

# **End-to-End Optimization of Lipid Nanoparticle Manufacturing for mRNA Delivery**

A thesis presented for the degree of  
Doctor of Philosophy  
from the Institute of Pharmacy and Biomedical Science  
at the University of Strathclyde  
*by*  
**Valeria Giacobbo**

## **Declaration of Authenticity**

*'This thesis is the result of the author's original research. It has been composed by the author and has not been previously submitted for examination which has led to the award of a degree.'*

*'The copyright of this thesis belongs to the author under the terms of the United Kingdom Copyright Acts as qualified by University of Strathclyde Regulation 3.50. Due acknowledgement must always be made of the use of any material contained in, or derived from, this thesis.'*

*Signed: Valeria Giacobbo*

*Date: 9<sup>th</sup> February 2025*

## Acknowledgements

First and foremost, I want to express my gratitude to my supervisor, Professor Yvonne Perrie. Her guidance over the past three years has been fundamental to both my professional and personal growth. She helped me stay on track with my PhD, provided brilliant scientific advice whenever I got stuck, and supported me when I needed it the most. After knowing her for four years now, I truly couldn't have asked for a better supervisor.

I'm also very thankful to Curia (Scotland) for sponsoring my PhD and making it possible for me to pursue my studies in the UK. Besides the financial support, I'm extremely grateful to the entire team – especially the development and analytical teams—for always helping me out over the past three years, making me feel welcome and part of the team during my time on site, and teaching me skills I wouldn't have learned elsewhere. Having an insight of how a pharmaceutical company works during an academic PhD is something I don't take for granted, and I had a great experience working there.

This PhD journey, with all its challenges, wouldn't have been the same without my lab mates at Strathclyde. Our lab is so big that I can't name everyone, but I feel lucky to have worked with such an amazing group. I've learned a lot from them, not just professionally but also on a personal level. I have to mention Ankita, who not only helped me with my *in vitro* and *in vivo* studies but also became one of my best friends, making Glasgow feel like home.

To my closest friends—Antonella, Camilla, Megan, Elena, Santi, and Domenica—thank you for being such a big part of my life and supporting me through everything. Thanks for always making me feel like you're right here, even when we're far apart.

Finally, I want to thank my family for their endless support and, most of all, for always believing in me from the time I was just a kid. My mum Lorena (who's convinced I'm the smartest girl in the world), my sister Laura, my brother-in-law Nik, and my Nonna Teta—I can't imagine life without them.

University of Strathclyde

End-to-end optimization of lipid nanoparticle manufacturing for mRNA delivery

Valeria Giacobbo

## Abstract

With the emergence of SARS-CoV-2 in 2020, mRNA vaccines have gained global attention. Currently, lipid nanoparticles (LNPs) are the most clinically advanced drug delivery system for the delivery of nucleic acids. Despite the extensive literature on LNPs in recent years, challenges persist regarding their development and production. In fact, most research papers focus on the therapeutic targets of LNPs, while less attention is given to understanding the challenges associated with their manufacturing, especially on an industrial-production scale, including scalability, reproducibility, encapsulation efficiency and long-term storage.

This thesis focused on the end-to-end workflow of LNPs manufacturing, covering production, purification, and freeze-drying, while also addressing storage conditions. Beginning with LNP production, the effects of microfluidic parameters on LNP manufacturing were investigated while the preclinical scalable production of LNPs using various microfluidic devices was also evaluated. Moving on to purification, the second step of LNP manufacturing, the typical bottlenecks associated with this stage were assessed, with a focus on tangential flow filtration (TFF) as this method is commonly used on an industrial level. The effect of TFF speed and diafiltration volumes on LNPs characteristics were evaluated, along with the challenges related to scaling up the purification process. mRNA LNPs storage also represents a challenge due to the fragile nature of mRNA. With the aim of exploring lyophilisation as a technique for preserving mRNA LNPs, a series of freeze-drying cycles were conducted to identify the optimal parameters for producing mRNA LNPs with acceptable critical quality attributes (CQAs) and the *in vitro* and *in vivo* activity of the lyophilised product was evaluated to determine the effectiveness of the method. This thesis also explored the role of lipid selection in shaping the quality, stability, and performance of the final product. In particular, the contribution of PEGylated lipids having different alkyl chain lengths (DMG-PEG 2000 versus DSG-PEG 2000) to the physicochemical characteristics and performance of mRNA LNPs was investigated, as well as the impact *in vitro* and *in vivo* of the ionisable lipid (ALC-0315, DLin-MC3, and SM-102).

The results presented demonstrate that all steps of LNP manufacturing influence the CQAs of the particles, from the choice of lipids, which can either limit or enhance their efficiency, to the selection of microfluidic parameters, buffers, purification methods, and lyophilisation conditions, highlighting the importance of carefully considering each individual step.

## List of Publications

Ankita Borah\*, **Valeria Giacobbo\***, Randal Baillie, Yvonne Perrie, From *In Vitro* to *In Vivo*: The Dominant Role of PEG-Lipids in LNP Performance, *European Journal of Pharmaceutics and Biopharmaceutics* (\*Equal authorship) – under revision

Swapnil Khadke, Carla B Roces, Rachel Donaghey, **Valeria Giacobbo**, Yang Su, Yvonne Perrie, Scalable solvent-free production of liposomes, *Journal of Pharmacy and Pharmacology*, Volume 72, Issue 10, October 2020, Pages 1328–1340, <https://doi.org/10.1111/jphp.13329>

## List of Poster Presentations

**V. Giacobbo**, A. Borah, Y. Perrie. Evaluating the *in vivo* effects of ionisable lipid/PEG-lipid combinations for optimised LNP compositions: a tool for route-specific and organ-targeted delivery. *15<sup>th</sup> APS PharmSci International Conference*, Huddersfield, September 2024

**V. Giacobbo**, A. Borah, Y. Perrie. The impact of the ionisable lipid choice on LNPs efficacy *in vivo*. *Liposome Research Days 2024*, Glasgow, June 2024

**V. Giacobbo**, R. Baillie, A. McFarlane, C. Allan, Y. Perrie. Simplification of the downstream process for LNPs. *CRS 2023 Annual Meeting and Exposition*, Las Vegas, July 2023

**V. Giacobbo**, R. Baillie, A. McFarlane, Y. Perrie. Post-manufacturing purification of LNPs: the impact of hold-time and temperature. *13<sup>th</sup> APS PharmSci International Conference*, Belfast, September 2022 (Oral presentation)

## List of External Projects

**Production of liposome formulations for the Statens Serum Institute (SSI), Copenhagen, Denmark:** Ran the Blaze microfluidic device to produce liposome formulations, optimising the process to meet their specific requirements.

**Lipid nanoparticle (LNP) production for Microfluidics, USA:** Independently prepared LNPs using the M110P Microfluidizer, handling all aspects of the process from calculations and material preparation to operating the instrument.

**Large-scale LNP production for Veterna Srl, Siena, Italy:** Successfully produced a large batch of LNPs, using the Ignite microfluidic device and purifying the nanoparticles via spin column, ensuring stability for -80°C storage.

**Liposome training and mentoring, University of Strathclyde, Glasgow, UK:** Trained and mentored students and colleagues on liposome preparation, characterization, and purification techniques, ensuring effective knowledge transfer and successful process replication.

***SaRNA LNP manufacturing for Curia (Scotland) Ltd, Glasgow, UK:*** Assisted Curia with the manufacturing of saRNA LNPs by troubleshooting formulation issues and optimising processes to achieve high-quality nanoparticles.

***SOPs and report writing for Curia (Scotland) Ltd, Glasgow, UK:*** Authored SOPs for Blaze and Dolomite instruments and prepared technical reports, ensuring compliance with industry standards.

# Table of Contents

<i>Declaration of Authenticity</i> .....	2
<i>Acknowledgements</i> .....	3
<i>Abstract</i> .....	4
<i>List of Publications</i> .....	5
<i>List of Poster Presentations</i> .....	5
<i>List of External Projects</i> .....	5
<i>List of Figures</i> .....	11
<i>List of Tables</i> .....	19
<i>Abbreviations</i> .....	21
<b>Chapter 1 General Introduction</b> .....	<b>24</b>
<b>1.1 Lipid Nanoparticles (LNPs) for Drug Delivery</b> .....	<b>25</b>
<b>1.2 From Liposomes to LNPs – A 60-Year-Old Journey</b> .....	<b>26</b>
<b>1.3 Approved LNPs</b> .....	<b>28</b>
<b>1.4 The Role of Different Lipids in LNPs</b> .....	<b>32</b>
1.4.1 Selection of the Appropriate Lipid Molar Ratio and Nitrogen to Phosphate (N/P) Ratio .....	35
<b>1.5 Mechanism of mRNA-LNPs Delivery System</b> .....	<b>37</b>
1.5.1 Liver Tropism and Strategies to Overcome Liver Tropism.....	39
<b>1.6 Lipid Nanoparticles Production and Storage</b> .....	<b>40</b>
1.6.1 Manufacturing.....	40
1.6.2 Purification .....	42
1.6.3 Storage.....	44
<b>1.7 Characterisation Techniques of LNPs</b> .....	<b>45</b>
<b>1.8 Future Directions of LNPs for mRNA Delivery</b> .....	<b>49</b>
<b>1.9 COVID-19 Mitigation</b> .....	<b>50</b>
<b>1.10 Aim and Objectives</b> .....	<b>51</b>

**Chapter 2 Investigating the Effects of Microfluidic Parameters on LNP Manufacturing and Evaluating Preclinical Scalable Production..... 53**

<b>2.1</b>	<b>Introduction.....</b>	<b>54</b>
2.1.1	Aim and Objectives.....	57
<b>2.2</b>	<b>Materials and Methods .....</b>	<b>58</b>
2.2.1	Materials.....	58
2.2.2	LNPs Microfluidic Manufacturing .....	58
2.2.3	LNPs Purification.....	59
2.2.3.1	Dialysis .....	59
2.2.3.2	Spin Column .....	59
2.2.4	Preclinical Scalable Process .....	59
2.2.4.1	Optimisation of the Use of the Dolomite .....	60
2.2.5	<i>In Vitro</i> mRNA Expression.....	61
2.2.5.1	<i>In Vitro</i> mRNA Expression Optimisation.....	61
2.2.6	Characterization of LNPs.....	62
2.2.6.1	Characterization of Particle Size and Zeta Potential.....	62
2.2.6.2	RNA Quantification.....	62
2.2.7	Statistical Analysis.....	63
<b>2.3</b>	<b>Results.....</b>	<b>63</b>
2.3.1	LNPs Microfluidic Manufacturing Considerations .....	63
2.3.1.1	Lipid Solvent Selection .....	63
2.3.1.2	RNA Solvent Selection .....	64
2.3.1.3	Focus on the Effect of TFR and FRR on LNP Microfluidic Manufacturing .....	65
2.3.1.4	Final Buffer Selection .....	67
2.3.2	Scalable Process for Preclinical Development .....	68
2.3.2.1	mRNA Expression .....	69
2.3.2.1.1	<i>In Vitro</i> Assay Optimisation .....	69
2.3.3	Manufacturing Parameters Optimisation Using Alternative Microfluidic Systems.....	70
<b>2.4</b>	<b>Discussion.....</b>	<b>73</b>
<b>2.5</b>	<b>Conclusion .....</b>	<b>78</b>

**Chapter 3 Simplification of the Downstream Process for LNPs..... 79**

<b>3.1</b>	<b>Introduction.....</b>	<b>80</b>
3.1.1	Aim and Objectives.....	81
<b>3.2</b>	<b>Materials and Methods .....</b>	<b>82</b>

3.2.1	Materials.....	82
3.2.2	Preparation of LNPs .....	82
3.2.2.1	Hold Time Before Purification Study .....	82
3.2.3	LNP Purification Methods.....	83
3.2.4	Residual Ethanol Detection .....	85
3.2.5	Quantification of PolyA Loading and Recovery.....	85
3.2.6	Physiochemical Characterization of Formulations.....	86
3.2.7	Statistical Analysis.....	86
<b>3.3</b>	<b>Results.....</b>	<b>86</b>
3.3.1	Post-Manufacturing Purification of LNPs.....	86
3.3.1.1	The Impact of Purification Methods .....	86
3.3.1.2	The Impact of Hold Time Prior to Purification .....	88
3.3.2	Investigating TFF as LNPs Purification Method.....	89
3.3.2.1	The Impact of the TFF Speed.....	89
3.3.2.2	The Impact of the Number of Diafiltration Volumes.....	92
3.3.2.3	GC Analysis to Confirm Ethanol Removal .....	95
3.3.2.4	Scaling Up the TFF Purification Process.....	96
<b>3.4</b>	<b>Discussion.....</b>	<b>101</b>
<b>3.5</b>	<b>Conclusions.....</b>	<b>105</b>
<b>Chapter 4</b>	<b>.....</b>	<b>107</b>
<b>4.1</b>	<b>Introduction.....</b>	<b>108</b>
4.1.1	Aim and Objectives.....	110
<b>4.2</b>	<b>Materials and Methods .....</b>	<b>111</b>
4.2.1	Materials.....	111
4.2.2	Preparation of LNPs .....	111
4.2.3	Purification Methods and Cryoprotectant Addition .....	111
4.2.4	Thermal Analysis by Differential Scanning Calorimetry (DSC) .....	112
4.2.5	Freeze Dry Microscopy (FDM) .....	113
4.2.6	Optimisation of the Freeze-Dry Parameters for PolyA LNPs.....	113
4.2.6.1	First Freeze-Drying Cycle .....	113
4.2.6.2	Second Freeze-Drying Cycle .....	114
4.2.6.3	Third Freeze-Drying Cycle.....	114
4.2.7	Measuring Critical Quality Attributes (CQAs) .....	115
4.2.7.1	Physiochemical Characterization.....	115
4.2.7.2	RNA Quantification.....	115

4.2.7.3	<i>In Vitro</i> Testing .....	115
4.2.7.4	<i>In Vivo</i> Testing .....	116
4.2.7.5	mRNA Integrity.....	116
4.2.7.6	Lipid Content.....	117
4.2.7.6.1	HPLC-CAD Conditions .....	117
4.2.7.6.2	Mobile Phases and Sample Separation .....	117
4.2.7.6.3	Linearity Solutions Preparation and Sample Preparation.....	117
4.2.7.6.4	Method Evaluation: Specificity, Linearity, Precision and Concordance .....	117
<b>4.3</b>	<b>Results.....</b>	<b>118</b>
4.3.1	DSC and FDM Results .....	118
4.3.2	Optimizing the Freeze-Dry Cycle Parameters .....	121
4.3.3	Evaluating the <i>In Vitro</i> Expression of Lyophilised mRNA LNPs .....	125
4.3.3.1	Evaluating the Lipid Content of Lyophilised mRNA-LNP.....	127
4.3.4	Evaluating the <i>In Vivo</i> Expression of Lyophilised mRNA LNP.....	128
<b>4.4</b>	<b>Discussion.....</b>	<b>128</b>
<b>4.5</b>	<b>Conclusion .....</b>	<b>135</b>
<b>Chapter 5</b>	<b><i>From In Vitro to In Vivo: The Dominant Role of PEG-Lipids in LNP Performance</i></b>	<b>137</b>
<b>5.1</b>	<b>Introduction.....</b>	<b>138</b>
5.1.1	Aim and Objectives.....	139
<b>5.2</b>	<b>Materials and Methods .....</b>	<b>140</b>
5.2.1	Materials.....	140
5.2.2	Fluc-mRNA Ionisable Lipid/DSG-PEG and DMG-PEG LNPs Preparation.....	141
5.2.3	Characterisation of Fluc-mRNA Ionisable Lipid/DSG-PEG and DMG-PEG LNPs.....	141
5.2.4	mRNA Extraction and Gel Electrophoresis .....	142
5.2.5	Cell Culture Maintenance .....	142
5.2.6	Determining the Endocytic Uptake Route of DiR-Labelled Ionisable Lipid/DSG-PEG and DMG-PEG LNPs Using Pharmacological Inhibitors.....	142
5.2.7	<i>In Vitro</i> mRNA Expression Study.....	143
5.2.8	<i>In Vivo</i> Biodistribution Studies by IVIS.....	143
5.2.9	Statistical Analysis.....	144
<b>5.3</b>	<b>Results.....</b>	<b>144</b>
5.3.1	LNPs Physicochemical Characterisation – The Impact of PEG-Lipid .....	144
5.3.2	Endocytic Pathway for LNPs Incorporating DSG-PEG or DMG-PEG .....	145
5.3.3	<i>In Vitro</i> Expression of DSG-PEG and DMG-PEG LNPs.....	147

5.3.4	<i>In Vivo</i> Expression of DSG-PEG and DMG-PEG LNPs.....	148
<b>5.4</b>	<b>Discussion</b> .....	<b>152</b>
<b>5.5</b>	<b>Conclusion</b> .....	<b>155</b>
<b>Chapter 6</b>	<b><i>General Discussion</i></b> .....	<b>156</b>
<b>6.1</b>	<b>Introduction</b> .....	<b>157</b>
<b>6.2</b>	<b>Parameters that can affect LNP microfluidic production</b> .....	<b>157</b>
<b>6.3</b>	<b>The crucial role of LNP purification</b> .....	<b>158</b>
<b>6.4</b>	<b>Freeze-dry as a promising technique for long term storage of LNPs</b> .....	<b>159</b>
<b>6.5</b>	<b>Evaluating LNPs Efficiency Considering Lipid Composition and site of administration</b> ...	<b>160</b>
<b>6.6</b>	<b>Future and Outlook</b> .....	<b>160</b>
	<b><i>Bibliography</i></b> .....	<b>162</b>

## List of Figures

**Figure 1.1** Schematic representing the principal mRNA elements to consider when designing an mRNA-LNP vaccine (the 5' cap, the UTR regions and the poly-A tail). Image produced using Biorender..... 25

**Figure 1.2** Liposome (with active compounds). The red triangles represent the encapsulated hydrophilic drug while the green squares represent the hydrophobic drug. Image created using Biorender..... 26

**Figure 1.3** Lipid nanoparticle (LNP) schematics. Black arrows indicate the components of the nanoparticle. Image produced using Biorender..... 32

**Figure 1.4** Chemical structures of the most commonly used lipids used to design LNP. The ratio of the lipids can vary, but the most used is 50:38.5:10:1.5 mol % (ionisable lipid: cholesterol: helper lipid: PEG-lipid), even if attempts have been made to evaluate the results with varying ratios. .... 36

**Figure 1.5** The delivery mechanism of mRNA-LNPs. (1) The nanoparticle is endocytosed inside the cell. (2) The ionisable lipid became protonated due to the acidic environment. (3) The payload is released into the cytoplasm. (4) The mRNA is translated into protein by the ribosome. (5) The epitopes are loaded onto MHC class I in the endoplasmic reticulum. (6) The MHC class I-peptide complex is

presented to CD8+ cells. (7) The cell takes up the exogenous protein. (8) The MHC class II processes the epitope. (9) The MHC class II-peptide complex activates the CD4+ cells, which will later activate B cells. The image was taken from (56)..... 38

**Figure 1.6** Schematic representation of a TFF system. The key components are illustrated: the feed reservoir, the filtration module and the permeate. The membrane selectively retains larger molecules in the retentate while allowing smaller molecules and solvents to pass into the permeate. .... 43

**Figure 1.7** . Cryo-TEM image of LNPs. Adapted from (165). Scale bar = 100 nm..... 47

**Figure 2.1** Microfluidic equipment from Precision NanoSystems used in this chapter. From left to right, The Spark, the NanoAssemblr, The Ignite and The Blaze..... 55

**Figure 2.2** The Dolomite ANP platform from Dolomite Microfluidics. Flow rates between 0.05 - 10 mL/min can be achieved with pressures up to 10 bar. In this chapter, LNPs were produced using this equipment with varying different microfluidic parameters..... 56

**Figure 2.3** Microfluidic chip geometries used to formulate LNPs in this chapter. The NanoAssemblr is equipped with a SHM micromixer, the Spark, the Ignite and the Blaze are equipped with a TrM micromixer while the Dolomite's chip contains a X-Junction. Image created using Biorender. .... 57

**Figure 2.4** Effect of organic solvent selection on LNPs manufactured using microfluidics. A) Size and PDI results; B) Zeta potential results. Results are expressed as mean  $\pm$  SD from 3 independent batches. Statistical significance was calculated:  $p < 0.05$  (\*). .... 64

**Figure 2.5** Effect of increasing citrate buffer concentration. Size (A), PDI (B) and zeta potential (C) were measured. Results are expressed as mean  $\pm$  SD from 3 independent batches. Statistical significance was calculated:  $p < 0.05$  (\*). .... 65

**Figure 2.6** Effect of different TFR/FRR combinations. The flow rate proportion of solvent to aqueous phases varied from 2:1 (A and D) to 3:1 (B and E) and 5:1 (C and F), with multiple speeds (5 mL/min, 10 mL/min, 15 mL/min, and 20 mL/min) examined. Data are expressed by mean  $\pm$  SD (n=3) and statistical analysis was performed (\* $p < 0.05$ ). .... 66

**Figure 2.7** Impact of the final buffer selection on LNP manufactured using microfluidics. Size, PDI (A) and zeta potential (B) were measured. Results are expressed as mean  $\pm$  SD from 3 independent batches. Statistical significance was calculated:  $p < 0.05$  (\*). .... 67

**Figure 2.8** In vitro expression of Fluc-mRNA LNPs. Confluent HeLa cells were treated with LNPs having mRNA doses in the concentrations of 2 µg/mL, 1 µg/mL, 0.5 µg/mL, and 0.25 µg/mL. The plate was incubated at 37°C for 24 hours. a) Results represent mean ± SEM of 3 independent batches produced at the Spark, the Ignite and the NanoAssemblr. Statistical analysis was conducted, and the results were considered significant with a p-value of less than 0.05 (\*). b) Cell work results for the LNPs manufactured using the Blaze. Data represent the average of three different cell-based assays performed in different days using the same LNP batch..... 69

**Figure 2.9** mRNA expression on HEK293 cells in three different days and in different types of plates. A) mRNA expression performed in black plates. B) mRNA expression performed in clear plates. C) mRNA expression performed in white plates. GenVoy-LNPs encapsulating Fluc-mRNA were transferred to cells, and luminescence was read after 24 h hour incubation at 37°C and 5 % CO<sub>2</sub>. Results represent mean ± SEM of 3 independent batches. .... 70

**Figure 2.10** Impact of TFR, FRR, head and tail cut volumes, and the priming step on LNP manufacture using the Dolomite ANP platform. LNPs were made with 50% mol of DOTAP (A) and SM-102 (B)..... 71

**Figure 2.11** Production of LNPs using the Dolomite ANP platform. A) DOTAP LNPs results. The X-Junction chip (100 µm) was used, and samples were dialysed for 1 h against PBS. B) SM-102 LNP results. The same chip was used to produce the LNPs, and samples were dialysed for 24 h against PBS to ensure complete buffer exchange. .... 72

**Figure 2.12** Relative polarities and chemical structures of methanol, ethanol and isopropyl alcohol. 73

**Figure 3.1** Schematic of LNP manufacturing process. Some of the bottlenecks of each step are highlighted. Image created using Biorender. .... 80

**Figure 3.2** Retentate flow rate range for the column used. Image derived from Repligen website..... 85

**Figure 3.3** Investigating the impact of hold time and temperature. After manufacturing, LNPs were purified via dialysis (A) or spin column (B) and particles' characteristics were monitored over 24 h. Results represent mean ± SD of three independent batches (\*p < 0.05). 0 h represents the LNPs immediately after purification. .... 87

**Figure 3.4** Investigating the impact of hold time and temperature on LNPs left unpurified for 24 h. A) LNPs were purified after 24 h from manufacturing while being stored at room temperature (RT). B) LNPs were purified after 24 h from manufacturing while being stored at 4°C (mean ± SD, n = 3, \*p < 0.05). .... 89

**Figure 3.5** Impact of TFF speed during purification. The effect of TFF speed was evaluated in terms of size (A), PDI (B) and zeta potential (C). Results are expressed as mean  $\pm$  SD from 3 independent batches. Statistical significance was calculated:  $p < 0.05$  (\*)..... 91

**Figure 3.6** Investigating the “wash cycles” number required to purify LNPs while maintain vesicle characteristics. The number of washes was decreased from 12 (A) to 7 (B), 5 (C), 3 (D) and 0 (E). pH stripes were used as an approximate tool to measure LNPs external pH (F). ..... 94

**Figure 3.7** Residual solvent levels after TFF expressed as parts per million (ppm). The internal standard used was ethyl acetate. All measurements were within the level of detection and level of quantification. The GC results represent  $n=1$ . ..... 95

**Figure 3.8** Optimising pre-clinical TFF purification process (LNP batch 1). LNP were divided into 3 aliquots so that various parameters could be tested: Aliquot 1 consisted of LNPs diluted 1:5 and purified via TFF at 212 mL/min against PBS for 12 diafiltration volumes, Aliquot 2 consisted of LNPs diluted 1:5, purified via TFF at 212 mL/min against Tris/sucrose for 12 diafiltration volumes and Aliquot 3 consisted of LNPs not diluted, purified via TFF at 212 mL/min against PBS for 12 diafiltration volumes. (A) Size and PDI, (B) encapsulation efficacy (EE) and mass balance (MB), (C) ethanol content of the resulting LNPs. Results represent  $n=1$ ..... 97

**Figure 3.9** Optimising pre-clinical TFF purification process (LNP batch 2). LNP were divided into 3 aliquots so that various parameters could be tested; Aliquot 1 consisted of LNPs purified via TFF at 106 mL/min against Tris/sucrose for 12 diafiltration volumes, Aliquot 2 consisted of LNPs purified via TFF at 212 mL/min against Tris/sucrose for 12 diafiltration volumes and Aliquot 3 consisted of LNPs purified via TFF at 212 mL/min against Tris/sucrose for 7 diafiltration volumes. (A) Size and PDI, (B) encapsulation efficacy (EE) and mass balance (MB), and (C) ethanol content of the resulting LNPs. Results represent  $n=1$ . ..... 99

**Figure 3.10** Optimising pre-clinical TFF purification process (LNP batch 3). LNP were divided into 3 aliquots so that various parameters could be tested; Aliquot 1 consisted of LNPs purified via TFF at 212 mL/min against Tris for 7 diafiltration volumes, Aliquot 2 consisted of LNPs purified via TFF at 212 mL/min against Tris for 7 diafiltration volumes (sucrose added after TFF), and Aliquot 3 consisted of LNPs purified via TFF at 265 mL/min against Tris for 7 diafiltration volumes. (A) Size and PDI, (B) encapsulation efficacy (EE) and mass balance (MB), and (C) ethanol content of the resulting LNPs. Results represent  $n=1$ . ..... 101

**Figure 4.1** Common components of freeze dryer. A) The product chamber is the chamber in which the product is placed for freeze-drying. B) The condenser chamber contains the condenser which is composed of plates or coils that are cooled to a very low temperature on which the solvent vapour (represented by a dotted arrow) condenses and freezes, thus acting like a “cold trap”. C) The vacuum pump applies a vacuum during the freeze-drying stages. Image created using Biorender. .... 109

**Figure 4.2** Purification methods used in this chapter. PolyA LNPs were purified via TFF (2 mL), and mRNA LNPs were purified via spin column (1 mL). In both cases, the cryoprotectant was added after the purification and concentration step under stirring. Image created using Biorender..... 112

**Figure 4.3** Thermal assessment on LNP formulations. A) 10 % sucrose LNPs; B) 5 % sucrose LNPs; C) 10 % trehalose LNPs; D) 5 % trehalose LNPs. The red trace is the initial freezing cycle from 25°C to -50°C and the loop represents the freezing exotherm. The pink trace is the heating cycle from -50°C to 25°C and the endothermic event is the melting event. .... 119

**Figure 4.4** Freeze-dried microscopy of LNPs containing different types and concentrations of cryoprotectants. Samples were frozen to -40°C to evaluate the freezing point and, after applying a vacuum, the collapsing point. Different morphology transitions are represented for A-E) 10% sucrose LNPs, F-J) 5% sucrose LNPs, K-O) 10% trehalose LNPs, and P-T) 5% trehalose LNPs. The intact LNP images (1) show the edge of the LNP solution drop on the glass slide placed on the FDM cryostage. (2) Represents the moment when the solution froze. The drying front (3), the visible boundary between the frozen portion of the sample and the area where sublimation (drying) has occurred, begins to appear at the edge of the sample solution drop. The collapsing point (4) indicates that the structural integrity is compromised due to excessive sublimation, resulting in deformation or shrinkage. Samples were observed under a microscope at 400× magnification (400p). .... 120

**Figure 4.5** Results of the first freeze-drying cycle. A) Size (nm) and PDI of the LNPs pre and post lyo; B) Zeta potential (mV) of the LNPs pre and post lyo; C) RiboGreen assay results pre and post lyo; D) Cake appearance in the presence of sucrose and trehalose; E) Lyotrace obtained at the end of the cycle showing the changes in temperatures and pressures mapping the freezing, primary drying and secondary drying steps. .... 122

**Figure 4.6** Results of the second freeze-drying cycle. A) Size and PDI of the LNPs pre and post lyo; B) Zeta potential of the LNPs pre and post lyo; C) RiboGreen assay results pre and post lyo; D) Cake appearance in the presence of sucrose and trehalose; E) Lyotrace obtained at the end of the cycle showing the changes in temperatures and pressures mapping the freezing, primary drying and secondary drying steps. The Chamber Pirani trace was not shown in the graph. .... 123

**Figure 4.7** Results of the third freeze-drying cycle. A to E represents the results for 2 mL LNPs lyophilised; A) Size and PDI; B) Zeta potential; C) RiboGreen assay results; D) Cake appearance in the presence of sucrose and trehalose; E) Lyotrace obtained at the end of the cycle. F to I represents the results for 1 mL LNPs lyophilised; F) Size and PDI; G) Zeta potential; H) Cake appearance in the presence of sucrose and trehalose; I) RiboGreen assay results..... 125

**Figure 4.8** mRNA expression results. Cells were seeded at 10 000 cells/100 µL and, after confluency was reached, LNPs were added to the wells. Luminescence was read after 24 h from LNP addition. The results shown compare control LNPs with lyophilised LNPs (containing 10 % sucrose and 10 % trehalose). Results represents mean ± SEM of two independent batches. .... 126

**Figure 4.9** Agarose gel electrophoresis for mRNA inside LNP. mRNA encapsulated within LNPs post lyophilisation was evaluated for stability by gel electrophoresis and compared to control mRNA LNPs. .... 127

**Figure 4.10** HPLC-CAD analysis for lipid quantification. Each of the lipids included in the reconstituted product was analysed after dilution in ethanol and centrifugation to separate the lipids from the mRNA. The recovery is shown as normalised lipid recovery (%) against the corresponding lipids in the control sample. .... 127

**Figure 4.11** In vivo results after the administration of control LNPs and lyophilised LNPs into mice. A) Quantification of the bioluminescence signal after 0h, 6h and 24h from administration. Results represent the average (± SEM) of the results obtained from three mice injected intramuscularly with each formulation. Statistical significance was calculated:  $p < 0.05$  (\*). B) Bioluminescence-mRNA expression IVIS images in mice at 0h, 6h and 24h after IM administration. The radiance photons colour scale is set at a minimum of  $9.32e6$  to a maximum of  $7.77e7$ . .... 128

**Figure 4.12** Vapor pressure over ice chart (from ATS Life Sciences Scientific website). All materials exert a vapour pressure on their surroundings and the vapour pressure differential describes the tendency for particle within a solid or liquid to be freed and join the gas phase. At equilibrium, particles leaving the surface are balanced by those becoming trapped and the vapour pressure over ice table describe equilibrium condition in which sublimation doesn't occur. For this reason, there needs to be a differential between the ice leaving the product and the ice at the vapour trap..... 131

**Figure 4.13** Summary of the results of the three freeze-drying cycles. Sucrose-LNPs showed physicochemical characteristics improvements after the 2<sup>nd</sup> and 3<sup>rd</sup> cycle. On the contrary, trehalose-LNPs never maintained good CQAs after lyophilisation across all cycles..... 133

**Figure 5.1** Agarose gel electrophoresis for Fluc-mRNA inside the LNPs to identify mRNA integrity. The LNPs were disrupted by centrifugation after adding ethanol and sodium acetate. mRNA pellets were mixed with formaldehyde loading dye, and mRNA strand lengths were confirmed by agarose gel electrophoresis in 1X MOPS buffer containing the SYBR Green Stain. .... 145

**Figure 5.2** Endocytic pathway determination of ionisable lipid/DSG-PEG LNPs. Cells, seeded at 25,000 cells/500  $\mu$ L, were treated with chlorpromazine hydrochloride, cytochalasin D, and filipin complex at the concentrations of 20  $\mu$ g/mL, 10  $\mu$ g/mL, and 2  $\mu$ g/mL respectively and incubated at 4  $^{\circ}$ C to selectively inhibit the clathrin-mediated, macropinocytosis, and caveolae-mediated internalisation of LNPs. Control cells were incubated with LNPs at 37  $^{\circ}$ C for 24-h (I-III, panel a-c). Clathrin-mediated endocytosis is involved in the mechanism of LNP uptake as the internalisation of the LNPs is compromised when cells are treated with chlorpromazine hydrochloride (I-III, panel d-f in all the LNPs). Macropinocytosis is observed to exist in the cells incubated with ALC-0315 and SM-102/DSG-PEG LNPs as a possible second route of an endocytic pathway to a lesser extent (I and III, panel g-i). Scale bar = 50  $\mu$ m. .... 146

**Figure 5.3** Endocytic pathway determination of ionisable lipid/DMG-PEG LNPs. Cells, seeded at 25,000 cells/500  $\mu$ L, were treated with chlorpromazine hydrochloride, cytochalasin D, and filipin complex at the concentrations of 20  $\mu$ g/mL, 10  $\mu$ g/mL, and 2  $\mu$ g/mL respectively and incubated at 4  $^{\circ}$ C to selectively inhibit the clathrin-mediated, macropinocytosis, and caveolae-mediated internalisation of LNPs. Control cells were incubated with LNPs at 37  $^{\circ}$ C for 24-h (I-III, panel a-c). Clathrin-mediated endocytosis is involved in the mechanism of LNP uptake as the internalisation of the LNPs is compromised when cells are treated with chlorpromazine hydrochloride (I-III, panel d-f in all the LNPs). Macropinocytosis and caveolae-mediated endocytic pathways were not involved in the DMG-PEG LNPs cellular internalisation (I-III, panel g-i and j-l). Scale bar = 50  $\mu$ m. .... 147

**Figure 5.4** In vitro expression of Fluc-mRNA LNPs. Confluent HeLa cells were treated with LNPs having mRNA doses in the concentrations of (2  $\mu$ g/mL, 1  $\mu$ g/mL, 0.5  $\mu$ g/mL, and 0.25  $\mu$ g/mL) and incubated at 37 $^{\circ}$ C for 24 hours. a) mRNA expression of Fluc-mRNA ALC-0315 LNPs. b) mRNA expression of Fluc-mRNA DLin-MC3 LNPs. In Fig. 5.4b, the embedded graph displays the data at a reduced luminescence range, providing a clearer view of the less apparent differences in the full-scale plot. c) mRNA expression of Fluc-mRNA SM-102 LNPs. Data are expressed by mean  $\pm$  SEM (n=3) and statistical analysis was performed by GraphPad Prism (\*p < 0.05)..... 148

**Figure 5.5** Representative bioluminescence IVIS images at different time points (1h, 6h, 24h, 48h) after IM, SC and IV injection of Fluc-mRNA ionisable lipid/DSG-PEG and DMG-PEG LNPs. The injected mRNA

dose was 5 µg mRNA encapsulated in LNP formulations. D-luciferin (30 mg/mL concentration) was administered subcutaneously at a dose rate of 150 mg/kg, and bioluminescence was measured after 10 min. The radiance photons colour scale is set at a minimum of 3.13e6 to a maximum of 3.05e7. .... 148

**Figure 5.6** a) Bioluminescence quantification in the muscle after IM injection of Fluc-mRNA ionisable lipid/DSG-PEG LNPs at different time points. b) Bioluminescence quantification in the muscle after IM injection of Fluc-mRNA ionisable lipid/DMG-PEG LNPs at different time points. c) Bioluminescence quantification in the liver after IM injection of Fluc-mRNA ionisable lipid/DSG-PEG LNPs at different time points. b) Bioluminescence quantification in the liver after IM injection of Fluc-mRNA ionisable lipid/DMG-PEG LNPs at different time points. Data are expressed by mean ± SEM (n=3) and statistical analysis was performed by GraphPad Prism (\*p < 0.05). (Y-axis scale bars are kept different for the two LNPs due to the significant difference in the total flux intensity values)..... 149

**Figure 5.7** Bioluminescence quantification in the subcut region after 1h, 6h, 24h, 48h from LNPs administration via SC route. a) Bioluminescence signal for Fluc-mRNA ionisable lipid/DSG-PEG LNPs at the different time points. b) Bioluminescence signal for Fluc-mRNA ionisable lipid/DMG-PEG LNPs at the different time points. Data are expressed by mean ± SEM (n=3), and statistical analysis was performed by GraphPad Prism (\*p < 0.05). ..... 150

**Figure 5.8** Bioluminescence quantification in the liver after 1h, 6h, 24h, 48h from LNPs administration via IV route. a) Bioluminescence signal for Fluc-mRNA ionisable lipid/DSG-PEG LNPs at the different time points. b) Bioluminescence signal for Fluc-mRNA ionisable lipid/DMG-PEG LNPs at the different time points. Data are expressed by mean ± SEM (n=3), and statistical analysis was performed by GraphPad Prism (\*p < 0.05). ..... 150

**Figure 5.9** Percentage bioluminescence at 6h in different organs after IM, SC, or IV administration. a) Percentage bioluminescence when administering AL-0315, DLin-MC3 or SM-102 Fluc-mRNA/DSG-PEG LNPs. b) Percentage bioluminescence when administering AL-0315, DLin-MC3 or SM-102 Fluc-mRNA/DMG-PEG LNPs..... 151

**Figure 5.10** 3D bioluminescence and micro-CT imaging. SM-102/DMG-PEG LNPs were administered via IM, SC or IV route and imaged at 6 h. Images were analysed by overlapping the bioluminescence images from the IVIS Spectrum and the micro-CT images using the Quantum GX2 micro-CT imaging system. .... 152

## List of Tables

<b>Table 1.1</b> List of USFDA-approved LNPs for biologics. ....	31
<b>Table 1.2</b> Common methods to characterise LNP. ....	49
<b>Table 2.1</b> Critical quality attributes for mRNA-LNP formulation (181). ....	54
<b>Table 2.2</b> Developmental microfluidic parameters covered in this chapter. ....	59
<b>Table 2.3</b> Microfluidic parameters selected for further preclinical scalable processes.....	60
<b>Table 2.4</b> Developmental microfluidic parameters for the DOTAP-LNPs formulation manufactured using the Dolomite platform. ....	61
<b>Table 2.5</b> Developmental microfluidic parameters for the SM-102-LNPs formulation manufactured using the Dolomite platform.....	61
<b>Table 2.6</b> Encapsulation efficiency (EE%) and mass balance (MB%) values for LNPs manufactured dissolving the lipids in ethanol, methanol or IPA. Results are expressed as the mean $\pm$ SD, n = 3 .....	64
<b>Table 2.7</b> Encapsulation efficiency (EE%) and mass balance (MB%) values for LNPs manufactured at increasing citrate concentrations. Results are expressed as the mean $\pm$ SD, n = 3.....	65
<b>Table 2.8</b> Encapsulation efficiency (EE%) and mass balance (MB%) of the TFR/FRR combinations tested. Results are expressed as the mean $\pm$ SD, n = 3. ....	67
<b>Table 2.9</b> Encapsulation efficiency (EE%) and mass balance (MB%) of the LNPs in the final buffer. Results are expressed as the mean $\pm$ SD, n = 3.....	68
<b>Table 2.10</b> LNPs characteristics manufactured by the Spark, Ignite, the NanoAssemblr and the Blaze. The results are expressed as mean $\pm$ SD from 3 independent batches, except for the mRNA-LNPs produced at Blaze, which were produced only once due to the high volume of mRNA required. ....	68
<b>Table 2.11</b> GenVoy-LNPs physiochemical characteristics. Results represent mean $\pm$ SD of 3 independent batches.....	70
<b>Table 2.12</b> List of LNP papers with the internal buffers used, along with the corresponding LNP formulations, buffer molarity, and pH. The * symbol next to a lipid indicates its specific type, which is listed immediately below. ....	75

<b>Table 2.13</b> Overview of the experimental parameters, as defined in this chapter, for use in the following chapters unless otherwise indicated. ....	78
<b>Table 3.1</b> Small-scale purification methods used in this chapter.....	83
<b>Table 3.2</b> Pre-clinical TFF conditions evaluated in this chapter.....	84
<b>Table 3.3</b> Encapsulation efficacy (EE %) and mass balance (MB %) of LNPs after 24 h storage at RT or 4°C. Results represent mean $\pm$ SD (n=3). ....	88
<b>Table 3.4</b> Encapsulation efficacy (EE %) and mass balance (MB %) of LNPs following purification after 24 h storage at RT or 4°C. Results represent mean $\pm$ SD (n=3). ....	89
<b>Table 3.5</b> Encapsulation efficacy (EE %) and mass balance (MB %) results following TFF purification at increasing speeds.....	92
<b>Table 3.6</b> RiboGreen assay results for LNPs purified decreasing the number of diafiltration volumes. ....	95
<b>Table 4.1</b> Experimental parameters of the first freeze-drying cycle. The primary drying duration reported in the table coincided with the CM pressure and the Pirani pressure convergence ( $\pm$ 3 mTorr) after $\sim$ 30 hours. However, the primary drying was extended for an extra 19 hours for logistic reasons. ....	114
<b>Table 4.2</b> Experimental parameters of the second freeze-drying cycle. The primary drying (which ended after $\sim$ 30 hours) had to be extended for an extra 29 hours due to logistic reasons.....	114
<b>Table 4.3</b> Experimental parameters of the third freeze-drying cycle. The primary drying duration was $\sim$ 30 hours but was extended for an extra 18 hours due to logistic reasons. ....	115
<b>Table 4.4</b> Physicochemical characteristics of control LNPs and mRNA LNPs post lyophilisation for in vitro testing. Results represent the average $\pm$ SD of 2 independent batches.....	126
<b>Table 5.1</b> Physicochemical characterisation of Fluc-mRNA ionisable lipid/DSG-PEG and DMG-PEG LNPs. Results are expressed as the mean $\pm$ SD, n = 3. ....	145

## Abbreviations

ALC-0159	Methoxypolyethyleneglycoloxy(2000)-N,N-ditetradecylacetamide
ALC-0315	6-((2-hexyldecanoyl)oxy)-N-(6-((2-hexyldecanoyl)oxy)hexyl)-N-(4-hydroxybutyl)hexan-1-aminium
ANOVA	Analysis of variance
ApoE	Apolipoprotein E
ARCA	Anti-Reverse Cap Analog
C12-200	1,1'-[[2-[4-[2-[[2-[bis(2-hydroxydodecyl)amino]ethyl](2-hydroxydodecyl)amino]ethyl]-1-piperazinyl]ethyl]imino]bis-2-dodecanol
Chol	Cholesterol
COVID-19	Coronavirus disease 2019
CPPs	Critical process parameters
CQAs	Critical quality attributes
cryo-TEM	Cryogenic transmission electron microscopy
DiIC	1,1'-Dioctadecyl-3,3,3',3'-tetramethylindocarbocyanine perchlorate
DiR	1,1-dioctadecyl-3,3,3,3-tetramethylindotricarbocyanine iodide
Dlin-DMA-MC3 (MC3)	(4-(dimethylamino)-butanoic acid, (10Z,13Z)-1-(9Z,12Z)-9,12-octadecadien-1-yl-10,13-nonadecadien-1-yl ester)
DLS	Dynamic light scattering
DMG-PEG2000	1,2-dimyristoyl-rac-glycero-3-methoxypolyethylene glycol-2000
DODAP	1,2-dioleoyl-3-dimethylammonium-propane
DOPE	Dioleoylphosphatidylethanolamine
DOTAP	1,2-dioleoyl-3-trimethylammonium-propane
DSC	Differential scanning calorimetry
DSG-PEG2000	1,2-distearoyl-rac-glycero-3-methylpolyoxyethylene
DSPC	Distearoylphosphatidylcholine
DSPE-PEG2000	1,2-distearoyl-sn-glycero-3-phosphoethanolamine-N-[amino(polyethylene glycol)- 2000]
EDTA	Ethylenediaminetetraacetic acid
EE %	Encapsulation Efficiency
EMA	European Medicines Agency

EtOH	Ethanol
Ex/Em	Excitation/emission
FBS	Foetal bovine serum
FDA	Food and Drug Administration
FDM	Freeze dry microscopy
Fluc mRNA	Firefly Luciferase RNA
FRR	Flow Rate Ratio
GMP	Good manufacturing practice
GUV	Giant unilamellar vesicles
HPLC-CAD	High-performance liquid chromatography with charged aerosol detection
HS-GC-FID	Headspace gas chromatography with flame ionization detection
ICH	International Conference of Harmonisation
IM	Intramuscular administration
IPA	Isopropanol alcohol or 2-propanol
IV	Intravenous administration
IVIS	In vivo imaging system
LDLR	Low-Density Lipoprotein Receptor
LNP	Lipid Nanoparticle
LUV	Large unilamellar vesicles
MB %	Mass Balance
MEM	Minimum Essential Medium
MeOH	Methanol
MHC	Major Histocompatibility Complex
MLV	Multilamellar vesicles
mPES	Modified polyethersulfone
mRNA	messenger RNA
MW	Molecular Weight
MWCO	Molecular weight cutoff
N/P ratio	Nitrogen to Phosphate ratio
PBS	Phosphate-buffered saline
PC	Phosphatidylcholine
PDI	Polydispersity Index
PEG	Polyethylene glycol

pKa	Acid Dissociation Constant
Post lyo	Post lyophilisation
Pre lyo	Pre lyophilisation
RPMI	Roswell Park Memorial Institute medium
SARS-CoV-2	Severe Acute Respiratory Syndrome Coronavirus 2
SAXS	Small-angle X-ray scattering
SC	Subcutaneous administration
SD	Standard deviation
SEM	Scanning Electron Microscopy
SHM	Staggered Herringbone Mixer
SM-102	9-Heptadecanyl 8-((2-hydroxyethyl)[6-oxo-6-(undecyloxy)hexyl]amino)octanoate
SORT	Selective Organ Targeting
SUV	Small unilamellar vesicles
TFA	Trifluoroacetic acid
TFF	Tangential Flow Filtration
TFR	Total Flow Rate
Tm	High phase transition temperature
TMP	Transmembrane pressure
Tris	2-amino-2-(hydroxymethyl)-1,3-propanediol
TrM	Toroidal micromixer
UTR	Untranslated region
ZP	Zeta potential

# **Chapter 1**

## **General Introduction**

## 1.1 Lipid Nanoparticles (LNPs) for Drug Delivery

Lipid nanoparticles (LNPs) are small, spherical particles composed of lipid molecules that act like non-viral carriers for various therapeutic agents, including genetic materials like DNA and RNA (1). LNPs protect nucleic acids against enzymatic degradation and enhance their cellular uptake, making them essential resources in advancing gene therapy research (2). The mRNA-based therapeutics began gaining widespread scientific interest when, in 1990, Wolf and his colleagues published a groundbreaking study which demonstrated that the injection of in vitro transcribed (IVT) messenger RNA (mRNA) or plasmid DNA directly into mouse skeletal muscle, resulted in protein expression (3). mRNA is a single-stranded ribonucleic acid derived from a DNA template that carries genetic information from DNA to the ribosomes, where it serves as a template for protein synthesis. Currently, the mRNA delivery systems are mainly divided into two categories: viral and non-viral vectors (4); viral vectors (such as adenovirus, retroviruses and lentiviruses) are efficient in cellular delivery, but their use is often limited due to safety concerns and the complexity of production. Non-viral vectors, on the contrary, such as LNPs, exosomes, or virus-like particles (VLPs), do not have any viral replication capability, reduce the risk of immune reactions and ensure greater safety. The main components of the mRNA LNPs are the nucleic acid and the lipid shell. Therefore, LNP design focuses on optimising both the nucleic acid payload (by modifying the sequence design) and the LNP formulation. The strategies to modify the mRNA comprise nucleotide modifications, mRNA capping modalities, and sequence modifications (5) (Figure 1.1).

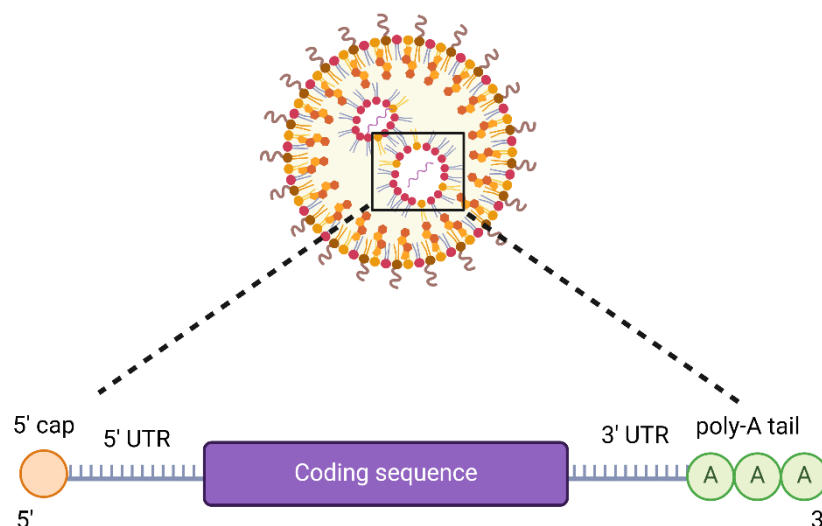


**Figure 1.1** Schematic representing the principal mRNA elements to consider when designing an mRNA-LNP vaccine (the 5' cap, the UTR regions and the poly-A tail). Image produced using Biorender.

Incorporating chemically modified nucleosides such as pseudouridine ( $\Psi$ ), 2-thiouridine (s2U), and 5-methylcytidine (m5C), reduces the immunogenicity of the mRNA, according to a study by Kariko et al. (6). Additional studies have also demonstrated that modified nucleosides stabilise the mRNA molecule, increasing protein translation (7). The strategy of including a modification has been employed in both authorised mRNA vaccines, mRNA-1273 (Spikevax) and BNT162b2 (Comirnaty), against COVID-19 (8). In particular, both these vaccines consist of N1-methylpseudouridine (m1 $\Psi$ )-modified mRNA encoding the viral spike antigen. The mRNA capping, another commonly used strategy, increases translation efficiency and mRNA stability (9). Several mRNA capping methods exist, such as the ARCA method, which ensures correct capping orientation (10), or the CleanCap technology (developed by TriLink Biotechnologies, San Diego, CA, USA) frequently used nowadays (11). UTR selection also should be considered. Roughly, the 5' UTR sequences influence protein expression, while the 3' UTRs are more likely to affect mRNA half-life (12). The poly-A tail is also important as it decreases the activity of the RNA exonuclease. Some studies suggest that longer poly-A tails (120–150 nucleotides) should be preferred as they increase mRNA stability, while other studies indicate that mRNA with short poly-A sequences (~33–34 nucleotides) resulted in higher translation efficiency (13). However, although mRNA plays a crucial role in the functionality of LNP-based delivery systems, this introduction will primarily focus on the lipidic carrier, as it is central to the stability, efficiency, and overall performance of LNP formulations.

## 1.2 From Liposomes to LNPs – A 60-Year-Old Journey

The rise of LNPs as a promising vehicle for gene delivery applications started from the development of phospholipid vesicles called “liposomes” in the 1960s after it was found that closed lipid bilayers vesicles spontaneously self-assemble in water (14–17) (Figure 1.2).

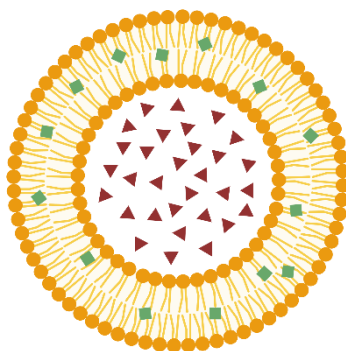


**Figure 1.2** Liposome (with active compounds). The red triangles represent the encapsulated hydrophilic drug while the green squares represent the hydrophobic drug. Image created using Biorender.

Liposomes consist of one or more lipid bilayers surrounding an aqueous core in which large quantities of aqueous buffer can be entrapped (18). The vesicles are typically made of phospholipids (such as phosphatidylcholines or phosphatidylethanolamines) and cholesterol, which stabilises the particles. Their structure depends on how they are prepared; liposomes can be unilamellar vesicles (in particular, depending on the size, they can be classified as small unilamellar vesicles (SUV), large unilamellar vesicles (LUV), giant unilamellar vesicles (GUV)) or multilamellar vesicles (MLV), forming an onion-like structure. SUV, whose size is usually around 100 nm, and smaller MLV are the most used as delivery systems (19). Size is a critical parameter in determining the *in vivo* circulation, as smaller liposomes are more successful at escaping phagocyte uptake (20) and, in general, especially for parenteral administration, particles need to be  $\leq 100$  nm (21). The surface charges of liposomes (expressed by their zeta potentials) control the interactions between particles and the stability of the nanoparticles. Particles with low charge densities or uncharged tend to aggregate over time, while charged particles repel each other, thus preventing aggregation. For this reason, zeta potential values lower than -30mV and higher than +30mV are optimal to maintain stability (22).

For nearly 30 years, liposomes have made significant progress in clinical applications, with the first USFDA-approved liposome preparation being Doxil, in 1995, to encapsulate the antitumor agent doxorubicin, used to treat ovarian cancer (23). Now, there are several liposomes-based drugs and vaccines to deliver anticancer, antibiotic, antifungal, aesthetic, and other drugs; among these, AmBisome (which encapsulates Amphotericin-B, approved in 1997), DaunoXome (Daunorubicin, 1996), Inflexal V (viroso-m-based trivalent influenza vaccine, 1997), Myocet (Doxorubicin, 2000), Estrasorb (Estradiol, 2003), Mepact (Mifamurtide, 2009), Vyxeos (Daunorubicin and Cytarabine, 2017), Nocita (Bupivacaine, 2017), Arikayce (Amikacin, 2018) and many more (24).

Liposomes are a versatile delivery system due to their ability to transport both hydrophobic drugs (in the hydrocarbon chain region of the lipid bilayer) and hydrophilic drugs (in the aqueous interior). In liposomes, efficient entrapment of anionic molecules like RNA or DNA is possible by using cationic lipids. The first examples of mRNA delivery through liposomes emerged in the late 70s. In 1978, Ostro et al. incorporated mRNA into liposomes for the first time, providing evidence that carcinoma cells treated with liposome-encapsulated rabbit globin mRNA produced a globin-like protein (25). At the same time, Dimitriadis et al. successfully introduced mRNA into mouse spleen lymphocytes through liposomes, directing the synthesis of globin (26). These findings started the era of gene-delivering liposomal formulations. In the beginning, liposomal formulations generally consisted of neutral phosphatidylcholine (PC) derived from egg or soy and cholesterol in different concentrations, and the major challenge was reaching a good encapsulation efficacy during production. The thin-film hydration method, one of the first methods developed to produce liposomes, which consists of dissolving the

hydrophilic drug in the aqueous buffer and then mixing it with dried lipid film to force the formation on multi-lamellar liposomes, comes with several challenges, the most significant one being the poor encapsulation inside the vesicles. The challenge was partially overcome when F. Szoka Jr. and D. Papahadjopoulos described the preparation of liposomes using the “reverse phase evaporation method” to form large unilamellar vesicles with improved encapsulation efficiency. The vesicles form when an aqueous buffer is introduced in a mixture of phospholipid and organic solvent, and then the organic solvent is evaporated under reduced pressure (27). However, more recently, microfluidic methods have gained prominence in liposome manufacturing, ensuring high reproducibility. Today, microfluidics is the most commonly used method for nanoparticle production (28). In the late 80s, cationic lipids started to be used for liposomal mRNA delivery as they can complex nucleic acids forming the so called “lipoplexes” (29,30). At the same time, pH-sensitive liposomes, achieved by incorporating pH-sensitive lipids engineered to remain stable at physiological pH but become destabilised in acidic conditions, started to be investigated (31,32). The strategy of incorporating a cationic pH-dependent lipid was also adopted to develop Onpattro, the first approved siRNA LNP delivery system. The structure of an LNP (Figure 1.3) is similar to the structure of a liposome, but a key aspect of LNPs is the presence of lipids and nucleic acid in the core, along with water (33). The LNP core contains lipids and small hydrophilic water pockets formed by the interaction between the ionisable lipids and nucleic acids. The nucleic acid molecules remain in the inner core, shelled by a lipid layer membrane, and are probably exposed to an aqueous environment (18). This core structure has been demonstrated by cryogenic transmission electron microscopy (cryo-TEM) analysis, which showed electron dense cores (33,34).

### 1.3 Approved LNPs

LNPs quickly became a big focus for mRNA delivery, as they offer a solution to the instability of the mRNA and its delivery challenges. As of January 2025, the only human mRNA products approved are the vaccines against SARS-CoV-2 (and variants) and against respiratory syncytial virus (RSV), but many are in ongoing trials involving mRNA products. On [clinicaltrials.gov](https://clinicaltrials.gov), there are over 250 entries under “mRNA” for phase 2 or 3 clinical trials involving respiratory viruses (such as a range of vaccines against SARS-CoV-2 but also respiratory syncytial virus and seasonal influenza), other infectious diseases (as Lyme disease and cytomegalovirus), cancers (among these malignant melanoma, solid tumours, pulmonary osteosarcoma, head and neck cancer) and also rare or metabolic diseases (such as ornithine transcarbamylase deficiency). Even though mRNA LNP vaccines gained the spotlight in 2020 during the COVID-19 pandemic, saving millions of lives globally, the first LNP product to reach the

market was a siRNA-based LNP for therapeutic purposes, namely Onpattro. The commercially approved LNP formulations and their specifications are reported below and summarised in Table 1.1.

### ***Patisiran (Onpattro)***

siRNA was discovered for posttranscriptional gene silencing by Hamilton and Baulcombe et al. in 1999, and it functions as a targeted mRNA degrader (35). Once inside the cell, siRNA binds to the RNA-induced silencing complex (RISC) that cleaves the target mRNA upon binding to a specific sequence on the mRNA molecule. This process prevents mRNA from being translated into the corresponding protein. In August 2018, Patisiran (Alnylam Pharmaceuticals Inc.) was approved by the United States Food and Drug Administration (FDA) and European Commission (EC) for the treatment of hereditary transthyretin-mediated (hTTR) amyloidosis in adults, a rare genetic disorder (36). The active pharmaceutical ingredient in Patisiran is patisiran sodium, a double-stranded siRNA that can reduce the synthesis of hTTR, which mutates and accumulates as insoluble amyloid fibrils in patients who suffer from this pathology. The target of Patisiran is the liver, the primary site of hTTR synthesis, where the siRNA is delivered using a lipid nanoparticle. The drug is administered over approximately 80 min via intravenous infusion of 0.3 mg/kg once every 3 weeks if the patient weighs < 100 kg or 30 mg once every 3 weeks if the patient weighs ≥ 100 kg (37).

### ***Comirnaty (Pfizer-BioNTech COVID-19 vaccine) and Spikevax (Moderna COVID-19 vaccine)***

The mRNA vaccines developed by Pfizer-BioNTech and Moderna were the first to receive emergency use authorization (EUAs) from regulatory agencies such as the MHRA, U.S. Food and Drug Administration (FDA) and the European Medicines Agency (EMA). Although mRNA vaccines had been under development for several years, their potential was not fully realised until the outbreak of COVID-19. The exceptional global health crisis created by SARS-CoV-2 enabled the rapid development of mRNA vaccines, making them central to the fight against the pandemic. Traditionally, vaccine platforms (such as inactivated or live-attenuated viruses) typically take years to develop as they require pathogen cultivation, inactivation, and formulation. In contrast, during the pandemic, vaccines (including the mRNA vaccines), were developed and entered clinical trials within a few months. This was due to different factors. When considering mRNA vaccines, the biohazard risks associated with mRNA LNPs manufacturing are low, and the scalability of production is simplified as mRNA vaccines do not require viral material for production; secondly, to target emerging viral variants or other disease targets, only changes to the mRNA sequences are needed, with very few adjustments required for the delivery technology (38). This was demonstrated by the fact that Moderna's vaccine started clinical trials only two months after the sequence of the viral genome was published (39).

The Pfizer-BioNTech COVID-19 vaccine, approved in 2020, contains Tozinameran (BNT162b2) while the Moderna COVID-19 vaccine, approved in the same year, contains Elasmomeran (mRNA-1273). Both the nucleoside-modified mRNAs encode for the viral spike protein of SARS-CoV-2 and, in both cases, the mRNAs use LNPs as delivery system (40,41). The viral mechanism of SARS-CoV-2 involves several steps that end with the immune response. At first, the spike glycoprotein (S protein) on the surface of the virus binds to the angiotensin-converting enzyme 2 (ACE2) receptor, highly expressed in the lungs and especially in alveolar epithelial type II, which serves as the site of viral replication (42,43). Specifically, spike protein (S) is very important because it is necessary for the SARS-CoV-2 virus to enter the cells (44). After administering the vaccines, the mRNA is released inside the cells and translated into the SARS-CoV-2 spike protein by ribosomes. When released into the bloodstream, this spike protein triggers the activation of the immune response.

These mRNA vaccines have shown a range of side effects during clinical trials. However, most of these side effects are mild (such as pain, swelling at the injection site, fatigue, headache, muscle pain, chills, fever, and nausea) and resolve within a few days after vaccination. More serious side effects, especially noted in younger male adults, are rare but include myocarditis and pericarditis and, in extremely rare cases, severe allergic reactions such as anaphylaxis (45).

#### **mRESVIA (Moderna respiratory syncytial virus (RSV) vaccine)**

mRESVIA is an mRNA respiratory syncytial virus (RSV) vaccine for the prevention of lower respiratory tract disease (LRTD) caused by RSV in adults  $\geq 60$  years old. This virus typically causes a mild upper respiratory tract infection in adults, but older adults, particularly those with underlying health conditions, have an increased risk of RSV-associated hospitalization. The mRNA encodes for the syncytial virus glycoprotein F which mediates viral fusion and host-cell entry and is encapsulated in a lipid nanoparticle (46).

mRESVIA was first approved by the U.S. FDA in May 2024, becoming the first mRNA vaccine authorised for a disease other than COVID-19. Later, the vaccine received a marketing authorisation valid throughout the EU in August 2024 and was approved in Canada in November 2024.

**Table 1.1** List of USFDA-approved LNPs for biologics.

<b>Trade Name</b>	<b>Payload</b>	<b>Lipid composition</b> (In order: ionisable cationic lipid, helper lipid, cholesterol, PEGylated lipid)	<b>Approved Indication</b>	<b>Dose/route of Administration</b>	<b>Molar lipid ratios (%)</b> (Ionisable cationic lipid : helper lipid: cholesterol : PEGylated lipid)	<b>Molar N/P ratios</b>
Onpattro	Patisiran sodium (siRNA)	- DLin-MC3-DMA ((6Z,9Z,28Z,31Z)-heptatriaconta-6,9,28,31-tetraen-19-yl-4-(dimethylamino) butanoate) - DSPC (1,2-distearoyl-sn-glycero-3-phosphocholine) - Cholesterol - PEG2000-C-DMG ( $\alpha$ -(3'-[[1,2 di(myristyloxy)propanoxy]carbonylamino]propyl)- $\omega$ -methoxy, polyoxyethylene)	Transthyretin-mediated amyloidosis	0.3 mg/kg, intravenous	50:10:38.5:1.5	3
Comirnaty	Tozinameran (mRNA)	- ALC-0315 ((4-hydroxybutyl)azanediyl)bis(hexane-6,1-diyl)bis(2-hexyldecanoate) - DSPC (1,2-Distearoyl-sn-glycero-3-phosphocholine) - Cholesterol - ALC-0159 (2-[(polyethylene glycol)-2000]-N,N-ditetradecylacetamide)	COVID-19 immunization	30 $\mu$ g; intramuscular	46.3:9.4:42.7:1.6	6
Spikevax	Elasomeran (mRNA-1273)	- SM-102 (heptadecan-9-yl 8-[(2-hydroxyethyl)[6-oxo-6-(undecyloxy)hexyl]amino]octanoate) - DSPC (1,2-distearoyl-sn-glycero-3-phosphocholine) - Cholesterol - PEG2000-DMG (1,2 Dimyristoyl-rac-glycero-3-methoxypolyethylene glycol-2000)	COVID-19 immunization	100 $\mu$ g; intramuscular	50:10:38.5:1.5	6 (estimate)
mRESVIA	mRNA-1345	- SM-102 (heptadecan-9-yl 8-[(2-hydroxyethyl) (6-oxo-6-(undecyloxy) hexyl) amino]octanoate) - DSPC (1,2-distearoyl-sn-glycero-3-phosphocholine) - Cholesterol - PEG2000-DMG (1,2 Dimyristoyl-rac-glycero-3-methoxypolyethylene glycol-2000)	Respiratory Syncytial Virus immunisation	50 $\mu$ g; intramuscular	50:10:38.5:1.5	6 (estimate)

## 1.4 The Role of Different Lipids in LNPs

LNPs are generally composed of four components: an ionisable cationic lipid, cholesterol, a helper lipid and a PEGylated lipid (Figure 1.3).

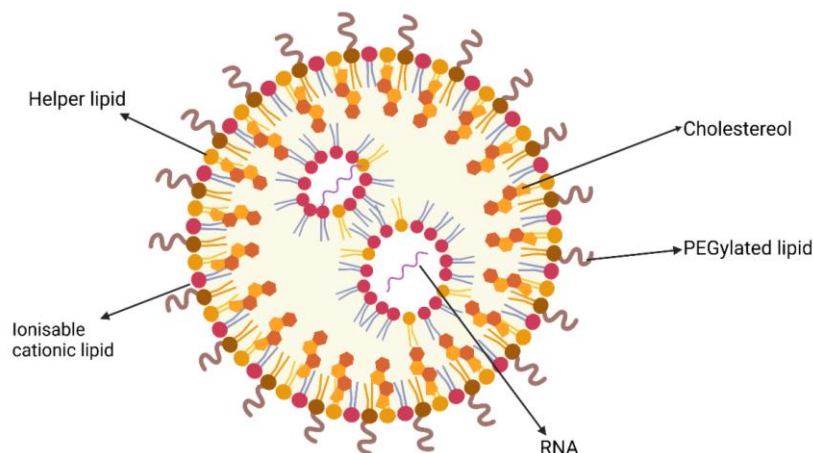


**Figure 1.3** Lipid nanoparticle (LNP) schematics. Black arrows indicate the components of the nanoparticle. Image produced using Biorender.

### *Ionisable cationic lipid*

Ionisable lipids (ILs) play a crucial role in the encapsulation of the nucleic acid. Their double nature allows them to exist in protonated or neutral forms: under acidic conditions, the lipids are protonated, and when neutrality is restored, the charge of the ionisable lipids decreases as they retrieve their neutral form. This duality has a double effect; from a manufacturing point of view, at low pH, they can self-assemble with negatively charged RNA via electrostatic interactions thus driving the formation of the particles (47). From an efficacy perspective, during circulation under physiological conditions (approximately pH 7.4), the lipids remain neutral, thereby reducing toxicity (48,49). However, upon entry into the endosome (where the pH is lower than the ionisable lipid pKa), the amine group on the head of the lipid becomes protonated, and this allows the lipid to interact with the anionic groups of the endosomal membrane, facilitating RNA release. The LNPs on the market have a pKa in the range of 6.1 – 6.7, which is considered to be optimal (50,51).

Generally, ILs are amphiphilic compounds composed of three domains: a polar head group, a linker and a hydrophobic tail region (52). The head group, based on the pH, can be neutral or positively charged depending on the pH of the surrounding environment. The ionisable lipid used in the FDA-approved LNP formulations (at date of publication) are DLin-MC3-DMA (Onpattro), SM-102 (Spikevax and mRESVIA), ALC-0315 (Comirnaty) and the headgroup of all these lipids is composed of a tertiary amine (53–56). One of the first ionisable lipids reported in literature (in 1994) was 1,2-dioleoyl-3-

dimethylammonium propane (DODAP), which was included in a liposomal formulation along with other lipids such as phosphatidylcholine (PC), dioleoylphosphatidylethanolamine (DOPE) and cholesterol (57). From DODAP (whose pKa is 6.58) other ionisable lipids with a creative structure were synthesised, enabling, in 2018, the first siRNA LNP formulation, Onpattro (36).

The linker connects the head to the tail region. It can be composed of more than one linker fragment, but the majority of ILs consist of a single fragment, usually an ester (58). The linkers can be biodegradable (such as esters and amides) or non-biodegradable (such as ethers and carbamates). However, ionisable lipids incorporating biodegradable linkers are often preferred because they demonstrate rapid elimination maintaining mRNA delivery efficacy (56,59). Moreover, Zhao et al. highlighted that, *in vivo*, lipids with ester bonds worked better than those with amide bonds (60).

The lipid tail usually consists of 1 to 4 hydrophobic tails (saturated or unsaturated) containing 8 to 20 carbon atoms each (61). DLin-MC3-DMA contains two linoleic acid tails, while SM-102 and ALC-0315 have two branched saturated tails. Because of their marked broader tails, the geometry of SM-102 and ALC-0315 is considered significantly “cone-shaped”, and it is this geometry that facilitates endosomal membrane destabilisation, enabling the intracytoplasmic release of nucleic acids (62). In particular, ILs with a cone-shaped morphology, when interacting with an endosomal membrane, likely form inverted hexagonal phases with the anionic endosomal phospholipids and promote release of the mRNA cargo into the cytosol (51,63).

### *Cholesterol*

Cholesterol is a rigid and hydrophobic molecule that is naturally present in the cell membrane, where it helps stabilise the membrane (64). It is generally included in the LNP formulations to confer stability, as it can regulate the integrity and rigidity of the vesicles, decreasing the membrane fluidity. It is usually included at high concentrations (>40% in molar ratio (65)) as, at high concentrations of cholesterol, the melting phase transition temperature of the lipids disappear, leaving highly stable vesicle (34). Moreover, a study revealed that this level of cholesterol is necessary to achieve almost complete and stable siRNA encapsulation in the absence of phospholipids (66). Because of its high proportion, different groups have investigated the effect of substituting cholesterol with analogues to investigate the effect on the delivery efficiency of LNPs, and it has been shown that the substitution of cholesterol with other sterol derivatives alters the gene delivery efficiency (67). For example, in 2020, Patel et al. screened a series of natural cholesterol analogues and discovered that, when included in LNPs,  $\beta$ -sitosterol allowed enhanced transfection efficiency and can therefore be considered a valid substitute (68).

### *Helper lipid*

Helper lipids (phospholipids) drive the formation of LNPs and facilitate endosomal escape by increasing membrane fusion (69,70). Typically employed phospholipids include saturated phosphatidylcholine (PC) lipids like DSPC (1,2-distearoyl-sn-glycero-3-phosphocholine) and unsaturated lipids like DOPE (dioleoylphosphatidylethanolamine), but commercially available LNPs only incorporate DSPC, probably due to its established role in stabilising commercial liposomes and the ability to disrupt the endosomal membrane (71). Kaufman et al., in their paper, showed that DSPC-containing LNPs had a higher mRNA encapsulation compared to DOPE-LNPs, despite a high protein expression being shown for DOPE-LNPs (34,72). Hence, adjusting the type of helper lipids can impact the delivery efficiency of LNPs and other aspects of their performance. A good example was provided in 2020 by Cheng et al., who demonstrated that the addition of negatively charged helper lipids to the nanoparticle formulation created LNPs with targeted delivery to the spleen (73).

### *PEGylated lipid*

First reported by Davis in 1977, PEGylation refers to the process of chemically conjugating polyethylene glycol on biomolecules (74). Since then, this strategy has been extensively evaluated as a mechanism to increase blood circulation time, and the first PEGylated liposomal formulation encapsulating doxorubicin reached the market in 1995 (75). Incorporating PEG-lipids has a crucial role in the structure and efficacy of LNPs, despite the small concentration (typically 1.5 mol %). One of the main reasons for including a PEG-lipid in the formulation is that PEGylation prolongs *in vivo* circulation time. In fact, the PEG-lipid chains extend on the outer surface of the vesicles, creating a barrier effect that prevents the binding of plasma proteins thereby avoiding the rapid clearance by the reticuloendothelial system (RES)(52). The hydrophilic spatial barrier created by the PEG-lipid on the surface of the LNPs also has a double effect on LNP stability: it improves the self-assembly during manufacturing (76) and it prevents aggregation, improving stability during storage (77,78). PEG-lipids also impact the encapsulation efficiency, the *in vivo* response, the circulation half-life and the transfection of LNPs (78,79). Additionally, considerations need to be made regarding the PEG-lipid molecular weight and length (80,81). For example, shorter carbon chains in PEGylated lipids led to faster desorption rates and better effects (52,81).

However, there are some safety concerns about using PEG-lipids *in vivo*. PEG-lipid has been named as the cause of an unexpected immunogenic response known as the "accelerated blood clearance" (ABC) effect that results in an increase in clearance and reduced efficacy of PEGylated nanocarriers (82). Another immune reaction to PEG-lipids is the "complement activation-related pseudoallergy" (CARPA); some studies revealed that DMG-PEG(2000) (the PEG-lipid included in the Moderna Covid vaccine)

produces more anti-PEG antibodies than ALC-0159 (the PEG-lipid included in the Pfizer/BioNTech Covid vaccine) (83). Figure 1.4 summarises the typical LNP components with the chemical structures of the most commonly used lipids.

#### **1.4.1 Selection of the Appropriate Lipid Molar Ratio and Nitrogen to Phosphate (N/P) Ratio**

Apart from selecting the appropriate lipids, the choice of the lipid molar ratio is crucial. The first liposomal formulations were mainly composed of high cholesterol and phospholipid content, but, in the case of LNPs, the major component is the ionisable cationic lipid. In general, the percentage of ionisable lipid is approximately 30-50 % of the total lipids, followed second by the cholesterol (20-50 %), phospholipid (10-20 %) and PEG-lipid (0.5-5 %)(58). The Moderna COVID-19 vaccine and Onpattro use a molar ratio of 50:38.5:10:1.5 mol % (representing the ionisable lipid: cholesterol: helper lipid: PEG-lipid) while the Pfizer/BioNTech vaccine uses slightly different ratios (46.3:42.7:9.4:1.6 mol %). In general, the 50:38.5:10:1.5 ratio is commonly used, but it may be modified depending on the lipids used, and in the literature, there are numerous examples (51,84,85). For example, Lam et al. demonstrated that increasing the PEG-lipid content from 1.6 % to 2.8 % resulted in better expression in primates when injected with siRNA LNPs (86). Roces et al. varied the ratio between cholesterol and the cationic lipid (DOTAP, MC3 and DDAB) to evaluate if modifications of the molar lipid content could be detected by the physicochemical characteristics of the formed particles and demonstrated a wide range of ratios could be adopted with minimal effect on the measured characteristics (87). More recently, AboulFotouh et al. studied the effect of lipid composition and molar ratios on the physicochemical properties of lipid nanoparticles and their stability during (thin-film) freeze-drying (88).

Another factor to consider when designing the LNPs is the nitrogen to phosphate (N/P) ratio, which represents the ratio between the amine group of the ionisable lipid and the phosphate groups of the mRNA backbone during LNP formation. Choosing the right N/P ratio is important to ensure successful mRNA complexation and the commonly used ratio *in vivo* is 6 (63,89–91). The N/P ratio of the Pfizer and Moderna COVID-19 vaccine is estimated at 6, while the Onpattro formulation N/P ratio is 3 (18). In 2021, Carrasco et al. made KC2 mRNA LNPs with N/P ratios in the range of 2–8. They reported that reducing the N/P ratio from 8 to 2 increased the LNP diameter and reduced encapsulation efficiency from 80 to 40% (51). In another study, Cheng et al. demonstrated that when the N/P ratio of their siRNA LNP was increased from 1 to 12, a progressive improvement in potency was observed up to an N/P ratio of 6, with little improvement in LNP activity beyond this point (92).

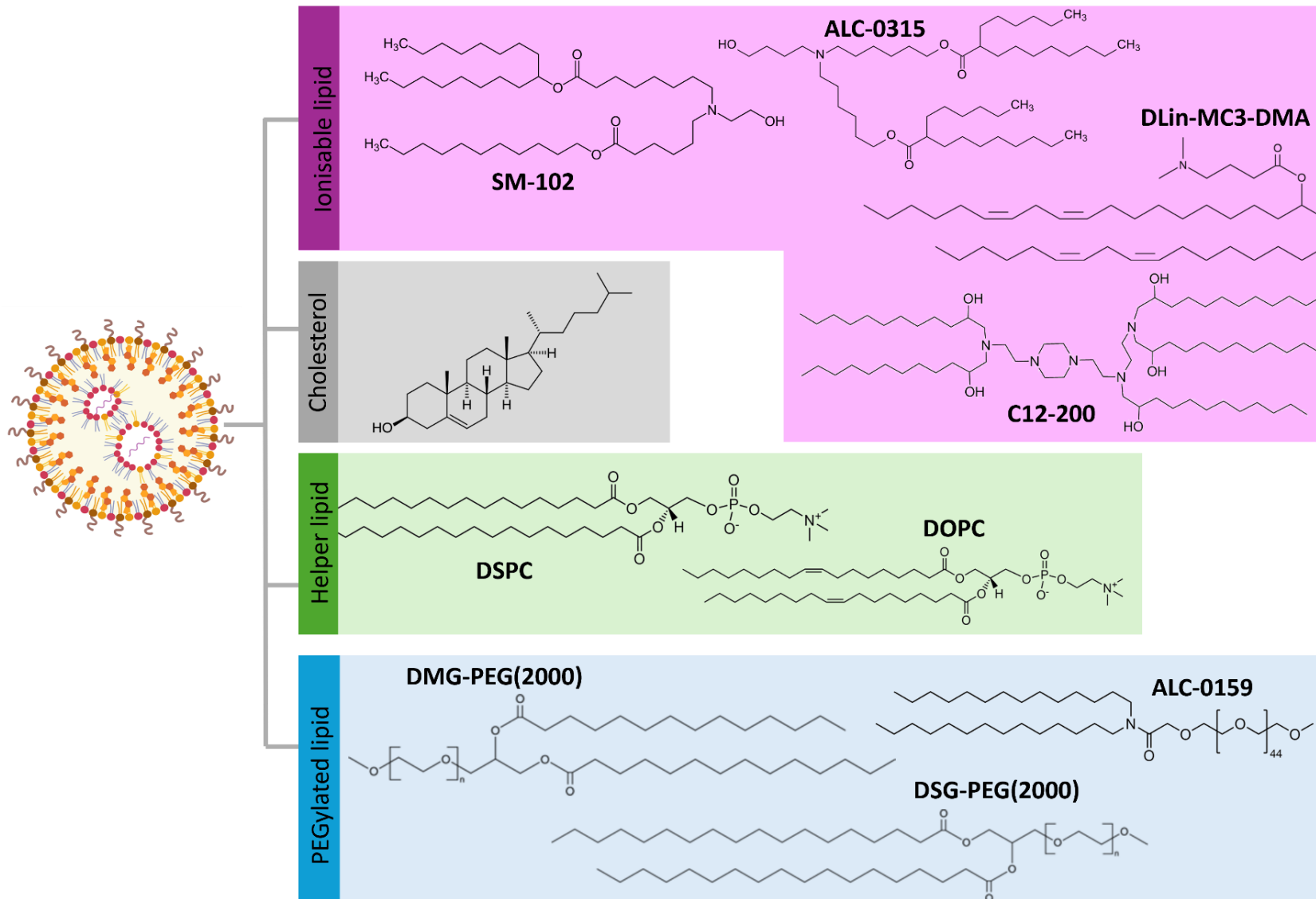


**Figure 1.4** Chemical structures of the most commonly used lipids used to design LNP. The ratio of the lipids can vary, but the most used is 50:38.5:10:1.5 mol % (ionisable lipid: cholesterol: helper lipid: PEG-lipid), even if attempts have been made to evaluate the results with varying ratios.

## 1.5 Mechanism of mRNA-LNPs Delivery System

mRNA LNPs need to overcome different extracellular and intracellular barriers to work *in vivo* (52). First, mRNA must be protected from RNases in physiological fluids. For this purpose, the LNP shell plays a crucial role by stabilising the mRNA molecules within the vesicles' core. This stabilisation occurs through electrostatic interactions between the mRNA and the lipids, preventing recognition and degradation by RNases. Additionally, the LNP shell further stabilises the mRNA in physiological fluids. Second, the LNPs should avoid interception by the mononuclear phagocyte system (MPS) and the post-administration renal clearance. PEG-lipid, often incorporated in the formulation, plays a crucial role in decreasing MSP recognition and renal filtration (93). Third, once they reach target cells, the mRNA must leave the endosome and reach the cytoplasm to start translation. This process is composed of different steps:

- a) The LNP is internalised inside the cell via multiple mechanisms such as macropinocytosis, clathrin-mediated endocytosis (CME) and caveolae-mediated endocytosis, depending on the vesicle type and the cell type (94,95). Macropinocytosis involves the formation of ruffles and cups on plasma membrane, which engulf the LNPs. This mechanism is a non-selective process where nanoparticles are lastly trapped in large vesicles called macropinosomes. The clathrin-mediated endocytosis involves the formation of clathrin-coated vesicles (CCVs) thanks to the action of a specific series of proteins (such as F-BAR and AP2) that are recruited to the plasma membrane (96). The caveolae-dependent endocytosis is another common way of internalisation of nanoparticles along with the CME (97); it involves the formation of the caveolae, flask-shaped invaginations of the plasma membrane.
- b) Even if the endosomal escape mechanism has not yet been fully understood, the most accredited theory suggests that, after the lipid nanoparticles are trapped in the endosomal compartments, the ionisable lipid becomes protonated because of the low pH of the environment, and this causes the electrostatic interaction and fusion with the negatively charged endosomal membranes. The LNP disruption facilitates the release of the RNA payload into the cytoplasm (47,98). However, it is important to state that only a small percentage of LNPs successfully escape from the endosome (99). After being freed outside the endosome, the mRNA binds to the host cell ribosomes, and it's translated into the antigen protein (98).
- c) Some antigens are released outside the cells, while others remain in the cell and are broken down by proteasomes into smaller fragments, including the antigenic epitopes. The epitopes

are loaded onto the major histocompatibility complex (MHC) class I in the endoplasmic reticulum (ER) and the MHC class I-epitope complexes are transported to the cell surface where they are presented to CD8+ T cells (100)

- d) The antigens that were released extracellularly are taken up by the antigen-presenting cells (APC), undergo endocytosis, and are subsequently loaded onto the major histocompatibility complex (MHC) class II. The MHC II-peptide complexes are transported to the cell surface thus activating CD4+ T cells (101). The activation of CD4+ T cells also stimulates B cells that will secrete antibodies specific to that antigen (102). The process is schematised in Figure 1.5.

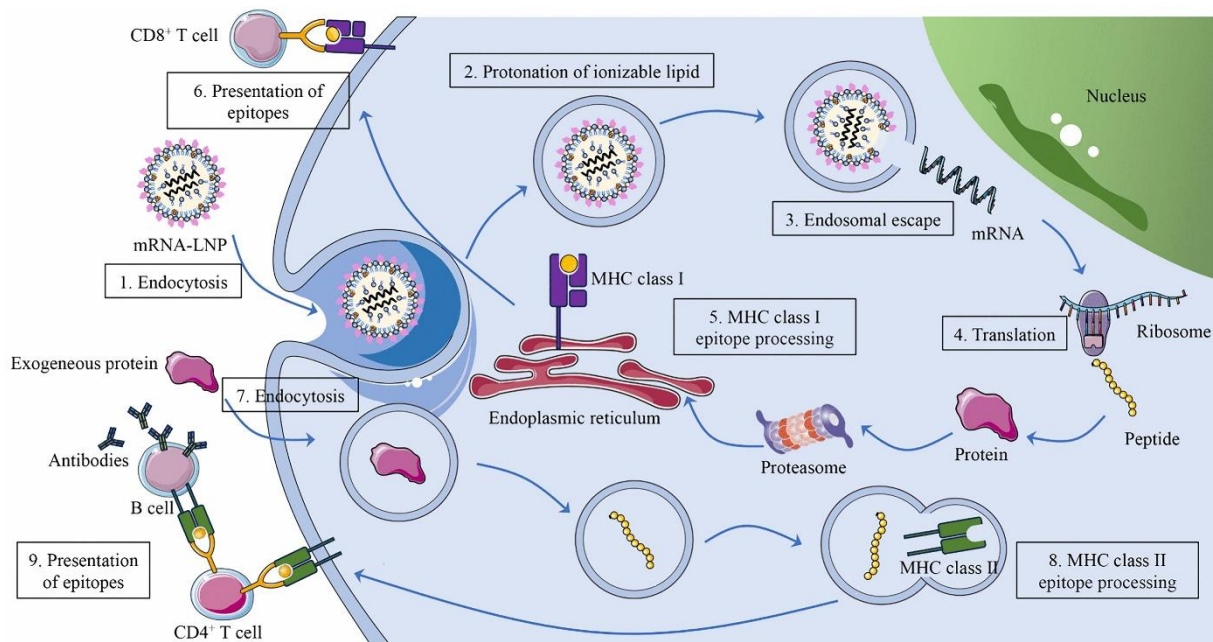


**Figure 1.5** The delivery mechanism of mRNA-LNPs. (1) The nanoparticle is endocytosed inside the cell. (2) The ionisable lipid became protonated due to the acidic environment. (3) The payload is released into the cytoplasm. (4) The mRNA is translated into protein by the ribosome. (5) The epitopes are loaded onto MHC class I in the endoplasmic reticulum. (6) The MHC class I-peptide complex is presented to CD8+ cells. (7) The cell takes up the exogenous protein. (8) The MHC class II processes the epitope. (9) The MHC class II-peptide complex activates the CD4+ cells, which will later activate B cells. The image was taken from (56).

One of the bottlenecks of this process is endocytosis of the LNPs, as the success of this step results in the release of the mRNA that will consequently trigger a series of events culminating in the immune response. The choice of lipids can impact this step; in fact, branched-tail lipids facilitate endosomal escape and consequent protein expression compared to linear lipids as they're strongly protonated at endosomal pH probably because the branch in the lipids creates additional space between the lipids that may facilitate protonation of the amines due to reduced repulsion between adjacent cations (103). Moreover, introducing double bonds into ILs and increasing the branching degree of the

nonpolar tail groups, thereby forming a more cone-like structure, causes the lipids to interact more effectively with the negatively charged lipids in the endosomal membrane. Their positive curvature helps disrupt the endosomal membrane leading to a membrane phase transition that allows the mRNA to escape from the endosome (104). Additionally, efforts have been made to produce LNPs that could achieve organ selectivity by, for example, coating nanoparticles with antibodies to deliver mRNA to specific cells (105), such as leukocytes (105), or modifying the ratios of lipid components (73,106).

### **1.5.1 Liver Tropism and Strategies to Overcome Liver Tropism**

When nanoparticles are injected into the bloodstream, plasma proteins adsorb on their surface, forming the so called “protein corona” (107). Some of these proteins function as markers for the mononuclear phagocyte system (MPS). The MPS includes different type of cells, such as dendritic cells, monocytes, and macrophages, and is responsible for detecting and removing foreign particles, like nanoparticles, from circulation. Kupffer cells, nonparenchymal cells present in the liver sinusoid, are the most abundant macrophages in the body and LNPs mainly accumulate in them (108). Along with Kupffer cells, other nonparenchymal liver cells are liver sinusoidal endothelial cells (LSECs) and hepatic stellate cells (HSCs), while hepatocytes constitute the parenchymal cells. Kupffer cells and LSECs are the first liver cells to interact with nanoparticles: generally, Kupffer cells take up particles larger than 100 nm while smaller particles are more readily taken up by LSECs (109). In general, if the nanoparticles bypass both Kupffer cells and LSECs, can interact with hepatocytes and exert their therapeutic function. This statement is supported by Park et al., who studied the distribution of PLGA nanoparticles in liver cells and noted that these particles are taken up by Kupffer cells and LSECs more than the hepatocytes. These findings make it clear that if the liver is the target organ for nanoparticles, achieving the therapeutic effect is quite straightforward due to the high liver tropism of the nanoparticles, even if the nonintentional accumulation in the nonparenchymal cells such as Kupffer cells and LSECs can present an issue (108,110). In fact, apart from particles with a very small size (less than 6 nm), that are eliminated through urinary excretion, all nanoparticles, independently of their size, charge or chemical composition, suffer from marked liver tropism (111). The liver tropism of LNPs is mainly due to the action of apolipoprotein E (ApoE), which in blood serum binds to LNPs, leading to LNP accumulation in the liver through low-density lipoprotein (LDL) receptors (112,113). However, in cases where the target organ differs from the liver, this constitutes a problem. In this context, extending the particle's circulation time to allow the particles to reach tissues other than the liver would be helpful. One approach commonly used to extend the circulation time is, as previously stated, PEGylation (especially if using a long PEG-lipid chain), thanks to the stealth effect of the PEG-lipid (114).

Different approaches are being explored to overcome the liver tropism namely passive, active, and endogenous targeting (115). In the passive targeting strategy, the physical attributes of the nanoparticle (such as size, shape, or charge) are adjusted to direct the particle to target tissues that present distinctive characteristics. This strategy is used, for example, for tumour targeting (116,117). The tumour tissue has, in fact, a very unique environment characterised by leaky blood vessels (the so-called “enhanced permeability and retention (EPR) effect” (118)); thus, only nanoparticles of specific sizes can access the tissue. Active targeting consists of binding, to the nanoparticle surface, a ligand (such as an antibody or peptide) that binds to a specific receptor on the target cell (118). By exploiting this strategy, LNPs have been used to target T cells (119) and bone marrow cells (120), but literature reports also note other sites such as the intestine (121), the blood-brain barrier (122), and more. The endogenous targeting strategy involves using additional lipid components to the LNPs. The methodology called “selective organ targeting (SORT)”, developed by Cheng et al., is an example (73). When the authors incorporated DOTAP as a “SORT molecule” into the traditional four-component LNP, mRNA delivery was exclusively directed to the lungs. On the contrary, when adding an anionic “SORT molecule,” delivery was directed to the spleen. This technique can be useful for directing the particles to specific sites that are otherwise difficult to reach.

## 1.6 Lipid Nanoparticles Production and Storage

### 1.6.1 Manufacturing

One of the traditional methods for liposomes and LNP manufacturing is the thin film hydration method (or the Bangham method), in which lipids are dissolved in an organic solvent, and then the solvent is removed via evaporation using a rotary evaporator, resulting in a thin lipid layer formation. This film is subsequently hydrated with an aqueous buffer containing the nucleic acid, which is passively encapsulated (123,124). The major disadvantage of this method, apart from the challenges in achieving reproducibility and scalability, is the fact that the resulting particles are large and show a low encapsulation efficiency. For these reasons, during the early 2000s, the spread of microfluidic techniques revolutionised the manufacturing of liposomes and LNPs to such an extent that, nowadays, microfluidic devices are primarily used in the upstream processes of LNP production (125,126). The microfluidic production of LNPs involves rapidly mixing lipids, solubilised in an organic solvent, with an aqueous phase containing the nucleic acid in a micromixer. The driving force behind particle formation is the interaction between the cationic or ionisable lipid and the negatively charged nucleic acid. If the

pH of the aqueous buffer is reduced to acidic values, the interaction with the RNA becomes stronger; on the contrary, if the buffer pH increases (for example, to values above the pKa of the ionisable lipid), the charge-charge interaction becomes weaker as the electron dissociation and association is in balance and therefore the ionisable lipid charge is neutralised (127).

The physicochemical properties, stability, and performance of LNP formulations of the resulting particles can be controlled by controlling the critical process parameters (CPPs). These parameters include temperature, lipid composition, lipid concentration, aqueous buffer molarity, lipid to RNA ratio as well as flow rate ratio (FRR) and total flow rate (TFR) (51,87,127–130). Proper control of these parameters is essential for optimising the drug delivery capabilities and ensuring the consistency of the formulation. The size of the LNP can also be manipulated by adjusting the excipients for the formulation, for example, changing the concentration of the cryoprotectant (131) and adding the cargo molecules (127).

The geometry of the microfluidic chip also plays a crucial role in the formation of LNPs, as it directly influences the mixing dynamics and self-assembly process. In a passive microfluidic system, fluid flows through microchannels, facilitating the mixing of two solutions under laminar flow conditions. This type of system offers precise control over LNP production by leveraging key fluid dynamics principles, such as Reynolds number, laminar flow, turbulence and shear stress (132,133). Reynolds number ( $Re = \rho v L / \mu$ ) is a dimensionless quantity that characterises the flow regime and is used to indicate the laminar or turbulent nature of a flow. It is influenced by some factors such as fluid velocity, channel size, and viscosity of the solution. In microfluidic systems, controlling flow rate directly impacts the Reynolds number and the flow behaviour. At low Reynolds numbers (<2000), flow remains laminar. In this situation, the mixing is controlled and is ideal for producing uniform nanoparticles (133). This is crucial for LNP production, as it ensures gradual and predictable mixing of lipids and mRNA, leading to stable encapsulation. On the contrary, at higher Reynolds numbers (>2000), turbulence can occur, and chaotic mixing is introduced. While turbulence might speed up the process, it risks instability and poor encapsulation of the payload. For LNP production, turbulence is generally undesirable, as it can lead to inconsistent particle sizes and reduced encapsulation efficiency. Maintaining laminar flow is crucial for producing stable, predictable LNPs, while avoiding the disruptive effects of turbulence. By adjusting the flow rate and managing Reynolds number, microfluidic devices can precisely control the size and uniformity of the LNPs, ensuring high encapsulation efficiency. A range of micromixer designs have been developed through the years; the staggered herringbone micromixer (SHM) for example, which has been widely used to produce size-controlled liposomes and LNPs, contains a series of herringbone structures that create chaotic flow in the fluid streams (134,135). Another example is the toroidal

mixer design (TrM) that includes circular structures within the flow path capable of increasing the number of vortices in the chip, allowing for better mixing (135,136).

The advantages of microfluidic devices include high reproducibility and scalability, largely due to their ability to achieve high production speeds (up to 200 mL/min), which reduces manufacturing time. For these reasons, they are also used for industrial-scale preparations other than for lab-scale manufacturing. In fact, if small-scale production is essential for identifying promising formulation candidates for further investigation and scaling up, large-scale production is equally crucial to meet the growing global demand for vaccines. A key requirement for advancing mRNA LNP therapeutics is the development of technology capable of producing particles that perform effectively on a small scale while also being scalable to meet the stringent manufacturing standards of the pharmaceutical industry, known as Good Manufacturing Practice (GMP) (137). Scaling-up can be achieved through parallelisation of the microfluidic chambers, longer flow duration, or increase of the mixer dimensions to enable comparable mixing at higher flow rates (132,138). Webb et al. assessed the ability to apply the toroidal mixer to produce liposomes at high production rates (>200 mL/min) using the NanoAssemblr GMP system and the NxGen 500 cartridge by Precision NanoSystems (139). The NxGen 500 cartridge has a larger cross-sectional area, resulting in lower fluidic resistance, but necessitating a higher flow rate to achieve the optimal mixing speed. The liposomes produced exhibited similar particle size distribution profiles and protein loading compared to those produced on a bench scale and larger preclinical scale. Another good example was given by Shepherd et al. in 2023 (140); with the aim of addressing the gap between formulation techniques at small-scale discovery stage and GMP-level production, the authors designed a microfluidic chip system to enable mRNA LNP vaccine production at both small discovery and large clinical testing scales (with scalable production rates of up to 17 L/h). Using this chip, they demonstrated that LNP physical properties and potency *in vivo* are unchanged as throughput is scaled. In particular, the authors formulated SARS-CoV-2 mRNA LNP vaccines that successfully triggered potent antibody responses in a preclinical study. Their chips (SCALAR chip) are fabricated out of silicon and glass substrates (while commonly used chips are made of polydimethylsiloxane, PDMS) which have excellent solvent compatibility, are compatible with pharmaceutical manufacturing, and can be reused and also suitable for high-temperature sterilizing methods.

### **1.6.2 Purification**

The production of LNPs mostly follows the same two steps: an upstream process to pre-assemble the particles and a downstream process to finalise the vesicles through buffer exchange (141).

Buffer exchange is important to raise the pH of the formulation to further sequester the payload inside the vesicles and ensure stability while removing ethanol to make the formulation suitable for clinical administration. In general, the methods commonly used are diafiltration and dialysis (87,142,143). Both methods require the use of a membrane. Diafiltration typically employs a filter made of polyethersulfone (PES) or modified polyethersulfone (mPES), while dialysis utilises tubing made of cellulose. These materials can interact to some extent with lipids forming nanoparticles. PES is a hydrophobic material, whereas mPES is surface modified to be more hydrophilic, which reduces, but does not eliminate, lipid binding. Cellulose, the primary component of dialysis membranes, is hydrophilic and generally less prone to binding lipids compared to PES.

Among the many downstream processing methods described in the literature, Tangential Flow Filtration (TFF) is often utilised due to its scalability (144) (Figure 1.6). The TFF system uses a membrane with a specific pore size to separate the molecules in solution. When the solution is introduced in the TFF system, it passes through the membrane and the large molecules (those larger than the membrane pore size) are retained by the membrane (in the “retentate”). In contrast, the smaller molecules pass through (into the “permeate”). The feed stream circulates through the membrane in a continuous flow mode, and the shear forces (produced by the tangential pumping of the liquid to the surface of the membrane) help reduce the accumulation of the cake layer on the surface.

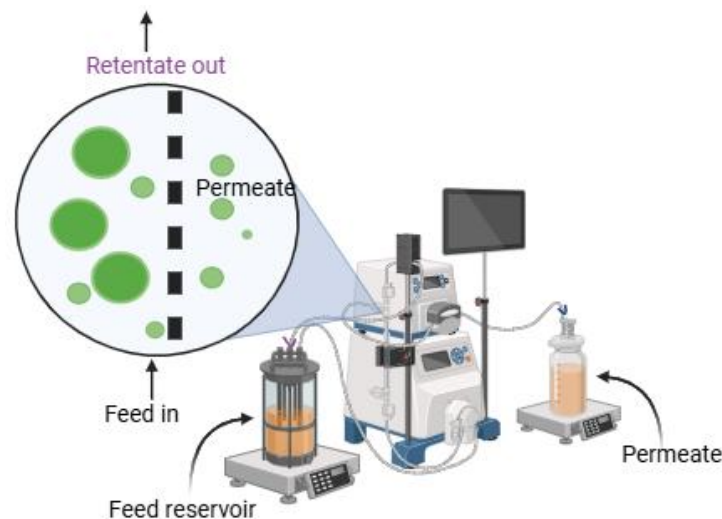


**Figure 1.6** Schematic representation of a TFF system. The key components are illustrated: the feed reservoir, the filtration module and the permeate. The membrane selectively retains larger molecules in the retentate while allowing smaller molecules and solvents to pass into the permeate.

### 1.6.3 Storage

Besides progress in scaling up mRNA LNP to GMP processes, LNP storage and transportation challenges persist. While conventional vaccines can be stored at 2–8°C for at least 6 months, mRNA vaccines require lower temperatures to ensure stability due to the unstable nature of mRNA and the fact that lipid-based delivery systems are easily corrupted. Moderna and Pfizer-BNT COVID-19 mRNA vaccines are examples of vaccines requiring ultra-low temperatures for long-term storage. Alternatively, they can be stored at 2°C to 8°C for up to 10 weeks (Pfizer-BNT) or up to 30 days (Moderna). An exception is the most recent development by Moderna's next-generation mRNA-1283 COVID-19 vaccine that can be stored for longer at 2–8°C due to the shorter mRNA length (145). The cold-chain approach can be a problem in countries with poor infrastructure. For this reason, lyophilisation (freeze-drying) of LNP-mRNA has been considered to increase the stability and shelf life of these vaccines and enable their worldwide shipping without freezing. Lyophilisation consists of removing the water from liquid drug formulations, which results in a stable solid ("cake") (146,147). To do so, the main steps are: (1) freezing the solution and (2) applying reduced pressure and heat to allow the frozen water sublimation. However, lyophilisation of mRNA is a challenging process due to the complexity of the LNPs. Generally, a sugar-based cryoprotectant (sucrose, trehalose, and mannitol) (148) is added to the formulation to ensure that particles are stable during the process because, although lyophilisation is effective in removing water, it can also cause particles to aggregate or collapse (149). In general, cryoprotectants are used not only when lyophilising a sample but also to improve the stability of LNPs during freeze-thawing and to ensure long storage at low temperatures. For example, Kim et al. discovered that mRNA LNP could be stored stably at –20 °C for at least 30 days in a PBS buffer with 10% sucrose (w/v) added as a cryoprotectant (148). Lyophilisation buffer, cryoprotectant and cycle process parameters such as temperatures and pressures must be carefully selected to ensure that LNP physicochemical characteristics are preserved during and after the process. Some studies have shown that LNPs containing siRNA or mRNA can be successfully lyophilised (149–151), but not all studies have reached the same conclusion. For example, Ball et al. experienced a significant decrease in gene silencing efficacy in cell culture after lyophilisation when LNPs were reconstituted with water (150). To date, research papers on optimizing the conditions for mRNA LNP lyophilisation remain limited, partly because customised solutions may be necessary for different types of mRNA and lipids, making it difficult to establish a standardised protocol for LNP lyophilisation.

## 1.7 Characterisation Techniques of LNPs

The characterisation of LNPs' critical quality attributes (CQAs) is essential to determine the success of the manufacturing processes and to check if the quality of the particles meets the standards and requirements of the pharmaceutical industry. The cellular uptake and the *in vivo* distribution of LNP are influenced by some physicochemical characteristics such as size, polydispersity (PDI), surface charge, surface morphology, encapsulation efficiency, pH and osmolarity of the final solution, integrity of the payload and crystallinity (152). The most common methods to characterise LNP are summarised in Table 1.2.

### *Particle size, polydispersity index (PDI), zeta potential and surface morphology*

Particle size can be measured through dynamic light scattering (DLS) (153,154). DLS measures variations in the intensity of scattered light caused by the Brownian motion of particles in a liquid. The sample is placed in a cuvette during the measurement, and a single-frequency laser is directed at it. The incident laser light scatters in all directions, and the scattered light is detected at a specific angle over time. This signal is analysed to determine particle size using the Stokes-Einstein equation (155):

$$D = \frac{k_B T}{6\pi\eta R_H}$$

Where:

$D$	Translational diffusion coefficient [m <sup>2</sup> /s] – “speed of the particles”
$k_B$	Boltzmann constant [m <sup>2</sup> kg/Ks <sup>2</sup> ]
$T$	Temperature [K]
$\eta$	Viscosity [Pa.s]
$R_H$	Hydrodynamic radius [m]

Nanoparticle size is a relevant factor as the size of the nanoparticles can influence their fate *in vivo*. Oussoren et al., for example, found that the subcutaneous injection of 40 nm liposomes, compared to larger particles, resulted in a higher lymphatic uptake (156). Younis et al. stated that only particles with a size smaller than 100 nm can target the liver after systemic administration (157) while, in their study, Uchiyama et al., found that liposomes that are 59 nm in diameter exhibit an enhanced tumour uptake than liposomes bigger than 100 nm in diameter (158).

When using the Stokes-Einstein equation in DLS measurements, several key assumptions are made. For example, the equation assumes that the particles being measured have a spherical shape, while particles could also be irregularly shaped, thus resulting in errors in the estimated particle size. Moreover, equation assumes that the particles remain monodisperse, which is a limitation as aggregates can affect the calculated value (159). Specifically, the scattering intensity generally increases with the size of the particles, but the relationship is not linear as it depends on several factors. According to the Rayleigh scattering law, when particles are much smaller than the wavelength of light, the scattering intensity of a particle in DLS is proportional to the sixth power of its diameter ( $d^6$ ) (160). This means that even a small number of large particles can dominate the measured signal, making the sample appear bigger than it actually is in such a way that, for small particles, even a small increase in diameter can result in a dramatic increase in the scattering intensity. For example, a single 100 nm particle will scatter 1,000,000× more light ( $100^6$ ) than a single 10 nm particle ( $10^6$ ). This can result in a distorted size distribution if large particles are present, even in very low quantities. To provide a more comprehensive understanding of the sample, DLS measurements can be considered not only by intensity but also by volume and number. The volume distribution is based on the actual physical volume of particles and gives the size distribution considering the volume of each particle. Larger particles will contribute more to the volume distribution even if they're present in smaller quantity because they occupy significantly more volume than smaller particles. The number distribution is based on the actual number of particles contained in the sample, independently of their size. The number distribution is particularly useful when smaller particles are the major population in terms of count but not in terms of scattering intensity.

Along with the particle size, the DLS also measures the polydispersity index (PDI), which provides information about the uniformity of particle sizes. The PDI ranges from 0 to 1, and the PDI value  $<0.2$  typically suggests uniform particle distribution. The charge on the surface of the particles is defined by the zeta potential (ZP), measured through electrophoretic light scattering (ELS), which is a useful parameter to predict long term stability of particles (161).

Different methods can be utilised to determine the surface morphology of nanoparticles such as transmission electron microscopy (TEM), scanning electron microscopy (SEM) and atomic force microscopy (AFM) that can provide insights into the shape and the dimensions of LNPs (152). SEM and TEM use electron beams that can scan the surface of particles to create an image of the structure, while AFM uses a sharp probe that scans the surface, mapping the outlines of the surface.

One of the most commonly used methods to obtain a detailed structure of LNPs is the cryo-transmission electron microscopy (cryo-TEM) (Figure 1.7). It preserves the structural integrity of the particles by freezing the nanoparticles in liquid nitrogen preventing the formation of ice crystal. Cryo-TEM investigations of LNPs have confirmed their electron dense core (162–164) .

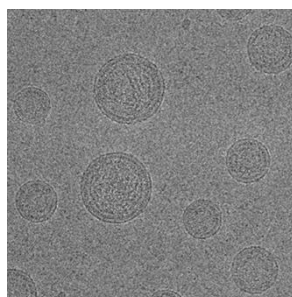


**Figure 1.7 .** Cryo-TEM image of LNPs. Adapted from (165). Scale bar = 100 nm.

In their paper, through a cryo-TEM analysis, Kulkarni et al. clarified the driving formation of siRNA LNPs. The authors hypothesised that siRNA is firstly sandwiched by the positively charged ionizable lipids at pH 4 aqueous buffer to form vesicular structures and, as the pH is raised to 7.4, it becomes trapped in these structures while the free ionizable lipids accumulates in the solid core (162). These findings have been utilised as a starting point to study the morphology of mRNA-loaded LNPs, while keeping in mind the larger size of mRNA compared to siRNA. Cryo-TEM based studies on the morphology of LNP-mRNA formulations identified different populations of particles; in their study, Brader et al. used thionine as a stain for RNA and demonstrated that the mRNA is located at the edges of the particle, likely sandwiched between closely apposed monolayers of lipid, or within aqueous compartments enclosed by bilayer protrusions. The authors discovered that mRNA can exist (a) fully encapsulated within the spherical particle or (b) dissociated within a large “bleb” (the name created to indicate protrusions on the surface of the particles) in the highly nonspherical particle or, alternatively, (c) in an intermediate state (162).

#### *Encapsulation efficiency (EE%)*

Encapsulation efficiency (EE%) is generally assessed through fluorescence assays, such as RiboGreen assay for RNA and PicoGreen assay for DNA. Achieving a high EE% is crucial to optimise drug delivery as high encapsulation efficiency ensures that a sufficient amount of therapeutic material is delivered to cells (166,167). During the experiment design process, it is crucial to define target attributes based on the intended use (for example, intramuscular, subcutaneous or intravenous delivery). Even if RiboGreen assay is one of the most commonly used methods to detect the mRNA concentration and it has been the method used in this thesis to measure RNA concentration, alternatives exist. HPLC-

based analytical methods, such as ion-pair reversed-phase HPLC (IP-RP-HPLC), size exclusion chromatography, and anion-exchange HPLC (AEX-HPLC) can be used for this purpose, assuring reproducibility. In the attempt of measuring mRNA concentration, Lokras et al. developed an IP-RP-HPLC method to quantify different mRNA cargos co-loaded into LNPs simultaneously (168). Bizmark et al. used size exclusion chromatography to measure the RNA content inside the LNPs and compared this technique to RiboGreen assay, concluding that RiboGreen assay can provide an estimate of EE with  $\approx 10\%$  error (169). An alternative method to evaluate the EE using an HPLC-based method was developed by Hara et al. In their study, the authors used an AEX-HPLC to quantify the poly(A) encapsulated in LNPs and determined the EE of this analytic method, concluding that this optimised HPLC method detects lipid nanoparticle degradation comparable to RiboGreen assay (170).

**Table 1.2** Common methods to characterise LNP.

Characterization criteria of LNPs	Impact	Assay
Particle size	To determine the size of nanoparticles	Dynamic light scattering (DLS) or NTA
Polydispersity index (PDI)	To measure the homogeneity of the sizes	
Zeta potential (ZP)	To determine the charge on the surface of nanoparticles	
Morphology	To evaluate structural characteristics	TEM, SEM, AFM, SAXS
Encapsulation efficacy (%)	To quantify the payload inside LNPs	RiboGreen assay or PicoGreen assay
pH	To ensure nanoparticles remain neutral at physiological levels (~7.4)	pH meter
Osmolarity	To verify nanoparticles are isotonic	Osmometer
Integrity of the nucleic acid	To detect the integrity of entrapped nucleic acid	Gel electrophoresis
Residual solvents	To ensure the solvent levels are in the range of the International Conference on Harmonisation (ICH) guidelines (171)	Gas chromatography
Lipid content	To identify and determine the contents of the lipids	HPLC-MS HPLC-ELSD HPLC-CAD
Gene transcription efficiency	To establish the success of LNP to deliver payload	<i>In vitro/in vivo</i> transfection

## 1.8 Future Directions of LNPs for mRNA Delivery

The advancements in LNP delivery systems and mRNA technology enabled the rapid development of mRNA vaccines against COVID-19. Nevertheless, some challenges remain. Translating preclinical successes into effective human therapies can be complex; for example, in April 2024, Verve Therapeutics halted their phase I clinical trial for VERVE-10, part of the Heart-1 trials, due to safety concerns. VERVE-101 is a CRISPR-based gene editing therapy to reduce low-density lipoprotein cholesterol (LDL-C) and PCSK9 levels in patients with heterozygous familial hypercholesterolemia (HeFH). VERVE-101 uses mRNA packaged in a lipid nanoparticle delivery vehicle to target the PCSK9

(148)(156,157)gene for lowering cholesterol. In response, Verve decided to replace LNP VERVE-101 with LNP VERVE-102, that uses a new original ionisable lipid that has been demonstrated to be safer in other trials (172). Although serious adverse reactions are rare in clinical trials of mRNA therapeutics and mRNA LNP vaccines are generally considered safe, some safety concerns persist. Three approaches have been proposed to improve the safety of mRNA drugs (4): (1) Reduce the dosage by enhancing the *in vivo* delivery efficiency of LNPs. (2) Identify alternatives, when possible, to replace the existing components of LNPs that might generate an immune response. For example, PEGylated lipids are usually used in mRNA–LNP vaccines, and it has been proved that they can induce anti-PEG antibodies in vaccinated individuals. These anti-PEG antibodies decrease the therapeutic efficacy, inducing faster clearance of systemically delivered PEGylated drugs (173,174). However, further studies are needed to understand the promoted clearance mechanism and the overall impact of these antibodies but given the spread of mRNA vaccine trials and delivery to large human populations (in the case of SARS-CoV-2 mRNA vaccines), this topic requires further research. (3) Optimise the composition of LNP to improve targeting. Another approach to improve the *in vivo* translation efficiency might be engineering RNA by modifying its five structural elements (the 5' cap, 3' poly(A) tail, protein-coding sequence, and the 5' and 3' untranslated regions) (175). Another challenge is linked to LNP manufacturing. As demonstrated by the extensive literature on this topic, numerous modifications can be made to LNPs to improve particle quality and achieve optimal CQAs. Factors such as the choice of lipids, buffers, and microfluidic mixing parameters are just some areas of interest. Moreover, scaling up from small-scale to large-scale production presents significant difficulties, as even minor variations in mixing or formulation can result in particles that are too large, unstable, or ineffective in delivering the payload. Large-scale production of LNPs is also challenging due to the difficulty of ensuring batch-to-batch consistency. Variations in particle size or drug encapsulation efficiency can lead to batches that fail to meet regulatory standards, making consistency across large volumes essential. During the COVID-19 pandemic, in fact, one major bottleneck identified was the scalability of the LNP formulation process (176,177). Moreover, as the number of highly efficient LNP delivery systems continues to grow, another important challenge is ensuring the long-term preservation of these formulations. The logistical demands of RNA therapies necessitate sub-zero temperatures, and this pose another challenge that should be faced.

## 1.9 COVID-19 Mitigation

The COVID-19 pandemic had a significant impact on the availability of key materials and consumables necessary for my research, particularly access to lipids. Due to global supply chain disruptions, it was

not always possible to source a consistent supply of specific lipids, which limited my ability to use the same lipid formulations across all experiments. As a result, different lipid nanoparticle (LNP) formulations were tested in different studies. However, given that the focus of my research was on the manufacturing process of LNPs rather than the specific formulations, this variability did not affect the key objectives or outcomes of this work.

## 1.10 Aim and Objectives

With the spread of the COVID-19 pandemic, scientific interest in lipid nanoparticle (LNP) vaccines has surged, leading to a significant rise in clinical trials involving LNPs, not only for vaccines but also for therapeutic applications. However, a lack of detailed understanding of their manufacture along with a lack of key indicators of efficacy that can be used to assess the product through the regulatory processes remain. This thesis, in collaboration with the pharmaceutical company Curia (Scotland), focused on developing microfluidic methods to mitigate risks in formulation, addressing the typical bottlenecks of microfluidic manufacturing from initial development (choice of lipids, upstream process, downstream process and filtration) to final product (including lyophilisation). To achieve this aim, the different steps typical of LNPs manufacturing were systematically examined:

- Upstream process – the effects of microfluidic parameters on LNP manufacturing were investigated by varying critical process parameters such as the lipid solvent, the mRNA internal and external buffers, the total flow rate (TFR), and the flow rate ratio (FRR). At the same time, different microfluidic devices with different geometries and volume capacities were tested to determine the possibility of scaling the process to a preclinical level.
- Downstream process – different LNP purification methods were optimised, including spin column, dialysis, and TFF. In particular, the focus of interest was the TFF process, as this technique is generally used for large productions. With the aim of simplify and speed up the process, the effects of speed and diafiltration volumes were evaluated on a bench scale. Additionally, the TFF purification process was scaled up to a preclinical level.
- Filtration – the impact of the 0.22 µm PES sterile filtration was evaluated and particles pre- and post- filtration were compared.
- Final product lyophilisation – the behaviour of LNPs during freeze-drying was investigated, with the aim of developing a suitable method of lyophilisation by varying the critical steps of freeze-drying and the nature of the cryoprotectant. Several freeze-drying cycles were conducted until the LNPs produced showed acceptable CQAs. The *in vitro* activity on HEK293

cells and the *in vivo* activity on BALB/c mice of the lyophilised mRNA LNPs was evaluated to determine if the process modified mRNA functionality.

- Impact of the choice of lipids – the effect of the choice of lipids on LNP performance was evaluated by varying the type of ionisable lipid and PEGylated lipid. The *in vitro* results of these changes were evaluated by measuring mRNA expression on HeLa cells and by evaluating the endocytic pathway that these LNPs adopt to enter the cells, to explore how much the ionisable lipid and PEG-lipid can impact on the way of internalisation. *In vivo* studies were also conducted following the intravenous, subcutaneous, and intramuscular administration, to investigate how different routes of administration can influence the effect of LNPs.

## **Chapter 2**

Investigating the Effects of Microfluidic Parameters on LNP Manufacturing and Evaluating Preclinical Scalable Production

## 2.1 Introduction

The development of lipid nanoparticles (LNPs) has emerged as a critical component in advancing RNA-based therapeutics, particularly in the context of vaccine delivery and gene therapy. As the demand for these therapeutics increases, so does the need for scalable and efficient manufacturing processes. Microfluidic technology offers a promising solution, enabling precise control over the formulation process, which is essential for producing LNPs with consistent size, polydispersity index (PDI), and RNA encapsulation efficiency (178–180).

In relation to lipid nanoparticle manufacturing, it is important to identify the critical quality attributes (CQAs) besides the critical process parameters (CPPs) that will impact the final formulation. CQAs and CPPs are often related as CPPs are production parameters that affect CQAs and should, therefore, be controlled. The CQAs regarding mRNA-LNP characterization are described in Table 2.1 (181). The suggested acceptance criteria are in accordance with existing regulatory guidelines for Moderna's (mRNA-1713) and Pfizer-BioNTech's (BNT162b2) vaccines and mainly reflect the requirements for RNA-based vaccines administered intramuscularly.

**Table 2.1** Critical quality attributes for mRNA-LNP formulation (181).

Quality attribute	QCAs influence	Acceptance criteria
Size	Affects LNP uptake and impact	<100–200 nm
Polydispersity Index	Impacts safety and efficacy as it's a measure of the homogeneity of the particles	<0.3
Surface charge	Affects the distribution of nanoparticles	±20 mV
Encapsulation efficacy (EE%)	Measures the amount of encapsulated mRNA and its crucial for delivery	>80%
Mass balance (MB%)	Important to track the loss of mRNA	70–95%
Lipid content	Impacts the efficacy of LNPs	N/A* *No acceptance criteria are currently documented

Key parameters that can be controlled in microfluidic systems include the flow rate ratio (FRR) (182), between the aqueous phase and the organic phase, and the total flow rate (TFR) (183), both of which can impact the physicochemical characteristics of the produced particles. The exploration of the flow rate performed in this chapter is aimed at pushing towards higher Reynolds numbers to enhance mixing intensity and assess how these changes impact the CQAs of the LNP formulations.

Besides FRR and TFR, the choice of aqueous buffer is also critical in LNP production. Citrate buffer, particularly at a lower pH (pH 4), is commonly used to dissolve the RNA and its concentration must be carefully optimised, as particle size is influenced by both the buffer type and its concentration (184). Other important factors are the solvent used to dissolve the lipids, and the external buffer used. The choice of external buffer is driven mainly by the intended storage conditions of the nanoparticles. For example, when LNPs are to be frozen or freeze-dried, Tris with a cryoprotectant is generally preferred over PBS due to PBS's tendency to cause pH shifts during lyophilisation.

A variety of microfluidic equipment is available for preclinical scalable production, ranging from small-scale to more industrial-scale systems. For the purposes of this chapter, the microfluidic devices used include the Spark, the NanoAssemblr, the Ignite and the Blaze from Precision NanoSystems (Figure 2.1).

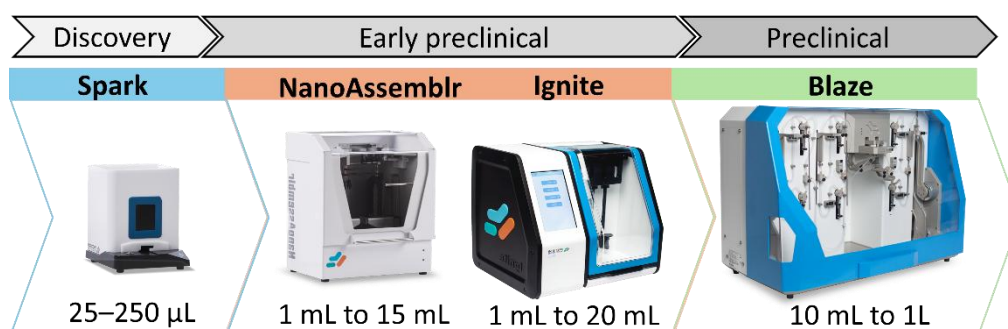


**Figure 2.1** Microfluidic equipment from Precision NanoSystems used in this chapter. From left to right, The Spark, the NanoAssemblr, The Ignite and The Blaze.

In addition to these devices, the Dolomite ANP platform from Dolomite Microfluidics was also employed for LNP production (Figure 2.2).

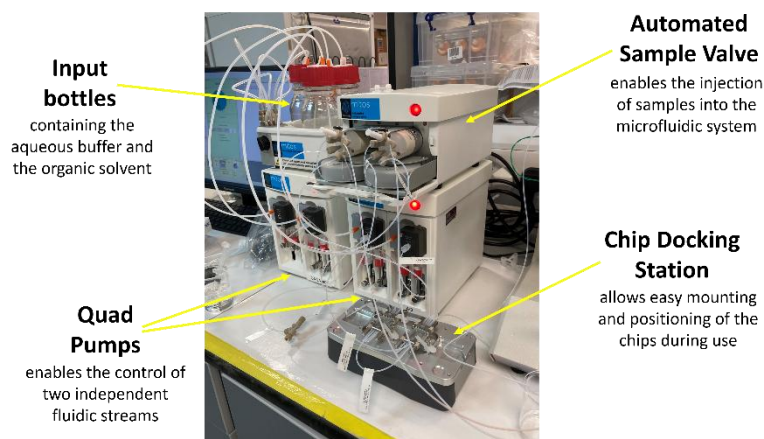


**Figure 2.2** The Dolomite ANP platform from Dolomite Microfluidics. Flow rates between 0.05 - 10 mL/min can be achieved with pressures up to 10 bar. In this chapter, LNPs were produced using this equipment with varying different microfluidic parameters.

These pieces of equipment feature mixers of different geometries as displayed in Figure 2.3. In a staggered herringbone micromixer (SHM, Figure 2.3A), the organic and aqueous phases are passed over a series of herringbone structures resulting in a chaotic flow while a toroidal micromixer (TrM, Figure 2.3B) contains circular structures that create vortices and centrifugal forces which can improve mixing and also allow reaching high fluid speeds (185–187). In a X-Junction chip (Figure 2.3C), particle formation occurs by diffusion and nanoprecipitation as the central channel is injected with the organic solution containing the lipids and the side channels are injected with the aqueous phase (188). In the chip, as the organic solution is mixed and diluted by the aqueous buffer streams, the lipids self-assemble vesicles (189). To evaluate which geometry offers optimal performance, mixing behaviour can be correlated to the CQAs of the resulting LNPs.

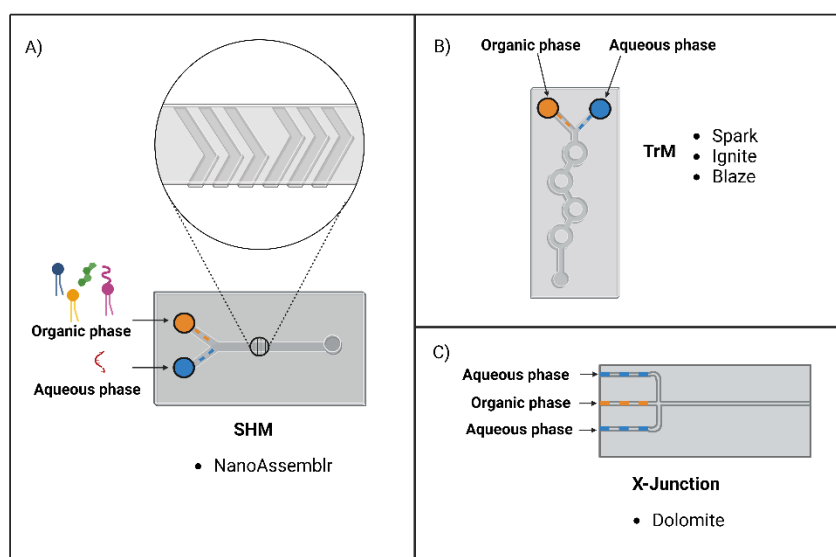


**Figure 2.3** Microfluidic chip geometries used to formulate LNPs in this chapter. The NanoAssemblr is equipped with a SHM micromixer, the Spark, the Ignite and the Blaze are equipped with a TrM micromixer while the Dolomite's chip contains a X-Junction. Image created using Biorender.

LNPs are crucial for the effective delivery of mRNA therapeutics (190). The ultimate goal of implementing LNP manufacturing is to produce nanoparticles suitable for injection into humans to achieve a therapeutic effect. By encapsulating mRNA, LNPs facilitate its transport into cells and enhance its stability. Once inside the cell, the mRNA is released and translated into protein, a process that can be measured to evaluate the effectiveness of the LNP formulation. Assessing mRNA expression involves quantifying the amount of protein produced from the delivered mRNA, which indicates the LNPs' performance in promoting gene expression.

### 2.1.1 Aim and Objectives

The aim of this work was to systematically investigate how key microfluidic parameters influence the formation and characteristics of LNPs, and to assess, for the first time, the preclinical scalability of LNP production across multiple distinct microfluidic platforms. This approach provides a comparative evaluation of device performance, offering new insights into optimizing LNP synthesis for translational applications. To achieve this, the objectives were:

- Perform a screening study by varying the CPPs in LNP manufacturing: lipid solvent, the mRNA internal and external buffers, the TFR, and the FRR.
- Evaluate the effects of different TFR/FRR combinations.

- Assess the feasibility of a preclinical scalable process using different microfluidic devices with varying geometries and capacities for producing different volumes of LNPs.
- Evaluate the *in vitro* performance of LNPs produced using different equipment by assessing mRNA expression in HEK293 cells.

## 2.2 Materials and Methods

### 2.2.1 Materials

Distearoylphosphatidylcholine (DSPC) was obtained from Lipoid (Ludwigshafen, Germany). Dioleoyl-3-trimethylammonium propane (DOTAP) and 1,2-dimyristoyl-rac-glycero-3-methoxypolyethylene glycol-2000 (DMG-PEG 2000) were purchased from Avanti Polar Lipids (Alabaster, AL, USA). The ionisable lipids (heptatriaconta-6,9,28,31-tetraen-19-yl-4-(dimethylamino)butanoate) (DLin-MC3-DMA) and (heptadecan-9-yl 8-((2-hydroxyethyl) (6-oxo-6-(undecyloxy) hexyl) amino) octanoate) (SM-102) were purchased from Broad Pharm, USA. Polyadenylic acid (PolyA), citric acid, sodium citrate tribasic dihydrate, Triton X-100 and cholesterol were purchased from Sigma Aldrich (St. Louis, MO, USA). EZ-Cap-modified firefly luciferase-mRNA (5-moUTP) was acquired from APEX BIO (USA). Quant-iT RiboGreen RNA Assay Kit, phosphate buffered saline tablets and diethylpyrocarbonate (DEPC) were purchased from Thermo Fisher Scientific (MA, USA). One-Glo Luciferase assay system was procured from Promega Corporation (USA). The organic solvents ethanol (EtOH), isopropanol (IPA), methanol (MeOH), D(+)-Sucrose and Tris-HCl were purchased from Fisher Scientific (Loughborough, UK). MEM cell culture media, TrypLE express, and L-glutamine were purchased from Gibco Life Technologies. Antibiotics penicillin/streptomycin and amphotericin B were purchased from Sigma Aldrich. The GenVoy-ILM™ Kit was provided by Precision Nanosystems Inc., Vancouver, BC, Canada. Dialysis tubing cellulose membrane (avg. flat width 25 mm), spin column 10 kDa/100 kDa MWCO, GenVoy-ILM™, Acrodisc® filter (0.2 µm pore size) Millex-GP Syringe Filter Unit were purchased from Merck Millipore Ltd (UK).

### 2.2.2 LNPs Microfluidic Manufacturing

Unless otherwise stated, microfluidic production of LNPs was achieved using the NanoAssembl Benchtop (Precision NanoSystems Inc, Vancouver, Canada) equipped with a SHM mixer. The two inlet streams comprised lipids dissolved in ethanol and aqueous buffer and to administer the solvent and aqueous components, disposable syringes (1 – 3 mL, Luer Lock) were used to attach the syringes to separate inlets on the microfluidic cartridge. Starting and end waste were 0.15 mL and 0.05 mL, respectively. Microfluidic parameters varied as described in Table 2.2.

The aqueous phase was composed of either polyA or Fluc-mRNA. The organic phase was made of DOTAP or SM-102, cholesterol, DSPC, DMG-PEG 2000 at a ratio of 50:38.5:10:1.5 mol %, respectively, and the starting lipid concentration was 5 mg/mL unless otherwise stated. The nitrogen/phosphate (N:P) ratio was 6:1 for all the formulations.

**Table 2.2** Developmental microfluidic parameters covered in this chapter.

Solvent selection (lipid)	Solvent selection (mRNA)	FRR (aq./org.)	TFR (mL/min)	Final buffer selection
Methanol, Ethanol, or IPA	Citrate 10, 50, 75, 100, 200 or 300 mM	2:1, 3:1, 5:1	5, 10, 15, 20	PBS 10 mM, Tris 10 mM, Tris 10 mM/sucrose 300 mM

## 2.2.3 LNPs Purification

### 2.2.3.1 Dialysis

Dialysis was used as a purification method to remove the organic solvent. Dialysis tubing with a molecular weight cut-off of 14 kDa was treated in a solution of 1 mM EDTA and 2% sodium bicarbonate at 80°C for 2 h to remove sulphites and glycine from the membrane. The membrane was then washed with deionised water and stored in a mixture of 50 % ethanol and 50 % water. After producing the LNPs via microfluidics, a 1 mL sample of LNPs was transferred into the dialysis membrane and dialysed against 200 mL of external buffer.

### 2.2.3.2 Spin Column

A 100kDa or 10kDa MWCO Amicon® Ultra Centrifugal filter was used to remove the organic buffer and perform a buffer exchange. 1 mL LNPs was diluted 1:40 in either PBS, Tris or Tris/sucrose and the column was centrifuged at 2,000 x g in a precooled centrifuge at +4°C for the required time. After finishing the first interval centrifugal process, the filtrate was removed from the filtrate tube, and the sample reservoir was filled with the remaining diluted sample. The sample was recovered to the initial volume.

## 2.2.4 Preclinical Scalable Process

Once established, the most effective microfluidic parameters (Table 2.3), LNPs were produced on different Precision NanoSystems instruments: the Spark, the Ignite, the Blaze, and the NanoAssemblr.

- *The spark*: The Spark can produce up to 250 µL LNPs. Disposable microfluidic chips (toroidal geometry) were loaded with 31 µL lipid stock and 93 µL PBS in the reaction chambers,

respectively. The formulation was prepared at room temperature, and the setting chosen from the Spark menu was 8.

- *The NanoAssemblr and the Ignite:* The NanoAssemblr and the Ignite were used to achieve microfluidic production of 1 mL LNPs. These systems use different microfluidic mixers: the NanoAssemblr uses a SHM mixer, and the Ignite cartridge is equipped with a TrM mixer.
- *The Blaze:* The Blaze was used to produce 10 mL LNPs. It uses the same TrM micromixer design as the Ignite. It dispenses fluid at precise flow rates and flow rate ratios using syringe pumps, which are controlled through the Blaze software installed on the accompanying laptop. The cartridge mixes the reagents from the centre, and the right channel under precisely controlled, non-turbulent conditions and the resulting formulation is then delivered to the collection vessels.

**Table 2.3** Microfluidic parameters selected for further preclinical scalable processes.

<b>Solvent selection (lipid)</b>	Ethanol
<b>Solvent selection (RNA)</b>	Citrate buffer 50 mM, pH 4
<b>FRR (aq./org.)</b>	3:1
<b>TFR (mL/min)</b>	15 mL/min
<b>Final buffer selection</b>	PBS

#### 2.2.4.1 Optimisation of the Use of the Dolomite

Alongside the production of LNPs using Precision NanoSystems instruments, LNPs were formulated with the Dolomite ANP platform from Dolomite Microfluidics (Royston, Hertfordshire, UK). As with any microfluidic device, the core of this system is the microfluidic chip. The system consists of two chips linked together: the first, the main chip (100  $\mu\text{m}$ ), allows the formation of the particles, and the second, the dilution chip (190  $\mu\text{m}$ ), directs the LNP stream from the first chip to the collector. If dilution is needed, the dilution chip introduces a buffer to the LNP stream, diluting the particles. The geometry of the chip can affect the final size of the LNPs. For this work, the 100  $\mu\text{m}$  X-Junction chip was used. The buffer and solvents used, including 50 mM citrate at pH 4, ethanol, and water, were filtered before starting the equipment. This step is necessary because the equipment is very sensitive to dust and debris, which can easily cause blockages.

Different runs were needed to produce LNPs with acceptable physicochemical characteristics, and key microfluidics parameters were modified during each run. Once the optimal parameters were

determined, LNPs were produced twice to confirm the results obtained from the initial run (n=1). The LNP formulations produced in duplicates at the Dolomite platform are described in Table 2.4 and Table 2.5.

**Table 2.4** Developmental microfluidic parameters for the DOTAP-LNPs formulation manufactured using the Dolomite platform.

<b>Chip type</b>	Junction chip (100 $\mu$ m, 190 $\mu$ m)
<b>FRR (aq./org.)</b>	2:1, 3:1, 4:1
<b>TFR (mL/min)</b>	6 mL/min, 8 mL/min, 10 mL/min
<b>Purification method</b>	1 h dialysis against PBS
<b>Final volume</b>	1 mL
<b>Head/cut volume</b>	300 $\mu$ L
<b>Priming</b>	No Priming

**Table 2.5** Developmental microfluidic parameters for the SM-102-LNPs formulation manufactured using the Dolomite platform.

<b>Chip type</b>	Junction Chip (100 $\mu$ m, 190 $\mu$ m)
<b>FRR (aq./org.)</b>	2:1, 3:1, 4:1
<b>TFR (mL/min)</b>	6 mL/min, 8 mL/min, 10 mL/min
<b>Purification method</b>	24 h dialysis against PBS
<b>Final volume</b>	1 mL
<b>Head/cut volume</b>	300 $\mu$ L
<b>Priming</b>	No Priming

## 2.2.5 *In Vitro* mRNA Expression

To determine the transfection efficiency of Fluc-mRNA LNPs, an *in vitro* luciferase assay system was employed using HEK293 cells. In a 96-well clear bottom white plate, 10,000 cells/100  $\mu$ L were seeded and grown to confluence. The confluent cells were treated with LNPs containing mRNA at concentrations of 0.25 to 2  $\mu$ g/mL, prepared in MEM media, and incubated for 24 hours. The following day, ONE-Glo luciferase reagent (100  $\mu$ L) was added to the cells, appropriately mixed, and allowed to stand for 3 minutes to ensure complete cell lysis before measuring luminescence using a microplate reader (Promega, Glo Max Discover Microplate reader).

### 2.2.5.1 *In Vitro* mRNA Expression Optimisation

To optimise the mRNA expression assay, mRNA expression was performed on three different days. Cells were seeded in three different 96-well plates (black, white, and clear plates with clear bottoms) to optimise this plate reader-based assay and choose the most suitable plate. Firefly Luciferase mRNA (5-

moUTP) was encapsulated into GenVoy-ILM™ by Precision NanoSystems (Vancouver, BC, Canada) by using the NanoAssemblr platform purchased from the same company. GenVoy-ILM™ is a commercially available proprietary lipid mix composition comprising DSPC: cholesterol: ionisable lipid: stabiliser at 10:37.5:50:2.5 mol% for encapsulating nucleic acids. At the NanoAssemblr, FRR was set at 3:1 and TFR at 12 mL/min as suggested by the manufacturer. The particles were purified via spin column against PBS until the solution was re-concentrated to the original volume. An Acrodisc® filter (0.2 µm pore size) was used to sterile-filter the concentrated LNPs-mRNA sample.

## 2.2.6 Characterization of LNPs

### 2.2.6.1 Characterization of Particle Size and Zeta Potential

The particle size (Z-average diameter), polydispersity index (PDI) and zeta potential (ZP) were measured by dynamic light scattering (DLS) using a Zetasizer Nano ZS (Malvern P analytical Ltd., Worcestershire, UK) equipped with a 4-mW 633 nm He-Ne laser and a detection angle of 173°. The measurement of particle size and polydispersity was carried out at 25 °C in the external buffer (1:10 dilution) with an attenuation value between 6 and 9. Zeta potential was measured in water (1:10 dilution) using a disposable folded capillary zeta cell. All measurements were undertaken in triplicate.

### 2.2.6.2 RNA Quantification

The Quant-iT Ribo Green RNA assay was performed to calculate the encapsulated nucleic acid according to the manufacturer's protocol. The samples were diluted to about 750 ng/mL final nucleic acid concentration in TE buffer in the presence or absence of 2 % Triton X-100 buffer, and the plate was incubated for 15 minutes at 37 °C to allow the Triton X-100 to break open the LNPs. 100 µL of the diluted fluorescent dye was added to the wells, and the fluorescence (resulting from the dye quantitatively binding free nucleic acid) was measured using either POLARstar Omega (BMG Labtech) or Glo Max Discover Microplate reader (Promega Corporation, Madison, WI) at 485 nm excitation and 525 nm emission wavelength. A 200-fold dilution of the RiboGreen reagent was used in Triton X-containing wells, where the RNA content is expected to be high. A 500-fold dilution was used in the TE-containing wells, where the RNA content is expected to be low. This method aims to minimise background noise in wells with low responses. The encapsulation efficiency was calculated using the following equation.

$$\text{Encapsulation efficiency (EE\%)} = \frac{\text{Total mRNA} - \text{Unencapsulated mRNA}}{\text{Total mRNA}} \times 100$$

The total mRNA concentration was based on results from triton (+), and the unencapsulated mRNA was based on results from triton (-) standard curves, respectively. The mass balance (or recovery) was calculated as follows:

$$\text{Mass balance (MB\%)} = \frac{\text{Total mRNA}}{\text{Theoretical mRNA concentration}} \times 100$$

### 2.2.7 Statistical Analysis

Unless stated otherwise, the results were calculated as mean  $\pm$  standard deviation (SD). For comparison, one-way or two-way ANOVA followed by Tukey post hoc analysis was performed, and significance was acknowledged for p values less than 0.05. All the calculations were made using GraphPad Prism 10.2.1.

## 2.3 Results

### 2.3.1 LNPs Microfluidic Manufacturing Considerations

LNPs were manufactured using the NanoAssemblr platform (from Precision NanoSystems Inc., Vancouver, BC, Canada). Unless otherwise stated, LNPs were made of DSPC, cholesterol, SM-102 and DMG-PEG 2000 at an initial concentration of 5 mg/mL and polyA was the payload of choice. After manufacturing, LNPs were purified via a spin column (100 kDa MWCO) against PBS. Some key manufacturing parameters for the LNP manufacturing were tested to check their effects on the LNP formulation. These included the selection of the lipid solvent used to dissolve the individual lipids, the RNA solvent for payload dilution, the TFR and FRR settings on the NanoAssemblr, and the choice of final solvent.

#### 2.3.1.1 Lipid Solvent Selection

The role of the organic solvent was investigated by dissolving the lipids in ethanol, methanol, or isopropanol (IPA). Figure 2.4A demonstrates the impact of solvent selection on LNP size, with an increase in size of around 30 nm when switching from ethanol to methanol and around 50 nm when using IPA, with the results being significantly different between ethanol and IPA ( $p < 0.05$ ). However, the PDI was not affected (remaining around 0.1; Figure 2.4A), nor was the zeta potential, which remained near neutral (Figure 2.4B). Similarly, the choice of solvent did not affect the encapsulation and mass balance, with EE% being high across all three LNP formulations (Table 2.6).

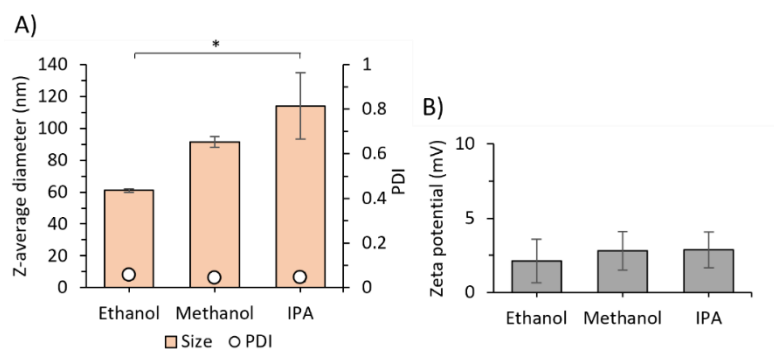


**Figure 2.4** Effect of organic solvent selection on LNPs manufactured using microfluidics. A) Size and PDI results; B) Zeta potential results. Results are expressed as mean  $\pm$  SD from 3 independent batches. Statistical significance was calculated:  $p < 0.05$  (\*).

**Table 2.6** Encapsulation efficiency (EE%) and mass balance (MB%) values for LNPs manufactured dissolving the lipids in ethanol, methanol or IPA. Results are expressed as the mean  $\pm$  SD,  $n = 3$

Lipid solvent	EE%	MB%
Ethanol	99 $\pm$ 1	79 $\pm$ 4
Methanol	100 $\pm$ 0.1	73 $\pm$ 29
IPA	99 $\pm$ 0.1	67 $\pm$ 11

### 2.3.1.2 RNA Solvent Selection

To explore the impact of aqueous phase concentration, the molarity of the citrate buffer was varied from 10 to 300 mM. The FRR was set at 15 mL/min, and TFR was set at 3:1. The initial lipid concentration was 6 mg/mL. The results in Figure 2.5A and B show that as the citrate buffer concentration increases from 10 mM to 75 mM, there is no significant impact on particle size or PDI. However, further increases in the concentration results in an increase in the size and PDI, peaking at 200 mM (174  $\pm$  30 nm size and PDI 0.65  $\pm$  0.22; Figure 2.5A and B). However, interestingly at 300 mM citrate, both the size and PDI drop again to within acceptable ranges (97  $\pm$  3 nm size and PDI 0.17  $\pm$  0.02; Figure 2.5A and B). In contrast to these changes in size and PDI, the zeta potential remained neutral at all conditions (Figure 2.5C). Similarly, the encapsulation efficacy of LNPs was generally not affected by the choice of buffer (Table 2.7) and it was approximately 100% under all conditions except for LNPs made with 200 mM citrate, which exhibited an encapsulation efficiency of 88  $\pm$  6%. Mass balance was above 80% for all LNPs except those made with 300 mM and 200 mM citrate, which showed 67  $\pm$  7% and 77  $\pm$  13%, respectively (Table 2.7).

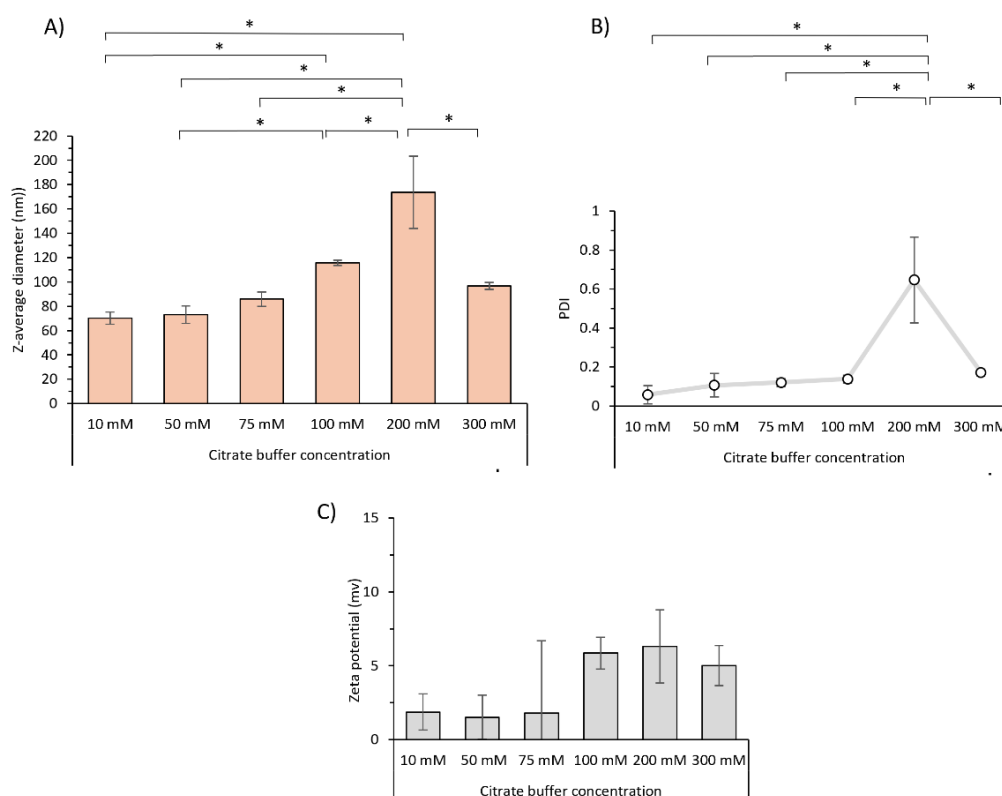


**Figure 2.5** Effect of increasing citrate buffer concentration. Size (A), PDI (B) and zeta potential (C) were measured. Results are expressed as mean  $\pm$  SD from 3 independent batches. Statistical significance was calculated:  $p < 0.05$  (\*).

**Table 2.7** Encapsulation efficiency (EE%) and mass balance (MB%) values for LNPs manufactured at increasing citrate concentrations. Results are expressed as the mean  $\pm$  SD,  $n = 3$ .

Citrate molarity	EE%	MB%
10 mM	100 $\pm$ 0.3	92 $\pm$ 4
50 mM	100 $\pm$ 0.1	86 $\pm$ 5
75 mM	100 $\pm$ 0.1	87 $\pm$ 5
100 mM	100 $\pm$ 0.1	90 $\pm$ 13
200 mM	88 $\pm$ 6	77 $\pm$ 13
300 mM	99 $\pm$ 1	67 $\pm$ 6

### 2.3.1.3 Focus on the Effect of TFR and FRR on LNP Microfluidic Manufacturing

To further assess the impact of process mixing and flow rate, different TFR and FRR combinations were tested to find the best TFR/FRR combination. The FRR of the solvent/aqueous phases varied from 2:1 to 5:1, with different speeds (5 mL/min, 10 mL/min, 15 mL/min, and 20 mL/min) tested (Figure 2.6). Instead of SM-102, the cationic lipid DOTAP was used in the formulation, and the initial lipid concentration was 10 mg/mL. After manufacturing, the solvent was removed by dialysis against PBS using a 14000 Da dialysis membrane.

At a flow rate of 5 mL/min, significantly ( $p < 0.05$ ) higher size and polydispersity values were observed at 2:1 and 3:1 ratios compared to the 10 mL/min, 15 mL/min, and 20 mL/min conditions ( $71 \pm 2$  nm at 2:1 ratio and  $65 \pm 2$  nm at 3:1 ratio; Figure 2.6A and B). LNPs produced at a flow rate of 5 mL/min and 5:1 ratio resulted in a size of  $68 \pm 8$  nm, approximately 10 nm bigger than the LNPs manufactured at higher speeds, even if results were not significantly different (Figure 2.6C). Conversely, generally, there were no significant differences in size or polydispersity between the 2:1, 3:1, and 5:1 ratios at the flow rates of 5 mL/min, 10 mL/min, 15 mL/min, and 20 mL/min, with all sizes being around 60 nm and  $PDI \leq 0.2$  (Figure 2.6A, B and C). Zeta potential remained neutral at all conditions (Figure 2.6D, E and F). In terms of RiboGreen assay results (Table 2.8) the 3:1 and 5:1 combinations consistently demonstrated the best outcomes at all speeds.

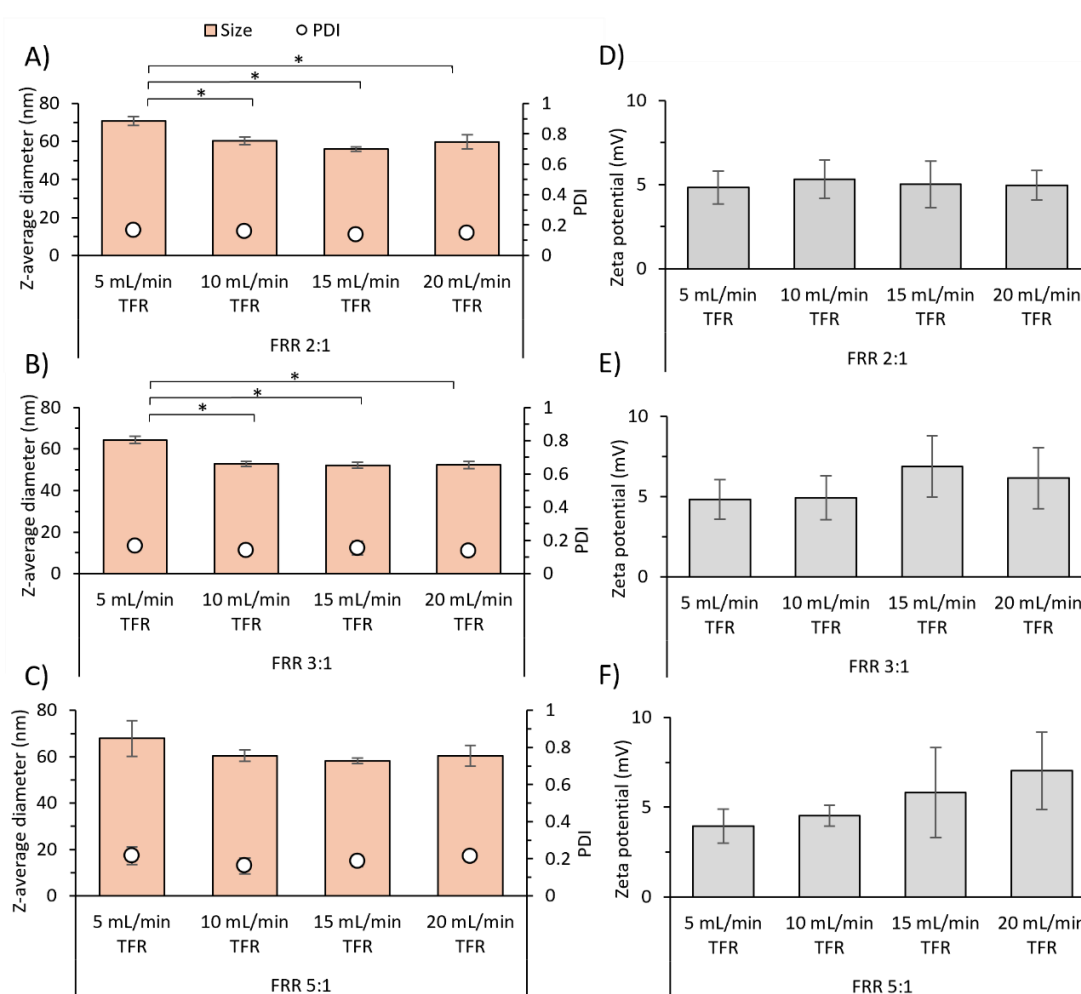


**Figure 2.6** Effect of different TFR/FRR combinations. The flow rate proportion of solvent to aqueous phases varied from 2:1 (A and D) to 3:1 (B and E) and 5:1 (C and F), with multiple speeds (5 mL/min, 10 mL/min, 15 mL/min, and 20 mL/min) examined. Data are expressed by mean  $\pm$  SD ( $n=3$ ) and statistical analysis was performed ( $*p < 0.05$ ).

**Table 2.8** Encapsulation efficiency (EE%) and mass balance (MB%) of the TFR/FRR combinations tested. Results are expressed as the mean  $\pm$  SD, n = 3.

	FRR	EE%	MB%
5 mL/min TFR	2:1	100 $\pm$ 1	69 $\pm$ 12
	3:1	100 $\pm$ 1	72 $\pm$ 4
	5:1	99 $\pm$ 1	82 $\pm$ 3
10 mL/min TFR	2:1	99 $\pm$ 1	69 $\pm$ 4
	3:1	99 $\pm$ 1	76 $\pm$ 5
	5:1	99 $\pm$ 1	84 $\pm$ 6
15 mL/min TFR	2:1	99 $\pm$ 0.4	67 $\pm$ 8
	3:1	99 $\pm$ 0.2	80 $\pm$ 8
	5:1	99 $\pm$ 0.2	81 $\pm$ 5
20 mL/min TFR	2:1	99 $\pm$ 0.05	76 $\pm$ 8
	3:1	99 $\pm$ 0.03	80 $\pm$ 10
	5:1	99 $\pm$ 0.3	86 $\pm$ 1

#### 2.3.1.4 Final Buffer Selection

The final external buffer was the last parameter examined. The final buffer selection can be chosen based on typical aqueous buffers used for LNPs, and the final choice depends mainly on the storage conditions of the LNP. The most used buffers are PBS and Tris (usually mixed with suitable cryoprotectant); hence, after LNP manufacturing, citrate buffer was exchanged for PBS and Tris via a spin column. No significant differences were noted with the LNP physicochemical characteristics when using PBS or Tris (Figure 2.7A and B). However, when sucrose was added to Tris buffer, the final LNP size was more variable between batches (Figure 2.7A). Low PDI (Figure 2.7A), neutral zeta potential results (Figure 2.7B) and high EE% (Table 2.9) were observed independently of the buffer chosen.

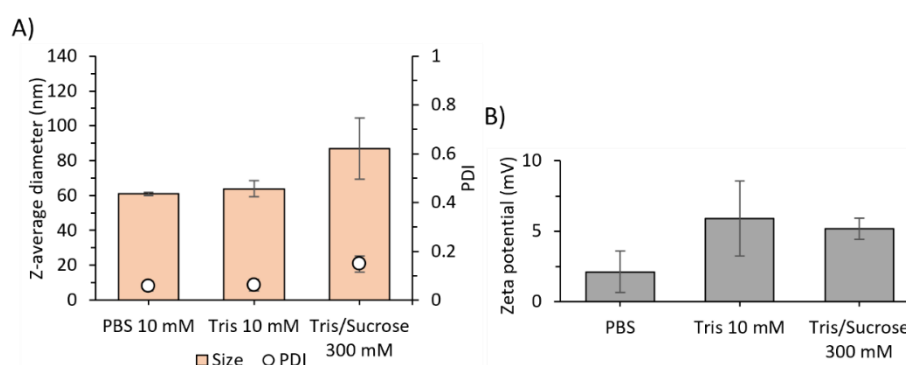


**Figure 2.7** Impact of the final buffer selection on LNP manufactured using microfluidics. Size, PDI (A) and zeta potential (B) were measured. Results are expressed as mean  $\pm$  SD from 3 independent batches. Statistical significance was calculated:  $p < 0.05$  (\*).

**Table 2.9** Encapsulation efficiency (EE%) and mass balance (MB%) of the LNPs in the final buffer. Results are expressed as the mean  $\pm$  SD, n = 3.

Final buffer	EE%	MB%
PBS 10 mM	99 $\pm$ 1	79 $\pm$ 4
Tris 10 mM	99 $\pm$ 1	79 $\pm$ 16
Tris/sucrose 300 mM	96 $\pm$ 3	62 $\pm$ 7

### 2.3.2 Scalable Process for Preclinical Development

The experiments outlined in the previous sections identified the most effective microfluidic parameters for producing LNPs. With these parameters established, LNPs were produced using various Precision NanoSystems instruments, including the Spark, the Ignite, the Blaze, and the NanoAssemblr. The microfluidic parameters for these instruments are detailed in Table 2.3. Each instrument was used to produce different volumes of LNPs—120  $\mu$ L with the Spark, 1 mL with the Ignite and the NanoAssemblr, and 10 mL with the Blaze. To assess the performance of the LNPs, firefly Luciferase mRNA (5-moUTP) was used as the payload instead of polyA, which enabled the mRNA expression study described in section 2.3.2.1. The final mRNA concentration across all LNPs was 57  $\mu$ g/mL.

The results, as shown in Table 2.10, were consistent with earlier research. Specifically, the size and polydispersity index (PDI) values of the LNPs after spin column purification were comparable across the instruments, with sizes consistently below 100 nm and PDIs < 0.2. The only statistically significant ( $p < 0.05$ ) differences were from LNPs produced using the Spark, as size and zeta potential values were statistically larger than those obtained from the Ignite and NanoAssemblr (Table 2.10). However, the LNPs manufactured using the Spark were not purified due to the low volume; they were diluted five-fold in PBS to dilute the ethanol. The Ribogreen assay results fell within the expected range, further validating the effectiveness of the microfluidic parameters used in the experiments.

**Table 2.10** LNPs characteristics manufactured by the Spark, Ignite, the NanoAssemblr and the Blaze. The results are expressed as mean  $\pm$  SD from 3 independent batches, except for the mRNA-LNPs produced at Blaze, which were produced only once due to the high volume of mRNA required.

	The Spark	The Ignite	The NanoAssemblr	The Blaze
<b>Z-Average diameter (nm)</b>	106.3 $\pm$ 3	74.6 $\pm$ 2	72.4 $\pm$ 3	73.2 $\pm$ 1
<b>PDI</b>	0.15 $\pm$ 0.03	0.05 $\pm$ 0.02	0.04 $\pm$ 0.02	0.05 $\pm$ 0.02
<b>Zeta potential (mV)</b>	10.88 $\pm$ 2	-4.39 $\pm$ 2	-7.12 $\pm$ 3	-5.65 $\pm$ 1
<b>EE (%)</b>	93 $\pm$ 2	88 $\pm$ 4	86 $\pm$ 7	88
<b>MB (%)</b>	103 $\pm$ 6	86 $\pm$ 7	84 $\pm$ 17	84

### 2.3.2.1 mRNA Expression

The LNPs manufactured in 2.3.2 were tested in HEK293 cells to evaluate mRNA expression. LNPs produced using the Spark, the Ignite and the NanoAssemblr were transferred to cells, and luminescence was read 24 h after LNP addition. The results (Figure 2.8A) showed a dose-response curve, with cells treated with LNPs at 2 mg/mL expressing higher luminescence values than cells treated with LNPs at 1 mg/mL, and so on. Higher fluorescence results were achieved by LNPs manufactured using the Ignite and the NanoAssemblr, while the results obtained from the LNPs produced using the Spark were comparably lower ( $p < 0.05$ ) (Figure 2.8A). LNPs produced on the Blaze were also tested at the same time; due to the larger volume required to manufacture samples using the Blaze (10 mL and the subsequent cost constraints), LNPs were only produced once ( $n=1$ ), and the mRNA expression results represent the average of three cell culture studies from the same LNP batch (Figure 2.8B).

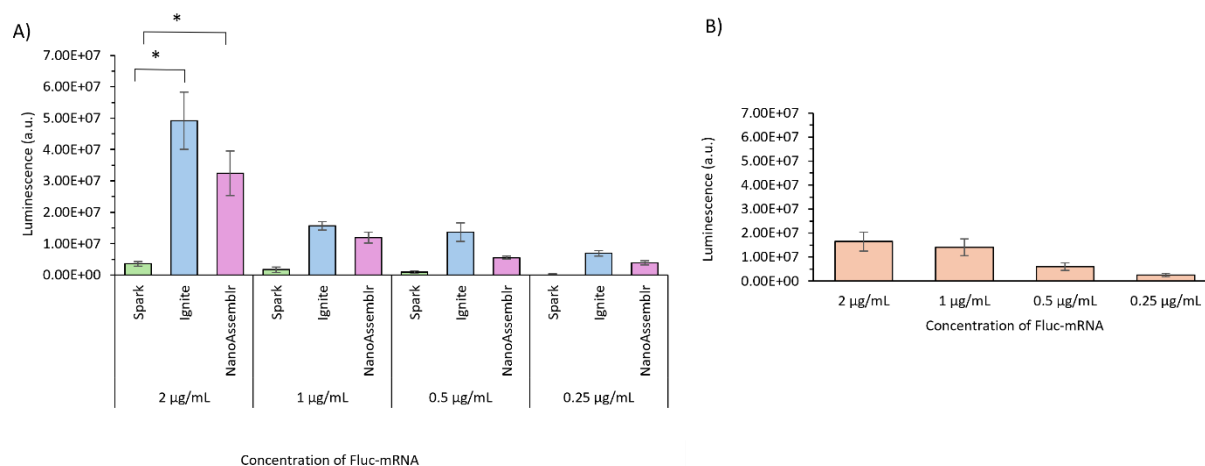


**Figure 2.8** *In vitro* expression of Fluc-mRNA LNPs. Confluent HeLa cells were treated with LNPs having mRNA doses in the concentrations of 2 µg/mL, 1 µg/mL, 0.5 µg/mL, and 0.25 µg/mL. The plate was incubated at 37°C for 24 hours. a) Results represent mean  $\pm$  SEM of 3 independent batches produced at the Spark, the Ignite and the NanoAssemblr. Statistical analysis was conducted, and the results were considered significant with a  $p$ -value of less than 0.05 (\*). b) Cell work results for the LNPs manufactured using the Blaze. Data represent the average of three different cell-based assays performed in different days using the same LNP batch.

#### 2.3.2.1.1 *In Vitro* Assay Optimisation

To further optimise the *in vitro* assay, Firefly Luciferase mRNA (5-moUTP) was encapsulated into a standard LNP formulation (GenVoy-ILM™ by Precision Nanosystems). Black, clear and white plates (with clear bottoms) were used to perform mRNA expression. The physicochemical characteristics of the LNPs are detailed in Table 2.11, and the mRNA transfection results are shown in Figure 2.9. The results in Figure 2.9 showed that mRNA expression values were higher when using the clear or white

plates (Figure 2.9B and C) rather than the black ones (Figure 2.9A); therefore, for further studies, white plates were used.

**Table 2.11** GenVoy-LNPs physicochemical characteristics. Results represent mean  $\pm$  SD of 3 independent batches.

LNPs physicochemical characteristics	
Z-average diameter (nm)	92 $\pm$ 9
PDI	0.12 $\pm$ 0.2
Zeta potential (mV)	4.85 $\pm$ 2
EE (%)	98 $\pm$ 1
MB (%)	112 $\pm$ 16

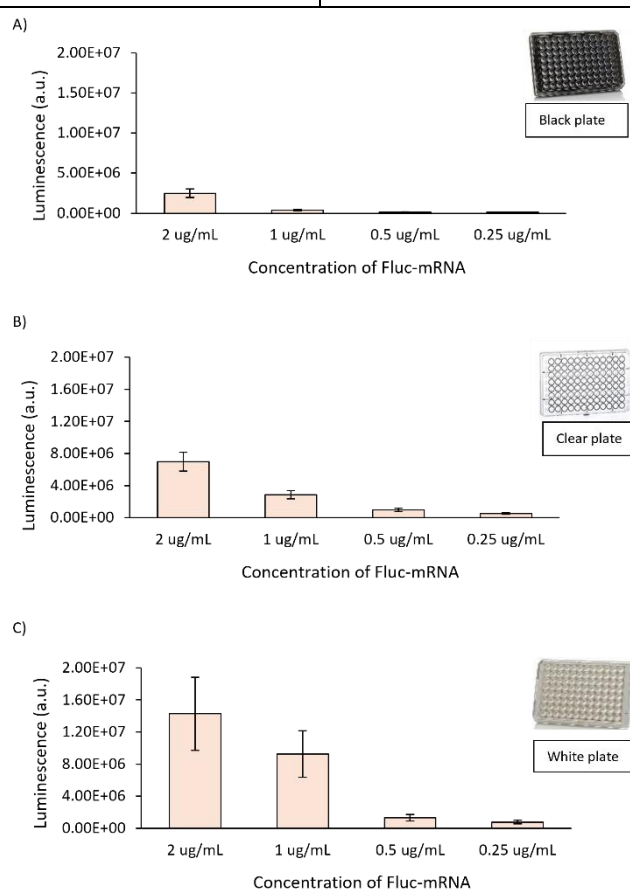


**Figure 2.9** mRNA expression on HEK293 cells in three different days and in different types of plates. A) mRNA expression performed in black plates. B) mRNA expression performed in clear plates. C) mRNA expression performed in white plates. GenVoy-LNPs encapsulating Fluc-mRNA were transferred to cells, and luminescence was read after 24 h hour incubation at 37°C and 5 % CO<sub>2</sub>. Results represent mean  $\pm$  SEM of 3 independent batches.

### 2.3.3 Manufacturing Parameters Optimisation Using Alternative Microfluidic Systems

LNPs were formulated using the Dolomite ANP platform (Dolomite Microfluidics, Royston, Hertfordshire, UK). As stated in section 2.1, LNP microfluidic production can vary depending on the manufacturing processes used, such as the TFR and the FRR. In relation to the Dolomite, the head and tail cut volumes are also important factors to consider, as well as the priming step. For optimisation of

the process and experimental conditions, LNPs made of DOTAP and SM-102 were produced at a millilitre scale, and results are shown in Figure 2.10A and Figure 2.10B, respectively. Results demonstrate that both the start/end cut volumes and the priming step can affect the results, as SM-102 LNPs produced after priming the microfluidic chip with the internal buffer (citrate buffer, pH 4) and setting the start/end cut volumes at 300  $\mu$ L, showed better results in terms of Z-average diameter (approx. 67 nm), PDI (consistently <0.2) and mass balance (>90%) across all the speed tested (Figure 2.10B). Therefore, the start/end cut volumes were set at 300  $\mu$ L for further studies. Regarding the priming step, even if it led to better results (Figure 2.10B), it also caused the chip to block, probably due to the crystallisation of the citrate inside the micro channels. For this reason, for further studies, the chip was not primed prior use.

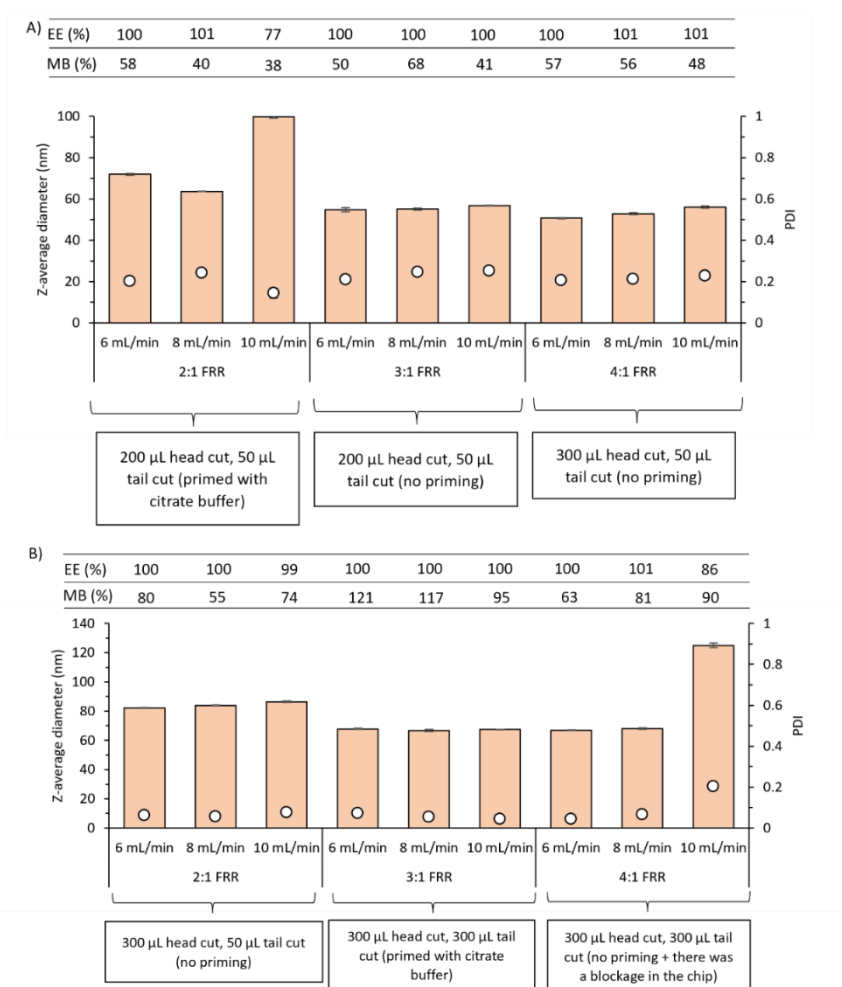


**Figure 2.10** Impact of TFR, FRR, head and tail cut volumes, and the priming step on LNP manufacture using the Dolomite ANP platform. LNPs were made with 50% mol of DOTAP (A) and SM-102 (B).

LNPs were produced again two times at the conditions described at Table 2.4 (DOTAP-LNPs) and Table 2.5 (SM-102-LNPs) to better understand the impact of the TFR (which was increased from 6 mL/min to

8 mL/min and 10 mL/min) and the FRR (which was varied from 2:1 to 3:1 and 4:1). Results for DOTAP-LNPs were shown in Figure 2.11A. LNPs were below 100 nm in size at all the FRR and TFR tested, while PDI was slightly higher than expected, between 0.2 and 0.24. Mass balance was around 60 % at the conditions tested, but due to the cationic nature of DOTAP, it is more likely that the Triton-X used in the Ribogreen assay didn't break the LNPs efficiently, leading to a lower fluorescent signal in the wells. In general, no significant differences were noticed at the different FRRs and TFRs considered. Results for SM-102-LNPs are shown in Figure 2.11B. The sizes of the SM-102-LNPs were between 65 nm and 90 nm, higher than those of the DOTAP-LNPs, even though always below 100 nm. The PDI values were lower than those obtained from the DOTAP-LNP runs and always below 0.2 (between 0.06 and 0.16, Figure 2.11B). Mass balance varied depending on the ratio and the speed considered, in the range of 60 to 96 % (Figure 2.11B).

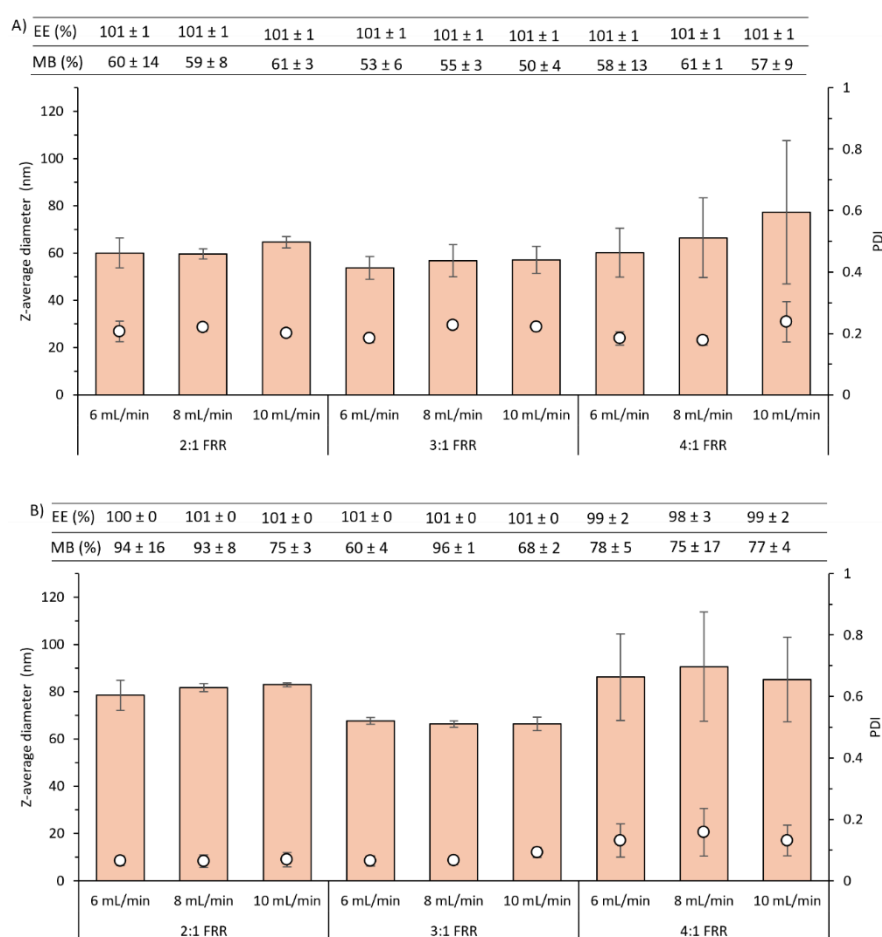


**Figure 2.11** Production of LNPs using the Dolomite ANP platform. A) DOTAP LNPs results. The X-Junction chip (100  $\mu$ m) was used, and samples were dialysed for 1 h against PBS. B) SM-102 LNP results. The same chip was used to produce the LNPs, and samples were dialysed for 24 h against PBS to ensure complete buffer exchange.

## 2.4 Discussion

Nanomedicine-based therapeutics (including RNA-based vaccines) are now recognised as playing a key role in national and global healthcare. Especially after the COVID-19 outbreak, RNA-based vaccines have played a decisive role in the fight against SARS-CoV-2 (191–193), and the general interest in this topic has increased. In this scenario, LNPs protect the mRNA from degradation, promote cell uptake and deliver the RNA inside the cytosol. Microfluidics is a well-established method of producing LNPs. However, a lack of detailed understanding of their manufacture remains, especially regarding reproducibility in scale-independent manufacturing. As detailed in Table 2.1, a range of CQAs are associated with mRNA-LNP characterization. This includes particle size, PDI, zeta potential, encapsulation efficacy (EE%), mRNA and lipid recovery when considering the drug product specifications. LNPs should generally be below 100 nm with a PDI of <0.2, near-neutral zeta potential, high encapsulation efficiency, and mRNA recovery (or mass balance). In this chapter, CPPs that drive the CQA of LNPs during microfluidic manufacturing have been evaluated.

### *The solvent composition pre-formation (organic and aqueous)*

Microfluidics is based on mixing two fluid streams: the organic phase containing the lipids and the aqueous phase in which the RNA is dissolved. For this reason, the choice of both solvents (organic and aqueous) can impact the LNP formation. In this chapter, the effect of three organic solvents (methanol, ethanol and IPA) was evaluated. In terms of polarity, methanol>ethanol>IPA (Figure 2.12); with increasing carbon chain length, the polarity decreases as the polar group (-OH) becomes a smaller component relative to the molecule.

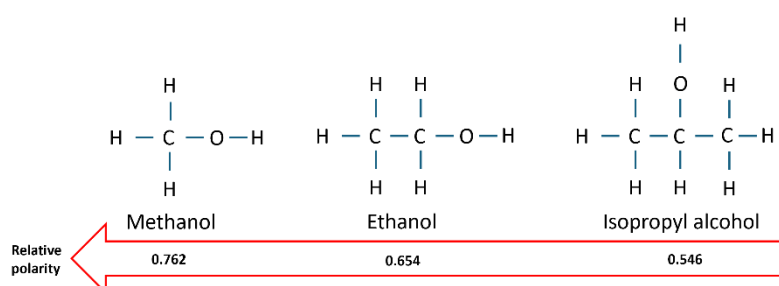


**Figure 2.12** Relative polarities and chemical structures of methanol, ethanol and isopropyl alcohol.

In 2010, Zook et al. (194) hypothesised that liposomes form in the microfluidic chip because, following the mixing of the aqueous and organic buffers, the polarity of the organic solvent increases, rendering the lipids less soluble, hence promoting their self-assembly into lipid bilayers. Results shown in Figure

2.4A demonstrate that when switching from ethanol to IPA, LNPs significantly increased in size by around 50 nm ( $p < 0.05$ ) (from approx. 60 nm to 110 nm). This might be due to the fact that, when decreasing the solvent polarity (ethanol to IPA), the shift in polarity that follows the mixing of the alcohol with water is slower. This causes lipid structures to form larger intermediate particles, resulting in bigger LNPs. However, in contrast, making the LNPs with methanol rather than ethanol as the initial solvent also increased the particle size from approximately 60 to 90 nm (Figure 2.4A). This suggests that polarity may not only be the driving factor in LNP formation and lipid solubility may also be a factor. Despite the impact on particle size, solvent choice did not impact other measured characteristics (PDI, zeta potential and encapsulation efficacy; Figure 2.4A-B and Table 2.6). Therefore, these results demonstrate that the choice of solvent adopted in manufacturing should be considered from a manufacturing perspective (with ethanol being a class 3 solvent (19)) and a drug product characteristics consideration.

Regarding the aqueous solvent used to dissolve the RNA, citrate buffer pH 4 was chosen to conduct all the experiments as this buffer is commonly used to prepare mRNA-LNPs because it reduces RNA hydrolysis due to the chelating effect of sodium citrate (87). A good example was given by Cheng et al., who demonstrated that LNPs manufactured in sodium citrate buffer (pH 4) displayed enhanced transfection efficiency on cells compared to LNPs produced in sodium acetate buffer at the same pH (195). The literature typically recommends using an aqueous buffer at 100 mM or less and pH 4 or 3 (Table 2.12). Choosing a low pH is important as, at low pH, the ionisable cationic lipid is protonated and can electrostatically interact with the negatively charged RNA, thus driving vesicle formation. To allow proper protonation, LNPs are commonly produced at a pH lower than the apparent pKa value of the ionisable lipids, which is typically around 6.5 (e.g. SM-102 pKa is 6.68) (196). In this chapter, citrate pH was kept constant at 4, but its concentration was varied from 10 to 300 mM, and results showed that increasing the molarity from 75 mM to 200 mM caused an increase in particle size and PDI (Figure 2.5A and B), while zeta potential remained neutral (Figure 2.5C). The increase in size might be due to the salting-out effect (197); when the ionic strength of the solution increases, the electrostatic repulsion between the LNPs is shielded, and LNPs can aggregate more. A good example was provided by Nakamura et al. in 2022 (197). In their study, the authors focused on the effect that salt concentration (ionic strength) in an acidic aqueous buffer has on the formation of LNPs. Their results showed that the mean particle diameters gradually increased in a NaCl concentration-dependent manner. Okuda et al. provided another good example; the authors demonstrated that the addition of salt (NaCl) to the aqueous buffer containing nucleic acids led to the synthesis of large LNPs (>200 nm), proving that the simple addition of salt is an easy and promising strategy to regulate the size of the

nanoparticles. However, the results in Figure 2.5A and B also showed that when further increasing citrate concentration to 300 mM, the size and PDI of the LNPs reached more typical values (below 100 nm and 0.2, respectively). Despite these changes in particle size, there was no effect on polyA encapsulation, except for LNPs made with high citrate concentrations (200 mM and 300 mM), which exhibited a lower encapsulation efficiency (Table 2.7). These findings were also supported by the work of Binici, Borah et al.; the authors compared the *in vitro* and *in vivo* activity of LNPs manufactured using citrate at increasing concentrations of 50 mM, 100 mM, and 300 mM. Their results demonstrated that higher citrate molarity (300 mM) produces LNPs with lower *in vitro* transfection efficiency compared to LNPs manufactured with citrate at 50 mM and 100 mM. This trend was also observed *in vivo*, where lower expression was noted for the 300 mM formulation compared to the 50 mM and 100 mM formulations. These results, combined with the cryo-TEM images showing increased bleb dissociation from the lipid particles when LNPs are prepared with a 300 mM citrate buffer, suggest that citrate buffer concentration may influence lipid packing during the production of LNPs (130).

**Table 2.12** List of LNP papers with the internal buffers used, along with the corresponding LNP formulations, buffer molarity, and pH. The \* symbol next to a lipid indicates its specific type, which is listed immediately below.

LNPs formulation components	pH and buffer used	Source
DLin-MC3-DMA, cholesterol, DSPC, PEG* *PEG-C14, PEG-C16 and PEG-C18	10 mM citrate buffer, pH 4	(198)
Ionisable lipid*, cholesterol, DSPC, DMPE-PEG2000 *DLin-MC3-DMA or DLin-DMA	50 mM citrate buffer, pH 3	(199)
Ionisable lipid*, cholesterol, DOPE, C14-PEG2000 *Different ionisable lipids were synthesised modifying the backbone structure of Dlin-MC3-DMA	10 mM citrate buffer, pH 3.5	(200)
DODMA or DLin-MC3-DMA, cholesterol, DOPE or DOPC, C16-PEG2000-Ceramide or pSar	100 mM citrate buffer, pH 5.4	(201)
cationic lipid*, DOPE, DMG-PEG2000 or cationic lipid/ionisable lipid*, cholesterol, DSPC, DMG-PEG2000 *DDA or DOTAP or DMTAP or DSTAP or DOBAQ	100 mM citrate buffer, pH 6	(202)
D-Lin-MC3-DMA, cholesterol, DSPC, PEG	50 mM citrate buffer, pH 4	(203)
Ionisable lipid*, cholesterol, DSPC, PEG * DLin-MC3-DMA and novel lipids	50 mM citrate buffer, pH 4 or 25 mM sodium acetate buffer, pH 5	(204)
Ionisable lipid*, cholesterol, DSPC, PEG * Various ionisable lipids were synthesised	6.25 mM sodium acetate buffer, pH 5	(205)
Ionisable lipid*, cholesterol, DOPE, C14-PEG2000 * Various ionisable lipids were synthesised	10 mM citrate buffer, pH 3	(206)

### *The mixing parameters (TFR and FRR)*

The influence of TFR on lipid-based delivery systems has been extensively described (e.g. (87,139,183)). Results in Figure 2.6 demonstrated that LNPs produced at speeds between 10 mL/min and 20 mL/min had similar characteristics. However, at lower speeds (5 mL/min), LNP sizes increased significantly ( $p < 0.05$ ) (Figure 2.6A-C). As hypothesised by Roces et al., this might be due to the fact that, at lower speeds, the slower dilution of the solvent enhances the formation of bigger particles (87). PDI and zeta potential, on the contrary, were unaffected (Figure 2.6A-F).

The impact of the FRR was also evaluated in this chapter. In general, as a result of increasing the FRR, particles tend to be smaller, and this might be because at the high proportion of aqueous buffer to ethanol, the ethanol (which contains the lipids) is diluted faster, and lipids have less opportunity to aggregate resulting in the formation of smaller particles (207). In 2024, McMillan et al. evaluated how the phase ratio and corresponding size ranges impact on the *in vitro* and *in vivo* expression of LNPs. In their study, the authors compared 1.3: 1, 1.5: 1, 2: 1 and 3: 1 FRRs emphasizing how a small increase in the ratio (e.g. 1.3: 1 to 1.5: 1) can create a big impact on the outcome of the formulation (207). Conversely, the results shown in this chapter demonstrated that there were no significant differences in size or polydispersity between the 2:1, 3:1, and 4:1 ratios when keeping the speed constant, with all sizes being around 60 nm and  $PDI \leq 0.2$  (Figure 2.6A-C). Zeta potential remained neutral at all conditions (Figure 2.6D-F). In terms of RiboGreen assay results (Table 2.8) the 3:1 and 5:1 combinations consistently demonstrated the best outcomes at all speeds.

### *The solvent composition post-formation*

The choice of the external buffer was also explored. After manufacturing, LNPs undergo purification to eliminate impurities, reduce the organic solvent content (171) and raise the pH to 7.4. In fact, the pH of the formulation needs to be increased so that the ionisable cationic lipids can adopt a neutral form which allows the formation of bigger particles having a “solid oil core” (165). In this condition, the RNA payload likely migrates into the polar “bleb” structures of the LNPs as it dissociates from the neutral ionisable lipid (195). Generally, the most commonly used buffers are PBS and Tris, often mixed with a cryoprotectant (208). Results showed in this chapter indicated that the choice of external buffer can impact the final characteristics of LNPs and should be carefully considered when selecting the parameters to achieve the desired LNP properties. In particular, from Figure 2.7A, it can be noted that there were no significant differences in the final LNPs' characteristics when using PBS or Tris. However, when sucrose was added to Tris buffer, size and PDI were variable between batches. The choice of the external buffer and its implications on the formulation's outcome will be further explored in Chapter

4. In that chapter, the issue of increased particle size after buffer exchange in Tris/sucrose is addressed by adding the cryoprotectant after the buffer exchange, resulting in smaller particle sizes. Zeta potential remained neutral regardless of the buffer used (Figure 2.7B). High EE% (Table 2.9) were observed independently of the buffer chosen.

After assessing the most common interrogatives about microfluidic manufacturing, LNPs were produced using different microfluidic equipment. In addition to the NanoAssemblr, LNPs were produced using the Spark, the Ignite, and the Blaze by Precision NanoSystems to assess the reproducibility of the formulation across different equipment supplied with different mixers geometries. While the NanoAssemblr cartridge uses a SHM mixer, the Ignite, the Spark, and the Blaze cartridges are equipped with a TrM mixer. All the final mRNA-LNPs showed acceptable physicochemical characteristics, demonstrating that, on a small-scale, both geometries can lead to the formation of good vesicles (Table 2.10). These results were consistent with those obtained by Webb, Forbes et al., who prepared three liposome formulations (anionic, cationic, and neutral) using both types of microfluidic mixers on a bench scale. The authors demonstrated that, across all formulations tested, the key physicochemical attributes were consistent between the two types of microfluidic mixers, with no significant difference in size and PDI. (139). LNPs were also manufactured using an alternative microfluidic system (the Dolomite System by Dolomite Microfluidics) which uses an X-junction (or "+" junction) geometry chip for droplet generation. After an initial optimisation, the nanoparticles displayed physicochemical features within the range (Figure 2.10 and Figure 2.11). These results demonstrate that LNPs can be produced using a range of equipment, proving their adaptability and reinforcing the importance of these findings for scalable production.

In addition to the CQAs for mRNA-LNP product development, the product potency is a key factor, and cell-based assays generally evaluate this. In this chapter, mRNA-LNPs produced using different microfluidic devices were therefore transferred to HEK293 cells to measure their transfection potency (Figure 2.8). Fluc-mRNA was also encapsulated inside GenVoy-LNPs, a pre-optimised lipid mixture designed to encapsulate RNA proprietary to Precision NanoSystems, and, after 24 hours, luciferase activity was measured. The aim of this work had two objectives: demonstrating that mRNA expression is reproducible and optimising the process by selecting the best type of plate among black, clear, and white with clear bottoms. The primary difference between white and black plates is their reflective properties. Black plates absorb light and reduce background and crosstalk for fluorescent assays, whereas white plates reflect light and maximize the light output signal for luminescent assays. For this reason, typically, white plates are commonly used for fluorescent assays (209). This is consistent with

the results shown in Figure 2.8, which showed that mRNA expression values were higher when using clear or white plates compared to black plates, which yielded lower overall values (Figure 2.9).

Based on the results obtained in this chapter, the parameters that will be utilised in the subsequent chapters, unless otherwise stated, are summarised in Table 2.13.

**Table 2.13** Overview of the experimental parameters, as defined in this chapter, for use in the following chapters unless otherwise indicated.

Solvent selection (lipid)	Solvent selection (mRNA)	FRR (aq./org.)	TFR (mL/min)	Final buffer selection
Ethanol	Citrate 50 mM, pH 4	3:1	15	PBS

## 2.5 Conclusion

In the course of this chapter, some of CPPs of microfluidic manufacturing have been systematically assessed. Among these, the aqueous and organic solvent selection, the TFR, the FRR and the external buffer can impact the CQAs of the LNPs, and by modifying some of these factors, it is possible to control LNP characteristics. This study provides a novel and systematic characterization of multiple CPPs and their combined effects on LNP critical quality attributes. Such an integrated evaluation contributes new insights into the rational design and optimisation of microfluidic processes. Additionally, this study demonstrates, for the first time, a direct comparison of multiple microfluidic platforms for LNP manufacturing under standardised conditions, proving that LNPs can be formulated on various microfluidic devices equipped with different chip geometries. Among the LNPs CQAs there's also the *in vitro* potency. The reproducibility of the *in vitro* mRNA expression assay has been evaluated considering the inter-day variation and the choice of the most suitable plate for this assay. In conclusion, as it is the first step of LNP production, manufacturing is a crucial phase, and measures must be taken to ensure the formation of particles that are worth undergoing the next stages of production, which are purification and filtration (if needed).

## **Chapter 3**

# Simplification of the Downstream Process for LNPs

### 3.1 Introduction

The steps leading to the production of LNPs are 1) microfluidic mixing 2) purification and 3) filtration and each step needs to overcome some obstacles to reach optimal LNP parameters. Some of the bottlenecks referred to each step are described in Figure 3.1.

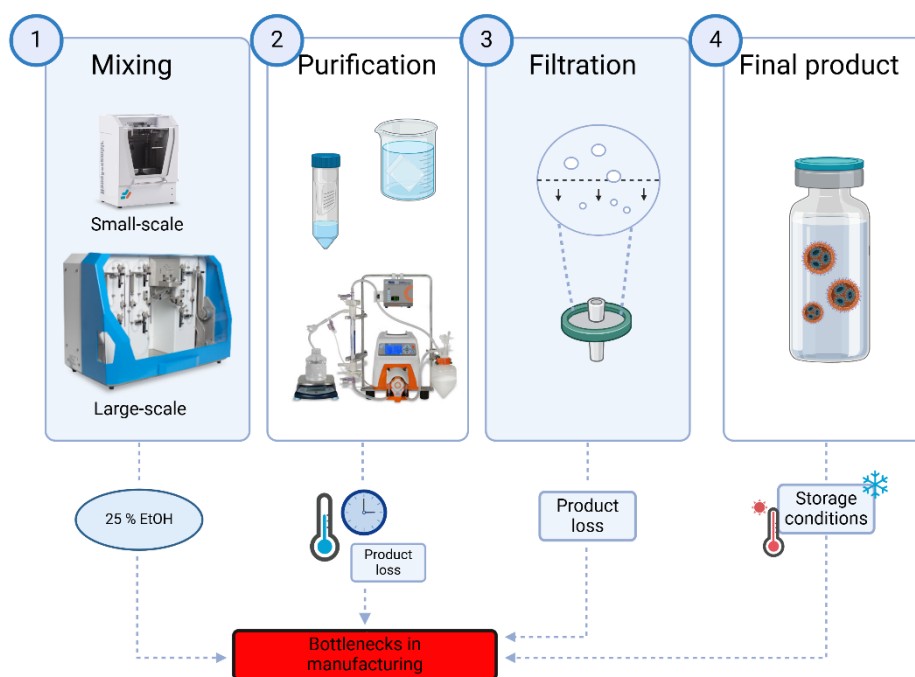


**Figure 3.1** Schematic of LNP manufacturing process. Some of the bottlenecks of each step are highlighted. Image created using Biorender.

LNP manufacturing by microfluidics results in particles containing the organic solvent in which the lipids were dissolved before mixing. The maximum allowable solvent concentration in pharmaceuticals is defined by the International Council for Harmonisation of Technical Requirements for Pharmaceuticals for Human Use (ICH) guidelines (171). These guidelines classify the solvents into three categories based on their possible risk to human health in (a) class 1 solvents (solvents to be avoided), (b) class 2 solvents (solvents to be limited, such as methanol), and (c) class 3 solvents (solvents with low toxic potential, including ethanol). As ethanol is defined as causing low risk to human health, it's often used for manufacturing pharmaceuticals (including liposomes and LNPs), and its maximum concentration limit is 5000 ppm. In consideration of this, decreasing the organic solvent concentration to authorised levels is crucial. Moreover, LNP purification is necessary for buffer exchange from the acidic buffer, which is typically used during manufacturing, with a more neutral physiological pH buffer (165).

Among the methods used to purify LNPs, spin column, dialysis and tangential flow filtration (TFF) are widely used (210,211). While spin column and dialysis are mostly used on a bench scale, TFF is often used by industries as the process can be scaled up owing to the availability of different column sizes and the different TFF devices on the market that allow the processing of high volumes. TFF is well documented in the literature (e.g., (150,212–214)) and is used in liposomes and LNP production to perform diafiltration for buffer exchange and to concentrate the sample if needed. When considering using TFF, it is important to evaluate some factors which are crucial for the good outcome of the formulation, such as the membrane pore size (MWCO), the membrane material, the feed flow rate (or speed), the transmembrane pressure (TMP), the number of diafiltration volumes, the exchange buffer type, and the temperature. Besides the many advantages of TFF, it also has some disadvantages. TFF can be time-consuming as 12 mL wash cycles are generally needed per 1 mL of formulation with external buffer added at the same speed as the permeate exits the column (212). Moreover, sometimes a loss of product (resulting in a lower recovery) is associated with using TFF, one of the causes being membrane fouling (213).

After manufacturing, besides the choice of the purification method, it is important to consider the impact of the temperature storage on LNP stability and the hold time before manufacturing and purification. While the impact of temperature on LNPs and similar drug delivery systems such as liposomes has been reported in literature (150,214,215), the impact of holding conditions for LNPs between manufacture and purification is less well understood.

### **3.1.1 Aim and Objectives**

The current chapter is focused on the purification and filtration step to assess the typical bottlenecks associated with these stages. To achieve this, the objectives were to:

- Develop protocols for LNP purification through different methods, including spin column, dialysis, and TFF, whose choice is generally based on the batch volume, thereby providing a practical framework for method selection.
- Evaluate and develop a TFF protocol to speed up and simplify the process on a bench scale.
- Investigate, for the first time in a systematic manner, the impact of hold time and temperature on LNPs between microfluidic manufacture and purification.
- Evaluate the impact of sterile filtration on LNPs, contributing to the understanding of how this critical step affects final product quality.

Collectively, these objectives represent a novel and comprehensive analysis of downstream processing conditions, integrating often-overlooked parameters such as post-manufacturing hold time and filtration impact. This chapter provides original insights into how these factors can be optimised to ensure the integrity and scalability of LNP production workflows.

## 3.2 Materials and Methods

### 3.2.1 Materials

Materials were purchased as described in Section 2.2.1. Additional materials specific to this chapter included MicroKros (500 kD MWCO, 20CM 500K MPES 0.5MM MLL X FLL 1/PK) and MidiKros hollow fibre filters (500 kD MWCO, 20CM 500K MPES 0.5MM FLL X FLL 1/PK) obtained from Spectrum Laboratories, Inc (UK). High-purity solvents dimethyl sulfoxide (DMSO,  $\geq 99.9\%$ ) and ethyl acetate ( $\geq 99.9\%$ ) were purchased from Sigma Aldrich (USA) while pH strips were obtained from Fisher Scientific (UK).

### 3.2.2 Preparation of LNPs

LNPs were produced using the NanoAssemblr benchtop (Precision NanoSystems Inc, Vancouver, Canada), as described in section 2.2.2. Briefly, the mixture of lipids in ethanol was combined with the aqueous phase via microfluidics and vesicles were collected in a 15 mL falcon tube. The total flow rate (TFR) for LNPs manufactured at the NanoAssemblr was set at 3:1 and the total flow rate (TFR) was fixed at 15 mL/min. The aqueous phase comprised polyA dissolved in citrate buffer 50 mM, pH 4. The organic phase was made of DLin-MC3 or SM-102, cholesterol, DSPC, DMG-PEG 2000 at a ratio of 50:38.5:10:1.5 mol %, respectively, and the starting lipid concentration was 5 mg/mL. The nitrogen/phosphate (N:P) ratio was 6:1 for all the formulations.

To scale up the purification process, LNPs were manufactured using the Blaze (Precision NanoSystems Inc, Vancouver, Canada) at a final volume of 100 mL using a classic cartridge (no dilution). The total waste volume was set at 1.3 mL. The total flow rate (TFR) was set at 18 mL/min, and the flow rate ratio (FRR) was set at 3:1. The sample bottle was positioned under the cartridge outlet, and the waste collection vessel was under the waste output.

#### 3.2.2.1 Hold Time Before Purification Study

For this investigation, LNPs consisting of DLin-MC3 (50% mol) were formulated at the NanoAssemblr. After manufacturing, the LNPs were separated into 3 aliquots: one was dialyzed against PBS for 1 h,

one was centrifuged using a spin column, and one was left unpurified. The samples were then stored at 4°C or room temperature (RT) in falcon tubes, and particle attributes were investigated over time (after 1, 2, 4, and 24 h).

### 3.2.3 LNP Purification Methods

After microfluidic manufacturing at the NanoAssemblr, LNPs were purified to eliminate the residual ethanol and to perform buffer exchange. The small-scale purification methods used in this chapter were dialysis, spin column, and tangential flow filtration (TFF –Spectrum® KrosFlo® Research 2i TFF System, Repligen Corporation, California, USA) (Table 3.1).

Dialysis was performed against 200 mL PBS pH 7.4 while spin column purification involved diluting samples 40 times in PBS and centrifuging at 4°C at 2000 g until the required volume was obtained. Details of these procedures are provided in section 2.2.3.

At the TFF, the effect of different filtration speeds (10 mL/min, 15 mL/min and 20 mL/min) was tested. After manufacturing of DLin-MC3 LNPs at the NanoAssemblr, LNPs were diluted 1:5 with the aqueous buffer used for manufacturing (citrate 50 mM, pH 4) to dilute the ethanol present in the sample and prevent it from entering the column. The sample was then purified using the TFF for 12 diafiltration volumes (or “washes”) utilising PBS as the external buffer. An aliquot of the LNPs was filtered using a 0.22 µm modified polyethersulfone (mPES) filter. After selecting the appropriate speed, to further evaluate the impact of the number of diafiltration volumes on the formulation outcome in terms of physiochemical characteristics as well as residual ethanol content, the number of TFF washes was decreased from 12 to 7, 5, 3 and 0 after diluting the DLin-MC3 LNPs five-fold with the external buffer (PBS). For this small-scale investigation, the TFF column used had a membrane area of 20 cm<sup>2</sup>, and the fibre diameter was 0.5 mm.

**Table 3.1** Small-scale purification methods used in this chapter.

	<b>Spin column</b>	<b>Dialysis</b>	<b>TFF</b>
<b>Membrane pore size</b>	14 kDa	10 kDa	500 kDa
<b>Sample volume</b>	1 mL	1 mL	2 mL
<b>Exchange buffer</b>	PBS	PBS	PBS

To scale up and optimise the TFF purification process, LNPs (100 mL) were manufactured in three different runs at the Blaze and divided into 3 aliquots of 30 mL each to be purified via TFF (Spectrum®

KrosFlo® MiniKros Pilot *i* TFF System, Repligen Corporation, California, USA) at different conditions. The TFF conditions for each run were described in Table 3.2. For this pre-clinical investigation, the TFF column used (500 kDa) had a membrane area of 115 cm<sup>2</sup> and a fibre diameter was 0.5 mm.

**Table 3.2** Pre-clinical TFF conditions evaluated in this chapter.

<b>1st run</b>				
<b>Aliquot</b>	<b>Dilution</b>	<b>Exchange buffer</b>	<b>Speed</b>	<b>Diafiltration volumes</b>
1	1:5 dilution	PBS	212 mL/min	12
2	1:5 dilution	Tris/sucrose 10 %	212 mL/min	12
3	No	PBS	212 mL/min	12
<b>2nd run</b>				
	<b>Dilution</b>	<b>Exchange buffer</b>	<b>Speed</b>	<b>Diafiltration volumes</b>
1	No	Tris/sucrose 10 %	106 mL/min	12
2	No	Tris/sucrose 10 %	212 mL/min	12
3	No	Tris/sucrose 10 %	212 mL/min	7
<b>3rd run</b>				
	<b>Dilution</b>	<b>Exchange buffer</b>	<b>Speed</b>	<b>Diafiltration volumes</b>
1	No	Tris	212 mL/min	7
2	No	Tris (sucrose 10 % added after buffer exchange)	212 mL/min	7
3	No	Tris	265 mL/min	7

The selection of the speeds to test was based on the shear condition graph related to the type of column used according to the manufacturer's instructions (Figure 3.2).

Retentate Flow Rate Range for Processing Shear Conditions					Membrane: 500 kD mPES	
2000 s <sup>-1</sup>	4000 s <sup>-1</sup>	6000 s <sup>-1</sup>	8,000 s <sup>-1</sup>	10,000 s <sup>-1</sup>	Membrane Area:	115 sq. cm
(L/min)	(L/min)	(L/min)	(L/min)	(L/min)	Fiber Diameter:	0.5 mm
0.053	0.106	0.159	0.212	0.265		

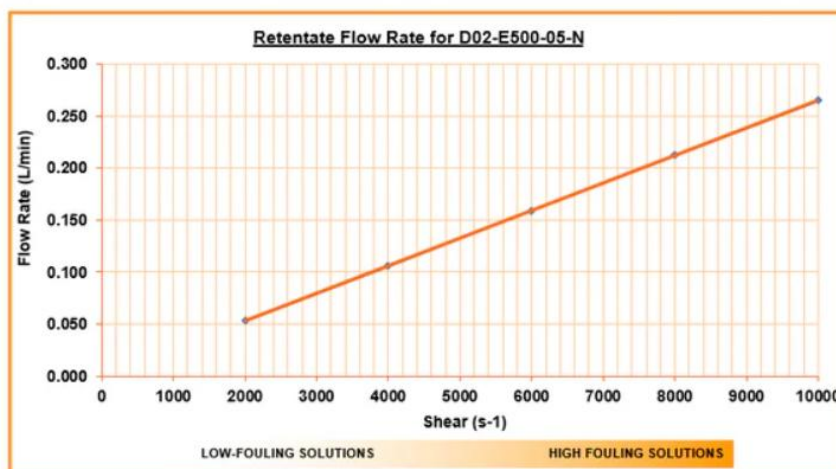


Figure 3.2 Retentate flow rate range for the column used. Image derived from Repligen website.

At the TFF, the TMP pressure values were maintained between 2 and 5 PSI as per the working limits set from literature (216,217).

### 3.2.4 Residual Ethanol Detection

Gas chromatography (HS-GC-FID, Agilent Technology) assessed the residual ethanol content in SM-102 LNP formulations purified via TFF. DMSO was used as the diluent, and ethyl acetate was the internal standard (0.04%). The column used was an Agilent DB-624, 30 m × 0.32 mm, 18 μm. The oven temperature was initially 50°C (held for 8 minutes), then was increased to 250°C at 50°C/min and held for 6 minutes. The detector temperature was 250°C. The carrier gas was helium, and the flow rate was 1.5 mL/min. All measurements were within the quantitative range of the method. The gas chromatography analysis was performed at Curia (Scotland) with the assistance of Norrie MacLeod, who provided technical guidance on optimizing the experimental parameters.

### 3.2.5 Quantification of PolyA Loading and Recovery

To measure polyA encapsulation efficacy (EE%) and recovery (or mass balance, MB%), RiboGreen assay was performed, as described in section 2.2.6.2. Briefly, samples were diluted to a final polyA concentration of 750 ng/mL in Tris-EDTA (TE) buffer in the presence or absence of 2 % Triton X-100 buffer. The plate was incubated at 37°C (15 minutes), and then the diluted RiboGreen reagent was added to the Triton (+) wells (1:200 dilution in TE buffer) and the Triton (-) wells (1:500 dilution in TE

buffer). Fluorescence was measured using either POLARstar Omega (BMG Labtech) or Glo Max Discover Microplate reader (Promega Corporation, Madison, WI) at 485 nm excitation and 525 nm emission wavelength.

### **3.2.6 Physiochemical Characterization of Formulations**

Zetasizer Nano ZS (Malvern, UK) was used to characterize the formulations in terms of Z-average diameter (nm), polydispersity index (PDI) and surface charge (zeta potential) by dynamic light scattering at 25°C, as described in Section 2.2.6.1. For the size, PDI, and zeta potential measurements, lipid concentration was diluted to approximately 0.1 mg/mL in PBS and distilled water, respectively.

### **3.2.7 Statistical Analysis**

For the statistical analysis, all experiments were conducted in triplicates unless otherwise stated, and the mean  $\pm$  standard deviation ( $\pm$  SD) was calculated. For statistical comparison, one- or two-way analysis of variance (ANOVA) followed by Tukey's Honest Significant Difference test was applied. P-values below 0.05 (\*) were considered significant and are indicated on the graphs.

## **3.3 Results**

### **3.3.1 Post-Manufacturing Purification of LNPs**

#### **3.3.1.1 The Impact of Purification Methods**

After producing DLin-MC3 LNPs at the NanoAssemblr, the LNPs were divided into three aliquots: one was subjected to purification by dialysis against PBS for 1 hour, another by centrifugation using a spin column, and the third was left unpurified. The first two aliquots were analysed together; the samples were stored at 4°C or RT, while particle attributes were investigated over time (after 1, 2, 4 and 24 h) (Figure 3.3). The particle size for LNPs purified via dialysis was  $71 \pm 6$  nm immediately after purification, with a PDI of  $0.14 \pm 0.02$  and a zeta potential of  $8.38 \pm 1$  mV. After 1 h, size remained around 70 nm, PDI <0.2 and zeta potential around 10 mV and no significant differences were observed for the dialysis group after 2, 4, and 24 h from purification, both at RT and 4°C (Figure 3.3A). The zeta potential values were consistently slightly positive, suggesting that buffer exchange might not be complete after 1 hour of dialysis.

After purification via spin column, the LNPs were approx. 10 nm larger in size compared to LNPs purified via dialysis ( $84 \pm 6$  nm; Figure 3.3B). After spin-column purification, the PDI was also lower ( $0.04 \pm 0.02$ ), and the zeta potential was closer to neutral ( $-2.21 \pm 1$  mV) (Figure 3.3B).

In terms of stability over the study period, again similar to the LNPs purified by dialysis, there was no significant change in size, PDI, or zeta potential measured over the period of the study irrespective of the temperature (Figure 3.3B). After 24 h, encapsulation efficacy (EE %) and mass balance (MB %) were measured and showed high nucleic acid encapsulation independent of the storage conditions (Table 3.3).

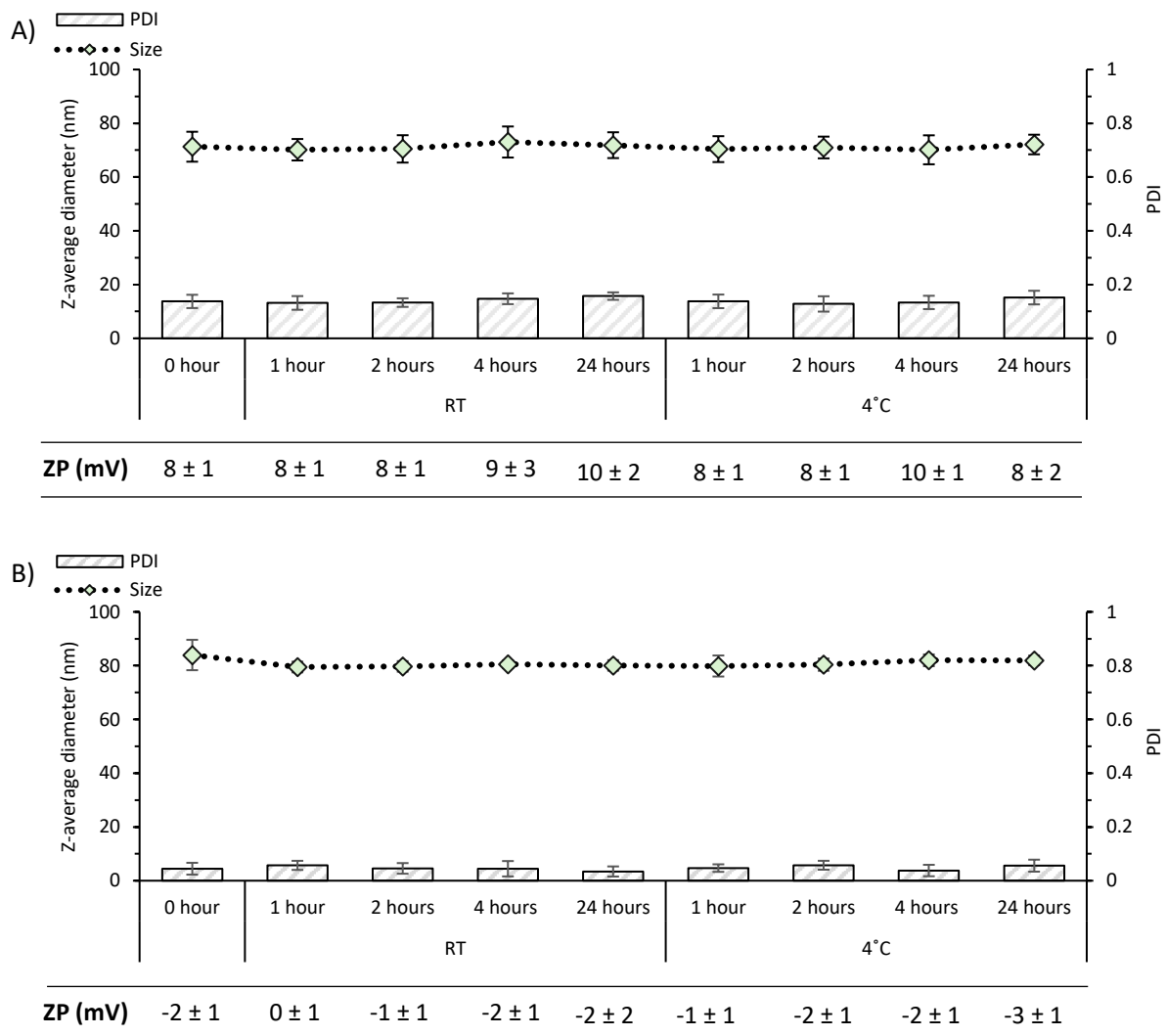


**Figure 3.3** Investigating the impact of hold time and temperature. After manufacturing, LNPs were purified via dialysis (A) or spin column (B) and particles' characteristics were monitored over 24 h. Results represent mean  $\pm$  SD of three independent batches ( $*p < 0.05$ ). 0 h represents the LNPs immediately after purification.

**Table 3.3** Encapsulation efficacy (EE %) and mass balance (MB %) of LNPs after 24 h storage at RT or 4°C. Results represent mean  $\pm$  SD (n=3).

	LNPs onto dialysis		LNPs onto spin column	
	EE (%)	MB (%)	EE (%)	MB (%)
RT	98 $\pm$ 0.5	83 $\pm$ 4	95 $\pm$ 0.9	70 $\pm$ 6
4°C	97 $\pm$ 1	85 $\pm$ 5	95 $\pm$ 2	76 $\pm$ 5

### 3.3.1.2 The Impact of Hold Time Prior to Purification

After assessing the stability of LNPs post-purification, the stability of LNPs before ethanol removal was also investigated to better understand the effects of ethanol exposure and hold times that are acceptable before ethanol removal. To achieve this, an aliquot of LNPs was left unpurified for up to 24 hours at RT or 4°C, then subjected to purification via spin column. Changes in the sample's size, PDI, and zeta potential were monitored over time and compared to the results obtained after its purification (Figure 3.4). The results indicate that LNPs exhibited minimal increases in size and PDI after 1, 2, 4, and 24 h when left unpurified whether stored at RT (Figure 3.4A) or 4°C (Figure 3.4B). Following purification after 24 hours, no significant differences in size were observed under either storage condition. In contrast, for unpurified samples stored at both RT and 4°C, PDI significantly decreased after purification, indicating a broader particle size distribution prior to purification (Figure 3.4A-B). In terms of EE % and MB %, after purification, LNPs showed high nucleic acid encapsulation (Table 3.4).

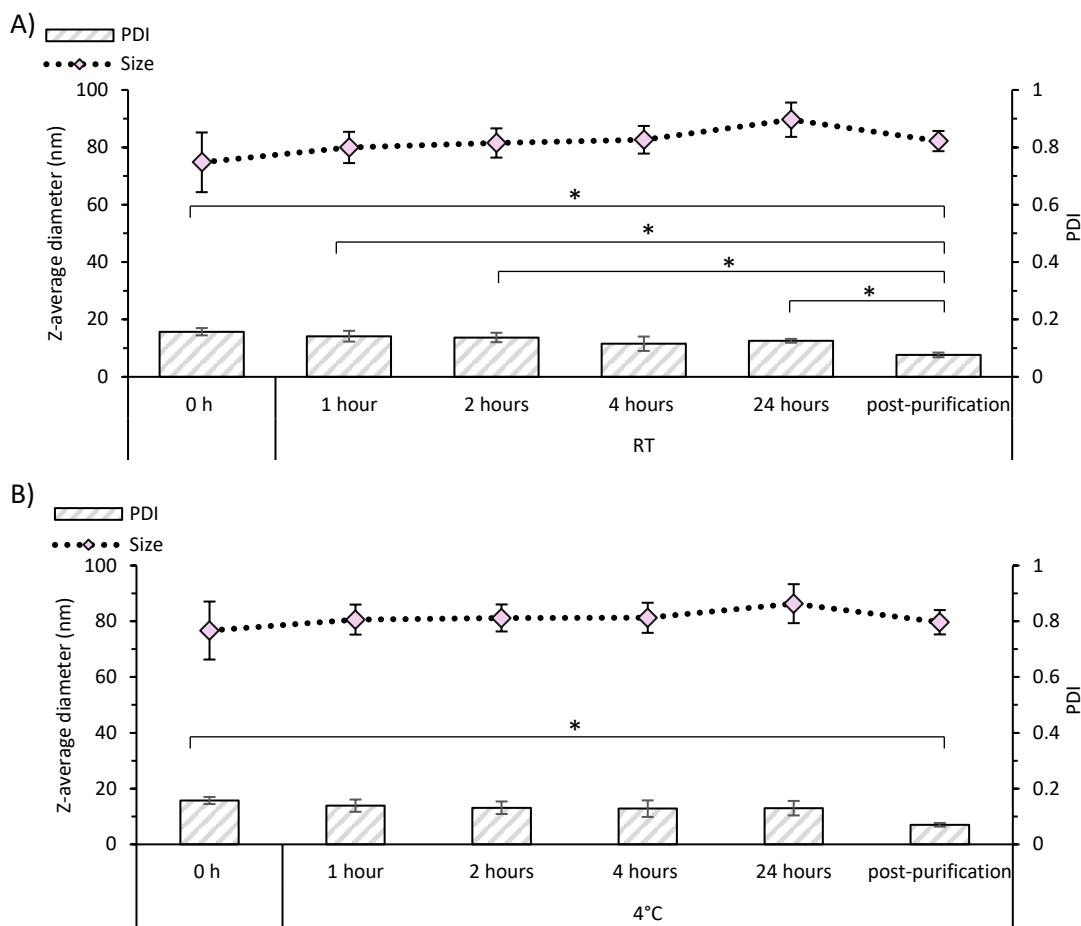


**Figure 3.4** Investigating the impact of hold time and temperature on LNPs left unpurified for 24 h. A) LNPs were purified after 24 h from manufacturing while being stored at room temperature (RT). B) LNPs were purified after 24 h from manufacturing while being stored at 4°C (mean ± SD, n = 3, \*p < 0.05).

**Table 3.4** Encapsulation efficacy (EE %) and mass balance (MB %) of LNPs following purification after 24 h storage at RT or 4°C. Results represent mean ± SD (n=3).

	Unpurified LNPs	
	EE (%)	MB (%)
RT	97 ± 2	73 ± 8
4°C	97 ± 0.2	91 ± 18

This study demonstrated that after manufacturing, a hold time of 24 h at RT or 4°C before the purification step can be used without detriment to the LNPs physicochemical characteristics.

### 3.3.2 Investigating TFF as LNPs Purification Method

#### 3.3.2.1 The Impact of the TFF Speed

To further investigate TFF purification as a small-scale method to purify LNPs, DLin-MC3 LNPs were

prepared at the NanoAssemblr. LNPs were diluted 1:5 in citrate buffer pH 4 and concentrated back to the initial volume at the TFF before starting the buffer exchange. Different TFF speeds were initially tested (10 mL/min, 15 mL/min and 20 mL/min) (Figure 3.5). TFF speed is important because it affects the rate of filtration and concentration (if required), influencing both the efficiency of the purification process and the potential for particle aggregation or deformation, which can ultimately impact the quality and stability of the final product.

Prior to purification, the LNPs sizes were 70 to 80 nm (Figure 3.5A) and following purification, the LNP size increased by approx. 15 to 20 nm with no significant difference between the LNPs purified at different speeds ( $92 \pm 3$  nm,  $91 \pm 7$  nm and  $88 \pm 4$  nm for 10 mL/min, 15 mL/min and 20 mL/min, respectively, Figure 3.5A). Similarly, the TFF purification speed did not significantly affect the PDI (Figure 3.5B) nor the zeta potential (Figure 3.5C).

These samples were also sterile-filtrated. Sterile filtration needs to be tested for LNPs because while it is essential for ensuring microbiological safety, the filtration process can potentially damage the LNPs, affecting their size, structure, and functionality, which could compromise their efficacy and stability. Following filtration, size decreased by around 5 nm, suggesting that either a small population of larger particles were retained in the 0.22  $\mu$ m filter or broken down due to shear to smaller LNPs (Figure 3.5A). After 0.22  $\mu$ m filtration, the PDI also decreased significantly ( $p < 0.05$ ) (Figure 3.5B). However, in all cases the PDI was well below 0.2. After filter-sterilisation, the zeta potential remained near neutral (Figure 3.5C).

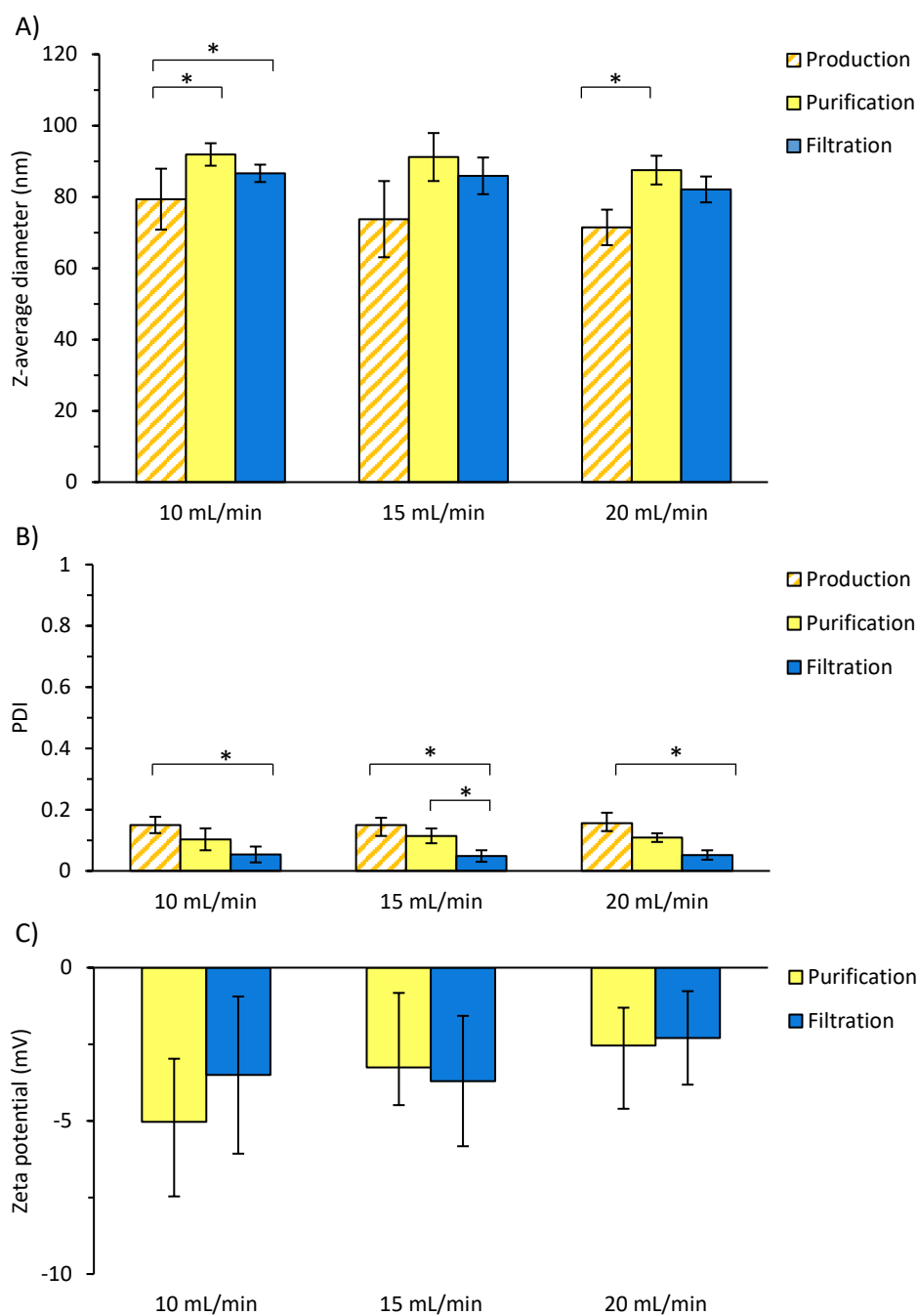


**Figure 3.5** Impact of TFF speed during purification. The effect of TFF speed was evaluated in terms of size (A), PDI (B) and zeta potential (C). Results are expressed as mean  $\pm$  SD from 3 independent batches. Statistical significance was calculated:  $p < 0.05$  (\*).

The LNPs purified at various speeds were also tested for mRNA encapsulation and total mRNA recovery (or mass balance, MB%) using the RiboGreen assay (Table 3.5). The results suggest that EE% was not affected by the speed of purification or by sterile filtration. Similarly, there was no notable difference in MB % for the LNPs purified at different speeds (Table 3.5).

**Table 3.5** Encapsulation efficacy (EE %) and mass balance (MB %) results following TFF purification at increasing speeds.

Speed	EE (%)		MB (%)	
	Unfiltered	Filtered	Unfiltered	Filtered
10 mL/min	94 ± 1	93 ± 2	82 ± 14	80 ± 19
15 mL/min	95 ± 1	94 ± 1	73 ± 11	70 ± 8
20 mL/min	95 ± 1	94 ± 1	80 ± 6	73 ± 9

Overall, speed seemed not to have a pivotal impact on the size, PDI and zeta potential and it did not interfere with the recovery of the RNA. Once it was determined that different speeds could lead to a similar outcome, further experiments were conducted at a rate of 20 mL/min to speed up the purification process.

### 3.3.2.2 The Impact of the Number of Diafiltration Volumes

The previous section focused on the impact of TFF speed, and for the purpose of that investigation, the number of diafiltration volumes was kept constant at 12. In this section, the impact of the number of diafiltration volumes on LNP characteristics was investigated while the TFF speed was kept constant at 20 mL/min. Diafiltration volume is important because it directly influences the efficiency of buffer exchange and the removal of unwanted components, ensuring that the final formulation of LNPs is purified to the desired specifications without compromising their stability or integrity. Additionally, it is crucial to balance the purification process with buffer use, as excessive diafiltration volume can lead to unnecessary buffer consumption, increasing costs and potentially affecting the overall efficiency of the process. Therefore, to investigate this, DLin-MC3 LNPs were diluted 1:5 in the external buffer (PBS 10 mM, pH 7.4), and the volume was concentrated back to the initial volume. After concentration, buffer exchange was performed, and the diafiltrate volume was decreased from 7-fold, to 5-fold and then 3-fold was tested. LNPs were also concentrated using the TFF without a washing step (“0 washes”).

The Z-average, PDI and zeta potential results comparing 12, 7, 5, 3, and 0 washes are shown in Figure 3.6A-E, and the external buffer's pH is shown in 3.6F. Initially, a pilot study (n=1) was conducted across all the TFF protocols (from 12 washes to 0 washes) to identify the possibly minimal volume that could be used to purify the LNPs.

The results in Figure 3.6 demonstrate that the particle size and PDI were generally retained across all wash protocols. Similarly, the zeta potential was the same (approx. -2 to -3 mV) for all samples except when skipping the washing step (“0 washes”, Figure 3.6E). This is in line with the fact that, in this case, LNPs were diluted in PBS but did not undergo a complete buffer exchange with PBS. Hence, the pH was not sufficiently raised from 4 to 7.4, and the ionisable lipid was still mainly protonated. This is confirmed by using pH stripes to indicate the external pH of the solutions (Figure 3.6F) (a pH probe was not used due to the limited batch volumes). The pH of the LNPs purified using 3 wash volumes is also shown to be approximately 7, indicating the success of the buffer exchange. In contrast, LNPs not purified (“0 washes”) retained a lower pH of around 5.

Once it was confirmed that reducing the washes to as few as 3 retained good attributes, LNPs were manufactured in triplicate using 3 washes to confirm the preliminary results from the engineering batches. Overall, irrespective of the number of washes, all the LNPs had a size of 100 nm or below and a PDI below 0.2 after purification. As a confirmation of the results shown in the previous section, filtration decreased both size and PDI. In terms of encapsulation efficiency and mRNA recovery (mass balance), all TFF wash protocols gave similar encapsulation and mass balance (Table 3.6), with EE% being  $\geq 95\%$  and MB% being  $\geq 80\%$ . However, when skipping the washing step, whilst LNPs maintained a high EE (96 %) the MB dropped to 52 %, suggesting mRNA (and potentially LNPs) were lost in this process (Table 3.6).

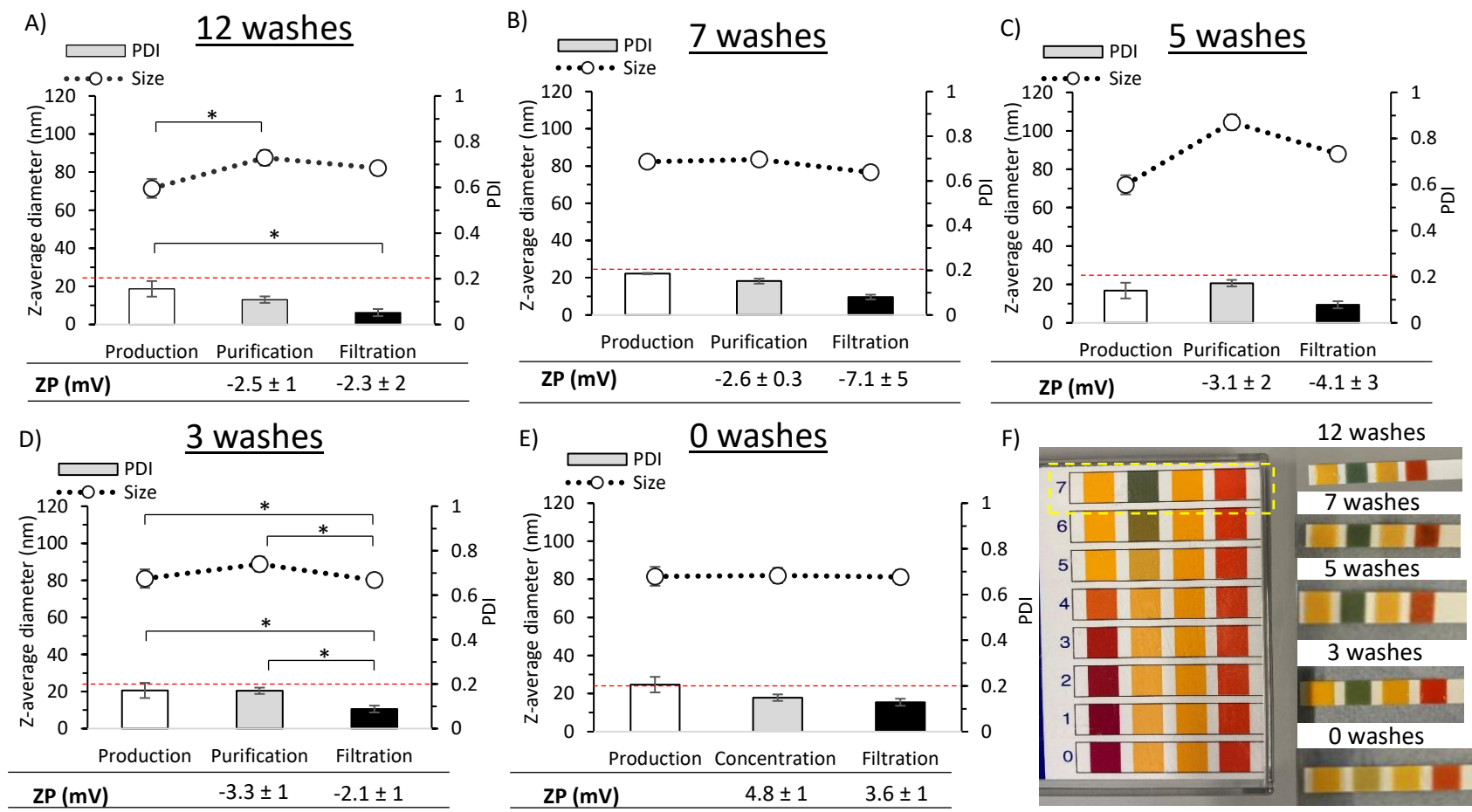


**Figure 3.6** Investigating the “wash cycles” number required to purify LNPs while maintain vesicle characteristics. The number of washes was decreased from 12 (A) to 7 (B), 5 (C), 3 (D) and 0 (E). pH stripes were used as an approximate tool to measure LNPs external pH (F).

**Table 3.6** RiboGreen assay results for LNPs purified decreasing the number of diafiltration volumes.

N° of washes	EE (%)		MB (%)	
	Unfiltered	Filtered	Unfiltered	Filtered
12	95 ± 1	94 ± 1	80 ± 6	73 ± 9
7	97	97	101	93
5	97	97	107	85
3	96 ± 1	96 ± 1	80 ± 8	81 ± 5
0	96	92	52	30

### 3.3.2.3 GC Analysis to Confirm Ethanol Removal

In addition to buffer exchange, a critical aspect of the LNP purification process is the effective removal of ethanol from the final product. The permissible residual ethanol volume varies depending on the specific application and regulatory standards. For pharmaceutical and biologic products, residual ethanol content is generally required to be below 0.5% (v/v) to ensure both safety and efficacy. However, this threshold may vary based on the product's intended use, making it essential to consult the appropriate guidelines for specific requirements. To assess the residual ethanol content, LNPs were manufactured and purified using TFF across decreasing diafiltration volumes (12 – 0). Ethanol content was quantified using gas chromatography. As shown in Figure 3.7, the results confirmed that a diafiltration volume of 5 represented the effective limit for ethanol removal, with a residual content of 2372 ppm. This value aligns with ICH guidelines for acceptable residual ethanol levels (171), indicating that the ethanol was sufficiently removed after the optimised TFF wash cycle.

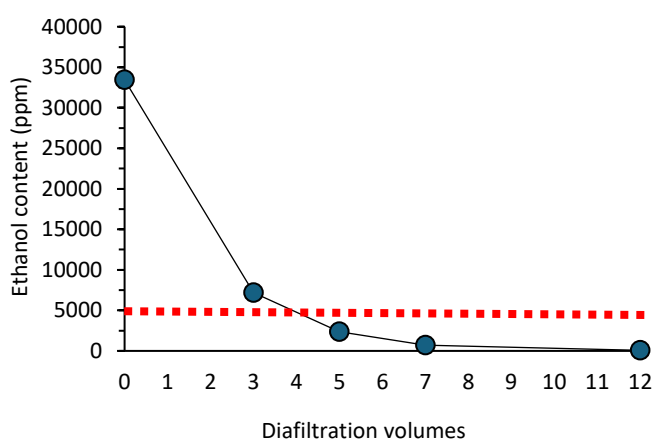


**Figure 3.7** Residual solvent levels after TFF expressed as parts per million (ppm). The internal standard used was ethyl acetate. All measurements were within the level of detection and level of quantification. The GC results represent n=1.

#### 3.3.2.4 Scaling Up the TFF Purification Process

To assess the impact of different purification conditions on the physicochemical consistency of LNPs during scaling-up, SM-102 LNPs were manufactured in the Blaze system at a volume of 100 mL. The sample was then aliquoted into three parts of 30 mL each (Aliquot 1, Aliquot 2, and Aliquot 3) and purified via TFF. In this study, the number of diafiltration volumes (12) and the speed (212 mL/min) were kept constant across all three aliquots, with a particular focus on the dilution step and the choice of external buffer (PBS vs Tris/sucrose). An industrial-scale TFF system was used to simulate industrial-scale production, as it accommodates larger product volumes and features a column with a larger membrane area (115 cm<sup>2</sup>). This scaling-up is critical, as transitioning from laboratory-scale to industrial-scale production requires careful optimization of key process parameters to ensure consistent product quality.

The three different protocols are summarised in Figure 3.8. PBS was the external buffer of Aliquots 1 and 3, and the only difference in terms of parameters was the dilution step: Aliquot 1 was diluted in the external buffer, while Aliquot 3 was not diluted. Aliquots 1 and 2 underwent the same in-line dilution; however, PBS was used as the external buffer for Aliquot 1, whilst Tris/sucrose was used as the external buffer for Aliquot 2.

Results for Aliquots 1 and 3 were comparable in terms of formulation outcome and ethanol removal. Specifically, LNPs from Aliquot 1 were  $91 \pm 0.3$  nm in size with a PDI of  $0.15 \pm 0.01$ , and LNPs from Aliquot 3 (no in-line dilution) were  $83 \pm 0.5$  nm in size with a PDI of  $0.17 \pm 0.004$  (Figure 3.8A). Similarly, the encapsulation efficiency and mass balance of these two LNP aliquots were similar (Figure 3.8B), demonstrating the addition of in-line dilution does not significantly impact the LNP physico-chemical attributes. However, when the external buffer was changed from PBS (in Aliquot 1) to Tris/Sucrose 10% (in Aliquot 2), a marked increase in size and PDI ( $162 \pm 4$  nm and  $0.27 \pm 0.03$ , respectively) and a decrease in encapsulation efficacy and mass balance (Figure 3.8A and B) were noted. Regarding residual solvent levels (Figure 3.8C), residual ethanol levels were below 80 ppm across all three aliquots. However, aliquots subjected to in-line dilution (Aliquots 1 and 2) had notably lower residual ethanol than Aliquot 3, which was not subjected to in-line dilution (Figure 3.8C).

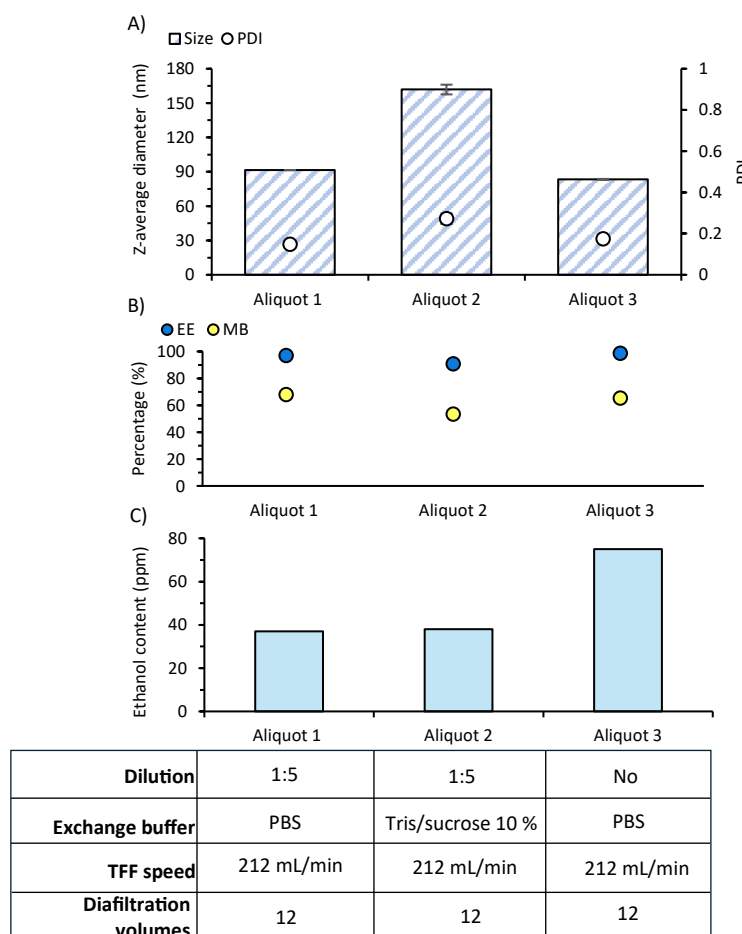


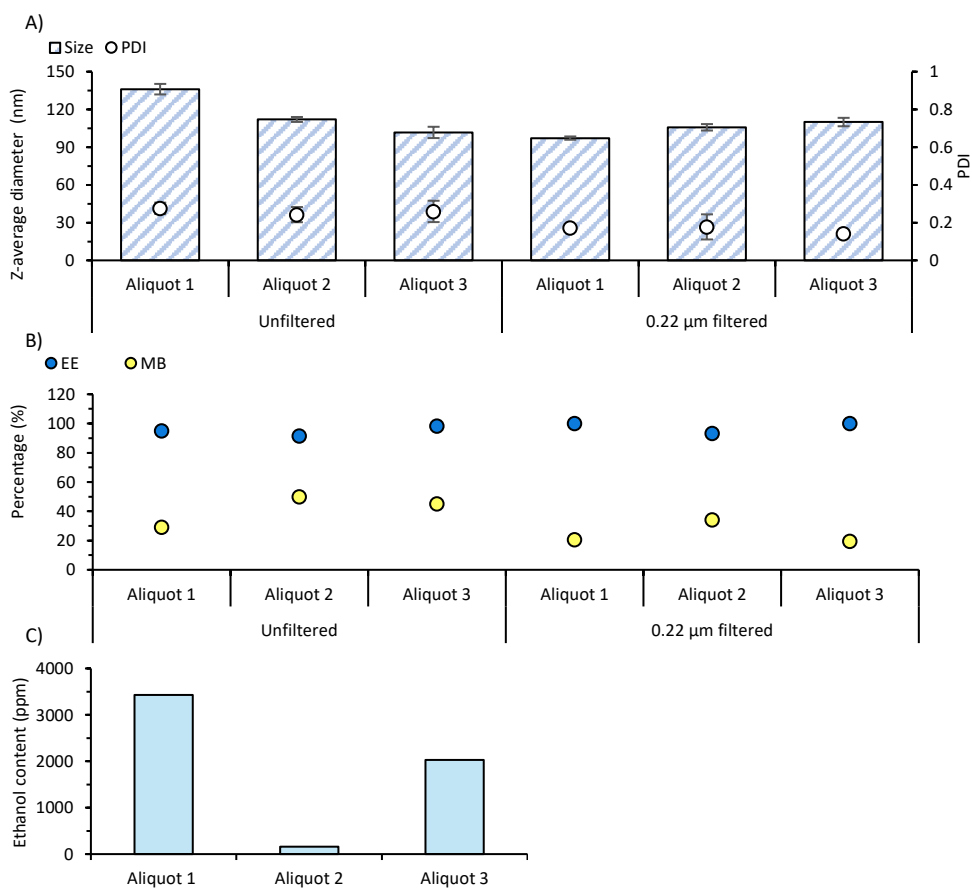
**Figure 3.8** Optimising pre-clinical TFF purification process (LNP batch 1). LNP were divided into 3 aliquots so that various parameters could be tested: Aliquot 1 consisted of LNPs diluted 1:5 and purified via TFF at 212 mL/min against PBS for 12 diafiltration volumes, Aliquot 2 consisted of LNPs diluted 1:5, purified via TFF at 212 mL/min against Tris/sucrose for 12 diafiltration volumes and Aliquot 3 consisted of LNPs not diluted, purified via TFF at 212 mL/min against PBS for 12 diafiltration volumes. (A) Size and PDI, (B) encapsulation efficacy (EE) and mass balance (MB), (C) ethanol content of the resulting LNPs. Results represent n=1.

Since dilution did not impact the LNP CQAs, from this point onwards, LNPs were not diluted in the external buffer to reduce the volume of buffer used and the length of the process. However, given the impact of switching external buffers (and the advantages of using Tris/sucrose 10% for LNPs to be frozen) a second batch of LNPs (100 mL, again divided into three aliquots) was produced to investigate the impact of external buffer further. In this phase of the study, only Tris/sucrose 10% was used as the external buffer, and adjustments were made to the speed and diafiltration volumes. The speed previously used (212 mL/min, corresponds to a shear of  $8,000 \text{ s}^{-1}$ ) was reduced to 106 mL/min (corresponding to a shear of  $4,000 \text{ s}^{-1}$ ) for Aliquot 1. For Aliquot 3, the diafiltration volume was reduced from 12 to 7.

The results in Figure 3.9 show that the speed change resulted in an increase in LNP size (to  $136.1 \pm 4$  nm; Figure 3.9A) and PDI (to  $0.28 \pm 0.03$ ; Figure 3.9A), a drastic decrease in mass balance (29 %, Figure 3.9B) and an increase in ethanol residual content (4000 ppm; Figure 3.9C), which nonetheless was below the safe limit of 5000 ppm.

Considering the length of the TFF process, for Aliquot 3, the number of diafiltration volumes was stopped at 7 to reduce time and costs. The ethanol content resulted to be  $< 5000$  ppm (2030 ppm) (Figure 3.9C). Decreasing the washes number did not impact on vesicles' characteristics which remained similar to those obtained when processing the LNPs with 12 diafiltration volumes (Aliquot 2). In particular, size was around 100 nm and PDI was approx. 0.2 for both Aliquots 2 and 3 (Figure 3.9A-B).

In the current paragraph, the LNP manufacturing process took a more industrial approach, which involved using the Blaze, a microfluidic device able to produce up to 1 L of product, as well as an industrial-scale TFF. As filtration is required for injectable products intended for the public use and it's used by industries to ensure sterility, LNPs were passed through a  $0.22 \mu\text{m}$  filter and their physiological characteristic were compared to those unfiltered. Filtration allowed bigger particles to be retained in the filtered and improved polydispersity (Figure 3.9A). On the other hand, filtration decreased mass balance (MB %) of the formulations (Figure 3.9B).



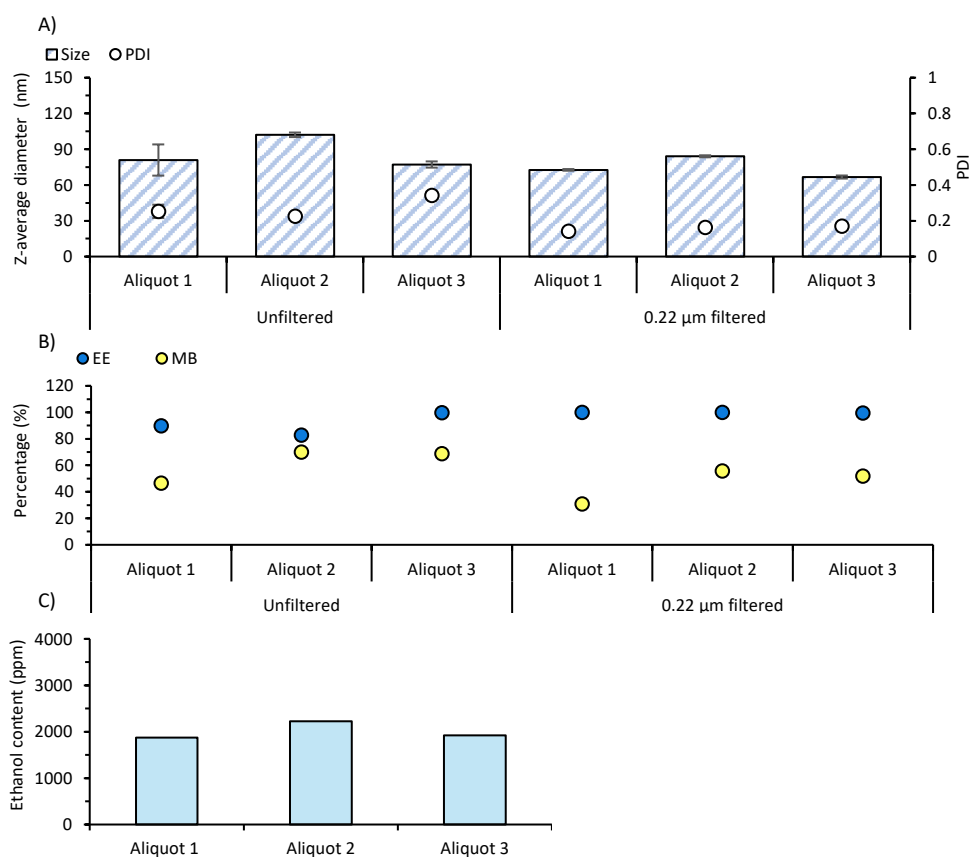
<b>Dilution</b>	No	No	No
<b>Exchange buffer</b>	Tris/sucrose	Tris/sucrose	Tris/sucrose
<b>TFF speed</b>	106 mL/min	212 mL/min	212 mL/min
<b>Diafiltration volumes</b>	12	12	7

**Figure 3.9** Optimising pre-clinical TFF purification process (LNP batch 2). LNP were divided into 3 aliquots so that various parameters could be tested; Aliquot 1 consisted of LNPs purified via TFF at 106 mL/min against Tris/sucrose for 12 diafiltration volumes, Aliquot 2 consisted of LNPs purified via TFF at 212 mL/min against Tris/sucrose for 12 diafiltration volumes and Aliquot 3 consisted of LNPs purified via TFF at 212 mL/min against Tris/sucrose for 7 diafiltration volumes. (A) Size and PDI, (B) encapsulation efficacy (EE) and mass balance (MB), and (C) ethanol content of the resulting LNPs. Results represent n=1.

Finally, a third batch of LNPs (100 mL) was manufactured and again divided into three aliquots, and in this part of the study, each of the three aliquots was purified via TFF, with the number of diafiltration volumes kept constant at 7 given this was shown to be effective in Figure 3.9. For Aliquot 1, buffer exchange was performed at a speed of 212 mL/min using Tris, with the intention of adding sucrose post-purification. The decision to add sucrose after TFF was made to avoid potential interference with the purification process, as sucrose can alter the properties of the LNPs during buffer exchange. By adding it after the TFF step, we aimed to maintain the integrity of the LNPs while also enabling the

cryoprotectant properties of sucrose, which are beneficial for preserving the LNPs during freezing and storage.

For Aliquot 1, LNPs were  $81 \pm 13$  nm in size with a PDI of  $0.25 \pm 0.04$  (Figure 3.10A), with 90 % encapsulation efficiency and 46 % mass balance (Figure 3.10B). Given that nearly 50% of polyA was lost during the process, Aliquot 2 was purified under the same conditions to evaluate the reproducibility of these results. Since the second purification showed improved mass balance, sucrose was added post-TFF, resulting in vesicles with a size of approximately 100 nm, a PDI of 0.2, and a mass balance of 70 %. Because adding the cryoprotectant after TFF seemed to have improved the final size and the mass balance of the LNPs, the third and last aliquot was purified against Tris only and the speed was increased to 265 mL/min (corresponding to  $10,000 \text{ s}^{-1}$ ). Results from this last run were promising as size was  $77 \pm 3$  nm and mass balance 70 %, even though PDI was  $0.34 \pm 0.02$  (Figure 3.10A-C). Filtration decreased the size and PDI of the vesicles but also resulted in a loss of polyA, confirming the results from run number 2.



<b>Dilution</b>	No	No	No
<b>Exchange buffer</b>	Tris	Tris (sucrose added after TFF)	Tris
<b>TFF speed</b>	212 mL/min	212 mL/min	265 mL/min
<b>Diafiltration volumes</b>	7	7	7

**Figure 3.10** Optimising pre-clinical TFF purification process (LNP batch 3). LNP were divided into 3 aliquots so that various parameters could be tested; Aliquot 1 consisted of LNPs purified via TFF at 212 mL/min against Tris for 7 diafiltration volumes, Aliquot 2 consisted of LNPs purified via TFF at 212 mL/min against Tris for 7 diafiltration volumes (sucrose added after TFF), and Aliquot 3 consisted of LNPs purified via TFF at 265 mL/min against Tris for 7 diafiltration volumes. (A) Size and PDI, (B) encapsulation efficacy (EE) and mass balance (MB), and (C) ethanol content of the resulting LNPs. Results represent  $n=1$ .

### 3.4 Discussion

This chapter focused on the purification of lipid nanoparticles using different purification methods, including dialysis, spin column, and TFF. Independently of the method used, one of the main issues in LNPs production is understanding the impact of temperature on LNPs storage and the hold time between manufacture and purification. Therefore, the aim of the study was to investigate the effect of temperature on LNPs after purification. This short-term stability study demonstrated that LNPs are stable up to 24 h after purification through dialysis and spin column when stored at RT and 4°C (Figure

3.3A and B). It should be noted that this study was only conducted for 24 hours, mainly assuming brief storage in the laboratory before, for example, measuring protein expression and the product stability after 24 h was not evaluated. However, longer-term stability has been reported as an issue. For example, Kamiya et al., demonstrated that LNPs stored at 4°C and RT for 7 days retained size, PDI and encapsulation efficiency but a drastic decrease in luciferase expression was noted compared to samples stored at -30°C (215). The authors hypothesised that this was due to the oxidation of lipids that also caused mRNA oxidation, which decreased mRNA activity along with mRNA hydrolysis (218). Within this current chapter, lipid and mRNA stability was not considered, and the CQAs measured particle size, PDI, EE%, and MB%. Whilst these attributes are more limited and do not directly test LNP efficacy, these CQAs are a good initial indicator of quality during manufacturing and support process development.

Additionally, the impact of hold time and storage temperature between microfluidic manufacture and purification was evaluated to support LNP production at both laboratory scales and particularly for larger batches where larger volumes may be subjected to longer hold times between production and purification. Results showed that, after manufacturing, unpurified LNPs (containing 25% ethanol) maintained stability for up to 24 h before the purification step, both at RT and 4°C (Figure 3.4A-B). The importance of the purification step after manufacturing of LNP and other drug delivery systems such as liposomes, besides removing impurities and exchanging the buffer, is to eliminate the ethanol (or another organic solvent) used to dissolve the lipids prior to microfluidic mixing. When using a flow rate ratio (FRR) of 3:1 (aqueous: organic), as per the LNPs manufactured in this chapter, ethanol content in the formulation is around 25 %, way above the concentration allowed by the ICH (0.5 %, corresponding to 5000 ppm) (171). Efforts have been made to produce liposomes without using organic solvents, and good examples are shown in the literature. In 2020, with the aim of facing the issue related to the presence of ethanol during liposome manufacturing, Khadke et al. described a complete solvent-free method for producing doxorubicin or amphotericin B-loaded liposomes which consisted of producing liposomes by high shear mixing dry powder lipids with an aqueous buffer and then downsizing the vesicles via microfluidic processing using the Microfluidizer processor (219).

Given the issues with achieving solvent-free production, purification is needed, and TFF is often used as a purification method for nanoparticles, especially on an industrial scale. In brief, the feed stream travels across the membrane surface, and particles smaller than the pore size leave the system (the so-called “permeate”) while, at the same time, the remainder (called “retentate”) is recirculated back to the feed reservoir. Among the process parameters that can be controlled, the feed flow rate, the transmembrane pressure (TMP), the number of diafiltration volumes, and temperature all play key

roles (220,221). The focus of this chapter was on the feed flow rate (or speed) and the number of diafiltration volumes. From Figure 3.5A-C, it has been shown that speed did not significantly impact the vesicles' final characteristics, either in terms of size, PDI, zeta potential or mRNA recovery (Table 3.5). Next, the focus shifted to simplifying the TFF process in terms of time and cost by reducing diafiltrate volumes, with the aim of scaling up the procedure. In 2018, Forbes et al., discussed on microfluidic manufacture of liposomes entrapping protein proving that solvent removal (in that case the solvent was MeOH) could be achieved within 12 diafiltration volumes when liposomes were purified via TFF (212). In contrast with these results, the findings showed in this chapter proved that it's possible to reduce the TFF diafiltrate volumes from 12 down to as low as 5 and successfully remove the ethanol as per the ICH guidelines without impacting LNP CQAs (Figure 3.6, Figure 3.7 and Table 3.6). With the intent of speeding up the purification process especially on a larger scale and, at the same time, reducing time and costs, this finding would be particularly useful. An alternative approach to the classic one-step TFF method used in this chapter (where ethanol is directly removed with increasing pH) is the two-step TFF method introduced by Geng et al. which involves removing ethanol before increasing the pH. Their proposed protocol includes an initial filtration in an acidic buffer to efficiently eliminate ethanol, followed by filtration in a basic buffer to gradually increase the pH. The reason behind this is that some reports suggest that ethanol residue in the LNP suspension significantly influences the stability of the lipid membrane. As a result, the LNPs exhibited larger particle sizes, fewer empty LNPs, excellent storage stability, enhanced *in vitro* transfection efficacy, and reduced distribution in the heart and blood *in vivo* (222).

As already mentioned, one of the bottlenecks of LNPs manufacturing is the loss of product during scaling up as sometimes is hard to translate what works on a bench scale on a bigger scale. In this chapter, SM-102 LNPs were manufactured at a pre-clinical scale and various TFF parameters were modified trying to match the good results achieved on the lab-bench scale. The parameters considered were the dilution, the exchange buffer type, the TFF speed and the number of diafiltration volumes. Dilution is often an option, as it reduces ethanol concentration, which is important because too much ethanol entering the column can adversely affect hollow fiber permeability (223). However, when looking at scaling up the TFF process question arises whether this extra step can be avoided to reduce time and costs. From the findings shown in section 3.3.2.4, dilution was not crucial for the outcome of the formulation (Figure 3.8A and B).

The optimal speed (for the type of column used) was 212 mL/min (corresponding to a shear of 8,000  $s^{-1}$ ), as a lower speed led to particles bigger in size and lowered the RNA recovery (Figure 3.9A and B). When a higher speed was adopted, particles retained good characteristics except for the

polydispersity which was above 0.2 (Figure 3.10A-C). Exchanging the buffer with Tris/sucrose resulted in a 50 % loss of RNA, and, with the aim of improving this aspect, buffer exchange was performed in Tris only (followed by the addition of the sucrose). The late addition of sucrose improved the mass balance outcome, raising it to 70 % (Figure 3.10A-B).

Another aspect that was considered in this chapter was the sterilisation step after purification. The techniques that can be used to sterilise LNPs are autoclaving, gamma irradiation and filtration through a 0.2  $\mu\text{m}$  membrane (224,225). Generally, filtration is used by industries to remove bacteria and particles from solutions (as particles bigger than the pores size are trapped in the filter), to achieve sterility and to follow the regulatory requirements. Some of the factors to consider relatively to filtration are the filter type, the filter pore size and the transmembrane pressure (TMP). Typically, polyethersulfone (PES) membrane filters are used for bioprocessing (226). Filtration is usually performed through a 0.2 or 0.22  $\mu\text{m}$  filter and, in order to be used, filters need to pass the test described in ASTM F838-05, Standard Test Method for Determining Bacterial Retention of Membrane Filters Utilized for Liquid Filtration, a test method designed to assess the retentivity of a sterilizing filter under standard challenge conditions (227). In particular, a filter is suitable to be used for sterilisation if it can retain a minimum of  $1 \times 10^7$  colony forming units (cfu) per  $\text{cm}^2$  of a challenge bacterium (usually *B. diminuta*). In their paper, Messerian et al. (228), focused on the behaviour of mRNA-containing lipid nanoparticles during sterile filtration when using a commercially available dual-layer polyethersulfone sterile filter (Sartopore 2 XLG), monitoring the transmembrane pressure (TMP). When increasing the TMP, the filter capacity increased and the resistance of the filter decreased. Authors hypothesised that working at high TMP may cause a change in the structure of the LNP-fouled filter and this would cause to a decrease in fouling resistance and concurred that, to further investigate the factors governing the resistance of the fouled filter, additional experiments would be required.

For the filtration assessments performed in this chapter, the TMP was not monitored, and the particles characteristics were evaluated after filtration and compared to those pre-filtration. On a bench scale (2 mL), filtration caused a decrease in LNP size and polydispersity without impacting significantly the mRNA encapsulation (Figure 3.5A-C, Table 3.5, Figure 3.6A-E, Table 3.6) but, on a pre-clinical scale, filtration did impact on the particles' attributes (Figure 3.9A-B and Figure 3.10A-B). This might be due to the fact that on a larger scale, the membrane was fouled faster because of the larger volume of LNPs, thus decreasing the effective surface area of the filter resulting in a reduced yield. Another hypothesis could be that, at larger volumes, LNP aggregated more easily, and this could have caused a major retention by the filter. It could also be possible that, for the filtration of larger volumes, a

filtration system should have been used to ensure uniform filtration and reproducibility to control the flow rates and the pressure.

### 3.5 Conclusions

This chapter intended to give new insights into LNP purification, showing different purification techniques with a focus on TFF, which is considered to be a key role in the pharmaceutical and life science industries. Starting from a bench-scale optimisation process and advancing to a pre-clinical level, efforts have been made to produce vesicles whose characteristics were within the range typically accepted for LNPs. Generally, scaling up the LNP purification process can be challenging because, very frequently, what works on a small scale doesn't match the results on higher volumes. From here, the necessity of investigating this aspect and evaluating the measures that need to be adopted to produce good vesicles. The results presented in this chapter demonstrate that on a small scale, TFF speed was not crucial for the outcome of the formulation, but speed seemed to have an impact on a larger scale. In fact, depending on the type of formulation, the column dimensions, and the volume to be processed, the appropriate speed should be selected. The external buffer and the dilution step are also aspects to be taken into consideration when using the TFF, and their impact has been demonstrated in this chapter. The number of diafiltration volumes is one of those parameters that can be monitored and scaled down to speed up the process, as it has been showed that 5 and 7, on a small scale and a pre-clinical scale, respectively, represent the minimum number of washes which allows to produce LNP with good characteristics and a residual ethanol content below the authorised range. Filtration, which is one of the methods to sterilise the LNPs, does have an impact on the size and PDI of the LNPs, often reducing their dimensions and polydispersity as the particles are retained in the filter, but additional considerations need to be done when it comes to filtration as this step affects the recovery of the particles, commonly decreasing the yield. The effect of temperature on LNP CQAs after 24 h from purification was also evaluated, with results showing that particle attributes are maintained at both RT and 4°C storage. Lastly, LNPs were left unpurified after manufacturing for 24 h to analyse if a late purification could impact the outcome of the process: from the findings presented in this chapter, LNP solutions containing 25 % ethanol can be left unpurified for up to 24 h and, once purified after 24 h, retain similar characteristics as before purification. Once examined in depth the problems related to purification, filtration and short-term handling of LNPs, the long-term storage conditions of the final product can be evaluated. This progression represents a novel, integrated approach that

connects upstream and downstream challenges with the stability of the end formulation, an aspect often addressed in isolation in previous studies.

## **Chapter 4**

# Optimisation of LNP Freeze-Drying Process

The DSC and FDM work, along with the UHPLC-CAD analysis and the freeze-drying optimization, were all performed at Curia, Scotland. Kiara Lobato assisted with the DSC and FDM work, while Dr. Chris Allan provided technical guidance for the UHPLC-CAD analysis. Dr. Jaclyn Raeburn contributed to the optimization of the freeze-drying cycles.

## 4.1 Introduction

When considering manufacturing any drug delivery system, it is important to consider its storage conditions. As for the liquid formulations, this aspect plays a central role as inappropriate storage conditions can affect the stability and the efficacy of the formulation, as well as microbial growth (229,230). Lipid nanoparticles (LNPs) face the same challenge. The two mRNA LNPs COVID-19 vaccines on the market, Comirnaty (Pfizer/BioNTech) and Spikevax (Moderna) require ultralow temperatures for long-term storage; Comirnaty vaccine needs to be stored between  $-90^{\circ}\text{C}$  and  $-60^{\circ}\text{C}$  and Spikevax vaccine between  $-50^{\circ}\text{C}$  and  $-15^{\circ}\text{C}$  (231). Alternatively, they can be stored at  $2^{\circ}\text{C}$  to  $8^{\circ}\text{C}$  but only for a limited time: Comirnaty for up to 10 weeks and Spikevax for up to 30 days. The stability of these vaccines at room temperature is even lower (only 12 hours) (232). The recently approved mRNA LNP vaccine (mRESVIA) for the prevention of lower respiratory tract disease (LRTD) in individuals 60 years of age and older, also requires low storage temperatures ( $-40^{\circ}\text{C}$  to  $-15^{\circ}\text{C}$ ) (233). Storing liquid formulations at low temperatures is problematic: the liquid-containing vials are bulky and difficult to transport, and the cold-chain storage is very costly. It is estimated that up to 80% of the cost of the vaccine is necessary to maintain the cold chain storage (234). In addition, this type of storage condition is difficult to maintain in low-resource countries which lack sufficient storage facilities. In the case of LNPs, cold storage is essential for preserving the efficacy of the mRNA payload, which is prone to rapid degradation, especially at high temperatures (231,235). Lyophilisation (freeze-drying) has emerged as a valuable strategy to overcome all these issues. Lyophilisation, removing water from the formulation, can decrease the risk of microbial growth and mRNA degradation (236). Moreover, the lyophilised product can be stored generally at higher temperatures (236), thus reducing the difficulties and costs related to cold chain storage.

Freeze-dry comprises three main steps: 1) freezing, 2) primary drying, and 3) secondary drying. In the first stage of freeze-drying, the product is frozen. When decreasing the temperature, bulk water starts to freeze leaving particles and solutes in the freeze-concentrate (237). During primary drying, the product is dried by a process known as sublimation in which frozen water is removed at low temperatures and low pressure: when the pressure/temperature balance is reached, the ice sublimates directly into a vapour without melting. Any unfrozen water is removed through desorption as the temperature is raised during secondary drying. The main components of freeze-dryer are shown in Figure 4.1 (vapour flow is also shown).

During all the stages of freeze-drying, mRNA LNPs undergo a series of stresses that can affect their CQAs. Among these are the crystallisation of the buffer components, the pH changes, the interfacial

stress between ice and liquid and many more (238). For example, in their paper, Meulewaeter et al. demonstrated that the ionisable lipid-to-mRNA weight ratio and the type of aqueous buffer affect the properties of mRNA LNPs after lyophilisation (239). In particular, their findings showed that a sufficiently high ratio is necessary to prevent leakage of mRNA and that Tris is more appropriate than PBS to lyophilise LNPs. When evaluating their morphology via cryo-EM, mRNA LNPs in PBS showed a higher concentration of bleb structures after dialysis in PBS (compared to Tris buffer) which showed similarities with liposomes. As leakage of encapsulated drugs after freeze-drying often occurs when lyophilising liposomes, the authors hypothesised that the similarity between LNPs and liposomes could explain their results. Formulation buffers with a low salt concentration (e.g. Tris buffer) should be preferred as salts can shield the charges on the ionisable lipids and decrease the ionic interactions between RNA and the ionisable lipid; as a result, the weaker intermolecular interactions contribute to the generation of blebs structures and, consequently, mRNA release during lyophilisation. Moreover, PBS causes shifts in the pH of solutions after freezing, and this contributes to the vesicles' instability (240). The same conclusions were achieved by Alejo et al. who confirmed that, independently of the cryoprotectant used, Tris is more efficient than PBS at preserving the functional properties of mRNA-LNPs during freeze-drying (241).

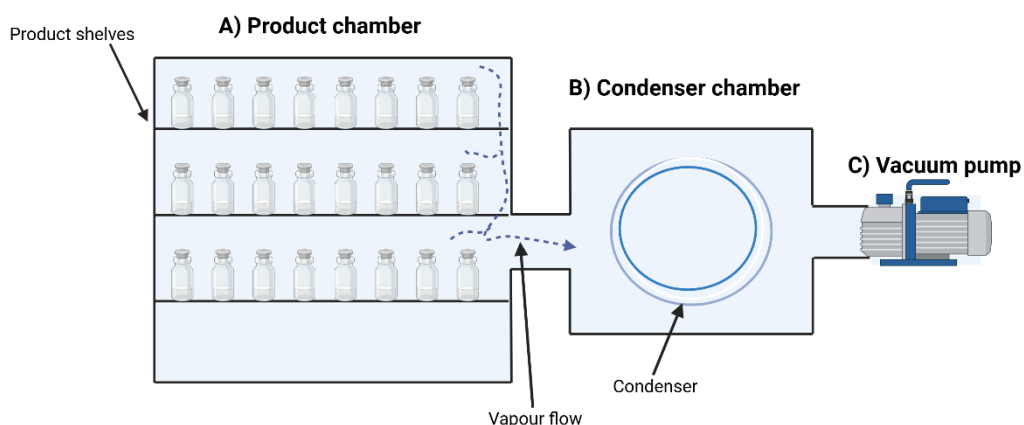


**Figure 4.1** Common components of freeze dryer. A) The product chamber is the chamber in which the product is placed for freeze-drying. B) The condenser chamber contains the condenser which is composed of plates or coils that are cooled to a very low temperature on which the solvent vapour (represented by a dotted arrow) condenses and freezes, thus acting like a “cold trap”. C) The vacuum pump applies a vacuum during the freeze-drying stages. Image created using Biorender.

Typically, cryoprotectants are added to protect liposomal and LNP structures during the process (242–244). The two most commonly accepted theories behind the cryoprotectant working mechanism are the water replacement theory and the vitrification theory. According to the water replacement theory, the structure of the lipid membrane (in the case of liposomes) is maintained because cryoprotectants replace water molecules and interact with phospholipids through hydrogen bonds (245,246). The vitrification theory states that, upon freezing, cryoprotectants form a glassy matrix (vitrification

process) that maintains the distance among vesicles, thus preventing changes in lipid membranes (246,247).

The freeze-drying process is critical, and it hasn't been thoroughly studied for lipid nanoparticles yet; In addition to the limited research on lyophilisation procedures and protectants, it is important to consider that the lyophilisation process itself is time-consuming. This poses a significant challenge to the production capacity and cost-effectiveness of mRNA vaccines (248). Consequently, additional research, which also considers this aspect and aims to shorten the process where possible, is extremely needed.

#### **4.1.1 Aim and Objectives**

The aim of this chapter was to investigate the behaviour of LNPs during freeze-drying and develop an optimised method for lyophilising mRNA LNPs, addressing common challenges associated with this complex process. To achieve this, the objectives were to:

- Investigate LNP behaviour during freeze-drying, using differential scanning calorimetry to study LNP behaviour and employ the freeze-drying microscope to examine the freeze-dried structure of the particles.
- Identify optimal freeze-drying parameters by conducting a series of freeze-drying cycles to determine the best conditions for producing LNPs with acceptable CQAs (including size, PDI, zeta potential, encapsulation efficiency, mass balance and cake appearance).
- Evaluate mRNA LNP activity by assess their *in vitro* and *in vivo* activity to determine if the freeze-drying process affects mRNA functionality.

This work presents a novel, stepwise optimisation strategy for mRNA LNP lyophilisation, rarely documented in literature in such detail. By experimentally refining the freeze-drying parameters across multiple cycles, this approach provides practical insights into how lyophilisation protocols can be tailored to improve nanoparticles' CQAs. Notably, the integration of advanced analytical tools such as differential scanning calorimetry and freeze-drying microscope for real-time observation of LNP freeze-drying behaviour, alongside functional validation, represents a unique contribution to the field.

## 4.2 Materials and Methods

### 4.2.1 Materials

Materials were purchased as described in Sections 2.2.1 and 3.2.1. Additional materials specific to this chapter included trifluoroacetic acid (TFA), purchased from Sigma Aldrich (USA), and D(+)-Trehalose, purchased from Life Sciences (St. Petersburg, FL, USA). Formaldehyde loading dye, SYBR Green Stain II and sodium acetate were purchased from Thermo Fisher Scientific (MA, USA). Agarose, MOPS 10X and Millennium RNA Marker were purchased from Invitrogen.

### 4.2.2 Preparation of LNPs

The aqueous phase was prepared by dissolving polyA (used to optimise the freeze-drying cycle) or Firefly Luciferase mRNA (for *in vitro* and *in vivo* experiments) in citrate buffer 50 mM (pH 4). The organic phase was composed of DSPC, cholesterol, SM-102 and DMG-PEG 2000 in ethanol at a molar ratio of 10:38.5:50:1.5 mol%, respectively, to mimic the Moderna Spikevax formulation. PolyA or mRNA concentrations were adjusted to maintain the nitrogen to phosphate ratio (N:P) of 6, the lipid phase concentration before microfluidics constant at 5 mg/mL and the aqueous:organic phase ratio (FRR) at 3:1. The NanoAssemblr benchtop (Precision Nanosystems Inc., Vancouver, Canada) was used to prepare the nanoparticles for all the experiments in this chapter, as detailed in section 2.2.2; the mixtures were placed in two plastic syringes connected to the microfluidic chip and the speed (TFR) was 15 mL/min for all the experiments.

### 4.2.3 Purification Methods and Cryoprotectant Addition

LNPs were purified either via tangential flow filtration (TFF) or spin column (Figure 4.2).

- *Purification via TFF*

The engineering batches of LNPs employed to optimise the freeze-drying protocol were purified via TFF (Spectrum® KrosFlo® Research 2i TFF System, Repligen Corporation, California, USA) against Tris 10 mM (pH 7.4). 8 mL of LNPs were diluted 1:5 in Tris 10 mM and concentrated back to the original volume at the TFF. LNPs were processed for 7 diafiltration volumes at a speed of 20 mL/min. At the end of the filtration process, LNPs were concentrated to 4 mL and divided into 4 aliquots of 1 mL each. The cryoprotectant (sucrose or trehalose) at the selected concentration (10 % or 5 %) was added to

the solutions and solubilised under stirring. The volume of each aliquot was adjusted with Tris 10 mM to 2 mL.

- *Purification via spin column*

The batches of LNPs used to test the formulations *in vitro* and *in vivo* were purified via spin column (100 kDa MWCO) to use less amount of mRNA. The procedure was described in section 2.2.3. Briefly, 2 mL LNPs were diluted 1:40 in Tris 10 mM and spun at 2000 g at 4°C for 15-40 minutes until sample was concentrated to 1 mL. LNPs were divided into two aliquots of 0.5 mL each and the cryoprotectants were added to each aliquot at different concentrations (10 % sucrose and 10 % trehalose). Lastly, Tris was added to each aliquot to reach the initial volume of 1 mL.

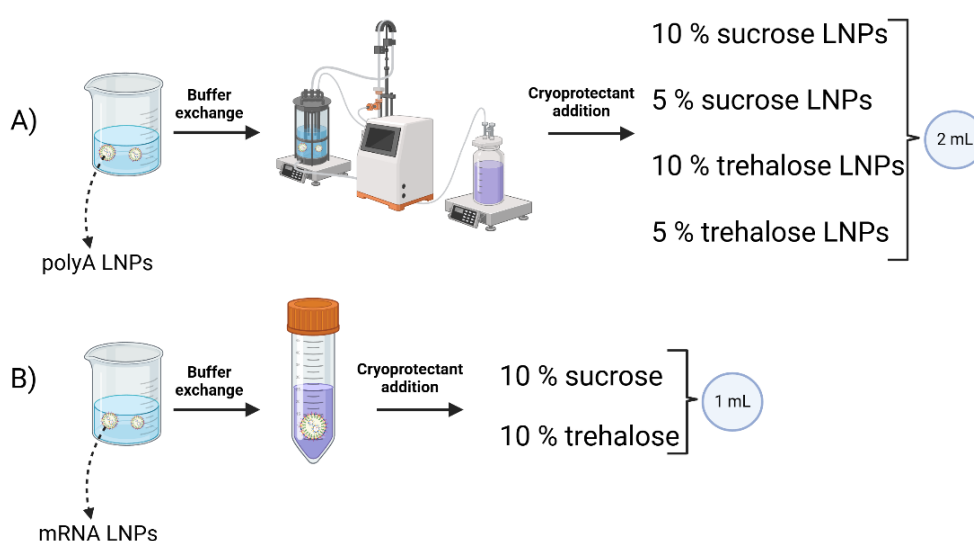


**Figure 4.2** Purification methods used in this chapter. PolyA LNPs were purified via TFF (2 mL), and mRNA LNPs were purified via spin column (1 mL). In both cases, the cryoprotectant was added after the purification and concentration step under stirring. Image created using Biorender.

#### 4.2.4 Thermal Analysis by Differential Scanning Calorimetry (DSC)

Differential scanning calorimetry studies were performed on a DSC2500 differential scanning calorimeter (TA Instruments, New Castle, USA). 20  $\mu$ L of the sample (10 % sucrose LNPs, 5 % sucrose LNPs, 10 % trehalose LNPs and 5 % trehalose LNPs) were pipetted in a pre-weighed sample pan and sealed hermetically using the DSC sample press and an empty pan was also prepared as a reference. The sample and reference were heated to 25°C, cooled to -50°C and heated back to 25°C at a rate of 10°C/min under an inert atmosphere to avoid reactions with the atmosphere (UHP nitrogen environment maintained at a flow rate of 50 mL/min). The results were repeated twice for reproducibility.

#### 4.2.5 Freeze Dry Microscopy (FDM)

Experiments were conducted using Lyostat5 Freeze Drying Microscope (Biopharma Ltd., Winchester, UK), whose main components are the Lyostat5 cryostage connected to the temperature control unit and the liquid nitrogen pump. On the cryostage, 2  $\mu$ L of each sample (10 % sucrose LNPs, 5 % sucrose LNPs, 10 % trehalose LNPs and 5 % trehalose LNPs) was loaded onto a circular glass slide and covered with another glass coverslip. Three cycles were necessary to get to know the freezing and the collapsing temperature of the samples:

1. A fast cycle where samples were cooled down to  $-40^{\circ}\text{C}$  at a rate of  $20^{\circ}\text{C}/\text{min}$  using liquid nitrogen, after which the vacuum was applied and held for 30 minutes. The temperature was then quickly increased from  $-40^{\circ}\text{C}$  to  $20^{\circ}\text{C}$ . This was useful for getting indicative information of the freezing temperature range and the collapse temperature range.
2. A slower run was used to provide a more definite indication of the freezing and melting temperatures. Images were taken every 20 seconds for the duration of the run.
3. A third run to confirm the results from the second run.

#### 4.2.6 Optimisation of the Freeze-Dry Parameters for PolyA LNPs

LNPs containing 10 % sucrose, 5 % sucrose, 10 % trehalose or 5 % trehalose were lyophilised using either the VirTis 25L Freeze Dryer (SP Scientific, Warminster, PA, USA) or the Lyostar 3 Freeze Dryer (SP Scientific, Warminster, PA, USA). Samples were pipetted into type I glass vials (2 ml) (Schott, Müllheim, Germany) and results from the DSC and the FDM were used to design the freeze-dry cycles. With the aim of improving the characteristics of the LNPs after lyophilisation, three different freeze-drying cycles were investigated.

##### 4.2.6.1 First Freeze-Drying Cycle

The first freeze-drying cycle involved freezing the samples down to  $-40^{\circ}\text{C}$  for 6 hours. The primary drying involved ramping the temperature up to  $-25^{\circ}\text{C}$  where it was held for  $\sim 30$  hours at 285 mTorr vacuum. Moving to the secondary drying, the temperature was increased to  $25^{\circ}\text{C}$  and held for 10 hours at a pressure of 20 mTorr. The heating and cooling temperature ramp rate was set at  $0.25^{\circ}\text{C}/\text{min}$ . The cycle parameters are summarised in Table 4.1.

**Table 4.1** Experimental parameters of the first freeze-drying cycle. The primary drying duration reported in the table coincided with the CM pressure and the Pirani pressure convergence ( $\pm 3$  mTorr) after  $\sim 30$  hours. However, the primary drying was extended for an extra 19 hours for logistic reasons.

	Temperature ( $^{\circ}\text{C}$ )	Pressure (mTorr)	Time (h)	Ramp rate ( $^{\circ}\text{C}/\text{min}$ )
Freezing	-40	N/A	6	0.25
Primary drying	-25	285	31	0.25
Secondary drying	25	20	10	0.25

#### 4.2.6.2 Second Freeze-Drying Cycle

For the second cycle, the freezing temperature was decreased to  $-50^{\circ}\text{C}$  (8 hours hold). The primary drying temperature was kept at  $-25^{\circ}\text{C}$  for  $\sim 30$  hours at a pressure of 120 mTorr. The temperature was increased to  $25^{\circ}\text{C}$  for the secondary drying and held for 6 hours at a pressure of 20 mTorr. The heating and cooling temperature ramp rate was set at  $0.2^{\circ}\text{C}/\text{min}$ . The cycle parameters are summarised in Table 4.2.

**Table 4.2** Experimental parameters of the second freeze-drying cycle. The primary drying (which ended after  $\sim 30$  hours) had to be extended for an extra 29 hours due to logistic reasons.

	Temperature ( $^{\circ}\text{C}$ )	Pressure (mTorr)	Time (h)	Ramp rate ( $^{\circ}\text{C}/\text{min}$ )
Freezing	-50	N/A	8	0.2
Primary drying	-25	120	32	0.2
Secondary drying	25	20	6	0.2

#### 4.2.6.3 Third Freeze-Drying Cycle

The freezing and secondary drying stages of the third cycle were equal to those of the second cycle. However, the primary drying temperature decreased to  $-30^{\circ}\text{C}$  while the pressure was further reduced to 20 mTorr. The heating and cooling temperature ramp rate was set at  $0.2^{\circ}\text{C}/\text{min}$ , the same as the second cycle. The cycle parameters are summarised in Table 4.3.

**Table 4.3** Experimental parameters of the third freeze-drying cycle. The primary drying duration was ~30 hours but was extended for an extra 18 hours due to logistic reasons.

	Temperature (°C)	Pressure (mTorr)	Time (h)	Ramp rate (°C/min)
Freezing	-50	N/A	8	0.2
Primary drying	-30	20	30	0.2
Secondary drying	25	20	6	0.2

#### 4.2.7 Measuring Critical Quality Attributes (CQAs)

The CQAs of the LNPs before lyophilisation were compared to those post lyophilisation, after being reconstituted in the same volume of nuclease-free water.

##### 4.2.7.1 Physicochemical Characterization

Particle size (Z-average diameter), polydispersity index (PDI) and zeta potential of LNPs were measured using the ZetaSizer Ultra (Malvern Panalytical Ltd., Worcestershire, UK), as detailed in section 2.2.6.1. In brief, size and PDI were measured using ZEN0040 disposable micro-cuvettes and samples were diluted to 0.1 mg/mL lipid concentration with Tris to achieve attenuation values between 7-9. For zeta potential measurements, DTS1070 folded capillary zeta cells were used; the same dilution used for size/PDI was applied but samples were diluted in ultrapure water. Z-average diameter, PDI and zeta potential results are expressed as mean  $\pm$  SD of three independent measurements.

##### 4.2.7.2 RNA Quantification

To quantify the amount of polyA or mRNA inside the LNP, RiboGreen assay was performed. The extensive procedure was outlined in section 2.2.6.2. Summarily, 50  $\mu$ L of the sample was added to the 96-well black plate in the presence and absence of 0.1 w/v% Triton X-100. The plate was incubated for 15 minutes at 37°C and then the fluorescent reagent (100  $\mu$ L) was added to the Triton (+) wells with 200x dilution and to the Triton (-) wells with 500x dilution. Fluorescence (excitation at 480 nm and emission at 520 nm) was detected using the GloMax plate reader (Promega, UK). The encapsulation efficacy (EE%) and mass balance (MB%) were calculated based on the standard curves with and without Triton to measure the “total” and “free” RNA, respectively.

##### 4.2.7.3 *In Vitro* Testing

After being lyophilised, reconstituted mRNA LNPs were transferred to HEK293 cells to measure mRNA expression along with fresh, non-lyophilised mRNA-LNPs (prepared in the same way as the lyophilised LNPs but without including the cryoprotectant) which were used as a control. After purification, the

mRNA-LNPs solutions (1 mL each) were freeze-dried following the protocol described in Table 4.3. Lyophilised LNPs were reconstituted using 1 mL of nuclease free water. HEK293 cells were cultured in minimal essential medium (MEM) supplemented with 10% fetal bovine serum (FBS), 1% penicillin/streptomycin, 1% sodium pyruvate and 2.5 mg/mL amphotericin-B. Cells were seeded at a density of  $1 \times 10^5$  cells/mL in white plates with clear bottoms. When cells reached confluency, reconstituted LNPs and fresh LNPs were added to the plates at decreasing mRNA concentrations (2  $\mu\text{g}/\text{mL}$ , 1  $\mu\text{g}/\text{mL}$ , 0.5  $\mu\text{g}/\text{mL}$ , 0.25  $\mu\text{g}/\text{mL}$ ) and, after 24 h from LNPs addition, the reagent was added and the luminescence was read using the GloMax plate reader (Promega, UK). The experiment was carried out twice for reproducibility. The full procedure was described in section 2.2.5.

#### 4.2.7.4 *In Vivo* Testing

The *in vivo* efficacy of 10 % sucrose mRNA LNPs and 10 % trehalose mRNA LNPs (post lyo) and fresh mRNA LNPs was compared. The lyophilised mRNA LNPs were reconstituted in water and diluted to the target *in vivo* mRNA concentration of 1  $\mu\text{g}/\text{mL}$  in Tris 10 mM. Three female BALB/c mice (10-12 weeks old) were injected intramuscularly with each formulation (50  $\mu\text{L}$  LNPs into each leg). To measure the bioluminescence signal at different time points (0, 6 and 24 hours after LNP injection), d-luciferin was injected subcutaneously at a dose of 150 mg luciferin/kg body weight. 10 min after the luciferin injection, mice were transferred to the IVIS chamber keeping the isoflurane level at 2% and imaged with an IVIS Spectrum *in vivo* imaging system (PerkinElmer, Buckinghamshire, UK). The images were normalised, and the bioluminescence signals were quantified using the Living Image 4.7.3 software. All animals were handled in accordance with the UK Home Office Animals Scientific Procedures Act of 1986 in accordance with an internal ethics board.

#### 4.2.7.5 mRNA Integrity

Gel electrophoresis was performed to check the mRNA integrity inside the LNPs freeze dried in the presence of cryoprotectant (10 % sucrose and 10 % trehalose). The mRNA integrity of fresh, not-lyophilised, LNPs was also analysed as a comparison. To disrupt the lipid nanoparticles, the mRNA-LNPs were diluted to 10  $\mu\text{g}/\text{mL}$  mRNA concentration in Tris 10 mM and mixed with 750  $\mu\text{L}$  ethanol and 25  $\mu\text{L}$  of 3 M sodium acetate at pH 5.2. The solution was centrifuged (twice) at 14 000 rpm for 20 min at 4°C. The supernatant was discarded, and the pellet was resuspended in 35  $\mu\text{L}$  RNAse free water and mixed with formaldehyde loading dye (1:3 v/v). The samples were heated to 70 °C for 10 minutes, cooled down to room temperature and then loaded in the agarose gel prepared in MOPS running buffer (10 mM) containing the SYBR Green Stain. The samples, the ladder and the naked mRNA were electrophoresed in a gel electrophoresis system at 90 V (Bio-Rad) and the gel was imaged using a gel doc EZ imager (Bio-Rad).

#### 4.2.7.6 Lipid Content

The Thermo Scientific Vanquish Flex Quaternary UHPLC system (Thermo Fisher Scientific, Germering, Germany) with charged aerosol detector (CAD) was used to quantify the lipid content after freeze-dry comparing the results to fresh, non-lyophilised, LNPs. The HPLC-CAD method described was based on the United States Pharmacopeia (USP) method for the identification of lipids for RP-UPLC-CAD described in the Analytical Procedures for Quality of mRNA Vaccines and Therapeutics draft guidelines (249).

##### 4.2.7.6.1 HPLC-CAD Conditions

For the CAD, the data collection rate was 2 Hz and the evaporator temperature was fixed to 35 °C. The lipids were separated using an ACE Excel SuperC18 column (90 Å pore size, 2.1 mm ID × 150 mm column) with a particle size of 2 µm from Avantor Performance Materials (Center Valley, PA). The column oven temperature was set to 60°C and the autosampler temperature to 15°C. The sample injection volume was 20 µL. Data were processed using Chromeleon Chromatography Data System software version 7.2.10.

##### 4.2.7.6.2 Mobile Phases and Sample Separation

Two mobile phases were used for this method, mobile phase A (0.1% TFA in water) and mobile phase B (50/50 IPA/MetOH with 0.1% TFA). The method started with a composition of 40 % mobile phase A and 60 % mobile phase B, followed by a gradient to 95 % mobile phase B over 8 minutes; mobile phase B was held at 95 % for 7 minutes and then decreased to the initial condition (60%) and equilibrated for 5 minutes before injecting the next sample (the total duration of the method was 21.5 minutes). The flow rate was set at 0.5 mL/min.

##### 4.2.7.6.3 Linearity Solutions Preparation and Sample Preparation

Linearity stock solutions were prepared in ethanol for each lipid (DSPC, Chol, SM-102 and DMG-PEG 2000) at 200 % of the working concentration based on the theoretical lipid concentrations (standard solution 1, SD1). The linearity stock solutions were diluted with ethanol to 60 %, 80 %, 100 %, 120 % and 140 % directly in the HPLC vials. A standard solution 2 (SD2) was also prepared by mixing SD1 and ethanol 1:1. Samples (already reconstituted in RNase free water) were prepared by diluting them with ethanol (1:10), followed by centrifugation at 10 000 rpm for 5 minutes.

##### 4.2.7.6.4 Method Evaluation: Specificity, Linearity, Precision and Concordance

Specificity was tested by injecting blanks to confirm the absence of interfering peaks; linearity was determined over the range of 60 – 140% of the working concentration. Precision was evaluated by injecting SD2 solution 5 times and concordance was determined by comparing SD2 to SD1.

## 4.3 Results

### 4.3.1 DSC and FDM Results

To design the freeze-drying cycle, samples containing the cryoprotectants were analysed using the DSC and the results were compared to a reference (an empty pan). The samples and the reference were analysed between -50 and 25°C to determine freezing and melting points. DSC provided valuable thermal data on the LNPs' behaviour, including their glass transition temperature ( $T_g$ ), freezing, and melting points, which is essential for developing an optimised freeze-drying protocol. The results in Figure 4.3A showed that, for 10 % sucrose LNPs, -19.89°C was the onset temperature at which the freezing transition began and -3.43°C was the onset temperature for the melting phase transition. Figure 4.3B shows the results for 5 % sucrose LNPs; -21.65°C and -1.90°C were the onset temperatures for the freezing and melting events, respectively. The onset temperatures for the freezing and melting events of 10 % trehalose LNPs are detailed in Figure 4.3C (-22.78°C and -2.96°C, respectively) and the phase transition events of 5 % trehalose LNPs are shown in Figure 4.3D (-24.31°C and -2.05°C, respectively).

To further investigate this, the FDM was used to know the freezing and the collapsing temperature of the samples and the physical changes of the LNP-cryoprotectant mixtures were investigated in real time. In particular, changes in the morphology were observed with the freezing (Figure 4.4B,G,L and Q), drying (Figure 4.4C,H,M and R) and collapse (Figure 4.4D, I, N and S) of the LNP-cryoprotectant solutions. In the figure, additional images of the intact LNPs before freezing (Figure 4.4A, F, K and P) and the total collapsed LNPs (Figure 4.4E, J, O and T) were included for context. The collapse temperatures were in a tight range, being -30°C for 10 % sucrose LNP (Figure 4.4D), -32°C for 5 % sucrose LNP (Figure 4.4I), -27°C for 10 % trehalose LNP (Figure 4.4N) and -26°C for 5 % trehalose LNP (Figure 4.4S).

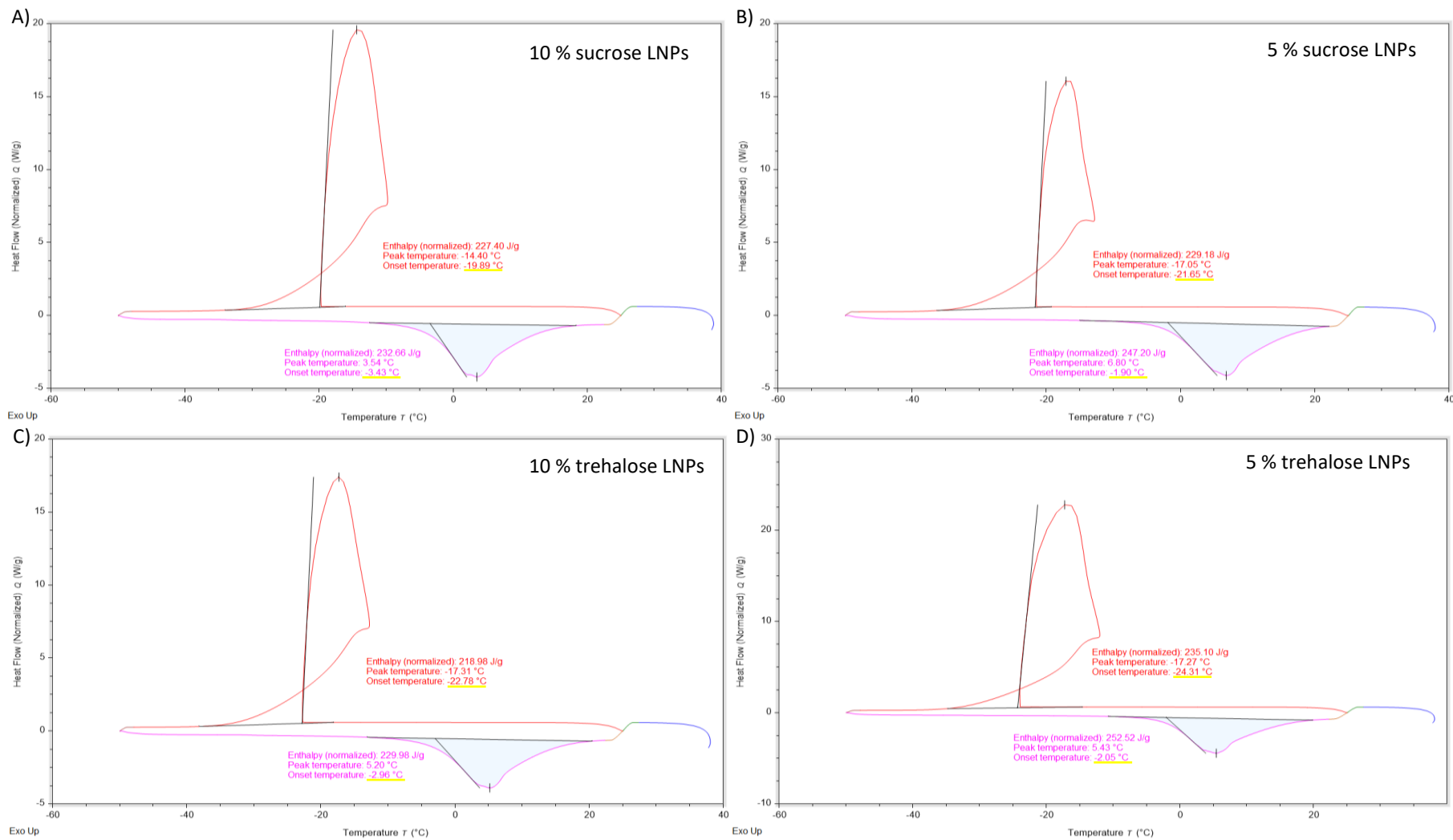


**Figure 4.3** Thermal assessment on LNP formulations. A) 10 % sucrose LNPs; B) 5 % sucrose LNPs; C) 10 % trehalose LNPs; D) 5 % trehalose LNPs. The red trace is the initial freezing cycle from 25°C to -50°C and the loop represents the freezing exotherm. The pink trace is the heating cycle from -50°C to 25°C and the endothermic event is the melting event.

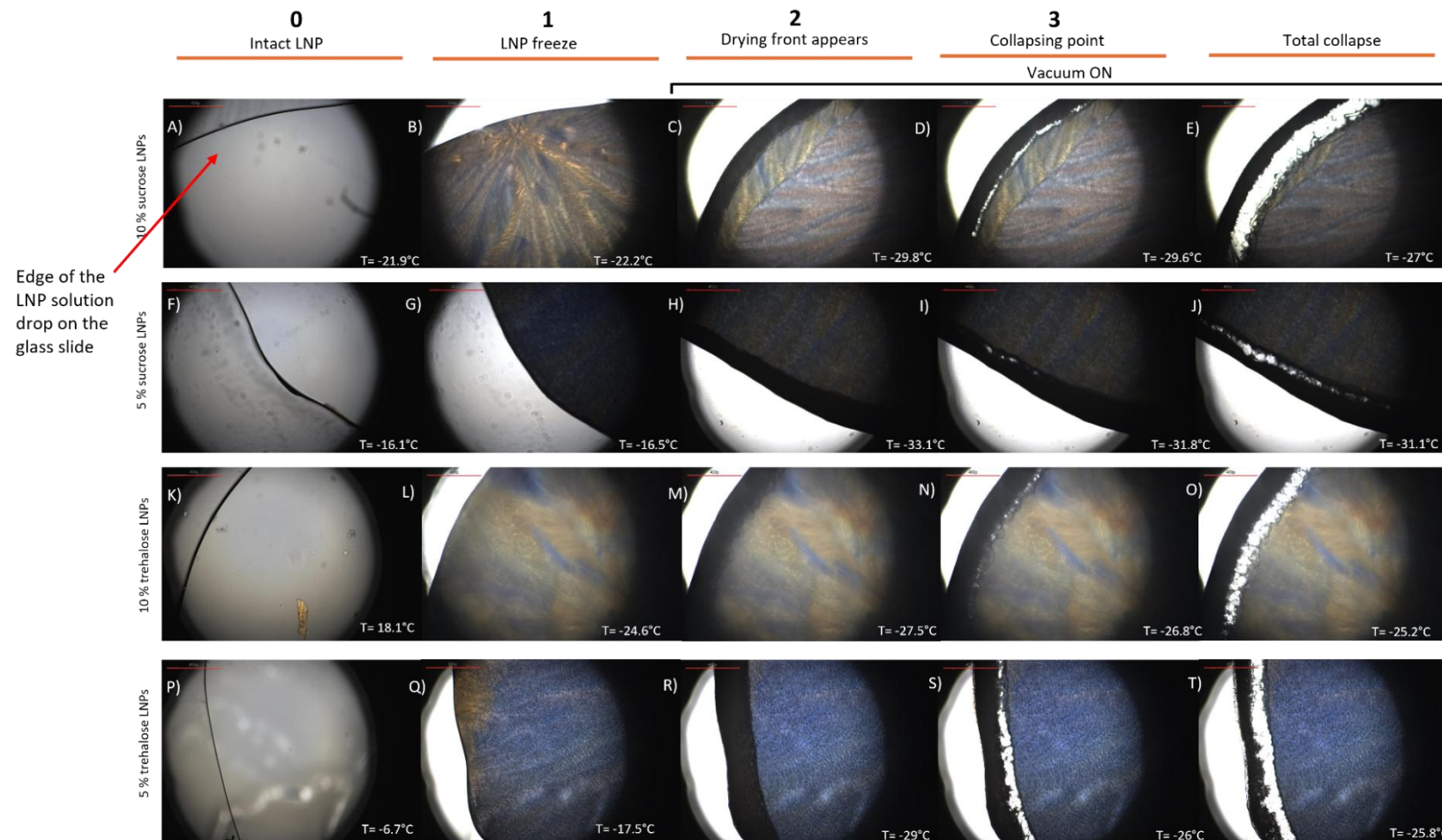


**Figure 4.4** Freeze-dried microscopy of LNPs containing different types and concentrations of cryoprotectants. Samples were frozen to  $-40^{\circ}\text{C}$  to evaluate the freezing point and, after applying a vacuum, the collapsing point. Different morphology transitions are represented for A-E) 10% sucrose LNPs, F-J) 5% sucrose LNPs, K-O) 10% trehalose LNPs, and P-T) 5% trehalose LNPs. The intact LNP images (1) show the edge of the LNP solution drop on the glass slide placed on the FDM cryostage. (2) Represents the moment when the solution froze. The drying front (3), the visible boundary between the frozen portion of the sample and the area where sublimation (drying) has occurred, begins to appear at the edge of the sample solution drop. The collapsing point (4) indicates that the structural integrity is compromised due to excessive sublimation, resulting in deformation or shrinkage. Samples were observed under a microscope at  $400\times$  magnification ( $400\times$ ).

### 4.3.2 Optimizing the Freeze-Dry Cycle Parameters

Three freeze-dry cycles were necessary to improve the characteristics of the resulting lyophilised LNPs.

#### First Cycle

Results from the DSC and the FDM were used to design the first cycle as described in Table 4.1, as primary drying temperature is based on the thermal characteristics of the formulations. The characteristics of the LNPs pre lyophilisation (“Pre lyo”) and post lyophilisation (“Post lyo”) were evaluated as shown in Figure 4.5. Independently of the type of cryoprotectant, the sizes of the LNPs after freeze-drying were double compared to their corresponding non-lyophilised (around 200 nm; Figure 4.5A). An increase in polydispersity (PDI) was also noticed, as PDI increased from  $0.1 \pm 0.01$  to  $0.17 \pm 0.04$  for 10 % sucrose LNPs and from  $0.14 \pm 0.02$  to  $0.18 \pm 0.04$  for 5 % sucrose LNPs (Figure 4.5A). Nevertheless, the most dramatic increase in PDI resulted after lyophilisation of trehalose-LNPs as the PDI of 10 % trehalose LNPs jumped from  $0.11 \pm 0.01$  to  $0.31 \pm 0.03$  and the PDI of 5 % trehalose LNPs jumped from  $0.10 \pm 0.01$  to  $0.36 \pm 0.05$  post lyo (Figure 4.5A). The zeta potential of the LNPs, independently of the cryoprotectant, became negative (ranging from 3.5 mV to -14.2 mV; Figure 4.5B). RiboGreen results showed a decrease of around 5 % and of around 14 % in encapsulation efficacy for sucrose and trehalose LNPs, respectively. Mass balance decreased at all conditions, the lowest result being that of 10 % trehalose LNPs (48 % after lyo; Figure 4.5C). Cake shrinkage was also observed, especially for the cake of the sucrose-containing LNPs (Figure 4.5D).

The lyotrace obtained from the freeze-drying process was reported in Figure 4.5E; the “Shelf Setpoint” (blue line) represent the temperature of the shelf, the “Product Probe” (yellow line) represents the temperature of the product probe, the “Chamber CM” (purple line) is the pressure set in the chamber while the “Chamber Pirani” (orange line) is the actual pressure in the chamber. It should be noted that the “Product Probe”, that has been used to monitor the temperature in the vials, refers to the temperature of a vial containing only the buffer instead of the actual product. From the lyotrace, it can be noted that, after the end of the freezing step that took ~6 hours (yellow line and blue line), the temperatures increased to -25°C and the primary drying started as the chamber CM value reached 285 mTorr (purple line). The primary drying ended after ~30 hours as the chamber CM pressure (purple line) and the Pirani pressure (orange line) converged but was extended for extra 19 hours for logistic reasons. The secondary drying started as the temperatures of both the shelf and the probe reached 25°C and the pressures decreased to 20 mTorr (duration was ~10 hours).

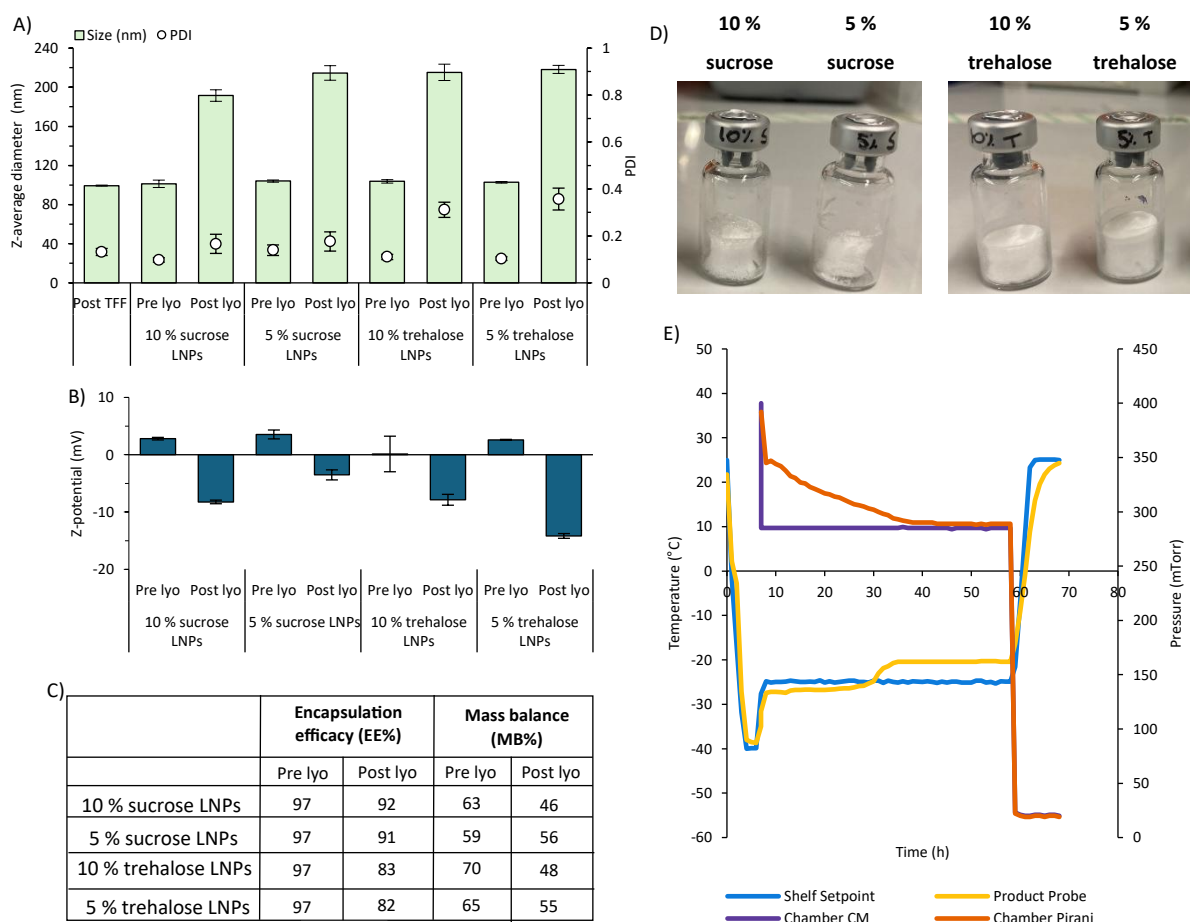


**Figure 4.5** Results of the first freeze-drying cycle. A) Size (nm) and PDI of the LNPs pre and post lyo; B) Zeta potential (mV) of the LNPs pre and post lyo; C) RiboGreen assay results pre and post lyo; D) Cake appearance in the presence of sucrose and trehalose; E) Lyotracer obtained at the end of the cycle showing the changes in temperatures and pressures mapping the freezing, primary drying and secondary drying steps.

## Second Cycle

The second cycle parameters were described in Table 4.2. In terms of physicochemical characteristics, size dimensions of sucrose-LNPs post lyo were  $133 \pm 1$  nm and  $151 \pm 1$  nm for 10 % and 5 % sucrose LNP, respectively (Figure 4.6A). The PDI was  $0.17 \pm 0.01$  for 10 % sucrose LNP and  $0.15 \pm 0.01$  for 5 % sucrose LNP (Figure 4.6A). The LNPs in trehalose showed bigger sizes ( $>170$  nm) and PDIs ( $\geq 0.6$ ) (Figure 4.6A). The zeta potential values of the sucrose-LNPs were neutral (between -11 mV and -7mV) while the zeta potential values of trehalose-LNPs were more negative (between -18 mV and -19mV) (Figure 4.6B). However, it should be noted that the zeta potential values pre lyo were already unusually negative. The RiboGreen assay results showed no big differences in the encapsulation efficacy and the mass balance between pre and post lyo samples (EE% $>90\%$ ; Figure 4.6C). The sucrose-LNP cakes resulted still slightly shrunk while trehalose-LNP cakes showed no signs of shrinkage (Figure 4.6D).

The lyotrace, shown in Figure 4.6E, gives an insight of what happened in the freeze-dryer during the cycle; vials were frozen down to  $-50^{\circ}\text{C}$  and the temperature was held for  $\sim 8$  hours (blue line represents the shelf temperature; the probe temperature was not recorded due to a failure in the equipment). The temperature was then increased to  $-25^{\circ}\text{C}$  while the CM pressure was set at 120 mTorr (purple line). The primary drying ended after  $\sim 30$  hours when the CM pressure and the pressure in the chamber (orange line) merged. However, the primary drying length was extended by 29 hours due to logistic reasons. The pressures then increased to 20 mTorr and the temperature reached  $25^{\circ}\text{C}$  to account for the secondary drying.

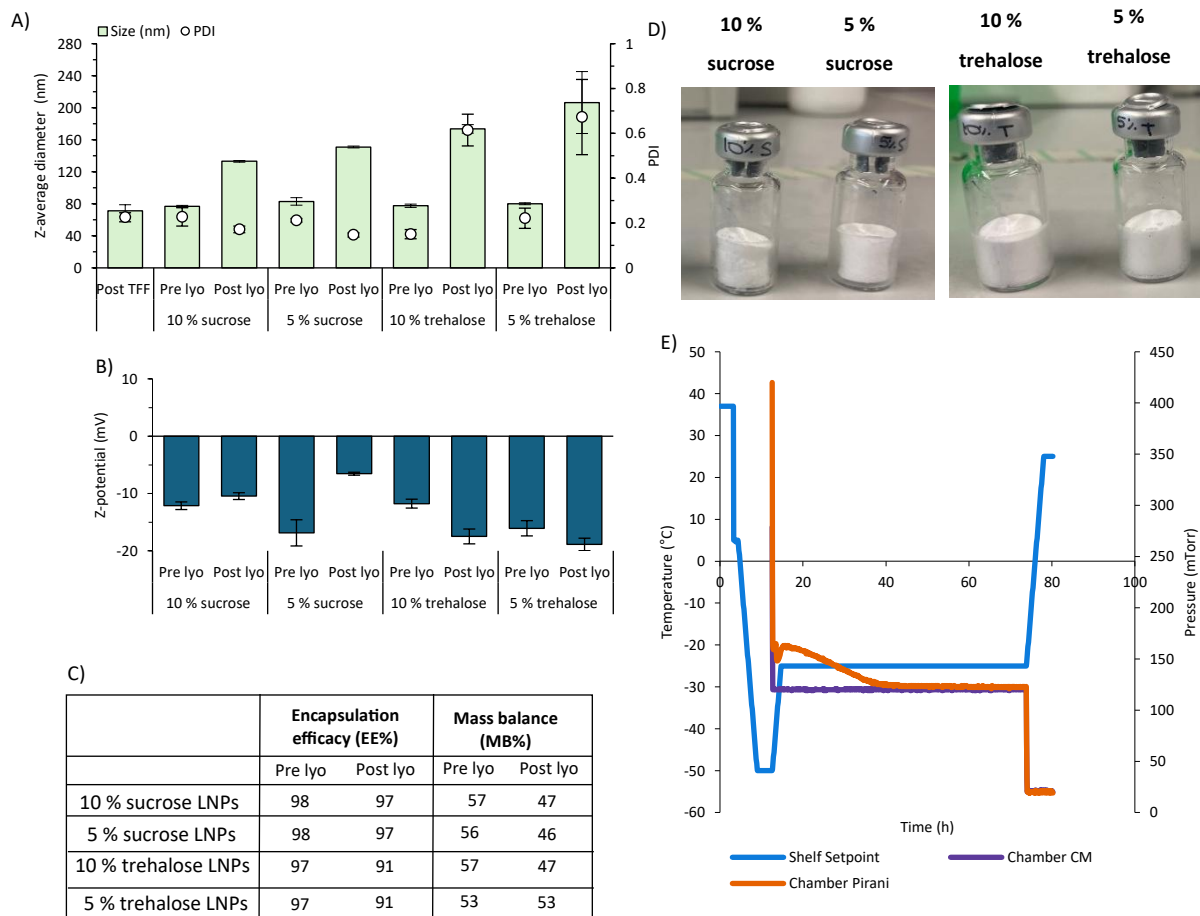
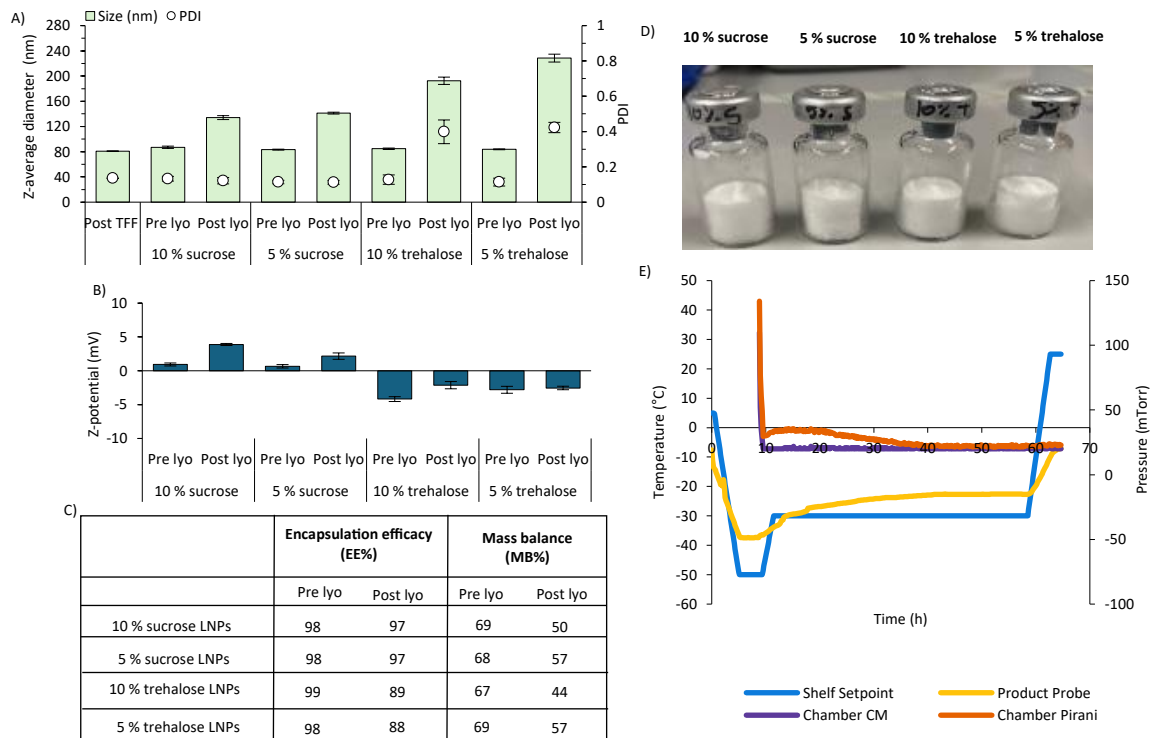


**Figure 4.6** Results of the second freeze-drying cycle. A) Size and PDI of the LNPs pre and post lyo; B) Zeta potential of the LNPs pre and post lyo; C) RiboGreen assay results pre and post lyo; D) Cake appearance in the presence of sucrose and trehalose; E) Lyotrace obtained at the end of the cycle showing the changes in temperatures and pressures mapping the freezing, primary drying and secondary drying steps. The Product Probe trace was not shown in the graph.

### Third Cycle

LNPs were lyophilised after changing the parameters of the cycle (Table 4.3). Figure 4.7A showed the size and PDIs pre and after lyophilisation. Size of sucrose-LNPs after lyophilisation was  $134 \pm 3$  nm and  $141 \pm 1$  nm for 10 % sucrose and 5 % sucrose, respectively, while PDI was around 0.11 at both conditions (Figure 4.7A). LNPs in trehalose displayed a bigger size (around 200 nm; Figure 4.7A) and PDIs  $\geq 0.4$  (Figure 4.7A). The zeta potential remained neutral after lyophilisation (ranging between 0.7 mV and -4.3 mV; Figure 4.7B). Encapsulation efficacy of sucrose-LNPs didn't decrease with lyophilisation, on the other hand, encapsulation efficacy decreased of  $\sim 10$  % for trehalose-LNPs. Mass balance decreased after lyophilisation at all conditions, with values ranging from 44 % to 57 % (Figure 4.7C). None of the cakes showed any sign of shrinkage (Figure 4.7D). The lyotrace reported in Figure 4.7E showed the changes in pressure and temperature during the process; starting from the freezing step at  $-50^{\circ}\text{C}$ , the temperature was then raised to  $-30^{\circ}\text{C}$  (blue and yellow line) while the pressure in the chamber reached 20 mTorr (purple line) during primary drying. The primary drying lasted  $\sim 30$  hours (pressure convergence represented by the purple line and orange line merging) but was extended, for logistic reasons, by 18 hours. The secondary drying was performed at  $25^{\circ}\text{C}$ , keeping the pressure constant at 20 mTorr. A lower volume of polyA LNPs (1mL) were lyophilised at the same conditions described in Table 4.3 in view of lyophilising mRNA LNPs and results are shown in Figure 4.7F-I. The same trend in the results was noticed when decreasing the samples volume: sizes increased after lyophilisation at all conditions, but LNPs in sucrose showed smaller sizes than LNPs in trehalose (Figure 4.7F). The same trend was observed for PDIs. Zeta potential remained neutral (Figure 4.7G). Cakes did not shrink during the process (Figure 4.7H) and RiboGreen results highlighted a decrease in EE % when using trehalose (while there was no encapsulation loss when using sucrose) and a general decrease in MB % (Figure 4.7I). For further studies involving mRNA, cryoprotectant concentrations of 10 % sucrose and 10 % trehalose were selected.

### TFF LNPs (2 mL volume)



### Spin column LNPs (1 mL volume)

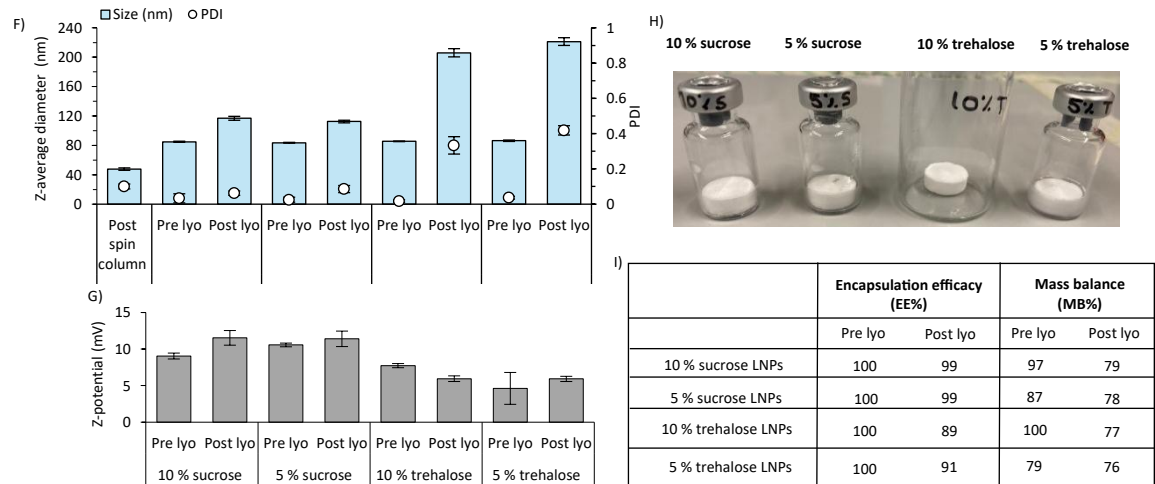


**Figure 4.7** Results of the third freeze-drying cycle. A to E represents the results for 2 mL LNPs lyophilised; A) Size and PDI; B) Zeta potential; C) RiboGreen assay results; D) Cake appearance in the presence of sucrose and trehalose; E) Lyotrace obtained at the end of the cycle. F to I represents the results for 1 mL LNPs lyophilised; F) Size and PDI; G) Zeta potential; H) Cake appearance in the presence of sucrose and trehalose; I) RiboGreen assay results.

### 4.3.3 Evaluating the *In Vitro* Expression of Lyophilised mRNA LNPs

Despite the changes in particle sizes, given that the EE% and MB% of the various LNPs remained within an acceptable range, the next step was to assess their potency. The *in vitro* expression of lyophilised

mRNA LNPs containing 10 % sucrose and 10 % trehalose was evaluated and compared to fresh LNPs (control LNPs). 1 mL of mRNA LNPs were freeze-dried following the parameters described in Table 4.3, and the physicochemical characteristics of the LNPs were evaluated in terms of size, PDI, zeta potential, encapsulation efficiency and mass balance (Table 4.4). The results of the lyophilised mRNA products were in line with those obtained for polyA LNPs (Figure 4.7F, G and I), apart from the size of the 10 % sucrose mRNA LNPs which was significantly ( $p < 0.05$ ) bigger ( $172 \pm 19$  nm; Table 4.4) than the size of the 10 % sucrose polyA LNPs freeze dried in the previous section ( $117 \pm 3$  nm; Figure 4.7F).

**Table 4.4** Physicochemical characteristics of control LNPs and mRNA LNPs post lyophilisation for *in vitro* testing. Results represent the average  $\pm$  SD of 2 independent batches.

	Z-average diameter (nm)	PDI	Zeta potential (mV)	Encapsulation efficiency (EE%)	Mass balance (MB%)
<b>Control LNPs</b>	$81 \pm 8$	$0.06 \pm 0.03$	$4.9 \pm 7$	$98 \pm 0.004$	$77 \pm 4$
<b>10 % sucrose LNPs</b>	$172 \pm 19$	$0.07 \pm 0.03$	$3.8 \pm 11$	$84 \pm 13$	$68 \pm 11$
<b>10 % trehalose LNPs</b>	$210 \pm 7$	$0.44 \pm 0.06$	$-4.2 \pm 19$	$73 \pm 8$	$71 \pm 9$

Regarding the cell response, control LNPs demonstrated having the highest luminescence values, followed by the trehalose-containing LNPs, while the sucrose-containing LNPs had the lowest response (Figure 4.8). To evaluate the integrity of the mRNA inside the LNPs, agarose gel electrophoresis was performed, and results were evaluated against the naked mRNA (Figure 4.9). The bands of the lyophilised products appeared to be lower than the naked mRNA band, suggesting a slower migration in the gel.

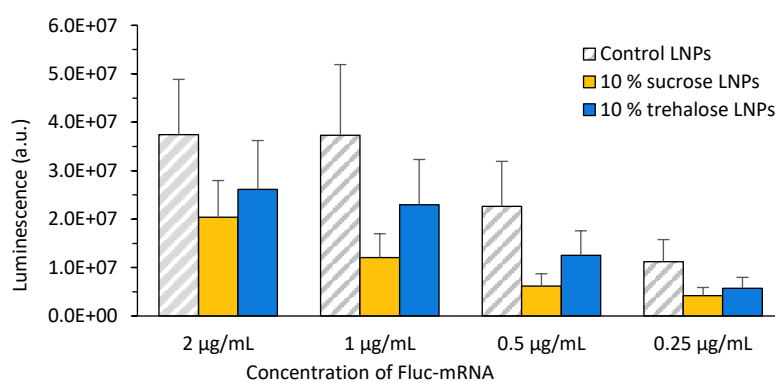


**Figure 4.8** mRNA expression results. Cells were seeded at 10 000 cells/100  $\mu$ L and, after confluency was reached, LNPs were added to the wells. Luminescence was read after 24 h from LNP addition. The results shown compare control LNPs with lyophilised LNPs (containing 10 % sucrose and 10 % trehalose). Results represents mean  $\pm$  SEM of two independent batches.

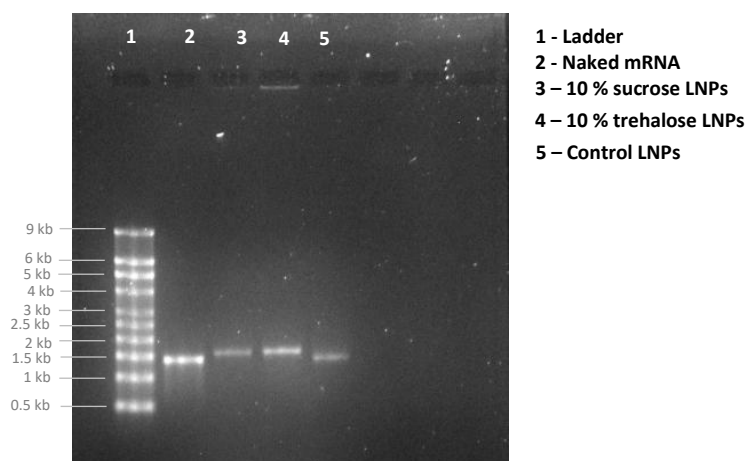


**Figure 4.9** Agarose gel electrophoresis for mRNA inside LNP. mRNA encapsulated within LNPs post lyophilisation was evaluated for stability by gel electrophoresis and compared to control mRNA LNPs.

#### 4.3.3.1 Evaluating the Lipid Content of Lyophilised mRNA-LNP

An HPLC-CAD method was developed to quantify the lipid content inside the freeze-dried vesicles and results were normalised against the control LNPs, taking the recovery measurement from each lipid (%) and dividing it by the recovery value of the control for that lipid (%). From the findings displayed in Figure 4.10 it is shown that independent of the cryoprotectant used, the recovery of each lipid included in the formulation (DSPC, Chol, SM-102 and DMG-PEG 2000) is close to the control.

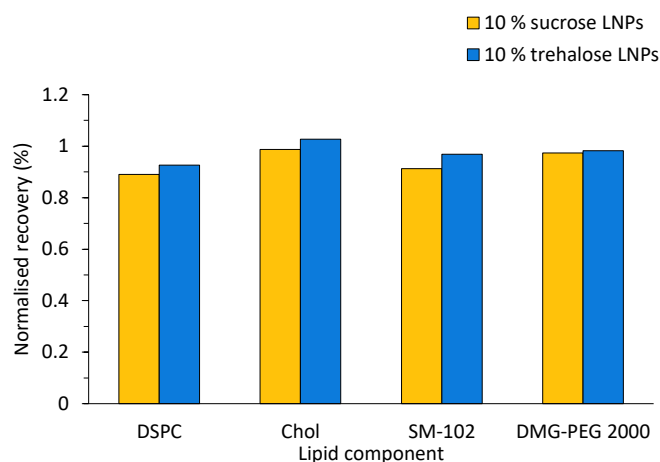


**Figure 4.10** HPLC-CAD analysis for lipid quantification. Each of the lipids included in the reconstituted product was analysed after dilution in ethanol and centrifugation to separate the lipids from the mRNA. The recovery is shown as normalised lipid recovery (%) against the corresponding lipids in the control sample.

#### 4.3.4 Evaluating the *In Vivo* Expression of Lyophilised mRNA LNP

Once the *in vitro* response was completed, the *in vivo* efficacy of the lyophilised mRNA LNPs was tested in female BALB/c mice. Each formulation was administered intramuscularly (IM), and 10 minutes after the luciferin subcutaneous injection, the bioluminescence signal was measured. Changes in the bioluminescence signal were monitored over 24 hours following LNP injection (at 0, 6, and 24-hour intervals).

*In vivo*, results showed that 6 h after administration, mice injected with the control LNPs expressed the highest bioluminescence signal, followed second by 10 % trehalose LNPs, which showed only a small reduction in the results. 10% sucrose LNPs, with significantly lower results ( $p < 0.05$ ) compared to both the control LNPs and sucrose-LNPs, expressed the lowest signal. After 24 hours, all the signals decreased, with the lyophilised formulations showing a significantly greater decrease compared to the control ( $p < 0.05$ ) (Figure 4.11A and B).

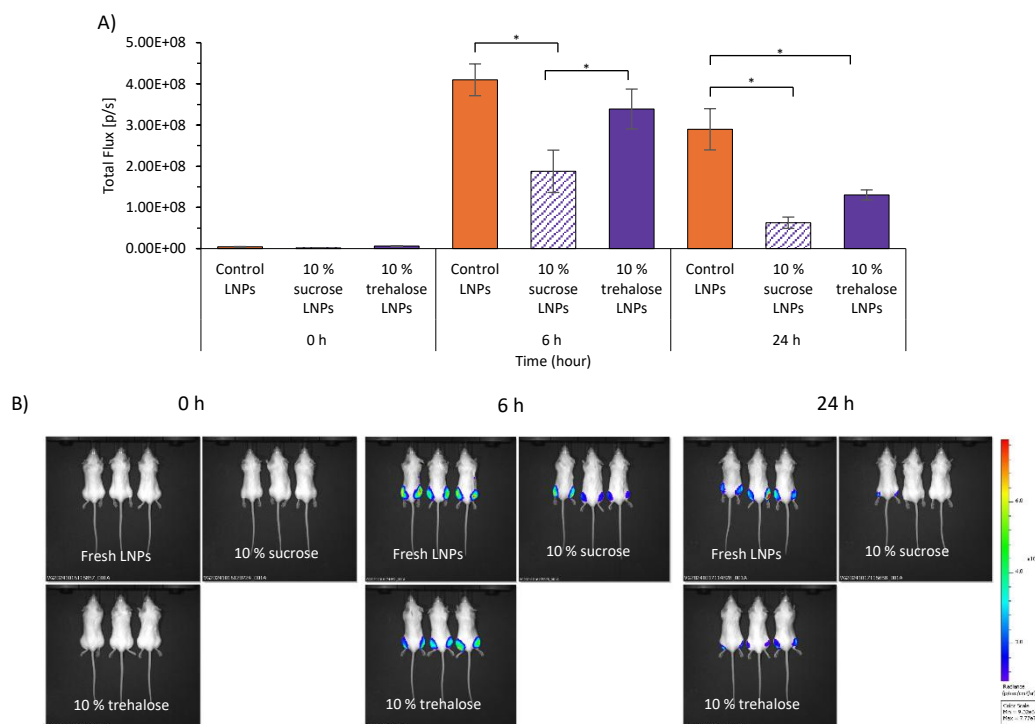


**Figure 4.11** *In vivo* results after the administration of control LNPs and lyophilised LNPs into mice. A) Quantification of the bioluminescence signal after 0h, 6h and 24h from administration. Results represent the average ( $\pm$  SEM) of the results obtained from three mice injected intramuscularly with each formulation. Statistical significance was calculated:  $p < 0.05$  (\*). B) Bioluminescence-mRNA expression IVIS images in mice at 0h, 6h and 24h after IM administration. The radiance photons colour scale is set at a minimum of  $9.32 \times 10^6$  to a maximum of  $7.77 \times 10^7$ .

## 4.4 Discussion

The building up of a freeze-dry method for LNPs has been extensively reported in this chapter. Sucrose

or trehalose were the cryoprotectants added to the formulations at increasing concentrations (5 % or 10 %) to help stabilise the particles during the process. The current mRNA vaccines on the market also contain a cryoprotectant for protection during freezing rather than lyophilisation. In particular, Moderna's Spikevax vaccine contains 8.7 m/V% sucrose (250) and Pfizer/BioNTech's Comirnaty includes 2 w/V % sucrose (251). During freeze-drying, stabilising the particles is important as freeze-drying can alter the CQAs of the nanoparticles. The process comprises of a freezing stage and two drying phases followed by reconstitution, and all these steps are known to cause stress to the formulation (242,252). The main difficulties encountered when freeze-drying LNPs are

- physical instability that results in an increase in size and/or PDI, which is often caused by partial aggregation of LNP after lyophilisation (251), and a negative shift of the zeta potential, which is considered to be one of the causes of aggregation. In their paper, Schwarz et al. (253) reported the results from the lyophilisation of solid lipid nanoparticles loaded with tetracaine and etomidate demonstrating that the entrapped drug in nanoparticles may, in some cases, influence the freeze-drying process. In particular, the presence of electrolytes (e.g., free protonated drug) in the dispersion medium reduces the zeta potential as the concentration increases. In case of LNPs, this shift towards more negative values has been partially attributed to the leakage of negatively charged mRNA molecules from the LNPs (239);
- chemical instability that manifests as reduced encapsulation of the mRNA payload and lipid components;
- decrease of efficacy, often due to aggregation upon reconstitution, as reported by Lball et al. (244), who noted a significant loss of gene silencing efficacy in HeLa cells when reconstituting LNPs with DI water.

Cake appearance could suggest, in some cases, a loss of CQAs and changes in LNP characteristics (254). Observing cake shrinkage, for example, which manifests as the cake pulling away from the walls and often the bottom of the vial, is often the first manifestation of collapse.

In this chapter, three cycles were evaluated, and at every cycle, the freeze-dry parameters were changed to improve the particles' physicochemical characteristics. A summary of the results for each cycle was described in Figure 4.13.

DSC and FDM were used to help determine from which parameters to start to design the first freeze dry cycle (Figure 4.3 and Figure 4.4). DSC provided an insight on the freezing and melting point of the formulations, while FDM was useful to know their collapsing point. All the samples (10 % sucrose LNPs, 5 % sucrose LNPs, 10 % trehalose LNPs and 5 % trehalose LNPs) started freezing between -24°C and -

20°C (Figure 4.3), melting between -2°C and -3°C (Figure 4.3) and collapsing in the range of -26°C to -32°C (Figure 4.4). To be more precise, the exothermal peak representing the “freezing” transition is the peak of the freezing of the bulk solution (heterogeneous ice nucleation) at approximately -20°C (255,256). Heterogeneous nucleation is a process in which the formation of the first small ice crystal (enough to initiate the crystallization of the entire liquid phase) is catalysed by a foreign particle instead of pure water (homogeneous nucleation). The “melting” transition refers to the ice melting, as the incorporation of cholesterol at high concentrations eliminates the phase transition temperature ( $T_m$ ) because it applies an ordering effect on the liquid phase that is defined liquid-ordered phase ( $l_o$ ) in the presence of cholesterol (257). In fact, depending on the context, cholesterol has a different role in membranes: in combination with phospholipids with low  $T_m$ , it increases the  $l_o$  by decreasing the membrane fluidity and, when it’s combined with high  $T_m$  lipids, it increases membrane fluidity. In both cases, cholesterol directs the lipids to a liquid-ordered phase (258).

Based on these results, the first cycle was developed: freezing was set at -40°C to ensure all the LNPs were completely frozen, and primary drying was set at -25°C / 285 mTorr (Table 4.1). Normally, it’s recommended a primary drying temperature 5 °C to 10 °C below collapse, but primary drying at -35 °C or lower would be very slow. Instead, the primary drying was performed at -25°C but with the pressure set equivalent to -30 °C (which is 285 mTorr) from the vapour pressure over ice chart (Figure 4.12) to prevent collapse and create a differential (of 5°C). Secondary drying was performed at 25°C / 20 mTorr.

**VAPOR PRESSURE OVER ICE CHART**

Temp			Temp		
Deg C	Vapor Pressure		Deg C	Vapor Pressure	
	mTorr	mBar		mTorr	mBar
0	4,584.00	6.111480	-50	29.500	0.039330
-2	3,883.00	5.176893	-52	23.000	0.030664
-4	3,281.00	4.374295	-54	17.900	0.023865
-6	2,765.00	3.686353	-56	13.800	0.018398
-8	2,325.00	3.099737	-58	10.600	0.014132
-10	1,949.00	2.598446	-60	8.100	0.010799
-12	1,630.00	2.173149	-62	6.160	0.008213
-14	1,359.00	1.811846	-64	4.660	0.006213
-16	1,130.00	1.506539	-66	3.510	0.004680
-18	936.80	1.248960	-68	2.630	0.003506
-20	774.40	1.032446	-70	1.960	0.002613
-22	638.20	0.850861	-72	1.450	0.001933
-24	524.30	0.699007	-74	1.060	0.001413
-26	429.40	0.572485	-76	0.780	0.001040
-28	350.50	0.467294	-78	0.570	0.000760
-30	285.10	0.380101	-80	0.410	0.000547
-32	231.20	0.308240	-82	0.290	0.000387
-34	186.80	0.249045	-84	0.210	0.000280
-36	150.30	0.200383	-86	0.150	0.000200
-38	120.60	0.160786	-88	0.100	0.000133
-40	96.30	0.128389	-90	0.072	0.000096
-42	76.70	0.102258	-92	0.049	0.000065
-44	60.80	0.081060	-94	0.034	0.000045
-46	48.00	0.063995	-96	0.023	0.000031
-48	37.70	0.050262	-98	0.015	0.000020




**Figure 4.12** Vapor pressure over ice chart (from ATS Life Sciences Scientific website). All materials exert a vapour pressure on their surroundings and the vapour pressure differential describes the tendency for particle within a solid or liquid to be freed and join the gas phase. At equilibrium, particles leaving the surface are balanced by those becoming trapped and the vapour pressure over ice table describe equilibrium condition in which sublimation doesn't occur. For this reason, there needs to be a differential between the ice leaving the product and the ice at the vapour trap.

Results from the first cycle showed that LNPs underwent drastic changes during freeze-drying, and this was anticipated by the collapsed appearance of the cakes (Figure 4.5D). Irrespective of the cryoprotectant incorporated in the formulations, all sizes were 200 nm or more (Figure 4.5A). PDI was in the acceptable range for sucrose-LNPs (between 0.14 and 0.18; Figure 4.5A) but high for trehalose-LNPs (around 0.3; Figure 4.5A). Zeta potential shifted to negative (Figure 4.5B), and both EE% and MB% decreased, especially in trehalose samples (Figure 4.5C).

To overcome these issues, the parameters were modified to generate a more conservative cycle to reduce the cake “bubbling” effect and possible collapse. In the second cycle, the parameters of the three main freeze-drying steps were modified; previous studies on liposomes (242,259) suggested that the freezing temperature is particularly important as these vesicles are sensitive to the formation of

ice crystals, and literature showed that a slow freezing rate may minimize the formation of ice crystals in the inner aqueous compartment and prevent drug leakage (260). For this reason, the ramp rate was further decreased to 0.2°C/min and the temperature adjusted to -50°C. For the primary drying, the temperature was kept at -25°C but the pressure was decreased to 120 mTorr, which is equivalent to -38°C on the vapour over ice chart (Figure 4.12). In this way, the primary drying was performed 6°C below the lowest onset of collapse (-32°C) in terms of vapour pressure (Figure 4.3A-D). As the shrinkage might have happened because the increase in temperature was too fast, the ramp rate was also slightly decreased from 0.25°C/min to 0.2 °C/min and the secondary drying was hold for 6 hours only instead of 10 (Table 4.2).

The results from the second cycle were better than those of the first cycle; the size values of the sucrose samples were smaller than the values obtained from the first cycle (between 133 and 151 nm; Figure 4.6A) while the PDIs were similar to those of the first cycle (Figure 4.6A). Trehalose samples, on the contrary, showed big sizes and high polydispersity (>170 nm and  $\geq 0.6$ , respectively; Figure 4.6A). All the zeta potential values were negative (Figure 4.6B) and there was an improvement in EE% (Figure 4.6C). The cake appearance also looked better, especially for trehalose-LNPs while sucrose-LNPs still demonstrated some signs of shrinkage (Figure 4.6D).

With the aim of optimising the cycle even further, a third cycle was designed (Table 4.3). The purpose was to make the cycle more conservative, and, to do so, the primary drying parameters were modified: the temperature was decreased to -30°C and the pressure was decreased down to 20 mTorr. With these new parameters set, the temperature differential (based on the vapour pressure over ice chart, Figure 4.12) was ~23°C. The reason behind this was to try to slow down the sublimation during primary drying because, even if a differential was created between the vapour pressure and set temperature, generally lyophilising at lower temperature slows down the process. To give an example, Suzuki et al. performed primary drying of lipid nanoparticles at very low temperature (40°C) and pressure (23 mTorr), and this extended the process time to 45 h (261). Another example is provided by Muramatsu et al. (262), who set the primary drying temperature higher, at -25°C, while simultaneously maintaining a low pressure of 23 mTorr. This created a temperature differential of 27°C, and the primary drying duration was reportedly 84 hours. In this case, the process was slow although a big differential was created, as low pressures are generally less efficient and slower at driving sublimation. The same strategy was adopted by Stitz et al. (263) who set the temperature and the pressure for primary drying at -10°C / 120 mTorr, thus creating a high differential (28°C). In this last example however, primary drying was shorter (“only” 17 hours) as the authors chose a much higher temperature which accelerated sublimation. These results suggest that the essence of a successful lyophilisation process

is striking a balance: if, on one end, lyophilising at very low temperatures slows down the process because ice turns into vapour more slowly, on the other hand, creating a big pressure differential fasten the process because the water vapour moves from the product chamber to the condenser faster. In the case of the third cycle, however, the primary drying duration was similar to that of the previous cycles (around 30 hours).

In general, this third cycle produced overall better lyophilised sucrose-LNPs, with sizes around 130nm, PDI around 0.1 (Figure 4.7A), neutral zeta potential (Figure 4.7B) and EE% results that didn't change significantly after the process (Figure 4.7C). Additionally, the cake appearance resulted to be elegant with no signs of shrinkage (Figure 4.7D). On the contrary, lyophilised trehalose-LNPs didn't show physicochemical characteristics improvements when compared to those produced previously in terms of size/PDI reduction and RiboGreen results (sizes were around 200 nm, PDIs  $\geq 0.4$  and EE% decreased of ~10 % after the process; Figure 4.7A-D).

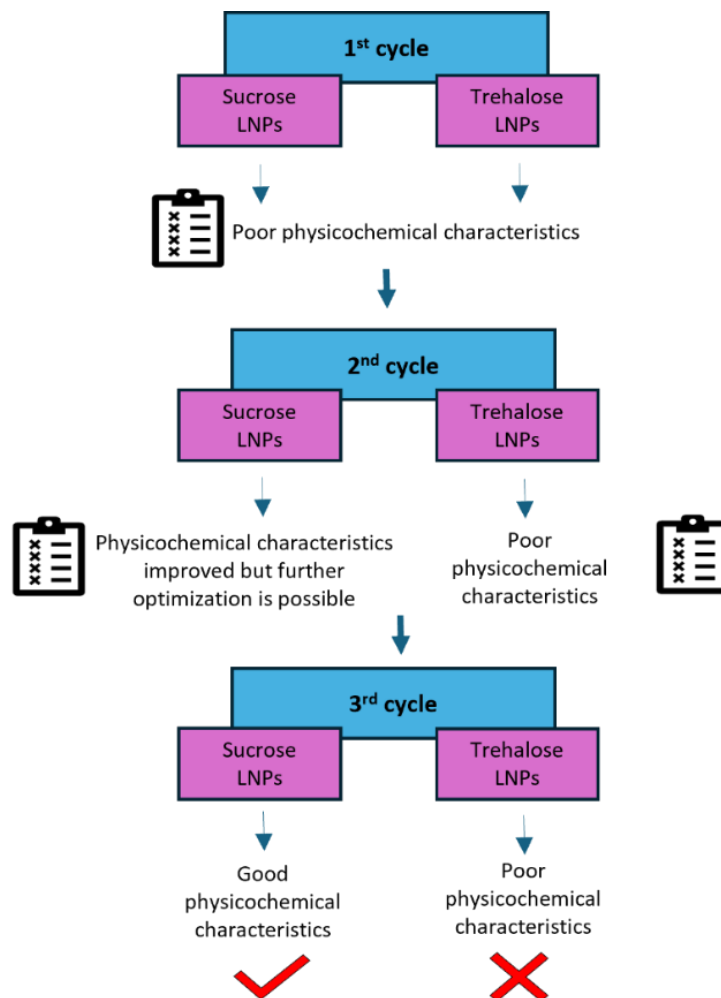


**Figure 4.13** Summary of the results of the three freeze-drying cycles. Sucrose-LNPs showed physicochemical characteristics improvements after the 2<sup>nd</sup> and 3<sup>rd</sup> cycle. On the contrary, trehalose-LNPs never maintained good CQAs after lyophilisation across all cycles.

Next, *in vitro* and *in vivo* efficacy of mRNA LNPs lyophilised according to the third cycle parameters were evaluated. For these experiments, a lower volume of sample (1 mL LNPs) was lyophilised with the aim of using less mRNA; the number of formulations tested was reduced to two: 10 % sucrose LNPs and 10 % trehalose LNPs, representing the “best” and the “worst” in terms of physicochemical attributes among the formulations previously tested. The fact that 10 % sucrose LNPs maintained good attributes after being freeze-dried aligns with the practice of considering 10 % sucrose as an optimal condition in many cases, even if the optimal cryoprotectant concentration is not fixed for every type of mRNA LNP and can vary depending on the formulation (251). For example, Kim et al. (264) demonstrated that mRNA LNPs composed of TT3, Dlin MC3-DMA, DOPE, cholesterol and DMG-PEG2000 at a molar ratio of 10:25:20:40:5 and containing 10 % sucrose (w/V) were able to maintain vaccine stability and function *in vivo* after 30 days of storage. For all the *in vitro* and *in vivo* experiments presented in this chapter, the results were compared to those of fresh (“control”) LNPs used as a reference. The characteristics of these mRNA LNPs mapped those of the respective polyA LNP (Table 4.4), even if an increase in size of around 50 nm was seen for sucrose LNPs containing the mRNA payload, resulting in a size of  $172 \pm 19$  nm. Particle size is a well-established CQA for LNPs, playing a crucial role in determining the overall quality and efficacy of the LNP formulation. Typically, LNPs used in clinic range between 50-100 nm size range when setting a phase ratio of 3:1 (aq./org.) (265). This size range can be further extended up to 150 nm, as demonstrated by Hassett et al. in their mRNA vaccine studies on the immune responses in mice and non-human primates, where LNPs with sizes up to 150 nm produced consistent results (265). However, the increase in size after lyophilisation has been observed previously in literature; for example, in a recently published paper, Wang et al. noticed an increase in size after freeze-drying of Comirnaty type LNPs and Spikevax type LNPs compared to the not lyophilised samples (251). Surprisingly, both *in vitro* and *in vivo* results revealed that trehalose-LNPs, whose physicochemical characteristics diverged significantly from typical LNP characteristics, performed better than sucrose-LNPs, whose characteristics more closely conformed to standard nanoparticle CQAs. In particular, control LNPs demonstrated having the highest cell response, followed second by trehalose-LNPs and third by sucrose-LNPs (Figure 4.8). In an attempt to explain these results, gel electrophoresis was carried out to check if the loss of mRNA integrity inside the LNPs decreased the response; however, the gel image (Figure 4.9) confirmed that the mRNA integrity inside the lyophilised samples was not compromised as the bands were well-defined (the slower migration of the mRNA bands that can be noticed in the lyophilised samples might be due to the presence of traces of the cryoprotectant that could have co-migrated with the mRNA during electrophoresis, slightly increasing the molecular weight or affecting its conformation). Moreover, the lipid profile of lyophilised LNPs was evaluated, revealing that there was no lipid loss after the process (Figure 4.10). It was then

hypothesised that the reason of the lower cell response was the structural changes that are often seen in lyophilised LNPs. In their paper, Fan et al. combined small-angle X-ray scattering (SAXS) and cryogenic transmission electron microscopy (cryo-TEM), showing that, in most lyophilised formulations, the mRNA LNPs core undergoes structural changes after lyophilisation, ranging from strong internal ordered phases, bleb structures, and highly disordered structures mixed with empty vesicles (238). The authors agreed that these structural changes could impact different aspects, such as the *in vitro* and/or *in vivo* performance and other critical parameters. The final check was injecting these formulations in mice. *In vivo*, the trend noticed *in vitro* was confirmed: when injected to BALB/c mice, control LNPs produced the highest bioluminescence signal followed by trehalose-LNPs and lastly by sucrose-LNPs, with sucrose-LNPs showing results that were significantly lower ( $p < 0.05$ ) than the other two. What is interesting to notice is that, *in vivo*, the difference in the response between control LNPs and lyophilised trehalose-LNPs was not significant, while sucrose LNPs did show a more significant decrease in response compared to fresh LNPs after 6 hours (Figure 4.11). The fact that, *in vivo*, control LNPs showed a slightly better results might be also due to their smaller size (~100 nm) compared to sucrose-LNPs (~180 nm) and trehalose-LNPs (~200 nm). In a recent paper, McMillan et al. observed that, *in vivo*, ALC-0315 LNPs in the size range of 60–120 nm outperformed LNPs with sizes >120 nm (207).

Although the CQAs, such as EE%, of the sucrose samples were optimised during the freeze-drying trial processes and yielded a formulation with favourable results, the *in vivo* performance of the sucrose-LNPs did not align with these expectations. This discrepancy highlights an important limitation of using CQAs like EE% as the principal indicators of formulation success. While EE% reflects the efficiency of encapsulation, it does not account for other crucial factors that influence the *in vivo* functionality of LNPs, such as their stability, biodistribution, and release mechanisms. For example, while mRNA encapsulation in the LNPs appeared to be efficient, the *in vivo* results suggested that other aspects, such as the LNPs ability to protect the mRNA during systemic circulation, their uptake by target cells, and the release of functional mRNA inside those cells, may play a more significant role in determining overall efficacy.

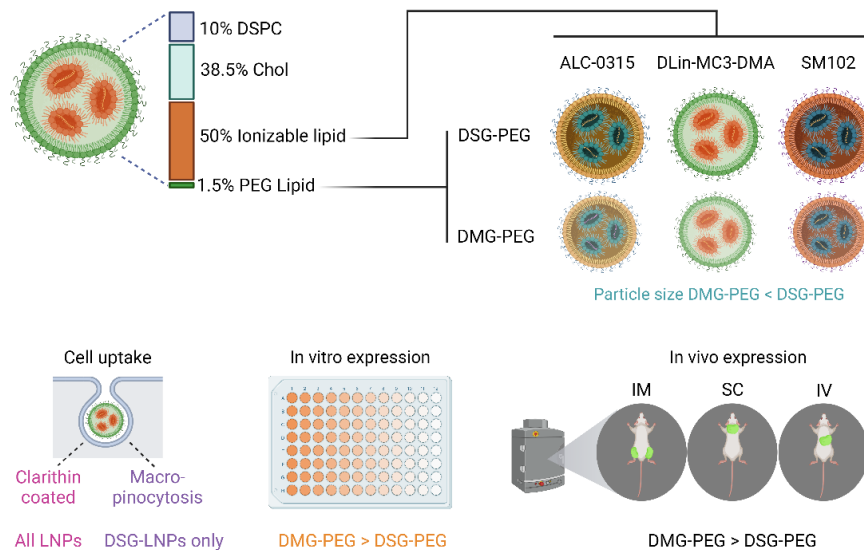
## 4.5 Conclusion

Unlike other vaccines that can be stored at room temperature or 4°C, mRNA LNPs require ultra-low temperatures to maintain their structural integrity and potency. Currently, LNP-based vaccines on the market, such as those for COVID-19 and respiratory syncytial virus (RSV), are stored frozen without undergoing lyophilisation, which presents challenges for transportation and long-term storage. To

enable storage at milder temperatures, lyophilisation is a promising approach. However, lyophilisation affects not only the structural features of nanoparticles but also their performance and stability. This chapter has extensively demonstrated that freeze-drying nanoparticles is possible if the three main stages of the process (freezing, primary drying, and secondary drying) are carefully controlled. Among the tested cycles, the most successful one involved conservative primary drying conditions characterised by low pressure, low temperature, and slow ramp rates. In addition to cycle parameters, the choice of cryoprotectant significantly impacted the formulation's outcome. While sucrose outperformed trehalose in producing nanoparticles with acceptable critical quality attributes (CQAs), trehalose-containing LNPs exhibited superior *in vitro* and *in vivo* performance after reconstitution in water. This chapter does not address all questions regarding LNP lyophilisation, such as evaluating a broader range of cryoprotectants, exploring different aqueous buffers, or understanding the impact of various lipid compositions on process outcomes and, while further optimization is required to produce lyophilised particles matching their fresh counterparts, these findings highlight that mRNA LNP lyophilisation, though challenging, is achievable. The approach presented in this chapter, which involved the experimental refinement of freeze-drying parameters across multiple cycles, provided practical insights into how lyophilisation protocols can be tailored to improve product quality, even if the final outcome was not yet fully optimised. It remains an essential strategy to explore, especially in light of the growing development of LNPs for various diseases.

# Chapter 5

## From *In Vitro* to *In Vivo*: The Dominant Role of PEG-Lipids in LNP Performance



DMG-PEG LNPs exhibit superior mRNA transfection and efficacy in vitro and in vivo, regardless of ionizable lipid or administration route. Created in <https://BioRender.com>

The data presented in this chapter are separate from the work discussed in earlier chapters and have been submitted as a paper in the European Journal of Pharmaceutics and Biopharmaceutics (under revision).

### Author Credit:

**Ankita Borah (A.B.):** conceptualisation, methodology, investigation, visualisation, formal analysis, software, validation, data curation, original draft preparation, review and editing.

**Valeria Giacobbo (V.G.):** conceptualisation, methodology, investigation, visualisation, formal analysis; software, validation, data curation, original draft preparation, review and editing.

**Yvonne Perrie (Y.P.):** conceptualisation, methodology, investigation, visualisation, formal analysis; resources, supervision, review and editing, project administration, funding acquisition.

All experimental work was conducted jointly by Dr. Ankita Borah and myself, with both of us contributing equally.

## 5.1 Introduction

Lipid nanoparticles (LNPs) are typically composed of four main lipid components: distearoylphosphatidylcholine (DSPC), an ionisable lipid, cholesterol and a PEG-lipid (266). Among these, the ionisable lipid (approximately 50% of the LNP composition) plays a critical role, facilitating nucleic acid complexation within the LNPs. First described by Semple et al. in 2001 for nucleic acid delivery (267), ionisable lipids are designed to change charge in response to the solution's pH, enabling the formation of particles that encapsulate the nucleic acid payload. In an acidic pH, these lipids acquire a positive charge, enabling high encapsulation efficiency of the negatively charged nucleic acids. During the particle formation process, the pH is subsequently raised, neutralising the ionisable lipid, rendering it more hydrophobic and thereby driving the ionisable lipid with mRNA into the interior of the lipid nanoparticles. As a result of this process, the potency of an LNP formulation is often reported to be linked to its pKa, with the most effective ionisable amino lipids having a pKa of around 6.5 (268). Currently, lipid nanoparticle-based mRNA products approved for human use include Comirnaty™ (269), SpikeVax™ (270,271), and mRESVIA® (272), all of which are vaccines administered via the intramuscular route. In contrast, Onpattro® is an LNP-based RNA interference therapeutic used to treat hereditary transthyretin-mediated amyloidosis and is given via the intravenous route. In terms of choice of ionisable lipid, Comirnaty™ uses ALC-0315 (4-hydroxybutyl) azanediy)bis (hexane-6,1-diyl)bis(2-hexyldecanoate), SpikeVax™ and mRESVIA® incorporates SM-102 (heptadecan-9-yl 8-((2-hydroxyethyl) (6-oxo-6-(undecyloxy) hexyl) amino) octanoate) and DLin-MC3-DMA (heptatriaconta-6,9,28,31-tetraen-19-yl-4-(dimethylamino)butanoate) is the ionisable lipid contained in Onpattro®. All three ionisable lipids have a common structure: an ionisable amine head group, a linker group, and hydrophobic tails, the latter of which confers a characteristic conical shape to the lipid. This conical shape is reported to facilitate LNP transfection to cells, as the broad shape of the tail region disrupts the endosomal membrane, rendering it easier for the mRNA to enter the cytosol (273).

Whilst representing only a small (1.5%) proportion of the lipid formulation, PEG-lipids are another essential component of LNP formulations, providing stability by improving the hydrophilicity of the LNPs (274,275). During LNP formation, PEG-lipids orientate with their hydrophilic head groups at the LNP exterior, improving the stability of LNPs during synthesis and storage and preventing LNP aggregation. However, the so-called “PEG dilemma” is based on the double effect that PEG can have on the fate of nanoparticles *in vivo*: PEGylation of particles can be used to extend the *in vivo* circulation time of particles by reducing particle opsonisation and clearance by the monophagocytic system. However, it can also decrease endosomal escape and LNP internalisation (276). Therefore, to overcome the “PEG dilemma”, LNP formulations generally include a low amount of PEGylated lipid (e.g., 1-2%)

(276,277). However, to address the “PEG dilemma” effectively, it is essential to consider the desorption dynamics of PEG-lipids. PEG desorption refers to the process by which PEG-lipids detach from the surface of lipid nanoparticles, a necessary step to expose the nanoparticle surface for interactions with proteins, which facilitates cellular uptake and transfection while maintaining a balance between stability and functional delivery. PEG desorption is influenced by the length of the hydrophobic carbon tails, with the rate of PEG desorption being inversely proportional to the length of the PEG-lipid hydrophobic anchor (278). PEGs with short lipid chains, such as DMG-PEG (C14), quickly dissociate in serum and are replaced by protein corona, including the liver-specific ApoE (279). The combination of the dissociation of PEG and rapid protein corona formation leads to improved LNP internalisation and expression.

Among the approved LNP formulations on the market, those designed for vaccination are administered intramuscularly into the deltoid muscle (269,280), whilst those designed for therapy (i.e. Onpattro®) are administered via intravenous infusion (281). For liver-targeting LNPs, intravenous administration is preferred since the liver is the primary organ of LNP accumulation (282). Nevertheless, liver accumulation also follows intramuscular administration (283,284). In fact, following intramuscular administration, mRNA-LNPs express at the injection site, the liver and draining lymph nodes (285,286), while mRNA-LNPs injected subcutaneously are generally retained at the site of injection (287). This suggests that the choice of PEG lipids with different alkyl chain lengths is crucial in LNP design and should be considered in combination with the route of administration.

### **5.1.1 Aim and Objectives**

This chapter investigated the influence of PEG lipid alkyl chain length on the physicochemical characteristics and performance of mRNA-loaded LNPs across different administration routes. In addition to the contribution of the PEGylated lipid, the impact of the ionisable lipid (ALC-0315, DLin-MC3, and SM-102) was also evaluated. This work intends to be a resource for choosing an ionisable lipid/PEG-lipid combination, depending on the administration route and the target site. To achieve this, the objectives were to:

- Investigate the physicochemical characteristics of the LNPs, including size, polydispersity index (PDI), zeta potential, encapsulation efficiency, and mRNA integrity, to determine the impact of chain length on these parameters.

- Evaluate the *in vitro* fate of these Fluc-mRNA ionisable lipids (ALC-0315, DLin-MC3, and SM-102)/DSG-PEG and DMG-PEG LNPs on HeLa cells by performing mRNA expression and their mechanism of endocytic uptake.
- Investigate the *in vivo* efficacy of the Fluc-mRNA ionisable lipids (ALC-0315, DLin-MC3, and SM-102)/DSG-PEG and DMG-PEG LNPs through three different routes of parenteral administration (intramuscular, subcutaneous, and intravenous).

## 5.2 Materials and Methods

### 5.2.1 Materials

The PEG-lipids 1,2-distearoyl-rac-glycero-3-methylpolyoxyethylene (DSG-PEG 2000) and 2-dimyristoyl-rac-glycero-3-methoxypolyethylene glycol-2000 (DMG-PEG-2000) were purchased from Avanti Polar Lipids (Alabaster, AL, USA) while 1,2-distearoyl-sn-glycero-3-phosphocholine (DSPC) was purchased from Lipoid (Ludwigshafen, Germany). The ionisable lipids (4-hydroxybutyl) azanediyl)bis (hexane-6,1-diyl)bis(2-hexyldecanoate) (ALC-0315), (heptatriaconta-6,9,28,31-tetraen-19-yl-4-(dimethylamino)butanoate) (DLin-MC3-DMA) and (heptadecan-9-yl 8-((2-hydroxyethyl) (6-oxo-6-(undecyloxy) hexyl) amino) octanoate) (SM-102) were purchased from Broad Pharm, USA. EZ-Cap-modified firefly luciferase-mRNA (5-moUTP) was acquired from APExBIO (USA). Polyadenylic acid (PolyA), citric acid, sodium citrate tribasic dihydrate, Triton X-100 and cholesterol were purchased from Sigma Aldrich (St. Louis, MO, USA). Agarose, MOPS 10 X, Millennium RNA marker and RNase-free PBS 10X were purchased from Invitrogen. Quant-iT Ribogreen RNA assay, 1,1-dioctadecyl-3,3,3,3-tetramethylindotricarbocyanine iodide (DiR), formaldehyde loading dye, SYBR green stain II and sodium acetate were procured from Thermo Fisher Scientific (MA, USA). Other chemicals were used at analytical grade and an in-house system provided RNA-se free water. DMEM cell culture media, TrypLE express, and L-glutamine were purchased from Gibco Life Technologies. Antibiotics penicillin/streptomycin and amphotericin B were purchased from Sigma Aldrich. The One-Glo Luciferase assay system and Vivo Glo Luciferin were bought from Promega. Endocytic pathway inhibitors chlorpromazine hydrochloride, cytochalasin D, and filipin complex ready-made solution were purchased from Sigma Aldrich. NucBlue live-ready probe was purchased from Invitrogen. All other chemicals were of analytical grade.

### 5.2.2 Fluc-mRNA Ionisable Lipid/DSG-PEG and DMG-PEG LNPs Preparation

All formulations were manufactured by mixing an aqueous phase containing Fluc-mRNA dissolved in 50 mM citrate buffer/pH 4.0 with an organic phase containing the lipids dissolved in ethanol at a concentration of 5 mg/mL. The two phases were mixed in a NanoAssemblr Ignite (Precision NanoSystems Inc., Vancouver, BC, Canada) at an aqueous/organic phase ratio of 3:1 and a total flow rate of 12 mL/min. The ratio between the amine groups on the ionisable and the phosphate groups on the mRNA (N:P ratio) was 6:1 for all the formulations. LNPs were composed of the ionisable lipid (ALC-0315, DLin-MC3, or SM-102), cholesterol, DSPC, PEG-lipid (DSG-PEG 2000 or DMG-PEG 2000) at a ratio of 50:38.5:10:1.5 mol %, respectively. For the *in vitro* endocytic pathway study, the ionisable lipid/DSG-PEG and DMG-PEG LNPs were labelled using the fluorescent dye DiR dissolved in the organic phase solution at a concentration of 1 % and poly A was used as a payload. After manufacturing, the resulting LNP suspension was purified using the 100kDa MWCO Amicon® Ultra Centrifugal filters to concentrate the LNPs and buffer exchange with PBS (10 mM) at pH 7.4.

### 5.2.3 Characterisation of Fluc-mRNA Ionisable Lipid/DSG-PEG and DMG-PEG LNPs

Particle size (nm), polydispersity index (PDI) and zeta-potential (ZP) were measured by dynamic light scattering (DLS) using a Zetasizer Nano ZS (Malvern P analytical Ltd., Worcestershire, UK) at 25 °C. LNPs were diluted to approximately 0.1 mg/mL lipid concentration in PBS (10 mM) to measure the size and PDI. The zeta potential was measured using a disposable folded capillary zeta cell using 1 mM PBS. All measurements were undertaken in triplicate. The Quant-iT RiboGreen RNA assay was used to calculate the encapsulated mRNA according to the manufacturer's protocol. The samples were diluted to about 750 ng/mL final mRNA concentration in TE buffer in the presence or absence of 2 % Triton X-100 buffer, and the plates were incubated for 15 minutes at 37 °C. Following the addition of the RiboGreen reagent at 1:200 and 1:500 to the Triton (+) and Triton (-) wells, respectively, the fluorescence was measured using a microplate reader (Promega Corporation, Madison, WI) at 485 nm excitation and 525 nm emission wavelength. The encapsulation efficiency was calculated using the following equation (1).

$$\text{Encapsulation efficiency (EE\%)} = \frac{\text{Total mRNA} - \text{Unencapsulated mRNA}}{\text{Total mRNA}} \times 100\%$$

The total mRNA concentration was based on Triton (+) results, and the unencapsulated mRNA was based on Triton (-) standard curve results.

#### **5.2.4 mRNA Extraction and Gel Electrophoresis**

The integrity of the mRNA strand inside the LNPs was confirmed by performing the agarose gel electrophoresis as previously described (288). Samples (200  $\mu$ L) were diluted to 10  $\mu$ g/mL mRNA concentration in PBS (10 mM) and centrifuged at 14,000 rpm for 20 min at 4 °C after the addition of 750  $\mu$ L ethanol and 25  $\mu$ L of 3 M sodium acetate at pH 5.2. Ethanol precipitation and centrifugation were repeated twice. mRNA pellets were resuspended in 35  $\mu$ L RNase free water and mixed with formaldehyde loading dye (1:3 v/v). The samples were heated to 70 °C for 10 min to denature and cooled down to room temperature, followed by loading in a 1 % agarose gel prepared in MOPS buffer (10 mM) containing the SYBR Green Stain. All samples, positive control, and the RNA ladder were electrophoresed in a gel electrophoresis system at 90 V (Bio-Rad). The gel was imaged using a gel doc EZ imager (Bio-Rad).

#### **5.2.5 Cell Culture Maintenance**

HeLa cells were used for the *in vitro* cell-based experiments, including the determination of the endocytic pathway and mRNA transfection studies. The cells were grown in Dulbecco's Modified Eagle Medium supplemented with 10 % fetal bovine serum, 1 % L-glutamine, 1 % penicillin/streptomycin, and 2.5  $\mu$ g/mL of amphotericin-B in a 5 % CO<sub>2</sub> humidified 37 °C incubator until confluent. The cells were passaged and seeded at the desired concentration for the respective cell-based experiments when they reached 80 % confluency.

#### **5.2.6 Determining the Endocytic Uptake Route of DiR-Labelled Ionisable Lipid/DSG-PEG and DMG-PEG LNPs Using Pharmacological Inhibitors**

To determine the endocytic pathway involved in the internalisation of different LNPs, confocal microscopy analysis was conducted (289) with slight modifications. Briefly, 25,000 cells/500  $\mu$ L were seeded in a glass-bottom confocal dish and grown till confluent. The following day, the cells were pre-treated with the pharmacological inhibitors' chlorpromazine hydrochloride, cytochalasin D, and filipin complex at the concentrations of 20  $\mu$ g/mL, 10  $\mu$ g/mL, and 2  $\mu$ g/mL respectively, and incubated for 40 minutes at 4 °C. After the incubation period, poly A encapsulated DiR-labelled ionisable lipid/DSG-PEG and DMG-PEG LNPs were added to the cells at 100  $\mu$ g/mL concentration and left for 24 hours at 37°C incubator. The next day, the LNPs were aspirated and washed with PBS to remove the inhibitors and

the non-internalised LNPs. Nuc Blue live-ready probes were added to the cells for 30 minutes to stain the nucleus. The stain was removed, followed by adding PBS and imaged under the LEICA SP8 confocal microscope using the 63 X oil-immersion objective lens. The excitation/emission wavelength of DiR and Nuc Blue live-ready probes used in the confocal microscope are 754 nm/778 nm and 360 nm/460 nm, respectively. In parallel to the endocytic pathway investigation, we also conducted cellular uptake of the LNPs at 37°C as a control.

### **5.2.7 *In Vitro* mRNA Expression Study**

An *in vitro* luciferase assay system was employed to determine the transfection efficiency of various Fluc-mRNA ionisable lipid/DSG-PEG and DMG-PEG LNPs. In a 96-well clear bottom white plate, 10,000 cells/100 µL were seeded and grown to confluence. The confluent cells were treated with LNPs at Fluc-mRNA concentrations of 2 µg/mL, 1 µg/mL, 0.5 µg/mL, and 0.25 µg/mL, prepared in DMEM media, and incubated for 24 hours. The following day, ONE-Glo luciferase reagent (100 µL) was added to the cells, mixed, and left for 3 minutes to ensure complete cell lysis before measuring luminescence using a microplate reader (Promega, Glo Max® Discover Microplate reader).

### **5.2.8 *In Vivo* Biodistribution Studies by IVIS**

The biodistribution studies of the different Fluc-mRNA ionisable lipid (ALC-0315, DLin-MC3, and SM-102)/DSG-PEG and DMG-PEG LNPs were investigated by three different parenteral routes of administration, i.e. intramuscular (IM), subcutaneous (SC), and intravenous (IV). Female BALB/c mice 7-10 weeks old, weighing between 18-21 grams, were used in the study and handled as per the UK Home Office Animals Scientific Procedures Act 1986, an internal ethics board at the University of Strathclyde, and a UK government-approved project and personal licence. The animals were divided into 18 groups (n=3) based on the six LNP types and the three routes of administration for each LNP type. Fluc-mRNA expression was assessed by bioluminescence on the luminescence filter using the IVIS Spectrum (Perkin Elmer).

The mice were injected with a mRNA dosage of 5 µg per 50 µL of the LNPs. For the IM route, the mice were injected on both the flanks (50 µL each leg), while the SC injection (50 µL) was administered in the loose skin of the neck, and finally, the IV injection (50 µL) via lateral tail vein. After an hour of LNP injection, mice received D-luciferin prepared in sterile PBS (30 mg/mL working concentration) at a dose rate of 150 mg/kg and were injected subcutaneously. After 10 minutes of D-luciferin injection, the

mice were imaged for bioluminescence signal. Bioluminescence imaging was repeated at time points 6 h, 24 h, and 48 h, and during the imaging period, the mice were kept under 3 % anaesthesia. All the animal experiments were conducted three times independently. For the data analysis, Living Image software was used to calculate the total flux from the muscle site and liver for the IM route, the subcutaneous region on the mouse neck for the SC route, and the liver and tail for the IV injection route for analysing the luciferase expression.

The *in vivo* micro-CT imaging of each route of administration was evaluated for one of the LNPs (SM-102/DMG-PEG LNPs) using the Quantum GX2 micro-CT imaging system. The mice were injected with the LNPs at the same mRNA dose via each parenteral route. Six hours later, D-luciferin was injected subcutaneously at the recommended dose rate, as mentioned. The mouse was imaged for bioluminescence on the IVIS Spectrum, followed by *in vivo* micro-CT imaging on the Quantum GX 2 with the following parameters (voltage= 90 kV; current= 88  $\mu$ A; radiation dose= 24 mGy; Fov= 72 mm; Voxel size= 144  $\mu$ m; X-ray filter=Cu 0.06+ Al 0.5; scan acquisition time= 8 sec $\times$ 3) to capture the micro-CT images. Images were processed and analysed by overlapping the bioluminescence images from the IVIS and micro-CT images from the Quantum GX 2 to get a 3D biodistribution.

### 5.2.9 Statistical Analysis

Statistical analysis was performed using GraphPad Prism 10.2.1. Data is represented as a mean of three independently conducted experiments, including LNP characterisation, *in vitro* mRNA transfection, and *in vivo* biodistribution studies. Two-way ANOVA was performed wherever applicable for all the above experiments using Sidak's and Tukey's multiple comparison method for the *in vitro* expression and *in vivo* mRNA expression respectively, and the statistical significance value was set to \*P-value < 0.05.

## 5.3 Results

### 5.3.1 LNPs Physicochemical Characterisation – The Impact of PEG-Lipid

The physico-chemical characteristics of various LNPs prepared with PEG-lipids of different chain lengths (DSG-PEG 2000 and DMG-PEG 2000) were initially investigated. LNPs were prepared with DSPC, cholesterol, an ionisable lipid (ALC-0315, DLin-MC3, or SM-102) and either DSG-PEG or DMG-PEG 2000 and DLS was used to measure size (Z-average), polydispersity (PDI), and zeta potential (ZP). As shown

in Table 5.1, all the formulations resulted in LNPs of approximately 70 - 90 nm in size with a PDI  $\leq$  0.05. In general, LNPs incorporating DMG-PEG were approximately 10 nm smaller than their DSG-PEG counterparts and particle sizes following the ALC-0315<SM012<DLin-MC3 trend. For all formulations, the LNPs were near neutral in charge with high mRNA encapsulation efficiency (>90%) (Table 5.1). Gel electrophoresis also confirmed similar mRNA loading and integrity inside the 6 LNP formulations (Figure 5.1).

**Table 5.1** Physicochemical characterisation of Fluc-mRNA ionisable lipid/DSG-PEG and DMG-PEG LNPs. Results are expressed as the mean  $\pm$  SD, n = 3.

PEG lipid	Ionisable lipid	Z-average diameter (nm) $\pm$ SD	PDI $\pm$ SD	Zeta Potential (mV) $\pm$ SD	Encapsulation Efficiency (%) $\pm$ SD
DSG-PEG 2000	ALC-0315	84 $\pm$ 6	0.02 $\pm$ 0.01	-5.3 $\pm$ 3	96 $\pm$ 3
	DLin-MC3	91 $\pm$ 3	0.03 $\pm$ 0.04	-4.5 $\pm$ 2	94 $\pm$ 5
	SM-102	88 $\pm$ 6	0.02 $\pm$ 0.01	4.6 $\pm$ 1	97 $\pm$ 3
DMG-PEG 2000	ALC-0315	69 $\pm$ 1	0.03 $\pm$ 0.02	-2.9 $\pm$ 4	94 $\pm$ 7
	DLin-MC3	80 $\pm$ 3	0.03 $\pm$ 0.01	2.6 $\pm$ 7	93 $\pm$ 3
	SM-102	75 $\pm$ 2	0.05 $\pm$ 0.02	7.2 $\pm$ 4	97 $\pm$ 3

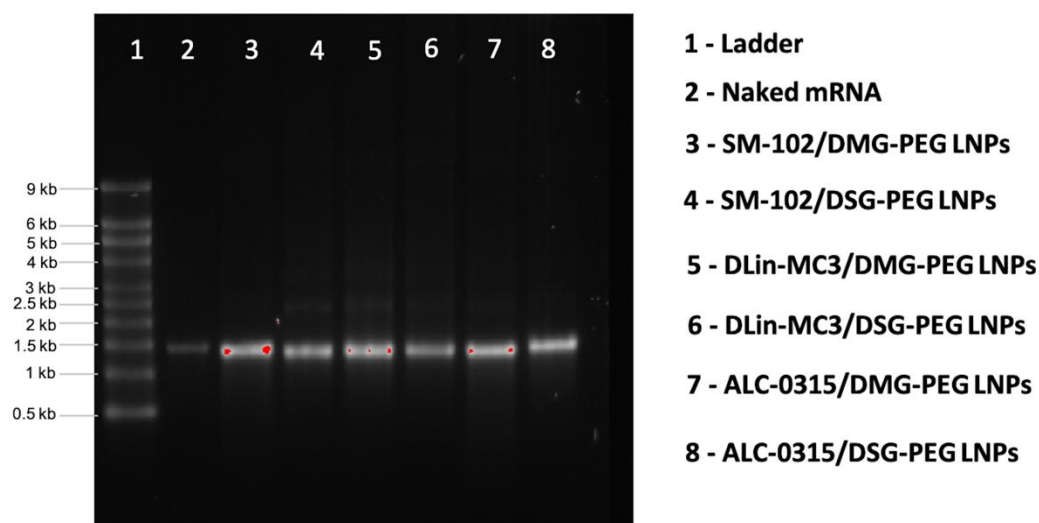


**Figure 5.1** Agarose gel electrophoresis for Fluc-mRNA inside the LNPs to identify mRNA integrity. The LNPs were disrupted by centrifugation after adding ethanol and sodium acetate. mRNA pellets were mixed with formaldehyde loading dye, and mRNA strand lengths were confirmed by agarose gel electrophoresis in 1X MOPS buffer containing the SYBR Green Stain.

### 5.3.2 Endocytic Pathway for LNPs Incorporating DSG-PEG or DMG-PEG

To investigate the endocytic uptake of LNPs incorporating either DSG-PEG (Figure 5.2) or DMG-PEG LNPs (Figure 5.3), HeLa cells were initially subjected to endocytic pharmacological inhibitors. LNPs were prepared with ALC-0315 (**panel I**), DLin-MC3 (**panel II**) or SM-102 (**panel III**). Cells were either untreated (control; **a-c**) or treated with chlorpromazine hydrochloride (**d-f**), cytochalasin D (**g-i**), and

filipin complex (j-l) as the endocytic inhibitors to block the three different endocytic pathway mechanisms, namely clathrin-mediated, macropinocytosis, and caveolae-mediated respectively, that are commonly involved in the internalisation of various nanoparticles.

In general, untreated/control cells incubated with DSG-PEG LNPs (Figure 5.2; I-III, panel a-c) had lower LNP internalisation than the DMG-PEG LNPs (Figure 5.3; I-III, panel a-c), suggesting the choice of PEG lipid impacts on cell uptake, irrespective of the ionisable lipid used. Furthermore, LNPs prepared using DLin-MC3 showed lower uptake in untreated/control cells than LNPs prepared using ALC-0315 or SM-102 (Figure 5.2 and Figure 5.3; I-III, panels a-c). When considering the various pre-treatment of cells, no cellular internalisation was observed for any of the six different LNPs in the chlorpromazine-treated cells, suggesting that inhibiting clathrin-mediated uptake blocks LNP uptake (Figure 5.2 and Figure 5.3; I-III, panels d-f). When considering cytochalasin D pre-exposed cells (Figure 5.2 and Figure 5.3; panels g-i), a reduction in DSG-PEG LNP uptake is seen compared to the untreated/control cells (Figure 5.2; panels a-c). In contrast, DMG-PEG LNPs did not show any such inhibition in cellular uptake (Figure 5.3; panels g-i). This suggests that inhibiting macropinocytosis uptake reduces DSG-PEG LNP uptake but not DMG-PEG LNP uptake. Finally, pre-treatment of cells with filipin complex did not inhibit LNP internalisation by the HeLa cells irrespective of their formulation, suggesting caveolae-mediated uptake is not an intracellular uptake route exploited by LNPs (Figure 5.2 and Figure 5.3; panels j-l).

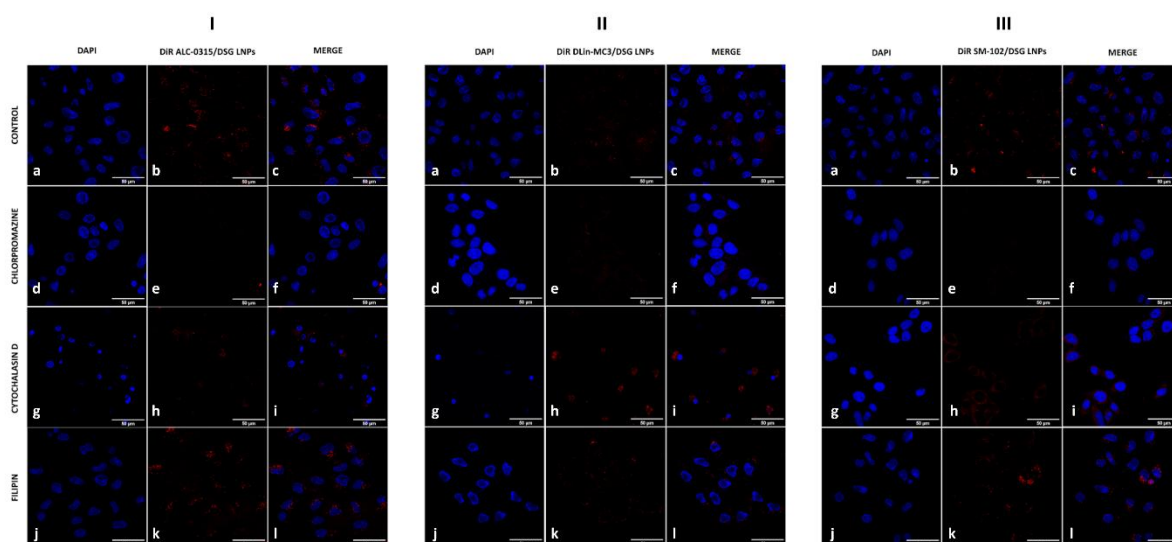


**Figure 5.2** Endocytic pathway determination of ionisable lipid/DSG-PEG LNPs. Cells, seeded at 25,000 cells/500  $\mu$ L, were treated with chlorpromazine hydrochloride, cytochalasin D, and filipin complex at the concentrations of 20  $\mu$ g/mL, 10  $\mu$ g/mL, and 2  $\mu$ g/mL respectively and incubated at 4  $^{\circ}$ C to selectively inhibit the clathrin-mediated, macropinocytosis, and caveolae-mediated internalisation of LNPs. Control cells were incubated with LNPs at 37  $^{\circ}$ C for 24-h (I-III, panel a-c). Clathrin-mediated endocytosis is involved in the mechanism of LNP uptake as the internalisation of the LNPs is compromised when cells are treated with chlorpromazine hydrochloride (I-III, panel d-f in all the LNPs). Macropinocytosis is observed to exist in the cells

incubated with ALC-0315 and SM-102/DSG-PEG LNPs as a possible second route of an endocytic pathway to a lesser extent (I and III, panel g-i). Scale bar = 50  $\mu\text{m}$ .

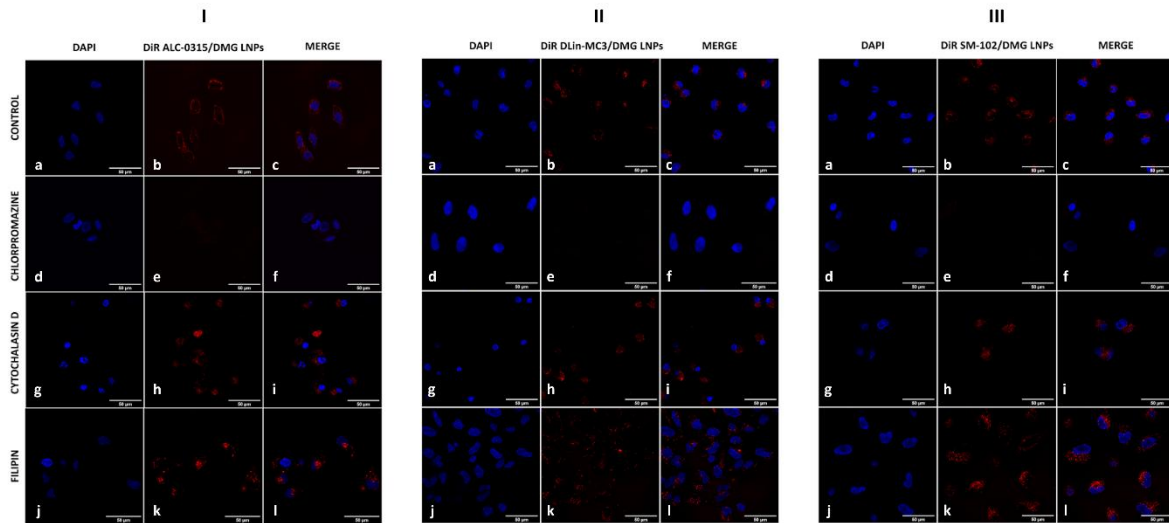


**Figure 5.3** Endocytic pathway determination of ionisable lipid/DMG-PEG LNPs. Cells, seeded at 25,000 cells/500  $\mu\text{L}$ , were treated with chlorpromazine hydrochloride, cytochalasin D, and filipin complex at the concentrations of 20  $\mu\text{g}/\text{mL}$ , 10  $\mu\text{g}/\text{mL}$ , and 2  $\mu\text{g}/\text{mL}$  respectively and incubated at 4  $^{\circ}\text{C}$  to selectively inhibit the clathrin-mediated, macropinocytosis, and caveolae-mediated internalisation of LNPs. Control cells were incubated with LNPs at 37  $^{\circ}\text{C}$  for 24-h (I-III, panel a-c). Clathrin-mediated endocytosis is involved in the mechanism of LNP uptake as the internalisation of the LNPs is compromised when cells are treated with chlorpromazine hydrochloride (I-III, panel d-f in all the LNPs). Macropinocytosis and caveolae-mediated endocytic pathways were not involved in the DMG-PEG LNPs cellular internalisation (I-III, panel g-i and j-l). Scale bar = 50  $\mu\text{m}$ .

### 5.3.3 *In Vitro* Expression of DSG-PEG and DMG-PEG LNPs

To consider the *in vitro* efficacy of the six different LNP formulations, HeLa cells were treated with LNPs across a dose concentration of 2 to 0.25  $\mu\text{g}/\text{mL}$  Fluc-mRNA incorporated into LNPs (Figure 5.4). The *in vitro* luciferase assay results show that in terms of ionisable lipids, the expression profiles followed the general trend of SM-102>ALC-0315>Dlin-MC3 for both the DSG-PEG and DMG-PEG LNPs and DMG-PEG-LNPs gave higher expression than DSG-PEG LNPs (Figure 5.4).

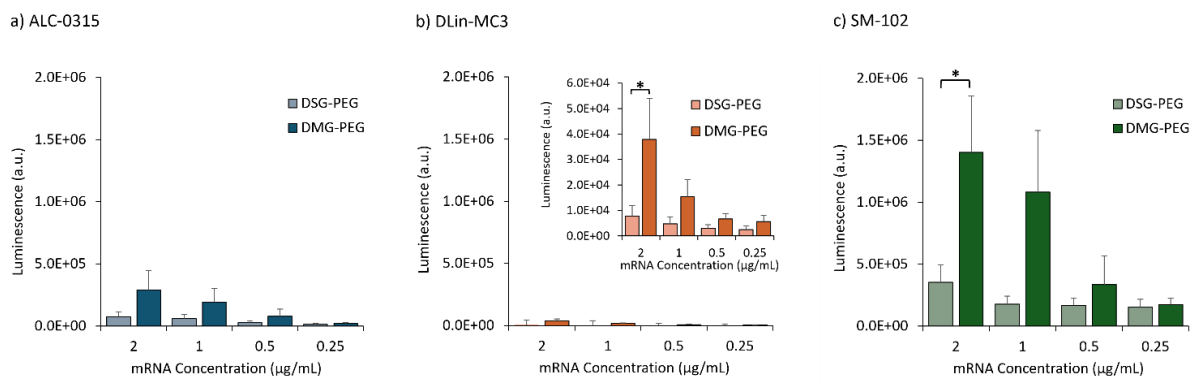


**Figure 5.4** *In vitro* expression of Fluc-mRNA LNPs. Confluent HeLa cells were treated with LNPs having mRNA doses in the concentrations of (2 µg/mL, 1 µg/mL, 0.5 µg/mL, and 0.25 µg/mL) and incubated at 37°C for 24 hours. a) mRNA expression of Fluc-mRNA ALC-0315 LNPs. b) mRNA expression of Fluc-mRNA DLin-MC3 LNPs. In Fig. 5.4b, the embedded graph displays the data at a reduced luminescence range, providing a clearer view of the less apparent differences in the full-scale plot. c) mRNA expression of Fluc-mRNA SM-102 LNPs. Data are expressed by mean ± SEM (n=3) and statistical analysis was performed by GraphPad Prism (\*p < 0.05).

### 5.3.4 *In Vivo* Expression of DSG-PEG and DMG-PEG LNPs

To consider the potency of the various formulations, it was investigated how different combinations of three ionisable lipids (ALC-0315, DLin-MC3, and SM-102) and two PEG-lipid moieties (DSG-PEG and DMG-PEG) influence luciferase expression profiles across three parenteral administration routes: intramuscular, subcutaneous and intravenous. Across all tested LNP formulations and administration routes, luciferase bioluminescence intensity consistently peaked at 6 hours post-administration (Figure 5.5, Figure 5.6, Figure 5.7, Figure 5.8 and Figure 5.9).

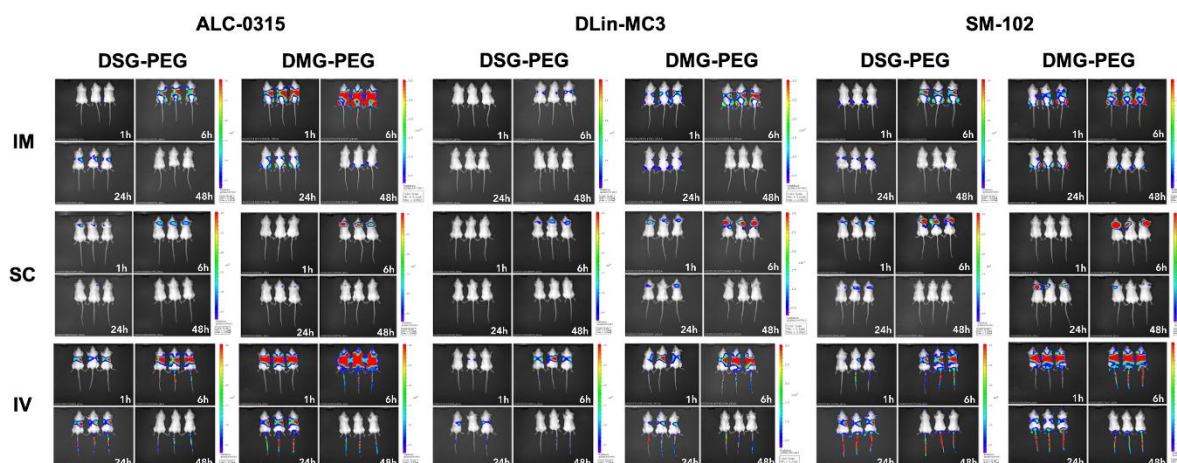


**Figure 5.5** Representative bioluminescence IVIS images at different time points (1h, 6h, 24h, 48h) after IM, SC and IV injection of Fluc-mRNA ionisable lipid/DSG-PEG and DMG-PEG LNPs. The injected mRNA dose was 5 µg mRNA encapsulated in LNP formulations. D-luciferin (30 mg/mL concentration) was administered subcutaneously at a dose rate of 150 mg/kg, and bioluminescence was measured after 10 min. The radiance photons colour scale is set at a minimum of 3.13e6 to a maximum of 3.05e7.

Bioluminescence signals in mice that received LNPs formulated with DSG-PEG and DMG-PEG were compared and quantified for each route of administration. Following IM administration, LNPs formulated with DMG-PEG demonstrated significantly higher expression at all measured time points compared to their DSG-PEG counterparts (Figure 5.6), consistent with *in vitro* trends. Among the ionisable lipids, DLin-MC3 LNPs consistently exhibited significantly lower expression levels ( $p < 0.05$ ) than ALC-0315 and SM-102 formulations at the muscle site. However, there was no significant

difference between ALC-0315 and SM-102 LNPs, regardless of the PEG-lipid used (Figure 5.6). This pattern was consistent across all time points.

Liver bioluminescence signals following IM administration were also quantified. DMG-PEG formulations again showed significantly higher expression compared to DSG-PEG formulations. Specifically, ALC-0315/DSG-PEG LNPs achieved significantly higher liver expression ( $p < 0.05$ ) at 6 hours compared to DLin-MC3/DSG-PEG LNPs, though the expression was comparable to SM-102/DSG-PEG LNPs (Figure 5.6c). With DMG-PEG formulations, ALC-0315/DMG-PEG LNPs achieved significantly higher IM expression ( $p < 0.05$ ) than both DLin-MC3/DMG-PEG and SM-102/DMG-PEG LNPs (Figure 5.6d).

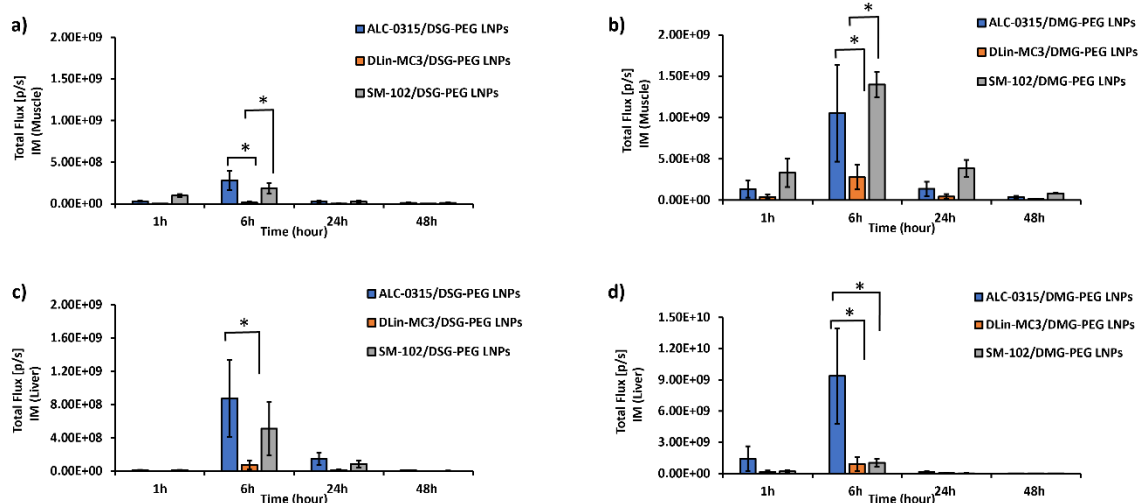


**Figure 5.6** a) Bioluminescence quantification in the muscle after IM injection of Fluc-mRNA ionisable lipid/DSG-PEG LNPs at different time points. b) Bioluminescence quantification in the muscle after IM injection of Fluc-mRNA ionisable lipid/DMG-PEG LNPs at different time points. c) Bioluminescence quantification in the liver after IM injection of Fluc-mRNA ionisable lipid/DSG-PEG LNPs at different time points. d) Bioluminescence quantification in the liver after IM injection of Fluc-mRNA ionisable lipid/DMG-PEG LNPs at different time points. Data are expressed by mean  $\pm$  SEM ( $n=3$ ) and statistical analysis was performed by GraphPad Prism ( $*p < 0.05$ ). (Y-axis scale bars are kept different for the two LNPs due to the significant difference in the total flux intensity values)

After SC administration, the LNPs gave a similar profile in terms of expression levels to those seen after IM administration, with DSG-PEG LNPs having lower expression than DMG-PEG LNPs (Figure 5.7). Similarly, when comparing the ionisable lipid groups, LNPs prepared by ALC-0315 or SM-102 promoted higher luciferase expression than their DLin-MC3 counterparts both when formulated with DSG-PEG (Figure 5.7a) and DMG-PEG (Figure 5.7b).

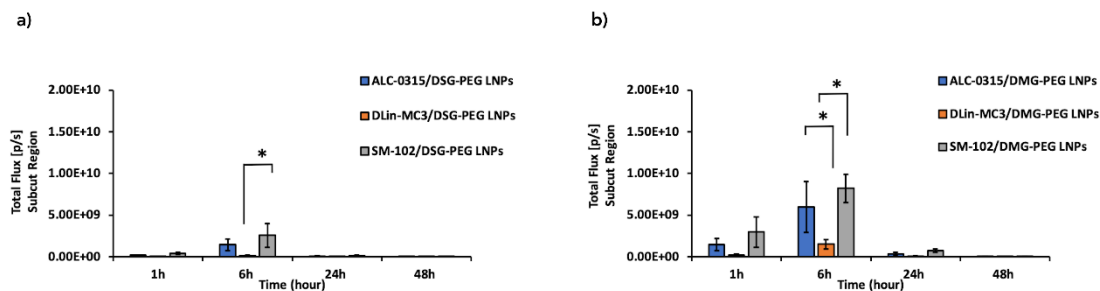


**Figure 5.7** Bioluminescence quantification in the subcut region after 1h, 6h, 24h, 48h from LNPs administration via SC route. a) Bioluminescence signal for Fluc-mRNA ionisable lipid/DSG-PEG LNPs at the different time points. b) Bioluminescence signal for Fluc-mRNA ionisable lipid/DMG-PEG LNPs at the different time points. Data are expressed by mean  $\pm$  SEM ( $n=3$ ), and statistical analysis was performed by GraphPad Prism ( $*p < 0.05$ ).

Next, the luciferase expression pattern of the various LNPs was analysed after administration via the IV route, and the primary site of expression was the liver for all formulations tested (Figure 5.5 and Figure 5.8). As with the other administration routes, LNPs prepared using DSG-PEG promoted lower luciferase expression levels compared to LNPs prepared using DMG-PEG and again, of the three ionisable lipids tested, DLin-MC3 was the least effective. However, when administrated IV, ALC-0315-based LNPs gave significantly higher ( $p < 0.05$ ) expression in the liver than SM-102-based and DLin-MC3-based LNPs (Figure 5.8b).

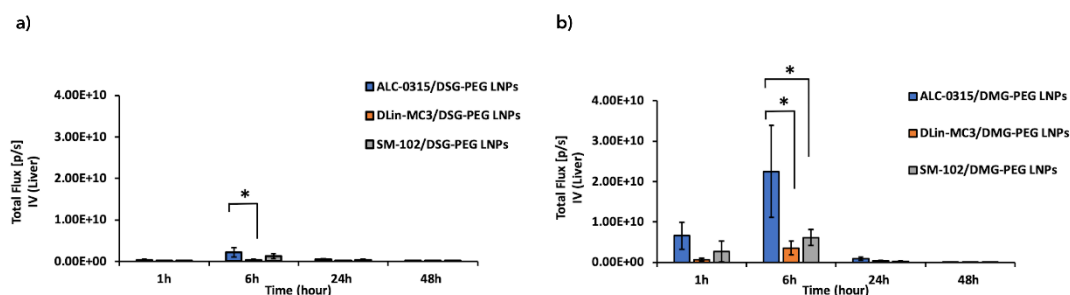


**Figure 5.8** Bioluminescence quantification in the liver after 1h, 6h, 24h, 48h from LNPs administration via IV route. a) Bioluminescence signal for Fluc-mRNA ionisable lipid/DSG-PEG LNPs at the different time points. b) Bioluminescence signal for Fluc-mRNA ionisable lipid/DMG-PEG LNPs at the different time points. Data are expressed by mean  $\pm$  SEM ( $n=3$ ), and statistical analysis was performed by GraphPad Prism ( $*p < 0.05$ ).

The mRNA expression was also quantified as per cent of the total signal to differentiate how much of the total bioluminescence was observed at the injection site and other organs 6 hours after injection (Figure 5.9). In general, a similar pattern was seen for DSG-PEG LNPs and DMG-PEG LNPs across the three administration routes, with the only notable differences being seen after IV injection with a higher percentage expression of DMG-LNPs at the liver than in the tail. Also, with the SM-102

formulations, when given IM, DMG-PEG LNPs had a higher percentage expression at the injection site than DSG-PEG LNPs (Figure 5.9e-f).

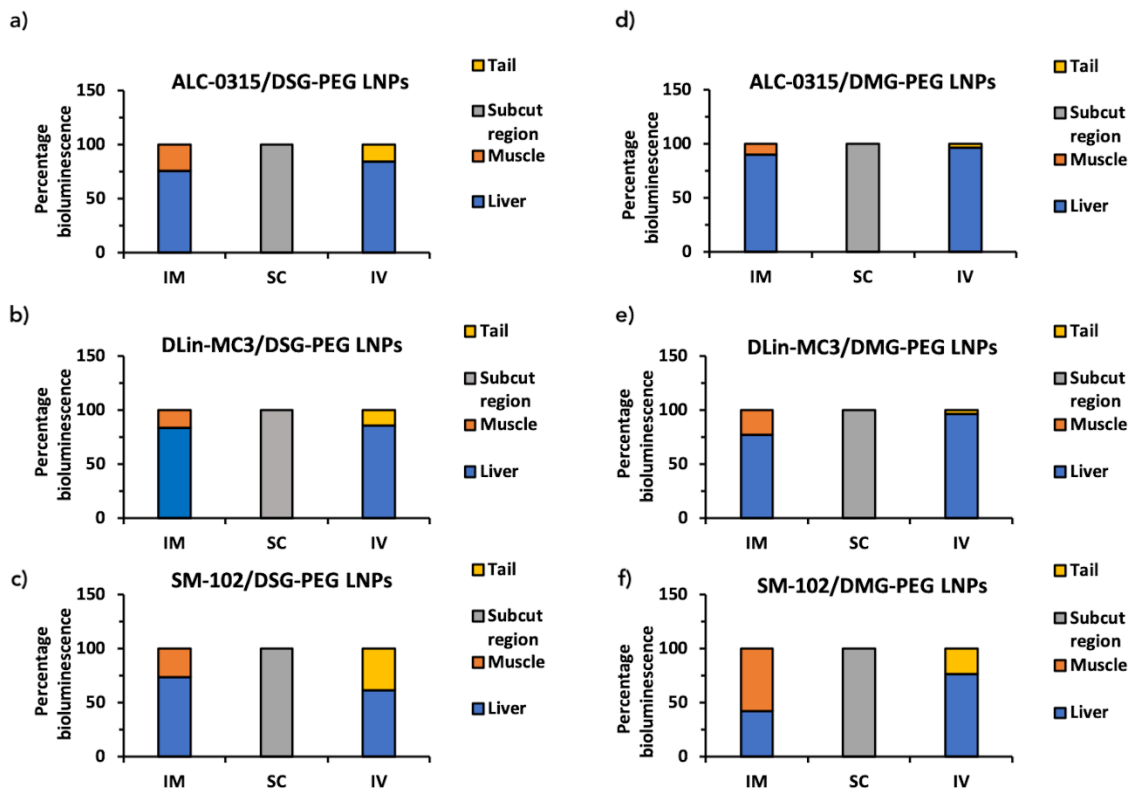


**Figure 5.9** Percentage bioluminescence at 6h in different organs after IM, SC, or IV administration. a) Percentage bioluminescence when administering AL-0315, DLin-MC3 or SM-102 Fluc-mRNA/DSG-PEG LNPs. b) Percentage bioluminescence when administering AL-0315, DLin-MC3 or SM-102 Fluc-mRNA/DMG-PEG LNPs.

Additionally, the mRNA expression after administration via the three routes (IV, IM and SC) was investigated using 3D bioluminescence and micro-CT imaging. The SM-102/DMG-PEG combination was selected as this LNP type displayed overall consistent luciferase expression via all three parenteral routes of administration. As observed in Figure 5.10, the IM route displayed bioluminescence both in the liver and the muscle site of the flanks, the SC route showed bioluminescence between the head and the shoulders when imaged dorsally, and the IV route had significant bioluminescence in the liver.

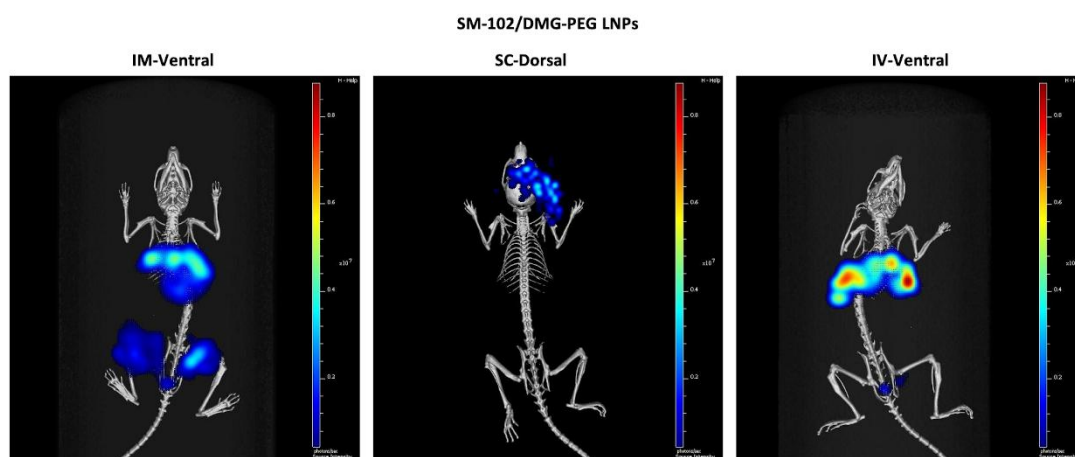


**Figure 5.10** 3D bioluminescence and micro-CT imaging. SM-102/DMG-PEG LNPs were administered via IM, SC or IV route and imaged at 6 h. Images were analysed by overlapping the bioluminescence images from the IVIS Spectrum and the micro-CT images using the Quantum GX2 micro-CT imaging system.

## 5.4 Discussion

When designing LNP formulations, despite its low percentage contribution to the LNP construct, the choice of PEG lipid is a critical factor, as PEG-lipid desorption kinetics have been reported to influence potency, stability, and biodistribution (264,266). Shorter-chain PEG lipids, like DMG-PEG, may desorb rapidly after administration, facilitating protein corona formation and enhancing cellular uptake. Conversely, longer-chain PEG lipids, such as DSG-PEG may desorb more slowly, promoting prolonged circulation and wider distribution. To explore these dynamics, the combination of three ionisable lipids with DSG-PEG and DMG-PEG in LNP formulations was systematically investigated, and their efficacy both *in vitro* and *in vivo* across three different routes of administration was assessed.

Regarding their physicochemical properties, there were only minor differences in particle size (with LNPs incorporating DMG-PEG being approx. 10 nm smaller than those made with DSG-PEG), and all LNPs were monodisperse, with neutral zeta potential (between -5 and 7 mV) and high encapsulation efficiency (>90%) (Table 5.1). This difference in size may result from the shorter DMG-PEG allowing the lipid components to pack more tightly together, reducing the overall size of the nanoparticles. In general, LNP particle size is driven by the manufacturing process used with the choice of buffer (284), choice of mixer, the aqueous-to-ethanol mixing ratio and the flow rate, all being critical process parameters that control size (290–293).

Particle size is recognised as a key factor in cellular uptake (294,295). This is shown in our studies where smaller DMG-PEG LNPs demonstrated higher internalization in HeLa cells than DSG-PEG LNPs (Figure 5.2 and Figure 5.3). The choice of ionisable lipid also influenced uptake, with DLin-MC3 LNPs showing reduced endocytosis relative to SM-102 and ALC-0315 LNPs. Cellular uptake begins with endocytosis, followed by endosomal escape, LNP degradation, and mRNA release into the cytosol (296). Pharmacological inhibition of endocytic pathways revealed that LNPs primarily enter cells via clathrin-mediated endocytosis, with macropinocytosis contributing specifically to DSG-PEG LNP uptake but not DMG-PEG LNPs, suggesting alternative routes for DSG-PEG (Figure 5.2 and Figure 5.3). Endocytosis is a crucial step in delineating the fate of nanoparticles to reach their intracellular target (297), and efficient LNP-mRNA transfection relies on an early and narrow endosomal escape window before lysosomal sequestration or exocytosis (298). These distinctions in uptake mechanisms translated to differences in transfection efficacy *in vitro*. DMG-PEG LNPs consistently produced higher levels of gene expression than DSG-PEG LNPs, suggesting their superior efficiency in mRNA delivery. Among the ionisable lipids tested, SM-102 > ALC-0315 > DLin-MC3 in performance, regardless of the PEG-lipid moiety. *In vivo* results mirrored these trends. DMG-PEG LNPs outperformed DSG-PEG LNPs across all administration routes (intramuscular, subcutaneous, and intravenous). At the injection sites for IM and SC, SM-102 and ALC-0315 LNPs achieved comparable gene expression, both significantly surpassing DLin-MC3. Only at the liver after IV injection did ALC-0315/DMG-PEG LNPs outperform SM-102/DMG-PEG LNPs (Figure 5.6, Figure 5.7, Figure 5.8, Figure 5.9).

When comparing physicochemical attributes to efficacy, the results suggest that smaller LNPs promote higher uptake and expression *in vitro*. However, previous studies comparing LNPs of the same formulation, but different sizes have reported that larger LNPs promote higher transfection *in vitro*, and it was hypothesised that larger LNPs are associated with enhanced mRNA functional delivery *in vitro* due to these larger LNPs having more mRNA copies per particle (299). Given that only small (<20 nm) differences in size were noted, this would suggest that the difference in performance in Figure 5.2, Figure 5.3 and Figure 5.4 is driven by lipid choice and not particle size. Both *in vitro* and *in vivo* (across all administration routes), DLin-MC3 LNPs, independent of the PEG-lipid used, showed low transfection. The low efficacy of DLin-MC3 was also reported by Binici et al. mouse studies (283) and by Escalona-Rayó et al. (300) using zebrafish; both studies found that LNPs prepared from SM-102 or ALC-0315 yielded significantly higher mRNA expression than LNPs prepared with DLin-MC3. This difference in potency has been related to the chemical structure of DLin-MC3 compared to ALC-0315 and SM-102 (301–303). ALC-0315 and SM-102 exhibit similar branching and comprise the same functional groups: one hydroxy, one tertiary amine, two esters and only saturated hydrocarbons. These

two lipids have enhanced stability, and an accentuated molecular cone shape compared to DLin-MC3, which facilitates fusion with the cellular membrane and disrupts the endosomal membrane.

Regarding PEG-lipid chain length, DMG-PEG lipid promoted higher *in vitro* and *in vivo* expression across the three administration routes tested. The improved potency of DMG-PEG LNPs has been attributed to the rate at which PEG-lipids shed from LNPs. Due to its shorter acyl chain, DMG-PEG forms weaker hydrophobic interactions with other lipids in the LNP, causing it to dissociate or "shed" more readily, particularly in the physiological environment (304). This faster PEG shedding enhances cellular uptake and promotes efficient endosomal escape, as the exposed LNP surface interacts more readily with cellular membranes. *In vitro*, while the simpler cell culture media lacks the complexity of the physiological environment, a protein corona may still form from proteins present in the media (e.g., serum proteins like albumin, transferrin, or immunoglobulins). However, the composition and properties of this corona depend on the specific proteins present in the medium and the conditions under which the nanoparticles are incubated. *In vivo*, PEG shedding exposes the LNP to interactions with serum proteins, leading to the rapid formation of a protein corona that includes Apolipoprotein E (ApoE). The choice of both the ionisable lipid and the PEG-lipid within the LNP significantly affects this protein binding (305). The protein corona influences cellular interactions, often promoting receptor-mediated uptake. ApoE, in particular, binds to low-density lipoprotein (LDL) receptors, which are abundant on hepatocytes, directing LNPs to the liver for uptake and processing (279). This mechanism aligns with the enhanced liver expression observed for DMG-PEG LNPs (Figure 5.8). Therefore, the rate and extent of PEG shedding influence both the composition of the protein corona and the biodistribution of LNPs, ultimately impacting their efficacy.

After subcutaneous injection, ApoE-bound LNPs are also recognised and internalised by other cell types, such as lymphatic endothelial cells (306), which likely contributes to the enhanced efficacy observed with DMG-PEG LNPs in this route (Figure 5.7). Similarly, DMG-PEG LNPs showed superior expression at the injection site following intramuscular (IM) administration (Figure 5.6a-b). Muscle-resident macrophages and recruited immune cells, such as dendritic cells, are early responders to IM injections. These cells, equipped with ApoE receptors (e.g., LRP1, LDLR, and scavenger receptors), may interact with LNPs directly, particularly if the LNPs have shed their PEG coating, exposing their lipid surface. Once exposed, LNPs are more readily taken up via phagocytosis or receptor-mediated endocytosis. However, while ApoE binding can facilitate macrophage uptake, it is not the primary driver of LNP efficacy in IM delivery. Instead, rapid PEG shedding plays a critical role in promoting cellular internalization and intracellular trafficking, enhancing LNP potency. Additionally, faster PEG

shedding reduces the production of anti-PEG IgM, which may lower the immunogenicity of PEGylated LNPs and improve their overall therapeutic profile LNPs (304).

## 5.5 Conclusion

The choice of PEG-lipid in LNP formulations has traditionally been regarded as important, primarily for stabilising LNPs during production and storage and for providing stability in blood circulation after intravenous delivery. To further investigate this, in this chapter, it was considered how the choice of PEG lipids with different alkyl chain lengths influences the physicochemical characteristics, biodistribution, and efficacy of LNPs across various routes of administration. Results show that while the physical properties of the LNPs, such as size (70–90 nm) and charge, remained comparable, the functional differences were pronounced. Despite contributing to only a small fraction of the total lipid composition, PEG-lipids play a pivotal role in shaping cellular uptake, nanoparticle potency, biodistribution, and overall efficacy. LNPs formulated with 1.5% DMG-PEG (shorter-alkyl chain) consistently outperformed those with 1.5% DSG-PEG both *in vitro* and *in vivo*, irrespective of the ionisable lipid tested and the route of administration. Crucially, these findings show that the influence of PEG-lipids extends beyond the traditional concept of PEG-shedding, as the choice of PEG-lipid significantly affects cellular uptake *in vitro* where the protein corona effect will be more limited. Furthermore, the ionisable lipid is shown as a key driver in the biodistribution of the expression irrespective of the choice of PEG lipid. After IM and SC administration, ALC-0315 and SM-102 LNPs had similar protein expression at the injection site. However, ALC-0315 promoted higher expression in the liver both after IV and IM injection. DLin-MC3, irrespective of PEG-lipids, exhibited the lowest transfection efficacy in all the routes tested. These findings challenge the traditional view of PEG-lipids as mere stabilisers and highlight their pivotal role in modulating LNP performance, particularly through mechanisms beyond PEG-shedding.

# **Chapter 6**

## **General Discussion**

## 6.1 Introduction

This thesis focused on optimising lipid nanoparticles manufacturing, starting from the early stages of research (including the choice of lipids to be included in the formulation, such as the PEG-lipid and the ionisable lipid) to manufacturing, purification, filtration, and ultimately assessing the conditions suitable for long-term storage of the nanoparticles. Each of these steps needs to be controlled in order to produce particles with CQAs that are accepted by the regulatory organisations. Parameters such as size, polydispersity index, surface charge, residual ethanol content, and encapsulation efficacy are crucial to produce particles that can deliver efficiently their payload to cells. This thesis also addressed a gap in existing research by focusing on translating knowledge from a lab-scale to a pre-clinical scale, as it is often difficult to reproduce small-scale results at a bigger scale, due to differences in equipment, reproducibility between batches and cost-effectiveness.

## 6.2 Parameters that can affect LNP microfluidic production

This thesis followed the end-to-end production of LNPs, with Chapter 1 focusing on the first step: microfluidic manufacturing. Microfluidics involves mixing the organic phase (containing the lipids) and the aqueous phase (containing the mRNA) at specific total flow rates (TFR) and flow rate ratios (FRR). The impact of these parameters was evaluated. Organic solvent selection primarily affected particle size (Figure 2.4), with ethanol producing smaller particles compared to methanol and IPA. The composition of the aqueous solvent before particle formation also proved to be crucial. As shown in Figure 2.5A and B, citrate buffer concentration significantly influenced the LNPs' physicochemical attributes. When the concentration was increased from 10 mM to 75 mM, the results were comparable. However, increasing it further to 200 mM caused an increase in particle size and PDI (Figure 2.5A and B) and a decrease in encapsulation efficiency (Table 2.7). Although no *in vitro* research was conducted to support these findings, they align with literature suggesting that citrate buffer concentration influences lipid packing during LNP production and, consequently, its efficacy.

The mixing parameters (TFR and FRR) were also assessed. At a low TFR of 5 mL/min, particle size increased (Figure 2.6A-C), while no significant differences in size or PDI were observed between the aqueous/organic ratios tested (2:1, 3:1, and 4:1) when the flow rate was kept constant (Figure 2.6A-C). Post-formation solvent composition also affected the results. LNPs suspended in PBS, Tris, and Tris/sucrose were compared, as these are common external buffers. The results showed that LNPs in

PBS or Tris had similar characteristics, while the addition of sucrose to Tris caused an increase in particle size (Figure 2.7).

After investigating these manufacturing parameters, LNPs were produced using different instruments equipped with various microfluidic chips (SHM, TrM, and T-Junction) to demonstrate the applicability of these findings (Table 2.10, Figure 2.10, Figure 2.11). The *in vitro* potency of LNPs produced with different equipment was also tested on HEK cells (Figure 2.8). To optimize the *in vitro* mRNA expression assay, an investigation was conducted to determine the most suitable plate (black, clear, or white) for measuring mRNA LNP expression, with the white plate yielding the best results in terms of maximizing the light output signal (Figure 2.9). This chapter helped establish the parameters that would be used throughout the rest of the thesis.

### 6.3 The crucial role of LNP purification

Chapter 3 focused on LNP purification, with the primary topics being the impact of temperature on LNP storage and the simplification of the TFF process. A short-term stability study was conducted, showing that LNPs remain stable for up to 24 h after purification via dialysis and spin column methods, both at 4°C and room temperature (Figure 3.3A and B), retaining the same physicochemical properties as at 0 h post-purification. Additionally, given that LNPs, especially in large batches, often experience long hold times between production and purification, the effects of hold time and storage temperature between microfluidic manufacturing and purification were evaluated. LNPs proved to be stable for up to 24 h before purification at both room temperature and 4°C (Figure 3.4A and B), indicating that the ethanol remaining from the manufacturing process (typically 25%) did not negatively affect particle stability.

The TFF process was also extensively evaluated with the aim of simplifying it, as it can be time-consuming and costly, particularly on a large scale. At a small scale, the impact of speed and the number of diafiltration volumes were assessed. The speed did not significantly affect the final characteristics of the vesicles (Figure 3.5A-C and Table 3.5), allowing for faster processing without compromising results. Additionally, it was demonstrated that the TFF diafiltration volumes could be reduced from the typical 12 volumes to 5 without impacting LNP CQAs (Figure 3.6 and Table 3.6), including effective ethanol removal, thereby saving time and costs (Figure 3.7).

The focus then shifted to a preclinical scale, where SM-102 LNPs were manufactured, and an industrial TFF was used for purification. The results described in section 3.3.2.4 confirmed several findings. First,

dilution was not crucial to the formulation outcome (Figure 3.8A and B). Second, the optimal speed for the column type used was 212 mL/min (Figure 3.9A and B). Finally, the type of buffer used for exchange impacted the results; performing the buffer exchange in Tris rather than Tris/sucrose improved the LNP CQAs. However, adding sucrose to Tris after the buffer exchange could be a valid alternative (Figure 3.10A and B).

Sterile filtration is commonly performed after purification to ensure sterility, especially in industrial-scale production. Therefore, after purification, LNPs underwent filtration both at bench scale and preclinical scale. At the bench scale, filtration reduced LNP size and PDI without significantly affecting yield (Figure 3.5A-C, Table 3.5, Figure 3.6A-E, Table 3.6). However, at the preclinical scale, filtration resulted in the degradation of the particles' attributes (Figure 3.9A and B and Figure 3.10A and B).

## 6.4 Freeze-dry as a promising technique for long term storage of LNPs

Long-term storage of LNPs is a crucial issue that needs to be addressed in the development of new LNP delivery systems. Currently, all LNP formulations on the market contain cryoprotectants and are stored at low temperatures to ensure long-term stability. Lyophilisation, which involves removing water from the formulation, is considered a promising solution to the storage challenge. However, this technology is still under development, and a standardised protocol has yet to be established. Chapter 4 focused on developing a lyophilisation method for storing mRNA LNPs, using the Moderna COVID-19 formulation as a benchmark. Three different lyophilisation cycles were compared, varying the three main stages of the process: freezing, primary drying, and secondary drying. The cycle that produced particles with good CQAs was very conservative, characterised by very low freezing and primary drying temperatures, low pressures, and slow ramp rates (Table 4.3). Sucrose and trehalose were compared as cryoprotectants, and even if the addition of sucrose resulted in LNPs with better CQAs than trehalose-LNPs (Figure 4.7A-D), trehalose-LNPs outperformed sucrose-LNPs in terms of cellular response when incubated with cells (Figure 4.8). These results were confirmed *in vivo*, where trehalose-LNPs gave a response similar to the control LNPs (Figure 4.11).

## 6.5 Evaluating LNPs Efficiency Considering Lipid Composition and site of administration

In Chapter 5, the attention was drawn to the importance of the lipid selection on LNP development. In particular, formulations containing different ionisable lipids and PEG-lipids with different alkyl chain lengths were extensively evaluated both *in vitro* and *in vivo*. The effects of DMG-PEG 2000 (C14) and DSG-PEG 2000 (C18) were compared, and results showed that despite the small fraction of the total lipid composition, the PEG-lipid plays a key role in cellular uptake, *in vitro* potency, *in vivo* biodistribution, and overall formulation efficacy. Independent of the rest of the LNP composition, LNPs containing shorter PEG-lipid chain consistently produced better results *in vitro* (Figure 5.4) and *in vivo* (Figure 5.6, Figure 5.7, Figure 5.8) than LNPs containing longer PEG-lipid chain. In addition, the effect of the ionisable lipid was evaluated by comparing SM-102, DLin-MC3 and ALC-0315, three lipids used in the LNPs formulation currently on the market. After IM and SC administration, SM-102 LNPs and ALC-0315 LNPs produced a similar signal in the injection site (the deltoid muscle and the subcut region, respectively), while ALC-0315 LNPs had better expression in the liver after IM and IV injections (Figure 5.6, Figure 5.7, Figure 5.8). Independently of the site of injection and the PEG-lipid used in the formulation, DLin-MC3 LNPs exhibited the lowest response.

## 6.6 Future and Outlook

This thesis addressed several common bottlenecks in LNPs manufacturing. In the attempt of examining the challenges related to LNP production, it has been shown that lot of issues remain. One key finding is the significant impact of LNP composition (in terms of lipid components) on the formulation's performance. For instance, altering the PEG-lipid, which commonly constitutes only 1.5 % of the formulation, greatly impacts the LNP faith *in vitro* and *in vivo*. Similarly, the choice of ionizable lipids has been shown to influence *in vivo* behaviour, emphasizing that the composition of LNPs must be carefully optimised depending on the therapeutic target. However, it should be noted that although these factors are critical, the exact mechanisms by which lipid composition influences LNP performance are still not fully understood. Future research could benefit from a deeper exploration of these mechanisms, potentially offering new strategies to tailor formulations for specific applications.

It has also been demonstrated that scaling up from bench scale to a larger manufacturing scale constitutes an issue as often, what works on a small scale, does not perform as expected on a larger scale. One major issue that remains is batch to batch consistency, with variations in particle size and

encapsulation efficacy becoming common on a bigger scale. This suggests that further optimisation of large-scale production methods is needed, particularly with regard to maintaining reproducibility and consistency across batches. In this context, more attention should be paid to the influence of production variables (such as mixing speeds, temperature, and solvent concentration) on the final product's quality.

Another challenge that should be carefully addressed in the near future, given the worldwide spread of LNP technology, is the long-term storage. To preserve LNP efficacy, lyophilisation constitutes a promising approach, yet research in this area is still lacking. This technique, even if promising, needs to be further explored as retaining the *in vivo* functionality of LNPs after lyophilisation is difficult due to the fragile nature of the mRNA. Improving this technique is necessary to allow LNP storage for longer periods at milder temperatures such as in refrigerators or even at room temperatures and, additionally, to simplify shipment to countries lacking ultra-low temperature storage facilities. Further studies should aim to identify stabilising agents or optimised lyophilisation cycles that can better preserve mRNA integrity and ensure the functionality of LNPs after storage.

Given the growing importance of LNP technology in both drug delivery and vaccines, it is crucial that these issues be addressed to enable broader, more reliable use of LNP-based therapies. As such, future research should not only focus on improving the technical aspects of LNP production but also explore novel strategies for scaling, stabilising, and optimising LNP formulations to meet the evolving demands of the pharmaceutical industry.

## Bibliography

1. Puri A, Loomis KH, Smith B, Lee JH, Yavlovich A, Heldman E, et al. Lipid-based nanoparticles as pharmaceutical drug carriers: from concepts to clinic. *Crit Rev Ther Drug Carrier Syst* [Internet]. 2009;26 6:523–80. Available from: <https://api.semanticscholar.org/CorpusID:13784203>
2. Yan Y, Liu XY, Lu A, Wang XY, Jiang LX, Wang JC. Non-viral vectors for RNA delivery. *Journal of Controlled Release* [Internet]. 2022;342:241–79. Available from: <https://www.sciencedirect.com/science/article/pii/S0168365922000220>
3. Wolff JA, Malone RW, Williams P, Chong W, Acsadi G, Jani A, et al. Direct Gene Transfer into Mouse Muscle in Vivo. *Science* (1979) [Internet]. 1990;247(4949):1465–8. Available from: <https://www.science.org/doi/abs/10.1126/science.1690918>
4. Jiao X, He X, Qin S, Yin X, Song T, Duan X, et al. Insights into the formulation of lipid nanoparticles for the optimization of mRNA therapeutics. Vol. 16, *Wiley interdisciplinary reviews. Nanomedicine and nanobiotechnology*. 2024. p. e1992.
5. Kon E, Elia U, Peer D. Principles for designing an optimal mRNA lipid nanoparticle vaccine. *Curr Opin Biotechnol* [Internet]. 2022;73:329–36. Available from: <https://www.sciencedirect.com/science/article/pii/S0958166921001932>
6. Karikó K, Buckstein M, Ni H, Weissman D. Suppression of RNA Recognition by Toll-like Receptors: The Impact of Nucleoside Modification and the Evolutionary Origin of RNA. *Immunity* [Internet]. 2005;23(2):165–75. Available from: <https://www.sciencedirect.com/science/article/pii/S1074761305002116>
7. Karikó K, Muramatsu H, Welsh FA, Ludwig J, Kato H, Akira S, et al. Incorporation of Pseudouridine Into mRNA Yields Superior Nonimmunogenic Vector With Increased Translational Capacity and Biological Stability. *Molecular Therapy* [Internet]. 2008;16(11):1833–40. Available from: <https://www.sciencedirect.com/science/article/pii/S1525001616326818>
8. Corbett KS, Edwards DK, Leist SR, Abiona OM, Boyoglu-Barnum S, Gillespie RA, et al. SARS-CoV-2 mRNA vaccine design enabled by prototype pathogen preparedness. *Nature* [Internet]. 2020;586(7830):567–71. Available from: <https://doi.org/10.1038/s41586-020-2622-0>
9. Xu S, Yang K, Li R, Zhang L. mRNA Vaccine Era—Mechanisms, Drug Platform and Clinical Prospection. *Int J Mol Sci* [Internet]. 2020;21(18). Available from: <https://www.mdpi.com/1422-0067/21/18/6582>
10. Sahin U, Karikó K, Türeci Ö. mRNA-based therapeutics — developing a new class of drugs. *Nat Rev Drug Discov* [Internet]. 2014;13(10):759–80. Available from: <https://doi.org/10.1038/nrd4278>
11. Pascolo S. Synthetic Messenger RNA-Based Vaccines: From Scorn to Hype. *Viruses* [Internet]. 2021;13(2). Available from: <https://www.mdpi.com/1999-4915/13/2/270>

12. Gergen J, Petsch B. mRNA-Based Vaccines and Mode of Action. In: Yu D, Petsch B, editors. mRNA Vaccines [Internet]. Cham: Springer International Publishing; 2022. p. 1–30. Available from: [https://doi.org/10.1007/82\\_2020\\_230](https://doi.org/10.1007/82_2020_230)
13. Lima SA, Chipman LB, Nicholson AL, Chen YH, Yee BA, Yeo GW, et al. Short poly(A) tails are a conserved feature of highly expressed genes. *Nat Struct Mol Biol* [Internet]. 2017;24(12):1057–63. Available from: <https://doi.org/10.1038/nsmb.3499>
14. Gregoriadis G. Liposomes and mRNA: Two technologies together create a COVID-19 vaccine. *Med Drug Discov* [Internet]. 2021;12:100104. Available from: <https://www.sciencedirect.com/science/article/pii/S2590098621000257>
15. Bangham AD, Standish MM, Watkins JC. Diffusion of univalent ions across the lamellae of swollen phospholipids. *J Mol Biol* [Internet]. 1965;13(1):238–IN27. Available from: <https://www.sciencedirect.com/science/article/pii/S0022283665800936>
16. Gregoriadis G. Liposomes in Drug Delivery: How It All Happened. *Pharmaceutics* [Internet]. 2016;8(2). Available from: <https://www.mdpi.com/1999-4923/8/2/19>
17. Weissig V. Liposomes came first: The early history of liposomology. In: *Methods in Molecular Biology*. Humana Press Inc.; 2017.
18. Schoenmaker L, Witzigmann D, Kulkarni JA, Verbeke R, Kersten G, Jiskoot W, et al. mRNA-lipid nanoparticle COVID-19 vaccines: Structure and stability. *Int J Pharm* [Internet]. 2021;601:120586. Available from: <https://www.sciencedirect.com/science/article/pii/S0378517321003914>
19. Laouini A, Jaafar-Maalej C, Limayem-Blouza I, Sfar S, Charcosset C, Fessi H. Preparation, Characterization and Applications of Liposomes: State of the Art. *Journal of Colloid Science and Biotechnology* [Internet]. 2012;1:147–68. Available from: <https://api.semanticscholar.org/CorpusID:23853943>
20. Harashima H, Sakata K, Funato K, Kiwada H. Enhanced Hepatic Uptake of Liposomes Through Complement Activation Depending on the Size of Liposomes. *Pharm Res* [Internet]. 1994;11(3):402–6. Available from: <https://doi.org/10.1023/A:1018965121222>
21. Nagayasu A, Uchiyama K, Kiwada H. The size of liposomes: a factor which affects their targeting efficiency to tumors and therapeutic activity of liposomal antitumor drugs. *Adv Drug Deliv Rev* [Internet]. 1999;40(1):75–87. Available from: <https://www.sciencedirect.com/science/article/pii/S0169409X99000411>
22. Smith MC, Crist RM, Clogston JD, McNeil SE. Zeta potential: a case study of cationic, anionic, and neutral liposomes. *Anal Bioanal Chem* [Internet]. 2017;409(24):5779–87. Available from: <https://doi.org/10.1007/s00216-017-0527-z>
23. Working PK, Dayan AD. Pharmacological-toxicological expert report. CAELYX. (Stealth liposomal doxorubicin HCl). *Hum Exp Toxicol* [Internet]. 1996;15 9:751–85. Available from: <https://api.semanticscholar.org/CorpusID:32031266>

24. Bobo D, Robinson KJ, Islam J, Thurecht KJ, Corrie SR. Nanoparticle-Based Medicines: A Review of FDA-Approved Materials and Clinical Trials to Date. *Pharm Res* [Internet]. 2016;33(10):2373–87. Available from: <https://doi.org/10.1007/s11095-016-1958-5>
25. OSTRO MJ, GIACOMONI D, LAVELLE DON, PAXTON W, DRAY S. Evidence for translation of rabbit globin mRNA after liposomemediated insertion into a human cell line. *Nature* [Internet]. 1978;274(5674):921–3. Available from: <https://doi.org/10.1038/274921a0>
26. DIMITRIADIS GJ. Translation of rabbit globin mRNA introduced by liposomes into mouse lymphocytes. *Nature* [Internet]. 1978;274(5674):923–4. Available from: <https://doi.org/10.1038/274923a0>
27. Szoka F, Papahadjopoulos D. Procedure for preparation of liposomes with large internal aqueous space and high capture by reverse-phase evaporation. *Proceedings of the National Academy of Sciences* [Internet]. 1978;75(9):4194–8. Available from: <https://www.pnas.org/doi/abs/10.1073/pnas.75.9.4194>
28. Yu B, Lee RJ, Lee LJ. Chapter 7 - Microfluidic Methods for Production of Liposomes. In: *Methods in Enzymology* [Internet]. Academic Press; 2009. p. 129–41. Available from: <https://www.sciencedirect.com/science/article/pii/S0076687909650072>
29. Felgner PL, Gadek TR, Holm M, Roman R, Chan HW, Wenz M, et al. Lipofection: a highly efficient, lipid-mediated DNA-transfection procedure. *Proceedings of the National Academy of Sciences* [Internet]. 1987;84(21):7413–7. Available from: <https://www.pnas.org/doi/abs/10.1073/pnas.84.21.7413>
30. Malone RW, Felgner PL, Verma IM. Cationic liposome-mediated RNA transfection. *Proceedings of the National Academy of Sciences* [Internet]. 1989;86(16):6077–81. Available from: <https://www.pnas.org/doi/abs/10.1073/pnas.86.16.6077>
31. Chu CJ, Dijkstra J, Lai MZ, Hong K, Szoka FC. Efficiency of Cytoplasmic Delivery by pH-Sensitive Liposomes to Cells in Culture. *Pharm Res* [Internet]. 1990;7(8):824–34. Available from: <https://doi.org/10.1023/A:1015908831507>
32. Ellens H, Bentz J, Szoka FC. pH-Induced destabilization of phosphatidylethanolamine-containing liposomes: role of bilayer contact. *Biochemistry* [Internet]. 1984 Mar 27;23(7):1532–8. Available from: <https://doi.org/10.1021/bi00302a029>
33. Arteta MY, Kjellman T, Bartesaghi S, Wallin S, Wu X, Kvist AJ, et al. Successful reprogramming of cellular protein production through mRNA delivered by functionalized lipid nanoparticles. *Proceedings of the National Academy of Sciences* [Internet]. 2018;115(15):E3351–60. Available from: <https://www.pnas.org/doi/abs/10.1073/pnas.1720542115>
34. Kulkarni JA, Witzigmann D, Leung J, Tam YYC, Cullis PR. On the role of helper lipids in lipid nanoparticle formulations of siRNA. *Nanoscale* [Internet]. 2019;11(45):21733–9. Available from: <http://europepmc.org/abstract/MED/31713568>

35. Hamilton AJ, Baulcombe DC. A Species of Small Antisense RNA in Posttranscriptional Gene Silencing in Plants. *Science* (1979) [Internet]. 1999;286(5441):950–2. Available from: <https://www.science.org/doi/abs/10.1126/science.286.5441.950>
36. Adams D, Gonzalez-Duarte A, O’Riordan WD, Yang CC, Ueda M, Kristen A V, et al. Patisiran, an RNAi Therapeutic, for Hereditary Transthyretin Amyloidosis. *New England Journal of Medicine* [Internet]. 2018;379(1):11–21. Available from: <https://www.nejm.org/doi/full/10.1056/NEJMoa1716153>
37. US Food and Drug Administration (FDA). ONPATTRO full prescribing information. 2018.
38. Lokras AG, Bobak TR, Baghel SS, Sebastiani F, Foged C. Advances in the design and delivery of RNA vaccines for infectious diseases. *Adv Drug Deliv Rev* [Internet]. 2024;213:115419. Available from: <https://www.sciencedirect.com/science/article/pii/S0169409X24002412>
39. Jackson LA, Anderson EJ, Roupheal NG, Roberts PC, Makhene M, Coler RN, et al. An mRNA Vaccine against SARS-CoV-2 — Preliminary Report. *New England Journal of Medicine* [Internet]. 2020;383(20):1920–31. Available from: <https://www.nejm.org/doi/full/10.1056/NEJMoa2022483>
40. Corbett KS, Flynn B, Foulds KE, Francica JR, Boyoglu-Barnum S, Werner AP, et al. Evaluation of the mRNA-1273 Vaccine against SARS-CoV-2 in Nonhuman Primates. *New England Journal of Medicine* [Internet]. 2020;383(16):1544–55. Available from: <https://www.nejm.org/doi/full/10.1056/NEJMoa2024671>
41. Center for Disease Control and Prevention. Pfizer-BioNTech COVID-19 Vaccine Overview and Safety. 2021.
42. Li F. Receptor recognition and cross-species infections of SARS coronavirus. *Antiviral Res* [Internet]. 2013;100(1):246–54. Available from: <https://www.sciencedirect.com/science/article/pii/S0166354213002222>
43. Zhao Y, Zhao Z, Wang Y, Zhou Y, Ma Y, Zuo W. Single-cell RNA expression profiling of ACE2, the putative receptor of Wuhan 2019-nCov. *bioRxiv* [Internet]. 2020; Available from: <https://www.biorxiv.org/content/early/2020/01/26/2020.01.26.919985>
44. Vitiello A, Ferrara F. Brief review of the mRNA vaccines COVID-19. *Inflammopharmacology* [Internet]. 2021;29(3):645–9. Available from: <https://doi.org/10.1007/s10787-021-00811-0>
45. Baden LR, Sahly HM El, Essink B, Kotloff K, Frey S, Novak R, et al. Efficacy and Safety of the mRNA-1273 SARS-CoV-2 Vaccine. *New England Journal of Medicine* [Internet]. 2021;384(5):403–16. Available from: <https://www.nejm.org/doi/full/10.1056/NEJMoa2035389>
46. EMA. Summary of product characteristics. 2024.
47. Kowalski PS, Rudra A, Miao L, Anderson DG. Delivering the Messenger: Advances in Technologies for Therapeutic mRNA Delivery. *Molecular Therapy* [Internet]. 2019 Apr 10;27(4):710–28. Available from: <https://doi.org/10.1016/j.ymthe.2019.02.012>

48. Kumar V, Qin J, Jiang Y, Duncan RG, Brigham B, Fishman S, et al. Shielding of Lipid Nanoparticles for siRNA Delivery: Impact on Physicochemical Properties, Cytokine Induction, and Efficacy. *Mol Ther Nucleic Acids* [Internet]. 2014 Jan 1;3. Available from: <https://doi.org/10.1038/mtna.2014.61>
49. Tam YYC, Chen S, Cullis PR. Advances in Lipid Nanoparticles for siRNA Delivery. *Pharmaceutics* [Internet]. 2013;5(3):498–507. Available from: <https://www.mdpi.com/1999-4923/5/3/498>
50. Patel P, Ibrahim NM, Cheng K. The Importance of Apparent pKa in the Development of Nanoparticles Encapsulating siRNA and mRNA. *Trends Pharmacol Sci* [Internet]. 2021;42(6):448–60. Available from: <https://www.sciencedirect.com/science/article/pii/S0165614721000493>
51. Carrasco MJ, Alishetty S, Alameh MG, Said H, Wright L, Paige M, et al. Ionization and structural properties of mRNA lipid nanoparticles influence expression in intramuscular and intravascular administration. *Commun Biol* [Internet]. 2021;4(1):956. Available from: <https://doi.org/10.1038/s42003-021-02441-2>
52. Hou X, Zaks T, Langer R, Dong Y. Lipid nanoparticles for mRNA delivery. *Nat Rev Mater* [Internet]. 2021;6(12):1078–94. Available from: <https://doi.org/10.1038/s41578-021-00358-0>
53. Samaridou E, Heyes J, Lutwyche P. Lipid nanoparticles for nucleic acid delivery: Current perspectives. *Adv Drug Deliv Rev* [Internet]. 2020;154–155:37–63. Available from: <https://www.sciencedirect.com/science/article/pii/S0169409X2030048X>
54. Tanaka H, Takahashi T, Konishi M, Takata N, Gomi M, Shirane D, et al. Self-Degradable Lipid-Like Materials Based on “Hydrolysis accelerated by the intra-Particle Enrichment of Reactant (HyPER)” for Messenger RNA Delivery. *Adv Funct Mater*. 2020 Aug 1;30(34).
55. Levien TL, Baker DE. Respiratory Syncytial Virus Vaccine (mRNA). *Hosp Pharm* [Internet]. 0(0):00185787241298140. Available from: <https://doi.org/10.1177/00185787241298140>
56. Wang B, Shen B, Xiang W, Shen H. Advances in the study of LNPs for mRNA delivery and clinical applications. *Virus Genes* [Internet]. 2024;60(6):577–91. Available from: <https://doi.org/10.1007/s11262-024-02102-6>
57. Bailey AL, Cullis PR. Modulation of Membrane Fusion by Asymmetric Transbilayer Distributions of Amino Lipids. *Biochemistry* [Internet]. 1994 Oct 1;33(42):12573–80. Available from: <https://doi.org/10.1021/bi00208a007>
58. Eygeris Y, Gupta M, Kim J, Sahay G. Chemistry of Lipid Nanoparticles for RNA Delivery. *Acc Chem Res* [Internet]. 2022 Jan 4;55(1):2–12. Available from: <https://doi.org/10.1021/acs.accounts.1c00544>
59. Maier MA, Jayaraman M, Matsuda S, Liu J, Barros S, Querbes W, et al. Biodegradable Lipids Enabling Rapidly Eliminated Lipid Nanoparticles for Systemic Delivery of RNAi Therapeutics. *Molecular Therapy* [Internet]. 2013;21(8):1570–8. Available from: <https://www.sciencedirect.com/science/article/pii/S1525001616319864>

60. Zhao X, Chen J, Qiu M, Li Y, Glass Z, Xu Q. Imidazole-Based Synthetic Lipidoids for In Vivo mRNA Delivery into Primary T Lymphocytes. *Angewandte Chemie - International Edition*. 2020 Nov 2;59(45):20083–9.
61. Zhang Y, Sun C, Wang C, Jankovic KE, Dong Y. Lipids and Lipid Derivatives for RNA Delivery. *Chem Rev* [Internet]. 2021 Oct 27;121(20):12181–277. Available from: <https://doi.org/10.1021/acs.chemrev.1c00244>
62. Zhang L, More KR, Ojha A, Jackson CB, Quinlan BD, Li H, et al. Effect of mRNA-LNP components of two globally-marketed COVID-19 vaccines on efficacy and stability. *NPJ Vaccines* [Internet]. 2023;8(1):156. Available from: <https://doi.org/10.1038/s41541-023-00751-6>
63. Buschmann MD, Carrasco MJ, Alishetty S, Paige M, Alameh MG, Weissman D. Nanomaterial Delivery Systems for mRNA Vaccines. *Vaccines (Basel)* [Internet]. 2021;9(1). Available from: <https://www.mdpi.com/2076-393X/9/1/65>
64. Singer SJ, Nicolson GL. The Fluid Mosaic Model of the Structure of Cell Membranes. *Science* (1979) [Internet]. 1972 Feb 18;175(4023):720–31. Available from: <https://doi.org/10.1126/science.175.4023.720>
65. Ricci M, Oliva R, Del Vecchio P, Paolantoni M, Morresi A, Sassi P. DMSO-induced perturbation of thermotropic properties of cholesterol-containing DPPC liposomes. *Biochimica et Biophysica Acta (BBA) - Biomembranes* [Internet]. 2016;1858(12):3024–31. Available from: <https://www.sciencedirect.com/science/article/pii/S0005273616303108>
66. Kulkarni JA, Witzigmann D, Leung J, Tam YYC, Cullis PR. On the role of helper lipids in lipid nanoparticle formulations of siRNA. *Nanoscale* [Internet]. 2019;11(45):21733–9. Available from: <http://dx.doi.org/10.1039/C9NR09347H>
67. Herrera M, Kim J, Eygeris Y, Jozic A, Sahay G. Illuminating endosomal escape of polymorphic lipid nanoparticles that boost mRNA delivery. *Biomater Sci* [Internet]. 2021;9(12):4289–300. Available from: <http://dx.doi.org/10.1039/D0BM01947J>
68. Patel S, Ashwanikumar N, Robinson E, Xia Y, Mihai C, Griffith JP, et al. Naturally-occurring cholesterol analogues in lipid nanoparticles induce polymorphic shape and enhance intracellular delivery of mRNA. *Nat Commun* [Internet]. 2020;11(1):983. Available from: <https://doi.org/10.1038/s41467-020-14527-2>
69. Álvarez-Benedicto E, Farbiak L, Márquez Ramírez M, Wang X, Johnson LT, Mian O, et al. Optimization of phospholipid chemistry for improved lipid nanoparticle (LNP) delivery of messenger RNA (mRNA). *Biomater Sci* [Internet]. 2022;10(2):549–59. Available from: <http://dx.doi.org/10.1039/D1BM01454D>
70. Kulkarni JA, Myhre JL, Chen S, Tam YYC, Danescu A, Richman JM, et al. Design of lipid nanoparticles for in vitro and in vivo delivery of plasmid DNA. *Nanomedicine* [Internet]. 2017;13(4):1377–87. Available from: <https://www.sciencedirect.com/science/article/pii/S1549963416302313>

71. Hald Albertsen C, Kulkarni JA, Witzigmann D, Lind M, Petersson K, Simonsen JB. The role of lipid components in lipid nanoparticles for vaccines and gene therapy. *Adv Drug Deliv Rev* [Internet]. 2022;188:114416. Available from: <https://www.sciencedirect.com/science/article/pii/S0169409X22003064>
72. Kauffman KJ, Dorkin JR, Yang JH, Heartlein MW, DeRosa F, Mir FF, et al. Optimization of Lipid Nanoparticle Formulations for mRNA Delivery in Vivo with Fractional Factorial and Definitive Screening Designs. *Nano Lett* [Internet]. 2015 Nov 11;15(11):7300–6. Available from: <https://doi.org/10.1021/acs.nanolett.5b02497>
73. Cheng Q, Wei T, Farbiak L, Johnson LT, Dilliard SA, Siegwart DJ. Selective organ targeting (SORT) nanoparticles for tissue-specific mRNA delivery and CRISPR–Cas gene editing. *Nat Nanotechnol* [Internet]. 2020;15(4):313–20. Available from: <https://doi.org/10.1038/s41565-020-0669-6>
74. Abuchowski A, McCoy JR, Palczuk NC, van Es T, Davis FF. Effect of covalent attachment of polyethylene glycol on immunogenicity and circulating life of bovine liver catalase. *Journal of Biological Chemistry* [Internet]. 1977;252(11):3582–6. Available from: <https://www.sciencedirect.com/science/article/pii/S0021925817402924>
75. Barenholz Y (Chezy). Doxil® — The first FDA-approved nano-drug: Lessons learned. *Journal of Controlled Release* [Internet]. 2012;160(2):117–34. Available from: <https://www.sciencedirect.com/science/article/pii/S0168365912002301>
76. Holland JW, Hui C, Cullis PR, Madden TD. Poly(ethylene glycol)–Lipid Conjugates Regulate the Calcium-Induced Fusion of Liposomes Composed of Phosphatidylethanolamine and Phosphatidylserine. *Biochemistry* [Internet]. 1996 Jan 1;35(8):2618–24. Available from: <https://doi.org/10.1021/bi952000v>
77. Holland JW, Hui C, Cullis PR, Madden TD. Poly(ethylene glycol)–Lipid Conjugates Regulate the Calcium-Induced Fusion of Liposomes Composed of Phosphatidylethanolamine and Phosphatidylserine. *Biochemistry* [Internet]. 1996 Jan 1;35(8):2618–24. Available from: <https://doi.org/10.1021/bi952000v>
78. Suzuki T, Suzuki Y, Hihara T, Kubara K, Kondo K, Hyodo K, et al. PEG shedding-rate-dependent blood clearance of PEGylated lipid nanoparticles in mice: Faster PEG shedding attenuates anti-PEG IgM production. *Int J Pharm* [Internet]. 2020;588:119792. Available from: <https://www.sciencedirect.com/science/article/pii/S0378517320307778>
79. Judge A, McClintock K, Phelps JR, MacLachlan I. Hypersensitivity and Loss of Disease Site Targeting Caused by Antibody Responses to PEGylated Liposomes. *Molecular Therapy* [Internet]. 2006;13(2):328–37. Available from: <https://www.sciencedirect.com/science/article/pii/S1525001605016205>
80. Oberli MA, Reichmuth AM, Dorkin JR, Mitchell MJ, Fenton OS, Jaklenec A, et al. Lipid Nanoparticle Assisted mRNA Delivery for Potent Cancer Immunotherapy. *Nano Lett* [Internet]. 2017 Mar 8;17(3):1326–35. Available from: <https://doi.org/10.1021/acs.nanolett.6b03329>
81. Mui BL, Tam YK, Jayaraman M, Ansell SM, Du X, Tam YYC, et al. Influence of Polyethylene Glycol Lipid Desorption Rates on Pharmacokinetics and Pharmacodynamics of siRNA Lipid

- Nanoparticles. *Mol Ther Nucleic Acids* [Internet]. 2013 Jan 1;2. Available from: <https://doi.org/10.1038/mtna.2013.66>
82. Abu Lila AS, Kiwada H, Ishida T. The accelerated blood clearance (ABC) phenomenon: Clinical challenge and approaches to manage. *Journal of Controlled Release* [Internet]. 2013;172(1):38–47. Available from: <https://www.sciencedirect.com/science/article/pii/S0168365913004367>
  83. Carreño JM, Singh G, Tcheou J, Srivastava K, Gleason C, Muramatsu H, et al. mRNA-1273 but not BNT162b2 induces antibodies against polyethylene glycol (PEG) contained in mRNA-based vaccine formulations. *Vaccine* [Internet]. 2022;40(42):6114–24. Available from: <https://www.sciencedirect.com/science/article/pii/S0264410X22010039>
  84. Kauffman KJ, Dorkin JR, Yang JH, Heartlein MW, DeRosa F, Mir FF, et al. Optimization of Lipid Nanoparticle Formulations for mRNA Delivery in Vivo with Fractional Factorial and Definitive Screening Designs. *Nano Lett* [Internet]. 2015 Nov 11;15(11):7300–6. Available from: <https://doi.org/10.1021/acs.nanolett.5b02497>
  85. Jayaraman M, Ansell SM, Mui BL, Tam YK, Chen J, Du X, et al. Maximizing the potency of siRNA lipid nanoparticles for hepatic gene silencing in vivo. *Angewandte Chemie - International Edition*. 2012 Aug 20;51(34):8529–33.
  86. Lam K, Schreiner P, Leung A, Stainton P, Reid S, Yaworski E, et al. Optimizing Lipid Nanoparticles for Delivery in Primates. *Advanced Materials*. 2023 Jun 28;35(26).
  87. Roces CB, Lou G, Jain N, Abraham S, Thomas A, Halbert GW, et al. Manufacturing Considerations for the Development of Lipid Nanoparticles Using Microfluidics. *Pharmaceutics* [Internet]. 2020;12(11). Available from: <https://www.mdpi.com/1999-4923/12/11/1095>
  88. Li Q, Shi R, Xu H, AboulFotouh K, Sung MMH, Oguin TH, et al. Thin-film freeze-drying of an influenza virus hemagglutinin mRNA vaccine in unilamellar lipid nanoparticles with blebs. *Journal of Controlled Release* [Internet]. 2024;375:829–38. Available from: <https://www.sciencedirect.com/science/article/pii/S0168365924006400>
  89. Chander N, Basha G, Yan Cheng MH, Witzigmann D, Cullis PR. Lipid nanoparticle mRNA systems containing high levels of sphingomyelin engender higher protein expression in hepatic and extra-hepatic tissues. *Mol Ther Methods Clin Dev* [Internet]. 2023 Sep 14;30:235–45. Available from: <https://doi.org/10.1016/j.omtm.2023.06.005>
  90. Hassett KJ, Benenato KE, Jacquinet E, Lee A, Woods A, Yuzhakov O, et al. Optimization of Lipid Nanoparticles for Intramuscular Administration of mRNA Vaccines. *Mol Ther Nucleic Acids* [Internet]. 2019 Apr 15;15:1–11. Available from: <https://doi.org/10.1016/j.omtn.2019.01.013>
  91. Oberli MA, Reichmuth AM, Dorkin JR, Mitchell MJ, Fenton OS, Jaklenec A, et al. Lipid Nanoparticle Assisted mRNA Delivery for Potent Cancer Immunotherapy. *Nano Lett* [Internet]. 2017 Mar 8;17(3):1326–35. Available from: <https://doi.org/10.1021/acs.nanolett.6b03329>
  92. Chen S, Tam YYC, Lin PJC, Sung MMH, Tam YK, Cullis PR. Influence of particle size on the in vivo potency of lipid nanoparticle formulations of siRNA. *Journal of Controlled Release* [Internet].

- 2016;235:236–44. Available from: <https://www.sciencedirect.com/science/article/pii/S0168365916303492>
93. Knop K, Hoogenboom R, Fischer D, Schubert US. Poly(ethylene glycol) in drug delivery: Pros and cons as well as potential alternatives. Vol. 49, *Angewandte Chemie - International Edition*. 2010. p. 6288–308.
  94. Zhang X, Zhao W, Nguyen GN, Zhang C, Zeng C, Yan J, et al. Functionalized lipid-like nanoparticles for in vivo mRNA delivery and base editing. *Sci Adv* [Internet]. 2020;6(34):eabc2315. Available from: <https://www.science.org/doi/abs/10.1126/sciadv.abc2315>
  95. de Almeida M, Susnik E, Drasler B, Taladriz-Blanco P, Petri-Fink A, Rothen-Rutishauser B. Understanding nanoparticle endocytosis to improve targeting strategies in nanomedicine. *Chem Soc Rev* [Internet]. 2021;50(9):5397–434. Available from: <http://dx.doi.org/10.1039/D0CS01127D>
  96. Kaksonen M, Roux A. Mechanisms of clathrin-mediated endocytosis. *Nat Rev Mol Cell Biol* [Internet]. 2018;19(5):313–26. Available from: <https://doi.org/10.1038/nrm.2017.132>
  97. Iversen TG, Skotland T, Sandvig K. Endocytosis and intracellular transport of nanoparticles: Present knowledge and need for future studies. *Nano Today* [Internet]. 2011;6(2):176–85. Available from: <https://www.sciencedirect.com/science/article/pii/S1748013211000181>
  98. Miao L, Lin J, Huang Y, Li L, Delcassian D, Ge Y, et al. Synergistic lipid compositions for albumin receptor mediated delivery of mRNA to the liver. *Nat Commun* [Internet]. 2020;11(1):2424. Available from: <https://doi.org/10.1038/s41467-020-16248-y>
  99. Sahay G, Querbes W, Alabi C, Eltoukhy A, Sarkar S, Zurenko C, et al. Efficiency of siRNA delivery by lipid nanoparticles is limited by endocytic recycling. *Nat Biotechnol* [Internet]. 2013;31(7):653–8. Available from: <https://doi.org/10.1038/nbt.2614>
  100. Alameh MG, Tombácz I, Bettini E, Lederer K, Ndeupen S, Sittplangkoon C, et al. Lipid nanoparticles enhance the efficacy of mRNA and protein subunit vaccines by inducing robust T follicular helper cell and humoral responses. *Immunity* [Internet]. 2021 Dec 14;54(12):2877–2892.e7. Available from: <https://doi.org/10.1016/j.immuni.2021.11.001>
  101. Lin PJC, Tam YYC, Hafez I, Sandhu A, Chen S, Ciufolini MA, et al. Influence of cationic lipid composition on uptake and intracellular processing of lipid nanoparticle formulations of siRNA. *Nanomedicine* [Internet]. 2013;9(2):233–46. Available from: <https://www.sciencedirect.com/science/article/pii/S1549963412002948>
  102. Lee Y, Jeong M, Park J, Jung H, Lee H. Immunogenicity of lipid nanoparticles and its impact on the efficacy of mRNA vaccines and therapeutics. *Exp Mol Med* [Internet]. 2023;55(10):2085–96. Available from: <https://doi.org/10.1038/s12276-023-01086-x>
  103. Hajj KA, Ball RL, Deluty SB, Singh SR, Strelkova D, Knapp CM, et al. Branched-Tail Lipid Nanoparticles Potently Deliver mRNA In Vivo due to Enhanced Ionization at Endosomal pH. *Small*. 2019 Feb 8;15(6).

104. Hagedorn L, Jürgens DC, Merkel OM, Winkeljann B. Endosomal escape mechanisms of extracellular vesicle-based drug carriers: lessons for lipid nanoparticle design. *Extracell Vesicles Circ Nucl Acids* [Internet]. 2024;5(3). Available from: <https://www.oaepublish.com/articles/evcna.2024.19>
105. Veiga N, Goldsmith M, Granot Y, Rosenblum D, Dammes N, Kedmi R, et al. Cell specific delivery of modified mRNA expressing therapeutic proteins to leukocytes. *Nat Commun* [Internet]. 2018;9(1):4493. Available from: <https://doi.org/10.1038/s41467-018-06936-1>
106. Liu S, Cheng Q, Wei T, Yu X, Johnson LT, Farbiak L, et al. Membrane-destabilizing ionizable phospholipids for organ-selective mRNA delivery and CRISPR–Cas gene editing. *Nat Mater* [Internet]. 2021;20(5):701–10. Available from: <https://doi.org/10.1038/s41563-020-00886-0>
107. Bilardo R, Traldi F, Vdovchenko A, Resmini M. Influence of surface chemistry and morphology of nanoparticles on protein corona formation. Vol. 14, *Wiley Interdisciplinary Reviews: Nanomedicine and Nanobiotechnology*. John Wiley and Sons Inc; 2022.
108. Ngo W, Ahmed S, Blackadar C, Bussin B, Ji Q, Mladjenovic SM, et al. Why nanoparticles prefer liver macrophage cell uptake in vivo. *Adv Drug Deliv Rev* [Internet]. 2022;185:114238. Available from: <https://www.sciencedirect.com/science/article/pii/S0169409X22001284>
109. Poon W, Zhang YN, Ouyang B, Kingston BR, Wu JLY, Wilhelm S, et al. Elimination Pathways of Nanoparticles. *ACS Nano* [Internet]. 2019 May 28;13(5):5785–98. Available from: <https://doi.org/10.1021/acsnano.9b01383>
110. Zhang YN, Poon W, Tavares AJ, McGilvray ID, Chan WCW. Nanoparticle–liver interactions: Cellular uptake and hepatobiliary elimination. *Journal of Controlled Release* [Internet]. 2016;240:332–48. Available from: <https://www.sciencedirect.com/science/article/pii/S0168365916300190>
111. Kim J, Eygeris Y, Ryals RC, Jozić A, Sahay G. Strategies for non-viral vectors targeting organs beyond the liver. *Nat Nanotechnol* [Internet]. 2024;19(4):428–47. Available from: <https://doi.org/10.1038/s41565-023-01563-4>
112. Akinc A, Querbes W, De S, Qin J, Frank-Kamenetsky M, Jayaprakash KN, et al. Targeted Delivery of RNAi Therapeutics With Endogenous and Exogenous Ligand-Based Mechanisms. *Molecular Therapy* [Internet]. 2010;18(7):1357–64. Available from: <https://www.sciencedirect.com/science/article/pii/S1525001616310814>
113. Sebastiani F, Yanez Arteta M, Lerche M, Porcar L, Lang C, Bragg RA, et al. Apolipoprotein E Binding Drives Structural and Compositional Rearrangement of mRNA-Containing Lipid Nanoparticles. *ACS Nano* [Internet]. 2021 Apr 27;15(4):6709–22. Available from: <https://doi.org/10.1021/acsnano.0c10064>
114. Kolate A, Baradia D, Patil S, Vhora I, Kore G, Misra A. PEG — A versatile conjugating ligand for drugs and drug delivery systems. *Journal of Controlled Release* [Internet]. 2014;192:67–81. Available from: <https://www.sciencedirect.com/science/article/pii/S0168365914004556>

115. Saber N, Senti ME, Schiffelers RM. Lipid Nanoparticles for Nucleic Acid Delivery Beyond the Liver. *Hum Gene Ther* [Internet]. 2024;35(17–18):617–27. Available from: <https://doi.org/10.1089/hum.2024.106>
116. Souri M, Soltani M, Moradi Kashkooli F, Kiani Shahvandi M. Engineered strategies to enhance tumor penetration of drug-loaded nanoparticles. *Journal of Controlled Release* [Internet]. 2022;341:227–46. Available from: <https://www.sciencedirect.com/science/article/pii/S0168365921006192>
117. Narum SM, Le T, Le DP, Lee JC, Donahue ND, Yang W, et al. Chapter 4 - Passive targeting in nanomedicine: fundamental concepts, body interactions, and clinical potential. In: Chung EJ, Leon L, Rinaldi C, editors. *Nanoparticles for Biomedical Applications* [Internet]. Elsevier; 2020. p. 37–53. Available from: <https://www.sciencedirect.com/science/article/pii/B9780128166628000047>
118. Marques AC, Costa PJ, Velho S, Amaral MH. Functionalizing nanoparticles with cancer-targeting antibodies: A comparison of strategies. *Journal of Controlled Release* [Internet]. 2020;320:180–200. Available from: <https://www.sciencedirect.com/science/article/pii/S0168365920300547>
119. U.S. Food and Drug Administration. Approved Cellular and Gene Therapy Products. 2024.
120. Swart LE, Fens MHAM, van Oort A, Waranecki P, Mata Casimiro LD, Tuk D, et al. Increased Bone Marrow Uptake and Accumulation of Very-Late Antigen-4 Targeted Lipid Nanoparticles. *Pharmaceutics* [Internet]. 2023;15(6). Available from: <https://www.mdpi.com/1999-4923/15/6/1603>
121. Dammes N, Goldsmith M, Ramishetti S, Dearling JJJ, Veiga N, Packard AB, et al. Conformation-sensitive targeting of lipid nanoparticles for RNA therapeutics. *Nat Nanotechnol* [Internet]. 2021;16(9):1030–8. Available from: <https://doi.org/10.1038/s41565-021-00928-x>
122. Nong J, Glassman PM, Shuvaev V V, Reyes-Estevés S, Descamps HC, Kiseleva RY, et al. Targeting lipid nanoparticles to the blood-brain barrier to ameliorate acute ischemic stroke. *Molecular Therapy* [Internet]. 2024 May 1;32(5):1344–58. Available from: <https://doi.org/10.1016/j.ymthe.2024.03.004>
123. Maclachlan I. Liposomal formulations for nucleic acid delivery. In: *Antisense Drug Technology: Principles, Strategies, and Applications*, Second Edition. 2007. p. 237–70.
124. Bangham AD, Horne RW. Negative staining of phospholipids and their structural modification by surface-active agents as observed in the electron microscope. *J Mol Biol* [Internet]. 1964;8(5):660-IN10. Available from: <https://www.sciencedirect.com/science/article/pii/S0022283664801157>
125. Jahn A, Vreeland WN, Gaitan M, Locascio LE. Controlled Vesicle Self-Assembly in Microfluidic Channels with Hydrodynamic Focusing. *J Am Chem Soc* [Internet]. 2004 Mar 1;126(9):2674–5. Available from: <https://doi.org/10.1021/ja0318030>

126. Shepherd SJ, Issadore D, Mitchell MJ. Microfluidic formulation of nanoparticles for biomedical applications. *Biomaterials* [Internet]. 2021;274:120826. Available from: <https://www.sciencedirect.com/science/article/pii/S0142961221001824>
127. Terada T, Kulkarni JA, Huynh A, Chen S, van der Meel R, Tam YYC, et al. Characterization of Lipid Nanoparticles Containing Ionizable Cationic Lipids Using Design-of-Experiments Approach. *Langmuir* [Internet]. 2021 Jan 26;37(3):1120–8. Available from: <https://doi.org/10.1021/acs.langmuir.0c03039>
128. Jahn A, Stavis SM, Hong JS, Vreeland WN, DeVoe DL, Gaitan M. Microfluidic Mixing and the Formation of Nanoscale Lipid Vesicles. *ACS Nano* [Internet]. 2010 Apr 27;4(4):2077–87. Available from: <https://doi.org/10.1021/nn901676x>
129. Jahn A, Vreeland WN, DeVoe DL, Locascio LE, Gaitan M. Microfluidic Directed Formation of Liposomes of Controlled Size. *Langmuir* [Internet]. 2007 May 1;23(11):6289–93. Available from: <https://doi.org/10.1021/la070051a>
130. Binici B, Borah A, Watts JA, McLoughlin D, Perrie Y. The influence of citrate buffer molarity on mRNA-LNPs: Exploring factors beyond general critical quality attributes. *Int J Pharm* [Internet]. 2025;668:124942. Available from: <https://www.sciencedirect.com/science/article/pii/S0378517324011761>
131. Li C, Deng Y. A novel method for the preparation of liposomes: Freeze drying of monophasic solutions. *J Pharm Sci* [Internet]. 2004;93(6):1403–14. Available from: <https://www.sciencedirect.com/science/article/pii/S0022354916315337>
132. O'Brien Laramy MN, Costa AP, Cebrero YM, Joseph J, Sarode A, Zang N, et al. Process Robustness in Lipid Nanoparticle Production: A Comparison of Microfluidic and Turbulent Jet Mixing. *Mol Pharm* [Internet]. 2023 Aug 7;20(8):4285–96. Available from: <https://doi.org/10.1021/acs.molpharmaceut.3c00390>
133. Capretto L, Cheng W, Hill M, Zhang X. Micromixing Within Microfluidic Devices. In: Lin B, editor. *Microfluidics: Technologies and Applications* [Internet]. Berlin, Heidelberg: Springer Berlin Heidelberg; 2011. p. 27–68. Available from: [https://doi.org/10.1007/128\\_2011\\_150](https://doi.org/10.1007/128_2011_150)
134. Tóth EL, Holczer EG, Iván K, Fürjes P. Optimized Simulation and Validation of Particle Advection in Asymmetric Staggered Herringbone Type Micromixers. *Micromachines (Basel)* [Internet]. 2015;6(1):136–50. Available from: <https://www.mdpi.com/2072-666X/6/1/136>
135. Webb C, Forbes N, Roces CB, Anderluzzi G, Lou G, Abraham S, et al. Using microfluidics for scalable manufacturing of nanomedicines from bench to GMP: A case study using protein-loaded liposomes. *Int J Pharm* [Internet]. 2020;582:119266. Available from: <https://www.sciencedirect.com/science/article/pii/S0378517320302507>
136. Lee CY, Wang WT, Liu CC, Fu LM. Passive mixers in microfluidic systems: A review. *Chemical Engineering Journal* [Internet]. 2016;288:146–60. Available from: <https://www.sciencedirect.com/science/article/pii/S138589471501596X>
137. European Commission. Eudralex – Vol. 4 – “Good Manufacturing Practice (GMP) guidelines.”

138. Ferhan AR, Park S, Park H, Tae H, Jackman JA, Cho NJ. Lipid Nanoparticle Technologies for Nucleic Acid Delivery: A Nanoarchitectonics Perspective. *Adv Funct Mater* [Internet]. 2022;32(37):2203669. Available from: <https://advanced.onlinelibrary.wiley.com/doi/abs/10.1002/adfm.202203669>
139. Webb C, Forbes N, Roces CB, Anderluzzi G, Lou G, Abraham S, et al. Using microfluidics for scalable manufacturing of nanomedicines from bench to GMP: A case study using protein-loaded liposomes. *Int J Pharm* [Internet]. 2020;582:119266. Available from: <https://www.sciencedirect.com/science/article/pii/S0378517320302507>
140. Shepherd SJ, Han X, Mukalel AJ, El-Mayta R, Thatte AS, Wu J, et al. Throughput-scalable manufacturing of SARS-CoV-2 mRNA lipid nanoparticle vaccines. *Proceedings of the National Academy of Sciences* [Internet]. 2023;120(33):e2303567120. Available from: <https://www.pnas.org/doi/abs/10.1073/pnas.2303567120>
141. Webb C, Ip S, Bathula N V, Popova P, Soriano SK V, Ly HH, et al. Current Status and Future Perspectives on mRNA Drug Manufacturing. *Mol Pharm* [Internet]. 2022 Apr 4;19(4):1047–58. Available from: <https://doi.org/10.1021/acs.molpharmaceut.2c00010>
142. Forbes N, Hussain MT, Briuglia ML, Edwards DP, Horst JH ter, Szita N, et al. Rapid and scale-independent microfluidic manufacture of liposomes entrapping protein incorporating in-line purification and at-line size monitoring. *Int J Pharm* [Internet]. 2019;556:68–81. Available from: <https://www.sciencedirect.com/science/article/pii/S037851731830886X>
143. Nag K, Sarker MdEH, Kumar S, Khan H, Chakraborty S, Islam MdJ, et al. DoE-derived continuous and robust process for manufacturing of pharmaceutical-grade wide-range LNPs for RNA-vaccine/drug delivery. *Sci Rep* [Internet]. 2022;12(1):9394. Available from: <https://doi.org/10.1038/s41598-022-12100-z>
144. Pattnaik P. Improving liposome integrity and easing bottlenecks to production. *Pharmaceutical Technology Europe*. 2009 Jun 1;21:24–8.
145. Yassini P, Hutchens M, Paila YD, Schoch L, Aunins A, Siangphoe U, et al. Interim analysis of a phase 1 randomized clinical trial on the safety and immunogenicity of the mRNA-1283 SARS-CoV-2 vaccine in adults. *Hum Vaccin Immunother* [Internet]. 2023 Jan 2;19(1):2190690. Available from: <https://doi.org/10.1080/21645515.2023.2190690>
146. Kasper JC, Winter G, Friess W. Recent advances and further challenges in lyophilization. *European Journal of Pharmaceutics and Biopharmaceutics* [Internet]. 2013;85(2):162–9. Available from: <https://www.sciencedirect.com/science/article/pii/S093964111300218X>
147. Chen C, Han D, Cai C, Tang X. An overview of liposome lyophilization and its future potential. *Journal of Controlled Release* [Internet]. 2010;142(3):299–311. Available from: <https://www.sciencedirect.com/science/article/pii/S0168365909007366>
148. Kim B, Hosn RR, Remba T, Yun D, Li N, Abraham W, et al. Optimization of storage conditions for lipid nanoparticle-formulated self-replicating RNA vaccines. *Journal of Controlled Release* [Internet]. 2023;353:241–53. Available from: <https://www.sciencedirect.com/science/article/pii/S0168365922007672>

149. Muramatsu H, Lam K, Bajusz C, Laczkó D, Karikó K, Schreiner P, et al. Lyophilization provides long-term stability for a lipid nanoparticle-formulated, nucleoside-modified mRNA vaccine. *Molecular Therapy* [Internet]. 2022 May 4;30(5):1941–51. Available from: <https://doi.org/10.1016/j.ymthe.2022.02.001>
150. Ball RL, Bajaj P, Whitehead KA. Achieving long-term stability of lipid nanoparticles: examining the effect of pH, temperature, and lyophilization. *Int J Nanomedicine* [Internet]. 2016;12:305–15. Available from: <https://api.semanticscholar.org/CorpusID:12793224>
151. Zhao P, Hou X, Yan J, Du S, Xue Y, Li W, et al. Long-term storage of lipid-like nanoparticles for mRNA delivery. *Bioact Mater* [Internet]. 2020;5(2):358–63. Available from: <https://www.sciencedirect.com/science/article/pii/S2452199X20300414>
152. Prabhakaran E, Hasan A, Karunanidhi P. Solid lipid nanoparticles: A review. 2011 Nov 30;2.
153. Danaei M, Dehghankhold M, Ataei S, Hasanzadeh Davarani F, Javanmard R, Dokhani A, et al. Impact of Particle Size and Polydispersity Index on the Clinical Applications of Lipidic Nanocarrier Systems. *Pharmaceutics* [Internet]. 2018;10(2). Available from: <https://www.mdpi.com/1999-4923/10/2/57>
154. Alexander M, Dalgleish DG. Dynamic Light Scattering Techniques and Their Applications in Food Science. *Food Biophys* [Internet]. 2006;1(1):2–13. Available from: <https://doi.org/10.1007/s11483-005-9000-1>
155. Gupta S, De Mel JU, Schneider GJ. Dynamics of liposomes in the fluid phase. *Curr Opin Colloid Interface Sci* [Internet]. 2019;42:121–36. Available from: <https://www.sciencedirect.com/science/article/pii/S1359029418301511>
156. Oussoren C, Zuidema J, Crommelin DJA, Storm G. Lymphatic uptake and biodistribution of liposomes after subcutaneous injection.: II. Influence of liposomal size, lipid composition and lipid dose. *Biochimica et Biophysica Acta (BBA) - Biomembranes* [Internet]. 1997;1328(2):261–72. Available from: <https://www.sciencedirect.com/science/article/pii/S0005273697001223>
157. Younis MA, Khalil IA, Elewa YHA, Kon Y, Harashima H. Ultra-small lipid nanoparticles encapsulating sorafenib and midkine-siRNA selectively-eradicate sorafenib-resistant hepatocellular carcinoma in vivo. *Journal of Controlled Release* [Internet]. 2021;331:335–49. Available from: <https://www.sciencedirect.com/science/article/pii/S0168365921000304>
158. Uchiyama K, Nagayasu A, Yamagiwa Y, Nishida T, Harashima H, Kiwada H. Effects of the size and fluidity of liposomes on their accumulation in tumors: A presumption of their interaction with tumors. *Int J Pharm* [Internet]. 1995;121(2):195–203. Available from: <https://www.sciencedirect.com/science/article/pii/037851739500015B>
159. Kastner E, Perrie Y. Particle Size Analysis of Micro and Nanoparticles. In: Müllertz A, Perrie Y, Rades T, editors. *Analytical Techniques in the Pharmaceutical Sciences* [Internet]. New York, NY: Springer New York; 2016. p. 677–99. Available from: [https://doi.org/10.1007/978-1-4939-4029-5\\_21](https://doi.org/10.1007/978-1-4939-4029-5_21)

160. Stetefeld J, McKenna SA, Patel TR. Dynamic light scattering: a practical guide and applications in biomedical sciences. *Biophys Rev* [Internet]. 2016;8(4):409–27. Available from: <https://doi.org/10.1007/s12551-016-0218-6>
161. Bhattacharjee S. DLS and zeta potential – What they are and what they are not? *Journal of Controlled Release* [Internet]. 2016;235:337–51. Available from: <https://www.sciencedirect.com/science/article/pii/S0168365916303832>
162. Brader ML, Williams SJ, Banks JM, Hui WH, Zhou ZH, Jin L. Encapsulation state of messenger RNA inside lipid nanoparticles. *Biophys J* [Internet]. 2021 Jul 20;120(14):2766–70. Available from: <https://doi.org/10.1016/j.bpj.2021.03.012>
163. Arteta MY, Kjellman T, Bartesaghi S, Wallin S, Wu X, Kvist AJ, et al. Successful reprogramming of cellular protein production through mRNA delivered by functionalized lipid nanoparticles. *Proceedings of the National Academy of Sciences* [Internet]. 2018;115(15):E3351–60. Available from: <https://www.pnas.org/doi/abs/10.1073/pnas.1720542115>
164. Eygeris Y, Patel S, Jozic A, Sahay G. Deconvoluting Lipid Nanoparticle Structure for Messenger RNA Delivery. *Nano Lett* [Internet]. 2020 Jun 10;20(6):4543–9. Available from: <https://doi.org/10.1021/acs.nanolett.0c01386>
165. Kulkarni JA, Darjuan MM, Mercer JE, Chen S, van der Meel R, Thewalt JL, et al. On the Formation and Morphology of Lipid Nanoparticles Containing Ionizable Cationic Lipids and siRNA. *ACS Nano* [Internet]. 2018 May 22;12(5):4787–95. Available from: [https://doi.org/10.1021/acsnano.8b01516](https://doi.org/10.1021/acs.nano.8b01516)
166. Yamamoto E, Miyazaki S, Aoyama C, Kato M. A simple and rapid measurement method of encapsulation efficiency of doxorubicin loaded liposomes by direct injection of the liposomal suspension to liquid chromatography. *Int J Pharm* [Internet]. 2018;536(1):21–8. Available from: <https://www.sciencedirect.com/science/article/pii/S0378517317310906>
167. Feczko T, Tóth J, Dósa Gy, Gyenis J. Optimization of protein encapsulation in PLGA nanoparticles. *Chemical Engineering and Processing: Process Intensification* [Internet]. 2011;50(8):757–65. Available from: <https://www.sciencedirect.com/science/article/pii/S0255270111001498>
168. Lokras A, Chakravarty A, Rades T, Christensen D, Franzyk H, Thakur A, et al. Simultaneous quantification of multiple RNA cargos co-loaded into nanoparticle-based delivery systems. *Int J Pharm* [Internet]. 2022;626:122171. Available from: <https://www.sciencedirect.com/science/article/pii/S0378517322007256>
169. Bizmark N, Nayagam S, Kim B, Amelemah DF, Zhang D, Datta SS, et al. Ribogreen Fluorescent Assay Kinetics to Measure Ribonucleic Acid Loading into Lipid Nanoparticle Carriers. *Adv Mater Interfaces* [Internet]. 2024;11(17):2301083. Available from: <https://advanced.onlinelibrary.wiley.com/doi/abs/10.1002/admi.202301083>
170. Hara S, Arase S, Sano S, Suzuki T, Mizogaki I, Sato S, et al. Anion exchange-HPLC method for evaluating the encapsulation efficiency of mRNA-loaded lipid nanoparticles using analytical quality by design. *Journal of Chromatography B* [Internet]. 2024;1247:124317. Available from: <https://www.sciencedirect.com/science/article/pii/S157002322400326X>

171. ICH, Harmonised Tripartite Guideline, Impurities: Guideline for residual solvents Q3C (R5). 2016. p. 1–25.
172. Miryam Naddaf. First trial of ‘base editing’ in humans lowers cholesterol — but raises safety concerns. *Nature*. 2023;
173. Chen BM, Cheng TL, Roffler SR. Polyethylene Glycol Immunogenicity: Theoretical, Clinical, and Practical Aspects of Anti-Polyethylene Glycol Antibodies. *ACS Nano* [Internet]. 2021 Sep 28;15(9):14022–48. Available from: <https://doi.org/10.1021/acsnano.1c05922>
174. Zhang P, Sun F, Liu S, Jiang S. Anti-PEG antibodies in the clinic: Current issues and beyond PEGylation. *Journal of Controlled Release* [Internet]. 2016;244:184–93. Available from: <https://www.sciencedirect.com/science/article/pii/S0168365916304175>
175. Kang DD, Li H, Dong Y. Advancements of in vitro transcribed mRNA (IVT mRNA) to enable translation into the clinics. *Adv Drug Deliv Rev* [Internet]. 2023;199:114961. Available from: <https://www.sciencedirect.com/science/article/pii/S0169409X23002764>
176. Kis Z, Kontoravdi C, Shattock R, Shah N. Resources, Production Scales and Time Required for Producing RNA Vaccines for the Global Pandemic Demand. *Vaccines (Basel)* [Internet]. 2021;9(1). Available from: <https://www.mdpi.com/2076-393X/9/1/3>
177. Rosa SS, Prazeres DMF, Azevedo AM, Marques MPC. mRNA vaccines manufacturing: Challenges and bottlenecks. *Vaccine* [Internet]. 2021;39(16):2190–200. Available from: <https://www.sciencedirect.com/science/article/pii/S0264410X21003194>
178. Geall AJ, Verma A, Otten GR, Shaw CA, Hekele A, Banerjee K, et al. Nonviral delivery of self-amplifying RNA vaccines. *Proc Natl Acad Sci U S A*. 2012 Sep 4;109(36):14604–9.
179. Leung AKK, Tam YYC, Chen S, Hafez IM, Cullis PR. Microfluidic Mixing: A General Method for Encapsulating Macromolecules in Lipid Nanoparticle Systems. *J Phys Chem B* [Internet]. 2015 Jul 16;119(28):8698–706. Available from: <https://doi.org/10.1021/acs.jpcc.5b02891>
180. Maeki M, Saito T, Sato Y, Yasui T, Kaji N, Ishida A, et al. A strategy for synthesis of lipid nanoparticles using microfluidic devices with a mixer structure. *RSC Adv* [Internet]. 2015;5:46181–5. Available from: <https://api.semanticscholar.org/CorpusID:53391028>
181. Daniel S, Kis Z, Kontoravdi C, Shah N. Quality by Design for enabling RNA platform production processes. *Trends Biotechnol* [Internet]. 2022;40(10):1213–28. Available from: <https://www.sciencedirect.com/science/article/pii/S0167779922000804>
182. Webb C, Forbes N, Roces CB, Anderluzzi G, Lou G, Abraham S, et al. Using microfluidics for scalable manufacturing of nanomedicines from bench to GMP: A case study using protein-loaded liposomes. *Int J Pharm* [Internet]. 2020;582:119266. Available from: <https://www.sciencedirect.com/science/article/pii/S0378517320302507>
183. Roces CB, Khadke S, Christensen D, Perrie Y. Scale-Independent Microfluidic Production of Cationic Liposomal Adjuvants and Development of Enhanced Lymphatic Targeting Strategies. *Mol Pharm* [Internet]. 2019 Oct 7;16(10):4372–86. Available from: <https://doi.org/10.1021/acs.molpharmaceut.9b00730>

184. Lou G, Anderluzzi G, Woods S, Roberts CW, Perrie Y. A novel microfluidic-based approach to formulate size-tuneable large unilamellar cationic liposomes: formulation, cellular uptake and biodistribution investigations. *Eur J Pharm Biopharm* [Internet]. 2019; Available from: <https://api.semanticscholar.org/CorpusID:201644549>
185. Zhigaltsev I V, Belliveau N, Hafez I, Leung AKK, Huft J, Hansen C, et al. Bottom-Up Design and Synthesis of Limit Size Lipid Nanoparticle Systems with Aqueous and Triglyceride Cores Using Millisecond Microfluidic Mixing. *Langmuir* [Internet]. 2012 Feb 21;28(7):3633–40. Available from: <https://doi.org/10.1021/la204833h>
186. Lee CY, Wang WT, Liu CC, Fu LM. Passive mixers in microfluidic systems: A review. *Chemical Engineering Journal* [Internet]. 2016;288:146–60. Available from: <https://www.sciencedirect.com/science/article/pii/S138589471501596X>
187. Tóth EL, Holczer EG, Iván K, Fürjes P. Optimized Simulation and Validation of Particle Advection in Asymmetric Staggered Herringbone Type Micromixers. *Micromachines (Basel)* [Internet]. 2015;6(1):136–50. Available from: <https://www.mdpi.com/2072-666X/6/1/136>
188. Tammaro O, Costagliola di Polidoro A, Romano E, Netti PA, Torino E. A Microfluidic Platform to design Multimodal PEG - crosslinked Hyaluronic Acid Nanoparticles (PEG-cHANPs) for diagnostic applications. *Sci Rep* [Internet]. 2020;10(1):6028. Available from: <https://doi.org/10.1038/s41598-020-63234-x>
189. Zhang G, Sun J. Lipid in chips: A brief review of liposomes formation by microfluidics. Vol. 16, *International Journal of Nanomedicine*. Dove Medical Press Ltd; 2021. p. 7391–416.
190. Maruggi G, Zhang C, Li J, Ulmer JB, Yu D. mRNA as a Transformative Technology for Vaccine Development to Control Infectious Diseases. *Molecular Therapy* [Internet]. 2019 Apr 10;27(4):757–72. Available from: <https://doi.org/10.1016/j.ymthe.2019.01.020>
191. Polack FP, Thomas SJ, Kitchin N, Absalon J, Gurtman A, Lockhart S, et al. Safety and Efficacy of the BNT162b2 mRNA Covid-19 Vaccine. *New England Journal of Medicine*. 2020 Dec 31;383(27):2603–15.
192. Jackson LA, Anderson EJ, Roupael NG, Roberts PC, Makhene M, Coler RN, et al. An mRNA Vaccine against SARS-CoV-2 — Preliminary Report. *New England Journal of Medicine*. 2020 Nov 12;383(20):1920–31.
193. Echaide M, Chocarro de Erauso L, Bocanegra A, Blanco E, Kochan G, Escors D. mRNA Vaccines against SARS-CoV-2: Advantages and Caveats. *Int J Mol Sci*. 2023 Mar 21;24(6):5944.
194. Zook JM, Vreeland WN. Effects of temperature, acyl chain length, and flow-rate ratio on liposome formation and size in a microfluidic hydrodynamic focusing device. *Soft Matter* [Internet]. 2010;6(6):1352–60. Available from: <http://dx.doi.org/10.1039/B923299K>
195. Cheng MHY, Leung J, Zhang Y, Strong C, Basha G, Momeni A, et al. Induction of Bleb Structures in Lipid Nanoparticle Formulations of mRNA Leads to Improved Transfection Potency. *Advanced Materials*. 2023 Aug 3;35(31).

196. Patel P, Ibrahim NM, Cheng K. The Importance of Apparent pKa in the Development of Nanoparticles Encapsulating siRNA and mRNA. *Trends Pharmacol Sci* [Internet]. 2021;42(6):448–60. Available from: <https://www.sciencedirect.com/science/article/pii/S0165614721000493>
197. Nakamura K, Aihara K, Ishida T. Importance of Process Parameters Influencing the Mean Diameters of siRNA-Containing Lipid Nanoparticles (LNPs) on the *in Vitro* Activity of Prepared LNPs. *Biol Pharm Bull*. 2022;45(4):497–507.
198. Mui BL, Tam YK, Jayaraman M, Ansell SM, Du X, Tam YYC, et al. Influence of Polyethylene Glycol Lipid Desorption Rates on Pharmacokinetics and Pharmacodynamics of siRNA Lipid Nanoparticles. *Mol Ther Nucleic Acids* [Internet]. 2013;2. Available from: <https://api.semanticscholar.org/CorpusID:18413960>
199. Maugeri M, Nawaz M, Papadimitriou A, Angerfors A, Camponeschi A, Na M, et al. Linkage between endosomal escape of LNP-mRNA and loading into EVs for transport to other cells. *Nat Commun* [Internet]. 2019;10. Available from: <https://api.semanticscholar.org/CorpusID:202733739>
200. Miao L, Lin J, Huang Y, Li L, Delcassian D, Ge Y, et al. Synergistic lipid compositions for albumin receptor mediated delivery of mRNA to the liver. *Nat Commun* [Internet]. 2020;11(1):2424. Available from: <https://doi.org/10.1038/s41467-020-16248-y>
201. Nogueira SS, Schlegel A, Maxeiner K, Weber B, Barz M, Schroer MA, et al. Polysarcosine-Functionalized Lipid Nanoparticles for Therapeutic mRNA Delivery. *ACS Appl Nano Mater* [Internet]. 2020; Available from: <https://api.semanticscholar.org/CorpusID:224998984>
202. Lou G, Anderluzzi G, Schmidt ST, Woods S, Gallorini S, Brazzoli M, et al. Delivery of self-amplifying mRNA vaccines by cationic lipid nanoparticles: The impact of cationic lipid selection. *Journal of Controlled Release* [Internet]. 2020;325:370–9. Available from: <https://www.sciencedirect.com/science/article/pii/S016836592030362X>
203. Zhang M, Sun J, Li M, Jin X. Modified mRNA-LNP Vaccines Confer Protection against Experimental DENV-2 Infection in Mice. *Mol Ther Methods Clin Dev* [Internet]. 2020;18:702–12. Available from: <https://www.sciencedirect.com/science/article/pii/S2329050120301625>
204. Hassett KJ, Benenato KE, Jacquinet E, Lee A, Woods A, Yuzhakov O, et al. Optimization of Lipid Nanoparticles for Intramuscular Administration of mRNA Vaccines. *Mol Ther Nucleic Acids* [Internet]. 2019;15:1–11. Available from: <https://api.semanticscholar.org/CorpusID:67857759>
205. Sabnis S, Kumarasinghe ES, Salerno T, Mihai C, Ketova T, Senn JJ, et al. A Novel Amino Lipid Series for mRNA Delivery: Improved Endosomal Escape and Sustained Pharmacology and Safety in Non-human Primates. *Molecular Therapy* [Internet]. 2018 Jun 6;26(6):1509–19. Available from: <https://doi.org/10.1016/j.ymthe.2018.03.010>
206. Riley RS, Kashyap M V, Billingsley MM, White B, Alameh MG, Bose SK, et al. Ionizable lipid nanoparticles for in utero mRNA delivery. *Sci Adv* [Internet]. 2021;7(3):eaba1028. Available from: <https://www.science.org/doi/abs/10.1126/sciadv.aba1028>

207. McMillan C, Druschitz A, Rumbelow S, Borah A, Binici B, Rattray Z, et al. Tailoring lipid nanoparticle dimensions through manufacturing processes. *RSC Pharmaceutics* [Internet]. 2024;1(4):841–53. Available from: <http://dx.doi.org/10.1039/D4PM00128A>
208. Schoenmaker L, Witzigmann D, Kulkarni JA, Verbeke R, Kersten G, Jiskoot W, et al. mRNA-lipid nanoparticle COVID-19 vaccines: Structure and stability. *Int J Pharm* [Internet]. 2021;601:120586. Available from: <https://www.sciencedirect.com/science/article/pii/S0378517321003914>
209. Auld Dsph . D, Coassin PS, Coussens Npph D. *Microplate Selection and Recommended Practices in High-throughput Screening and Quantitative Biology*. 2020.
210. Hussain M, Binici B, O'Connor L, Perrie Y. Production of mRNA lipid nanoparticles using advanced crossflow micromixing. *Journal of Pharmacy and Pharmacology* [Internet]. 2024 Oct 9;rgae122. Available from: <https://doi.org/10.1093/jpp/rgae122>
211. Vargas R, Romero M, Berasategui T, Narváez-Narváez DA, Ramirez P, Nardi-Ricart A, et al. Dialysis is a key factor modulating interactions between critical process parameters during the microfluidic preparation of lipid nanoparticles. *Colloid Interface Sci Commun* [Internet]. 2023;54:100709. Available from: <https://www.sciencedirect.com/science/article/pii/S221503822300016X>
212. Forbes N, Hussain MT, Briuglia ML, Edwards DP, Horst JH ter, Szita N, et al. Rapid and scale-independent microfluidic manufacture of liposomes entrapping protein incorporating in-line purification and at-line size monitoring. *Int J Pharm* [Internet]. 2019;556:68–81. Available from: <https://www.sciencedirect.com/science/article/pii/S037851731830886X>
213. Belfort G, Davis RH, Zydney AL. The behavior of suspensions and macromolecular solutions in crossflow microfiltration. *J Memb Sci* [Internet]. 1994;96(1):1–58. Available from: <https://www.sciencedirect.com/science/article/pii/0376738894001197>
214. Aso Y, Yoshioka S. Effect of Freezing Rate on Physical Stability of Lyophilized Cationic Liposomes. *Chem Pharm Bull (Tokyo)*. 2005;53(3):301–4.
215. Kamiya M, Matsumoto M, Yamashita K, Izumi T, Kawaguchi M, Mizukami S, et al. Stability Study of mRNA-Lipid Nanoparticles Exposed to Various Conditions Based on the Evaluation between Physicochemical Properties and Their Relation with Protein Expression Ability. *Pharmaceutics*. 2022 Nov 1;14(11).
216. Merk. *A Hands-On Guide to Ultrafiltration/Diafiltration Optimization using Pellicon® Cassettes*. 2013. p. 1–12.
217. G.H. Bio-Science. *Cross Flow Filtration Method Handbook*. 2014. p. 1–82.
218. Pogocki D, Schöneich C. Chemical Stability of Nucleic Acid-Derived Drugs. *J Pharm Sci* [Internet]. 2000 Apr 1;89(4):443–56. Available from: [https://doi.org/10.1002/\(SICI\)1520-6017\(200004\)89:4<443::AID-JPS2>3.0.CO](https://doi.org/10.1002/(SICI)1520-6017(200004)89:4<443::AID-JPS2>3.0.CO)

219. Khadke S, Roces CB, Donaghey R, Giacobbo V, Su Y, Perrie Y. Scalable solvent-free production of liposomes. *Journal of Pharmacy and Pharmacology* [Internet]. 2020 Oct 1;72(10):1328–40. Available from: <https://doi.org/10.1111/jphp.13329>
220. Dalwadi G, Sunderland VB. Purification of PEGylated nanoparticles using tangential flow filtration (TFF). *Drug Dev Ind Pharm*. 2007 Sep;33(9):1030–9.
221. Dalwadi G, Benson HAE, Chen Y. Comparison of diafiltration and tangential flow filtration for purification of nanoparticle suspensions. *Pharm Res*. 2005 Dec;22(12):2152–62.
222. Geng C, Zhou K, Yan Y, Li C, Ni B, Liu J, et al. A preparation method for mRNA-LNPs with improved properties. *Journal of Controlled Release* [Internet]. 2023;364:632–43. Available from: <https://www.sciencedirect.com/science/article/pii/S0168365923007344>
223. Worsham RD, Thomas V, Farid SS. Impact of ethanol on continuous inline diafiltration of liposomal drug products. *Biotechnol J*. 2023 Nov 1;18(11).
224. John R, Monpara J, Swaminathan S, Kalhapure R. *Chemistry and Art of Developing Lipid Nanoparticles for Biologics Delivery: Focus on Development and Scale-Up*. Vol. 16, Pharmaceuticals. Multidisciplinary Digital Publishing Institute (MDPI); 2024.
225. Vetten MA, Yah CS, Singh T, Gulumian M. Challenges facing sterilization and depyrogenation of nanoparticles: Effects on structural stability and biomedical applications. *Nanomedicine* [Internet]. 2014;10(7):1391–9. Available from: <https://www.sciencedirect.com/science/article/pii/S154996341400135X>
226. van Reis R, Zydney A. Bioprocess membrane technology. *J Memb Sci* [Internet]. 2007;297(1):16–50. Available from: <https://www.sciencedirect.com/science/article/pii/S0376738807001159>
227. ASTM. Standard test method for determining bacterial retention of membrane filters utilized for liquid filtration. 2013. p. 1–6.
228. Messerian KO, Zverev A, Kramarczyk JF, Zydney AL. Pressure-dependent fouling behavior during sterile filtration of mRNA-containing lipid nanoparticles. *Biotechnol Bioeng*. 2022 Nov 1;119(11):3221–9.
229. Moreira M, Sarraguça M. How can oral paediatric formulations be improved? A challenge for the XXI century. *Int J Pharm* [Internet]. 2020;590:119905. Available from: <https://www.sciencedirect.com/science/article/pii/S0378517320308905>
230. Kumru OS, Joshi SB, Smith DE, Middaugh CR, Prusik T, Volkin DB. Vaccine instability in the cold chain: Mechanisms, analysis and formulation strategies. *Biologicals* [Internet]. 2014;42(5):237–59. Available from: <https://www.sciencedirect.com/science/article/pii/S1045105614000487>
231. Schoenmaker L, Witzigmann D, Kulkarni JA, Verbeke R, Kersten G, Jiskoot W, et al. mRNA-lipid nanoparticle COVID-19 vaccines: Structure and stability. *Int J Pharm* [Internet]. 2021;601:120586. Available from: <https://www.sciencedirect.com/science/article/pii/S0378517321003914>

232. Crommelin DJA, Anchordoquy TJ, Volkin DB, Jiskoot W, Mastrobattista E. Addressing the Cold Reality of mRNA Vaccine Stability. *J Pharm Sci* [Internet]. 2021;110(3):997–1001. Available from: <https://www.sciencedirect.com/science/article/pii/S0022354920307851>
233. Committee for Medicinal Products for Human Use (CHMP). Assessment report mResvia. 2024.
234. Ghaemmaghamian Z, Zarghami R, Walker G, O'Reilly E, Ziaee A. Stabilizing vaccines via drying: Quality by design considerations. *Adv Drug Deliv Rev* [Internet]. 2022;187:114313. Available from: <https://www.sciencedirect.com/science/article/pii/S0169409X22002034>
235. Chheda U, Pradeepan S, Esposito E, Strezsak S, Fernandez-Delgado O, Kranz J. Factors Affecting Stability of RNA – Temperature, Length, Concentration, pH, and Buffering Species. *J Pharm Sci* [Internet]. 2024;113(2):377–85. Available from: <https://www.sciencedirect.com/science/article/pii/S0022354923004987>
236. Aves KL, Janitzek CM, Fougeroux CE, Theander TG, Sander AF. Freeze-Drying of a Capsid Virus-like Particle-Based Platform Allows Stable Storage of Vaccines at Ambient Temperature. *Pharmaceutics* [Internet]. 2022;14(6). Available from: <https://www.mdpi.com/1999-4923/14/6/1301>
237. Luo WC, Zhang W, Kim R, Chong H, Patel SM, Bogner RH, et al. Impact of controlled ice nucleation and lyoprotectants on nanoparticle stability during Freeze-drying and upon storage. *Int J Pharm*. 2023 Jun 25;641.
238. Fan Y, Rigas D, Kim LJ, Chang FP, Zang N, McKee K, et al. Physicochemical and structural insights into lyophilized mRNA-LNP from lyoprotectant and buffer screenings. *Journal of Controlled Release* [Internet]. 2024;373:727–37. Available from: <https://www.sciencedirect.com/science/article/pii/S0168365924005078>
239. Meulewaeter S, Nuytten G, Cheng MHY, De Smedt SC, Cullis PR, De Beer T, et al. Continuous freeze-drying of messenger RNA lipid nanoparticles enables storage at higher temperatures. *Journal of Controlled Release* [Internet]. 2023;357:149–60. Available from: <https://www.sciencedirect.com/science/article/pii/S0168365923002067>
240. Thorat AA, Suryanarayanan R. Characterization of Phosphate Buffered Saline (PBS) in Frozen State and after Freeze-Drying. *Pharm Res* [Internet]. 2019 May;36(7):98. Available from: <https://doi.org/10.1007/s11095-019-2619-2>
241. Alejo T, Toro-Córdova A, Fernández L, Rivero A, Stoian AM, Pérez L, et al. Comprehensive Optimization of a Freeze-Drying Process Achieving Enhanced Long-Term Stability and In Vivo Performance of Lyophilized mRNA-LNPs. *Int J Mol Sci* [Internet]. 2024;25(19). Available from: <https://www.mdpi.com/1422-0067/25/19/10603>
242. Franzé S, Selmin F, Samaritani E, Minghetti P, Cilurzo F. Lyophilization of Liposomal Formulations: Still Necessary, Still Challenging. *Pharmaceutics* [Internet]. 2018;10(3). Available from: <https://www.mdpi.com/1999-4923/10/3/139>
243. Trenkenschuh E, Friess W. Freeze-drying of nanoparticles: How to overcome colloidal instability by formulation and process optimization. *European Journal of Pharmaceutics and*

- Biopharmaceutics [Internet]. 2021;165:345–60. Available from: <https://www.sciencedirect.com/science/article/pii/S0939641121001545>
244. Lball R, Bajaj P, Whitehead KA. Achieving long-term stability of lipid nanoparticles: Examining the effect of pH, temperature, and lyophilization. *Int J Nanomedicine*. 2017;12:305–15.
  245. Pereira CS, Lins RD, Chandrasekhar I, Freitas LCG, Hünenberger PH. Interaction of the Disaccharide Trehalose with a Phospholipid Bilayer: A Molecular Dynamics Study. *Biophys J*. 2004;86(4).
  246. Chen C, Han D, Cai C, Tang X. An overview of liposome lyophilization and its future potential. Vol. 142, *Journal of Controlled Release*. 2010.
  247. Koster KL, Webb MS, Bryant G, Lynch D V. Interactions between soluble sugars and POPC (1-palmitoyl-2-oleoylphosphatidylcholine) during dehydration: vitrification of sugars alters the phase behavior of the phospholipid. *BBA - Biomembranes*. 1994;1193(1).
  248. Li M, Jia L, Xie Y, Ma W, Yan Z, Liu F, et al. Lyophilization process optimization and molecular dynamics simulation of mRNA-LNPs for SARS-CoV-2 vaccine. *NPJ Vaccines*. 2023;8(1).
  249. usp.org. Analytical Procedures for Quality of mRNA Vaccines and Therapeutics - Draft Guidelines: 3rd Edition.
  250. CHMP. COVID-19 Vaccine Moderna, INN-COVID-19 mRNA Vaccine (nucleoside modified) [Internet]. 2021. Available from: [www.ema.europa.eu/contact](http://www.ema.europa.eu/contact)
  251. Wang T, Yu T, Li W, Liu Q, Sung TC, Higuchi A. Design and lyophilization of mRNA-encapsulating lipid nanoparticles. *Int J Pharm* [Internet]. 2024;662:124514. Available from: <https://www.sciencedirect.com/science/article/pii/S0378517324007488>
  252. Trenkenschuh E, Friess W. Freeze-drying of nanoparticles: How to overcome colloidal instability by formulation and process optimization. *European Journal of Pharmaceutics and Biopharmaceutics* [Internet]. 2021;165:345–60. Available from: <https://www.sciencedirect.com/science/article/pii/S0939641121001545>
  253. Schwarz C, Mehnert W. Freeze-drying of drug-free and drug-loaded solid lipid nanoparticles (SLN). *Int J Pharm* [Internet]. 1997;157(2):171–9. Available from: <https://www.sciencedirect.com/science/article/pii/S0378517397002226>
  254. Patel SM, Nail SL, Pikal MJ, Geidobler R, Winter G, Hawe A, et al. Lyophilized Drug Product Cake Appearance: What Is Acceptable? Vol. 106, *Journal of Pharmaceutical Sciences*. 2017.
  255. Izutsu KI, Yomota C, Kawanishi T. Stabilization of liposomes in frozen solutions through control of osmotic flow and internal solution freezing by trehalose. *J Pharm Sci*. 2011;100(7).
  256. Kaasgaard T, Mouritsen OG, Jørgensen K. Freeze/thaw effects on lipid-bilayer vesicles investigated by differential scanning calorimetry. *Biochim Biophys Acta Biomembr*. 2003;1615(1–2).
  257. Filippov A, Orädd G, Lindblom G. The effect of cholesterol on the lateral diffusion of phospholipids in oriented bilayers. *Biophys J*. 2003;84(5).

258. Hald Albertsen C, Kulkarni JA, Witzigmann D, Lind M, Petersson K, Simonsen JB. The role of lipid components in lipid nanoparticles for vaccines and gene therapy. *Adv Drug Deliv Rev* [Internet]. 2022;188:114416. Available from: <https://www.sciencedirect.com/science/article/pii/S0169409X22003064>
259. van Winden ECA, Zhang W, Crommelin DJA. Effect of Freezing Rate on the Stability of Liposomes During Freeze-Drying and Rehydration. *Pharm Res* [Internet]. 1997;14(9):1151–60. Available from: <https://doi.org/10.1023/A:1012142520912>
260. Ingvarsson PT, Yang M, Nielsen HMØ, Rantanen J, Foged C. Stabilization of liposomes during drying. Vol. 8, *Expert Opinion on Drug Delivery*. 2011.
261. Suzuki Y, Miyazaki T, Muto H, Kubara K, Mukai Y, Watari R, et al. Design and lyophilization of lipid nanoparticles for mRNA vaccine and its robust immune response in mice and nonhuman primates. *Mol Ther Nucleic Acids*. 2022;30.
262. Muramatsu H, Lam K, Bajusz C, Laczkó D, Karikó K, Schreiner P, et al. Lyophilization provides long-term stability for a lipid nanoparticle-formulated, nucleoside-modified mRNA vaccine. *Molecular Therapy* [Internet]. 2022;30(5):1941–51. Available from: <https://www.sciencedirect.com/science/article/pii/S1525001622000843>
263. Stitz L, Vogel A, Schnee M, Voss D, Rauch S, Mutzke T, et al. A thermostable messenger RNA based vaccine against rabies. *PLoS Negl Trop Dis*. 2017;11(12).
264. Kim B, Hosn RR, Remba T, Yun D, Li N, Abraham W, et al. Optimization of storage conditions for lipid nanoparticle-formulated self-replicating RNA vaccines. *Journal of Controlled Release*. 2023;353.
265. Hassett KJ, Higgins J, Woods A, Levy B, Xia Y, Hsiao CJ, et al. Impact of lipid nanoparticle size on mRNA vaccine immunogenicity. *Journal of Controlled Release* [Internet]. 2021;335:237–46. Available from: <https://www.sciencedirect.com/science/article/pii/S0168365921002376>
266. Schroeder A, Levins CG, Cortez C, Langer R, Anderson DG. Lipid-based nanotherapeutics for siRNA delivery. *J Intern Med*. 2010 Jan;267(1):9–21.
267. Semple SC, Klimuk SK, Harasym TO, Dos Santos N, Ansell SM, Wong KF, et al. Efficient encapsulation of antisense oligonucleotides in lipid vesicles using ionizable aminolipids: formation of novel small multilamellar vesicle structures. *Biochimica et Biophysica Acta (BBA) - Biomembranes*. 2001 Feb;1510(1–2):152–66.
268. Patel P, Ibrahim NM, Cheng K. The Importance of Apparent pKa in the Development of Nanoparticles Encapsulating siRNA and mRNA. *Trends Pharmacol Sci*. 2021 Jun;42(6):448–60.
269. Polack FP, Thomas SJ, Kitchin N, Absalon J, Gurtman A, Lockhart S, et al. Safety and Efficacy of the BNT162b2 mRNA Covid-19 Vaccine. *New England Journal of Medicine*. 2020 Dec 31;383(27):2603–15.
270. Jackson LA, Anderson EJ, Roupheal NG, Roberts PC, Makhene M, Coler RN, et al. An mRNA Vaccine against SARS-CoV-2 — Preliminary Report. *New England Journal of Medicine*. 2020 Nov 12;383(20):1920–31.

271. Echaide M, Chocarro de Erauso L, Bocanegra A, Blanco E, Kochan G, Escors D. mRNA Vaccines against SARS-CoV-2: Advantages and Caveats. *Int J Mol Sci.* 2023 Mar 21;24(6):5944.
272. Papi A, Ison MG, Langley JM, Lee DG, Leroux-Roels I, Martinon-Torres F, et al. Respiratory Syncytial Virus Prefusion F Protein Vaccine in Older Adults. *New England Journal of Medicine.* 2023 Feb 16;388(7):595–608.
273. Mendonça MCP, Kont A, Kowalski PS, O'Driscoll CM. Design of lipid-based nanoparticles for delivery of therapeutic nucleic acids. *Drug Discov Today.* 2023 Mar;28(3):103505.
274. Cheng X, Lee RJ. The role of helper lipids in lipid nanoparticles (LNPs) designed for oligonucleotide delivery. *Adv Drug Deliv Rev.* 2016 Apr;99:129–37.
275. Tang X, Zhang Y, Han X. Ionizable Lipid Nanoparticles for mRNA Delivery. *Adv Nanobiomed Res.* 2023 Aug 13;3(8).
276. Mui BL, Tam YK, Jayaraman M, Ansell SM, Du X, Tam YYC, et al. Influence of Polyethylene Glycol Lipid Desorption Rates on Pharmacokinetics and Pharmacodynamics of siRNA Lipid Nanoparticles. *Mol Ther Nucleic Acids.* 2013 Dec 17;2(12):e139.
277. Waggoner LE, Miyasaki KF, Kwon EJ. Analysis of PEG-lipid anchor length on lipid nanoparticle pharmacokinetics and activity in a mouse model of traumatic brain injury. *Biomater Sci.* 2023;11(12):4238–53.
278. Wilson SC, Baryza JL, Reynolds AJ, Bowman K, Keegan ME, Standley SM, et al. Real Time Measurement of PEG Shedding from Lipid Nanoparticles in Serum via NMR Spectroscopy. *Mol Pharm.* 2015 Feb 2;12(2):386–92.
279. Akinc A, Querbes W, De S, Qin J, Frank-Kamenetsky M, Jayaprakash KN, et al. Targeted Delivery of RNAi Therapeutics With Endogenous and Exogenous Ligand-Based Mechanisms. *Molecular Therapy.* 2010 Jul;18(7):1357–64.
280. Wallace M, Moulia D, Blain AE, Ricketts EK, Minhaj FS, Link-Gelles R, et al. The Advisory Committee on Immunization Practices' Recommendation for Use of Moderna COVID-19 Vaccine in Adults Aged ≥18 Years and Considerations for Extended Intervals for Administration of Primary Series Doses of mRNA COVID-19 Vaccines — United States, February 2022. *MMWR Morb Mortal Wkly Rep.* 2022 Mar 18;71(11):416–21.
281. Adams D, Gonzalez-Duarte A, O'Riordan WD, Yang CC, Ueda M, Kristen A V., et al. Patisiran, an RNAi Therapeutic, for Hereditary Transthyretin Amyloidosis. *New England Journal of Medicine.* 2018 Jul 5;379(1):11–21.
282. Di J, Du Z, Wu K, Jin S, Wang X, Li T, et al. Biodistribution and Non-linear Gene Expression of mRNA LNPs Affected by Delivery Route and Particle Size. *Pharm Res.* 2022 Jan 26;39(1):105–14.
283. Binici B, Rattray Z, Zinger A, Perrie Y. Exploring the impact of commonly used ionizable and pegylated lipids on mRNA-LNPs: A combined in vitro and preclinical perspective. *Journal of Controlled Release.* 2025 Jan;377:162–73.

284. Binici B, Borah A, Watts JA, McLoughlin D, Perrie Y. The influence of citrate buffer molarity in mRNA-LNPs: Exploring factors beyond general critical quality attributes. *Int J Pharm.* 2024 Nov;124942.
285. Bahl K, Senn JJ, Yuzhakov O, Bulychev A, Brito LA, Hassett KJ, et al. Preclinical and Clinical Demonstration of Immunogenicity by mRNA Vaccines against H10N8 and H7N9 Influenza Viruses. *Molecular Therapy.* 2017 Jun;25(6):1316–27.
286. Carrasco MJ, Alishetty S, Alameh MG, Said H, Wright L, Paige M, et al. Ionization and structural properties of mRNA lipid nanoparticles influence expression in intramuscular and intravascular administration. *Commun Biol.* 2021 Aug 11;4(1):956.
287. Davies N, Hovdal D, Edmunds N, Nordberg P, Dahlén A, Dabkowska A, et al. Functionalized lipid nanoparticles for subcutaneous administration of mRNA to achieve systemic exposures of a therapeutic protein. *Mol Ther Nucleic Acids.* 2021 Jun;24:369–84.
288. Lou G, Anderluzzi G, Schmidt ST, Woods S, Gallorini S, Brazzoli M, et al. Delivery of self-amplifying mRNA vaccines by cationic lipid nanoparticles: The impact of cationic lipid selection. *Journal of Controlled Release.* 2020 Sep;325:370–9.
289. Martins S, Costa-Lima S, Carneiro T, Cordeiro-da-Silva A, Souto EB, Ferreira DC. Solid lipid nanoparticles as intracellular drug transporters: An investigation of the uptake mechanism and pathway. *Int J Pharm.* 2012 Jul;430(1–2):216–27.
290. Webb C, Forbes N, Roces CB, Anderluzzi G, Lou G, Abraham S, et al. Using microfluidics for scalable manufacturing of nanomedicines from bench to GMP: A case study using protein-loaded liposomes. *Int J Pharm.* 2020 May;582:119266.
291. Roces CB, Lou G, Jain N, Abraham S, Thomas A, Halbert GW, et al. Manufacturing Considerations for the Development of Lipid Nanoparticles Using Microfluidics. *Pharmaceutics* [Internet]. 2020 Nov 1 [cited 2023 May 2];12(11):1–19. Available from: <https://pubmed.ncbi.nlm.nih.gov/33203082/>
292. Webb C, Khadke S, Tandrup Schmidt S, Roces CB, Forbes N, Berrie G, et al. The Impact of Solvent Selection: Strategies to Guide the Manufacturing of Liposomes Using Microfluidics. *Pharmaceutics* [Internet]. 2019;11(12). Available from: <https://www.mdpi.com/1999-4923/11/12/653>
293. McMillan C, Druschitz A, Rumbelow S, Borah A, Binici B, Rattray Z, et al. Tailoring lipid nanoparticle dimensions through manufacturing processes. *RSC Pharmaceutics.* 2024;
294. Hoshyar N, Gray S, Han H, Bao G. The Effect of Nanoparticle Size on *In Vivo* Pharmacokinetics and Cellular Interaction. *Nanomedicine.* 2016 Mar 22;11(6):673–92.
295. He C, Hu Y, Yin L, Tang C, Yin C. Effects of particle size and surface charge on cellular uptake and biodistribution of polymeric nanoparticles. *Biomaterials.* 2010 May;31(13):3657–66.
296. Swingle KL, Hamilton AG, Mitchell MJ. Lipid Nanoparticle-Mediated Delivery of mRNA Therapeutics and Vaccines. *Trends Mol Med.* 2021 Jun;27(6):616–7.

297. Al Khafaji AS, Donovan MD. Endocytic Uptake of Solid Lipid Nanoparticles by the Nasal Mucosa. *Pharmaceutics*. 2021 May 20;13(5):761.
298. Sayers EJ, Peel SE, Schantz A, England RM, Beano M, Bates SM, et al. Endocytic Profiling of Cancer Cell Models Reveals Critical Factors Influencing LNP-Mediated mRNA Delivery and Protein Expression. *Molecular Therapy*. 2019 Nov;27(11):1950–62.
299. Cui L, Hunter MR, Sonzini S, Pereira S, Romanelli SM, Liu K, et al. Mechanistic Studies of an Automated Lipid Nanoparticle Reveal Critical Pharmaceutical Properties Associated with Enhanced mRNA Functional Delivery In Vitro and In Vivo. *Small*. 2022 Mar 16;18(9).
300. Escalona-Rayo O, Zeng Y, Knol RA, Kock TJF, Aschmann D, Slütter B, et al. In vitro and in vivo evaluation of clinically-approved ionizable cationic lipids shows divergent results between mRNA transfection and vaccine efficacy. *Biomedicine & Pharmacotherapy*. 2023 Sep;165:115065.
301. Hou X, Zaks T, Langer R, Dong Y. Lipid nanoparticles for mRNA delivery. *Nat Rev Mater*. 2021;6(12):1078–94.
302. Ferrareso F, Strilchuk AW, Juang LJ, Poole LG, Luyendyk JP, Kastrup CJ. Comparison of DLin-MC3-DMA and ALC-0315 for siRNA Delivery to Hepatocytes and Hepatic Stellate Cells. *Mol Pharm*. 2022 Jul 4;19(7):2175–82.
303. Han X, Zhang H, Butowska K, Swingle KL, Alameh MG, Weissman D, et al. An ionizable lipid toolbox for RNA delivery. *Nat Commun*. 2021 Dec 13;12(1):7233.
304. Suzuki T, Suzuki Y, Hihara T, Kubara K, Kondo K, Hyodo K, et al. PEG shedding-rate-dependent blood clearance of PEGylated lipid nanoparticles in mice: Faster PEG shedding attenuates anti-PEG IgM production. *Int J Pharm*. 2020 Oct;588:119792.
305. Paunovska K, Da Silva Sanchez AJ, Lokugamage MP, Loughrey D, Echeverri ES, Cristian A, et al. The Extent to Which Lipid Nanoparticles Require Apolipoprotein E and Low-Density Lipoprotein Receptor for Delivery Changes with Ionizable Lipid Structure. *Nano Lett*. 2022 Dec 28;22(24):10025–33.
306. Zechner R, Moser R, Newman TC, Fried SK, Breslow JL. Apolipoprotein E gene expression in mouse 3T3-L1 adipocytes and human adipose tissue and its regulation by differentiation and lipid content. *J Biol Chem*. 1991 Jun 5;266(16):10583–8.